DEVELOPMENT OF SYSTEM ANALYSIS METHODOLOGIES AND TOOLS FOR MODELING AND OPTIMIZING VEHICLE SYSTEM EFFICIENCY

by

Melody L. Baglione

A dissertation submitted in partial fulfillment
of the requirements for the degree of
Doctor of Philosophy
(Mechanical Engineering)
in the University of Michigan
2007

Doctoral Committee:

Professor Dionissios N. Assanis, Co-Chair
Professor Jun Ni, Co-Chair
Professor Levi T. Thompson, Jr.
Professor Huei Peng
Mark Duty, Chrysler LLC

DEDICATION

To my mother for her devotion,
To my brothers for their inspiration,
And to my husband for his love and support.

ACKNOWLEDGEMENTS

I would like to thank my advisor Professor Jun Ni for his direction and guidance in my research as well as for all his advice and encouragement throughout my academic career at the University of Michigan. I would also like to thank Professor Dennis Assanis, co-chair of my dissertation committee, for his powertrain research insight and helpful advice. I also appreciate Professor Levi Thompson and Professor Huei Peng for taking the time to serve on my dissertation committee.

I gratefully acknowledge the financial support of the Graduate Research Fellowship awarded by the National Science Foundation. I would also like to recognize the University of Michigan for the Rackham Engineering Award Fellowship.

I am sincerely grateful to Mark Duty and Greg Pannone at Chrysler for presenting me with challenging research opportunities and for the chance to see my work implemented in industry. I greatly acknowledge the hard work and contribution of Georg Thomann, a mechanical engineering student at the University of Applied Sciences in Esslingen, Germany, whom I advised on the performance simulation development. Special thanks to all those at Chrysler who helped me along the way, including John Rzepecki, Kevin Roth, Laurie Emerson, Dr. Jim Li, Chris Tuckfield, Lixin Zhao, Craig Ashmore, Jason Huang, Dr. Bruce Geist, Mike Bonne, John Bucknell, Pradeep Attibele, Mike Fingerman, Sashi Velnati, Mike Hagen, Harish Sivasubramanian, Brandon Brigham, Tim Tuttle, Mark Poublon, Mike Prucka, John Mitchell, Ben Moeggenberg,

along with many others. I also thank Bob Lee, Meg Novacek and Mike Donoughe for their mentoring.

I cannot begin to express my gratitude to all of my family and friends. Most importantly, I am forever indebted to my Mom, the most caring and giving woman I know, for her strength to single-handedly raise my brothers and me with very little means and for instilling in me a love of learning. I would also like to thank my older brothers, Brian and Darrel, whom I always looked up to, for inspiring me to become an engineer. Finally, I thank my loving husband, Thomas, for his constant support and for always being there for me.

TABLE OF CONTENTS

LIST OF FIGURES

LIST OF TABLES

CHAPTER 1

INTRODUCTION

1.1 Motivation and Problem Statement

The automotive industry is increasing its focus on developing fuel efficient vehicles. Growing worldwide oil demand and concerns about a supply base that is largely dependent on foreign oil has led to uncertainty with respect to fuel price stability. Heightened environmental awareness among the public and within the government has resulted in larger demand for fuel efficient vehicles and increased legislation on fuel economy. While increased attention is being given to hybrids and other alternatives to conventional powertrains, often other opportunities for fuel economy savings within current vehicle system designs are overlooked. Focusing current vehicle development efforts on optimizing fuel efficiency at a vehicle systems level is a low cost, practical and necessary solution to increasing overall fuel economy.

Too often when considering fuel economy only engine efficiency is taken into account. While achieving the highest feasible engine efficiency is desirable, often other vehicle attributes and components that affect fuel economy are disregarded. The potential fuel economy benefits of an efficiently designed engine can be futile if drivetrain and accessory components are not properly integrated or if the engine is not matched to the vehicle application. Furthermore, vehicle weight, aerodynamic drag, and

rolling resistance play a key role in influencing fuel economy. In order to develop more fuel efficient vehicles, a greater understanding of the energy demand within the vehicle system is essential. Considering energy demand at a vehicle subsystem level will expose the effect of individual component design and system integration decisions on the fuel economy of the vehicle system. Existing vehicle system models have the ability to predict overall fuel economy but lack the capability to accurately and systematically account for when and where fuel energy is being demanded within the vehicle system over different drive cycles.

In addition to the need to better understand fuel energy demand from a vehicle subsystem standpoint, optimal hardware and control design is essential to developing more fuel efficient vehicles. Vehicle systems are becoming increasingly complex as are drivers expectations for both fuel economy and performance. At the same time, there is increased need to shorten the product development time resulting in less time available to evaluate alternative hardware configurations and to design control strategies. Often the interrelationship between hardware selection and control design and their further dependence on driver application is overlooked during the design process. The challenge in successful vehicle system design is to optimally match hardware and control system design to specific vehicle attributes and driver applications.

Fuel economy testing completed with a proof-of-concept vehicle during this research demonstrates that incremental hardware and control strategy changes that add little or no cost to the current vehicle system design can increase real world fuel economy by four to eight percent. Further development of vehicle system hardware and system

integration optimization methodologies and tools offers the potential to reveal further opportunities to improve fuel economy for advanced powertrain system designs.

1.2 Research Objectives and Framework

The first portion of this research involves the development and application of a vehicle energy analysis methodology and tool that uses empirical vehicle data and first principles to simulate energy conversion throughout the vehicle system. The objective of the energy analysis tool is to accurately model where the fuel energy supplied to a vehicle system is being demanded. An accurate analysis requires that the vehicle model be populated with drive cycle data and other vehicle and component information. Once the tool is populated with vehicle specific data, the model can be used to investigate prevailing fuel economy effects and potential fuel saving hypothetical scenarios.

The goal of the second portion of this research is to develop a predictive model and optimization methodology that facilitates hardware and control optimization for multiple vehicle configurations and driving scenarios. The research includes the development of a reverse torque-based model that applies the same first principles used in the energy analysis tool albeit with reverse causality and the application of an optimization algorithm to address the optimal hardware and control design problem. The reverse tractive road load demand model and dynamic optimization technique will be used to optimize the hardware system and determine optimal operating states for different drive cycles.

1.2.1 Development of Vehicle Energy Analysis Model

The first step to improving fuel economy requires a detailed understanding of where the fuel energy supplied in a vehicle system is being demanded. An energy analysis tool will be created using MATLAB®/Simulink® and will use drive cycle data, vehicle data, measured component efficiencies, and basic physics and thermodynamics equations to quantify energy demand. The simulation models will represent various vehicle subsystems and calculate the power passed from one component to another and the corresponding parasitic losses over different drive cycles.

1.2.1.1 Test Based Methods and Energy Analysis Model Structure

It is often difficult to determine detailed subsystem parasitic losses over drive cycles. Accurate component and vehicle simulation data will be critical to obtaining valid energy analysis results. The numerous parasitic losses within the vehicle system will be accounted for by performing various tests to collect performance and efficiency data for each of the modeled components. To calculate inertial energy required for each vehicle component, computer-aided engineering (CAE) models will be used to determine moments of inertia for individual components.

Once the tool is populated with the necessary vehicle and component specific information, empirical data from drive cycles will be acquired. The vehicle model can be populated with any drive cycle data, such as the Environmental Protection Agency's (EPA) urban and highway Federal Test Procedures (FTP) for fuel economy and emissions as well as other real world consumer drive cycles. Drive cycle tests are conducted on standard chassis dynamometer rolls with constant volume sampling (CVS) and modal exhaust gas analyzers that measure fuel economy and emissions or on test

tracks using fuel flow meters. Vehicles will be further instrumented to collect additional measurements necessary to understand the component speeds and loads encountered over drive cycles and to understand the energy usage.

1.2.1.2 Investigation of Vehicle System Energy Supply and Demand

After the appropriate drive cycle and vehicle data are incorporated into the model, the tool will be used to investigate various effects on fuel economy. An energy analysis tool offers the potential to quickly evaluate possible fuel saving hypothetical scenarios by modeling the effect of vehicle and component changes on energy demand. The potential of the energy analysis tool extends beyond assisting in evaluating design alternatives. For instance, the tool can be used to explore the predominant fuel economy factors for different drive cycles as in the differences between idle, city, highway, and aggressive driving. Parametric analyses can also be performed. In addition, the overarching differences in where fuel energy is being demanded between different classes of vehicles, such as passenger cars, trucks and sport utility vehicles can be investigated. In summary, the energy analysis tool can serve to explore numerous fuel economy factors and potential fuel saving scenarios.

1.2.2 Development of Reverse Tractive Road Load Demand Model and Dynamic Optimization Methodology

To address the challenge of matching the powertrain hardware and control strategy to specific vehicle attributes and driver applications, a reverse tractive road load demand model and dynamic optimization methodology will be developed. The vehicle simulation and optimization algorithm will be developed in Matlab®/Simulink® and will propagate the required wheel torque and speed derived from the tractive road load

demand through the powertrain system to determine the fuel flow required for all possible states within the hardware constraints of the system. To expedite the simulation and optimization process, the model will be derivative based with inverted physical causality in that the force required to achieve the corresponding acceleration will be iteratively calculated from the desired speed trace. Then a dynamic programming algorithm will be applied to minimize the accumulated fuel required to traverse the given vehicle speed trace. The research goal is to facilitate optimal powertrain hardware and control design by simulating the vehicle system with an optimum powertrain system control strategy for given drive cycles.

1.2.2.1 Powertrain Control Strategy Assessment

The dynamic optimization technique offers the potential to quickly assess the potential fuel economy benefit of alternative powertrain control strategies. The dynamic optimization simulation tool will be applied to assess different torque converter clutch control strategies. By determining the most efficient state over various drive cycles, the tool will be used to develop more efficient transmission gear shift schedules. The reverse tractive road load demand model can further be used to help develop pedal calibrations for electronic throttle control vehicles. Also the methodology can be used to investigate how drive cycle characteristics influence the optimal powertrain system control design.

1.2.2.2 Dynamic Optimization of Variable Displacement Engine Operation

The reverse model and dynamic optimization technique will be extended to include optimizing variable displacement engine operation, also known as cylinder deactivation. Using the reverse dynamic optimization approach, control strategies for

variable displacement engines that take the transmission gear and torque converter clutch control interaction effects into account will be studied virtually.

1.2.2.3 Advanced Powertrain Hardware Design and System Integration Optimization

The model's reverse approach yields the required speeds and loads to traverse drive cycles, which can be used as design criteria for future powertrain programs, such as for the selection of optimal transmission gear ratios or minimum engine part throttle torque requirements. It will also be shown that evaluating alternative hardware configurations with an optimized control strategy that exploits the full capability of the powertrain can yield less biased and more rapid evaluations compared to the state-of-the-art vehicle simulations.

1.3 Literature Review

Modeling, simulation, and optimization of vehicle systems is becoming more relied upon as vehicle systems become increasingly complex and product development time decreases. Vehicle system modeling started in the early 1990's as efforts were made to find alternatives to in-vehicle testing. Around the same time, a growing amount of electronic control units (ECUs) were beginning to be installed in vehicles and hardware-in-the-loop (HIL) simulations became a prevalent method of testing ECUs. Since then an array of vehicle models with optimization capabilities have been developed by vehicle manufacturers, suppliers, universities, and research institutions. The following is a discussion of vehicle system modeling research and their approaches as well as optimization techniques that have been employed in vehicle system design.

1.3.1 Forward- vs. Backward-Looking Modeling Approaches

Current vehicle simulation models generally employ either a forward- or backward-looking approach. The following includes a brief description of both approaches and their inherent advantages and disadvantages along with their intended applications.

A forward-looking simulation includes a driver model and iteratively alters vehicle subsystem and component commands until the desired response of the system is achieved. The driver model considers the current and required speed to determine the appropriate throttle and brake commands often using a proportional-integral (PI) controller. The throttle command is translated into a fuel flow rate and engine torque, which is subsequently input into the transmission model, where the transmission output torque is computed from the transmission's efficiency and gear ratio. The transmission output torque is propagated forward through the drivetrain until the tractive force at the road and corresponding acceleration is calculated.

Backward-looking models assume the vehicle meets the desired driver trace and therefore do not require a driver model. Unlike in the forward-looking case, the force required to achieve the corresponding acceleration is directly calculated step by step from the desired speed trace. The required force is then converted into the required torque and rotational speed that must be provided by the component directly upstream. This calculation approach is continued in the reverse direction of the road load tractive force through the drivetrain until the energy demand that would be necessary to meet the driver trace is determined.

Forward-looking models have high fidelity but their major weakness is their long run times. Forward modeling is well-suited to control hardware development and simulations as in HIL applications. Other useful applications of forward-looking simulations include predicting vehicle dynamics and wide open throttle acceleration events. On the other hand, power calculations and the corresponding energy usage throughout the drivetrain rely on vehicle states and component speeds that must be computed by integration routines. The individual component speeds and power computations can result in unstable and inaccurate results if the individual component models do not accurately reflect reality or if higher order integration schemes with relatively small time steps are not employed. Thus, forward-looking models can be overly time-consuming for use in preliminary design studies. Wipke, *et al.* concluded that the backward-looking approach used in the Advanced Vehicle Simulator (ADVISOR), simulates vehicle performance on standard drive cycles between 2.6 and 8.0 times faster than a representative forward-looking model (1999).

The backward-looking approach is useful because the efficiencies of individual automotive drivetrain components can be obtained on laboratory test benches. Once efficiency tables are obtained, relatively simple calculations can be carried out to derive the energy loss throughout the drivetrain. In addition, since the calculations are relatively straight-forward, simple integration routines, such as Euler, with relatively large time steps on the order of one second can be used. One shortfall of the backward-looking approach is in the assumption that the desired driver trace is met. Furthermore, since efficiency maps are usually obtained at steady-state, transient effects are not represented in the model. Backward models are often preferred for fuel economy predictions,

component sizing, and road load analysis due to their low run times and simple integration routines. The benefits of a backward-looking approach will be demonstrated in Section 4.2.1.

1.3.2 Existing Advanced Vehicle Models

Vehicle modeling and simulation has become an essential tool to evaluate vehicle system performance early in the design phase. One model, Advanced Vehicle Simulator (ADVISOR), was developed by the National Renewable Energy Laboratory (NREL) to assist the Department of Energy (DOE) in developing technology for hybrids (Markel, *et al.* 2002). ADVISOR was developed to quantify the fuel economy, performance, and emissions of vehicles including alternative technologies, such as fuel cells, batteries, electric motors, internal combustion engines, and hybrids. ADVISOR is a quasi-static, empirical tool that combines component efficiency maps with a vehicle dynamics model to predict system performance. ADVISOR was developed using MATLAB®/Simulink® and operates on the backward-looking principle. ADVISOR limits the power requirements of a drivetrain component to that of which it's nearest upstream component can use. Since ADVISOR's component models are quasi-static, they are not well suited to predicting dynamic phenomena. Furthermore, ADVISOR uses the required vehicle speed as an input to ascertain the drivetrain torque and speeds required to meet that vehicle speed. A limited version of NREL's ADVISOR is available to the public and an advanced version has been commercialized by AVL Powertrain Engineering (http://www.nrel.gov/vehiclesandfuels/vsa/related_links.html).

Argonne National Laboratory under the direction of the Partnership for a New Generation (PNGV), a partnership that includes General Motors, Ford, Chrysler, and the

U.S. Department of Energy, developed a Vehicle Systems Analysis Toolkit (P-SAT) (Rousseau, *et al.* 2001; Feng, *et al.* 2001). PSAT is a forward-looking simulation that calculates the power generated by the powertrain by modeling the driver following a pre-defined cycle. While the forward approach is more computationally challenging, it is better suited for investigating dynamic response as well as control design since the method captures transient behavior. It is for this reason that HIL simulators also operate using the forward-looking approach. PSAT-PRO is an additional tool developed by Argonne capable of real-time simulation, HIL and rapid-prototyping (Pasquier and Roussau 2001).

Southwest Research Institute (SwRI) and Chrysler co-developed a Rapid Automotive Performance Simulator (RAPTOR) for virtual powertrain simulation (Berry, *et al.* 2001; McBroom 2005). Various vehicle powertrain components along with their mathematical descriptions can be selected by the user and simulated over different driving schedules. Typical inputs to RAPTOR include vehicle weight, aerodynamic drag, tire rolling resistance, engine and drivetrain component maps, and transmission and drivetrain losses. RAPTOR has the capability of performing both forward- and backward-looking simulations. The backward-looking simulation is typically used for fuel economy predictions, component sizing and road load analysis. Forward-looking simulations are utilized in performance characterization.

The Automotive Research Center at the University of Michigan developed a Vehicle Engine Simulation (VESIM) composed of engine, driveline and vehicle dynamics modules to simulate the dynamic response of a Class VI heady duty diesel truck using feed forward logic (Assanis, *et al.* 2000). The simulation replaces the driver

model with a vehicle speed controller. VESIM does not require component look-up tables and thus can be used to study non-existing designs. The high-fidelity engine model was coded in FORTRAN and consists of the corresponding number of single cylinder engine models that include thermodynamic models of the in-cylinder processes. The individual engine, drivetrain, and vehicle dynamics modules were then integrated into SIMULINK blocks that simulate the torque and angular speed propagation from the engine through the driveline. VESIM has been used to simulate the effects of varying control strategies, such as fueling and shift duration. The driveline and shift logic along with the differential equations representing the vehicle dynamics was constructed using the bond graph modeling language and implemented into 20SIM (Louca, *et al.* 2001). Hierarchical methodologies for optimally designing a complex vehicle system are explored in Kim, *et al.* (2002). The VESIM platform has been further expanded and utilized for investigating a number of research issues related to advanced and hybrid truck propulsion. The fuel economy potential of selected hybrid electric and hydraulic hybrid configurations has been evaluated by Lin, *et al.* (2004a) and Filipi, *et al.* (2004). Finally, integration of an engine hardware system in the loop with the virtual driveline and vehicle models has been demonstrated by Filipi, *et al.* (2006).

The unified approach of power flow, where mechanical, electrical and chemical power are universally represented by effort and flow, was applied to the modeling and analysis of hybrid vehicles in a computer simulation called, Vehicle Performance Simulator (VP-SIM) (Rizzoni, *et al.* 2000). Other analytically-driven approaches to quantifying energy flow from the tank-to-wheel in passenger vehicles have also been explored (Farzaneh and Saboohi 2005; Mortimer 2002).

In addition to the aforementioned vehicle simulation models, an array of other modeling software and tools has been developed both in industry and academia. Numerous commercial products have been introduced by companies such as Bosch, AVL, MathWorks, and Ricardo, each with their unique functionality.

While the aforementioned vehicle simulations are adequate at providing approximate predications for future vehicle system configurations where prototypes are not yet available, their predictive nature can sometimes yield inaccurate results. Such analytical simulations may fall short of predicting the actual component speeds and loads that result in "real-world" driving scenarios. As a consequence, CHAPTER 2 will explore a method to analytically determine how power is passed from component to another in vehicle systems using empirical speed and load data.

Another challenge associated with the virtual simulations discussed here is that they require control calibrations as inputs. A problem arises when studying future hypothetical hardware designs for which calibrations do not exist. To properly evaluate different hardware configurations, each requiring difficult control calibrations, such simulations require the user to manually alter the calibrations for different vehicle parameters which can be extremely time consuming given multiple design alternatives. A further complication arises since many existing methods to develop powertrain calibrations are subjective and do not take into account system interaction effects. CHAPTER 4 will introduce a reverse dynamic optimization methodology to address these challenges.

1.3.3 Vehicle System Design and Optimization

The following is a review of literature on vehicle system design optimization. Model predictive control (MPC) originated in the late 1970's and employs a model to predict the output and calculate a control sequence by minimizing an objective function. Initial vehicle design optimization work concentrated on optimizing engine control parameters. A powertrain model with reverse power flow to predict the engine speed and load trajectory for a given drive cycle was developed by Blumberg (1976). The model was then used to optimize the air/fuel ratio, spark timing and percentage of exhaust gas recirculation in the engine calibration using dynamic programming to allocate emissions contributions while maximizing fuel economy (Auiler, *et al.* 1977). These same engine parameters were optimized by choosing optimal control settings for the mapped speed and torque points of a given drive schedule using linear programming by Rishavy, *et al.* (1977). Rao, *et al.* introduced non-linear programming and Lagrange multipliers as a technique to optimize these engine control parameters over select speed and load points (1979).

Initial work that extended the optimization problem beyond the engine to the driveline by incorporating powertrain matching techniques for improving fuel economy was performed by Wong and Clemens (1979) and Porter (1979). The work included vehicle and component testing, using semi-empirical mathematical models to project fuel economy, performance and emissions trade-offs, and applying the models to evaluate powertrain system design alternatives (e.g., Torque Converter A versus Torque Converter B).

More recent work involves optimizing the calibration of advanced engine technologies. Kolmanovsky, *et al.* (1999; 2005) and Kang, *et al.* (2001) applied multi-objective dynamic programming to gasoline direct injection and hybrid diesel applications and their corresponding exhaust aftertreatment systems to optimize for fuel economy and emissions. Research to reduce the time to find optimal variable cam timing and corresponding spark with minimal engine dynamometer data was studied by Jankovic and Magner via a combination of steepest accent/descent search methods, Design of Experiments, and inverse distance interpolation schemes (1999). Artificial neural networks were proposed by Wu, *et al.* (2006) to optimize variable cam timing for fuel consumption and NO_x emissions.

The transmission control strategy also plays a major role in the vehicle fuel economy, performance, and driver perception. Figure 1-1 depicts an example shift schedule or shift map for a four-speed vehicle for which earliest torque converter lock-up (LU) occurs in third gear. The x-axis is transmission output speed or a scaled version of vehicle speed based on the tire size and final drive ratio. The y-axis conveys the driver intent by either the throttle or pedal percent. For electronic throttle engines, the relationship between the driver intent and engine throttle opening can be calibrated to yield a desired response (e.g., bias throttle response towards a performance feel at low pedal percents). To illustrate how the schedule controls the gear choice, suppose a driver accelerates from a stop by depressing the pedal to 30 percent of maximum. As the transmission output speed increases during vehicle acceleration, the vehicle will upshift to second gear as it crosses the 1-2 upshift curve at approximately 750 revolutions per minute.

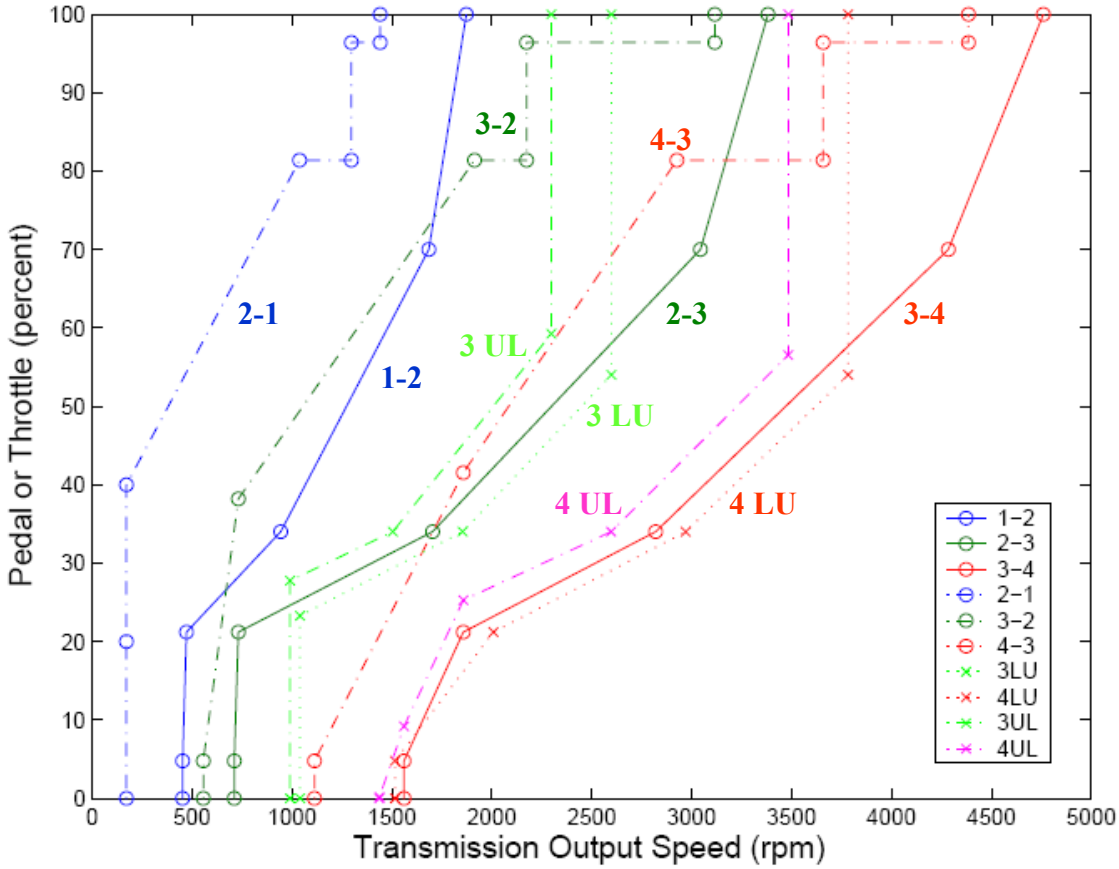

Figure 1-1 Example Shift Schedule

Suppose thereafter the driver depresses the accelerator pedal to 85 percent, the vehicle first crosses the 3-2 downshift curve but because the vehicle is not in third gear, crossing this curve has no effect. However, as the 2-1 downshift curve is crossed, a 2-1 downshift occurs. As the operating point crosses the 3 LU while in third gear, a lock-up event may be triggered assuming other enable conditions are also met. An unlock (UL) event will occur as either the vehicle slows down or if the pedal is increased such that the 3 UL curve is crossed (Geist 2004).

While optimal gear shifting for maximum performance is well known to be the intersections of the tractive force or wheel torque for consecutive gears as depicted in Figure 1-2 (Gillespie 1992), optimal gear shifting for fuel economy is more complicated

and a function of driver demand. Optimal gear shift scheduling for minimal fuel consumption and the corresponding acceleration trade-off was explored by Minowa, *et al.* by comparing the efficiency of the torque transmitted to the wheels at each gear shift ratio (1996). Abenavoli, *et al.* studied the trade-off between shifting for maximum fuel economy versus shifting for maximum acceleration for busses over sequential velocity intervals at varying road grades (1999). A math model based approach to gear shift schedule optimization was also developed at the University of Michigan by Kim (2006). Using a forward-looking model and dynamic programming, constant throttle inputs were optimized to determine a gear shift schedule map for fuel economy. Then scaling factors were used to scale between the shift schedule optimized for overall mile per gallon and the shift schedule optimized for maximum power. Kim also used dynamic programming and a forward-looking model to study the efficiency of an existing powertrain system over a drive cycle.

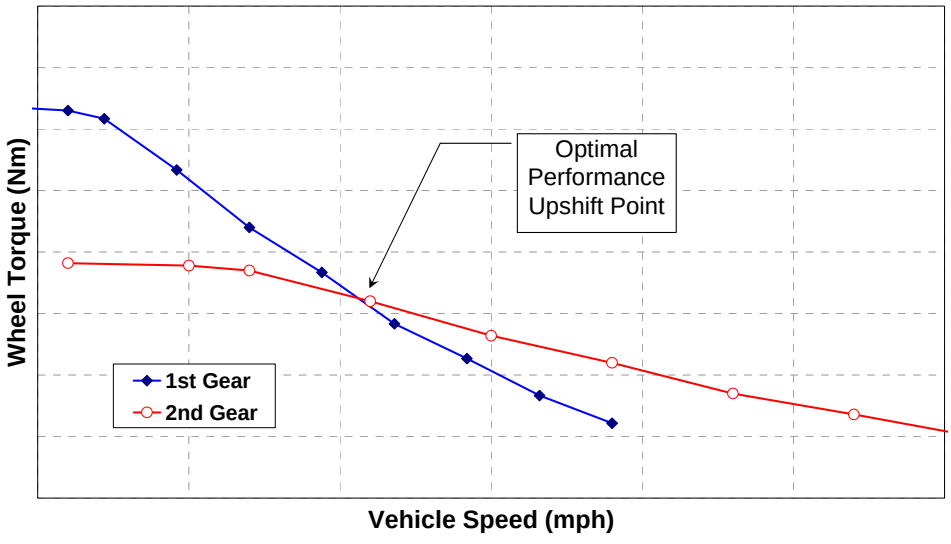

Figure 1-2 Optimal Upshift Point for Maximum Performance

In the area of hardware optimization, Song and El-Sayed developed a multi-objective optimization procedure to find the optimal combination of powertrain and chassis design parameters, including transmission gear ratios, axle ratio, vehicle weight, tire size, wheel base and position of center of gravity that optimizes the acceleration time, steady-state fuel economy, ride quality and steering stability (2002). The optimization algorithm selected was the Modified Feasible Directions Algorithm which first determines a search direction and iterates the design variables until it converges on an optimum.

Additionally, various optimization algorithms have been applied to the vehicle system models in Section 1.3.2. NREL studied the effectiveness of various commercial gradient based and non-gradient based optimization algorithms on hybrid vehicle design parameters using ADVISOR (Markel and Wipke 2001). Lin, *et al.* used a simplified version of VESIM to study the optimal power management and gear shifting strategy of a hybrid-electric heavy duty truck using a dynamic programming optimization algorithm (2001; 2003; 2004a; 2004b). Kheir, *et al.* proposed fuzzy logic to implement the energy management control strategy for hybrid vehicle system optimization and integrated the logic into Argonne's PSAT (2004). Various global optimization algorithms – specifically DIRECT, Simulated Annealing, and Genetic Algorithm – were also applied to the design optimization of a parallel hybrid vehicle in PSAT, where the maximum engine power, maximum motor power, number of battery cells and state-of-charge, as well as final drive ratio were included as design variables (Gao and Porandla 2005; Gao and Mi 2007).

While optimization in vehicle system design is growing, there exists a need to fully explore the capabilities of the powertrain system by developing a model based

approach that combines optimal hardware design with optimal control. The research discussed in CHAPTER 4 proposes using a reverse dynamic optimization modeling technique to match the powertrain hardware configuration and the transmission gear shift and torque converter clutch control strategies to specific vehicle and drive cycle attributes. More work is also needed to assist in developing control strategies that effectively take into account the trade-off between performance and fuel economy over different drive cycles. New methods to analytically determine optimal gear shifting, torque converter lock-up clutch, and engine cylinder deactivation control strategies that take into account system interaction effects will be introduced in CHAPTER 5 and CHAPTER 6. How the research approach introduced here can expedite consistent evaluation of hardware design alternatives early in the design process and reduce the time to evaluate a plurality of design alternatives will be demonstrated in CHAPTER 7.

1.4 Research Approach

The approach proposed for this research addresses some of the needs associated with the current state-of-the-art virtual vehicle system simulations.

1.4.1 Research Approach for Vehicle System Energy Analysis

The research approach for the development of energy analysis tool involves elements of both forward- and backward-looking simulations combined with empirical chassis dynamometer rolls data to overcome some of their shortfalls. Since this research tool is intended to analyze opportunities for improving fuel economy, real-time fuel consumption data is measured using modal exhaust emissions on a chassis dynamometer with a real driver following a prescribed trace. The approach is forward-looking in that

the indicated torque from in-cylinder pressure measurements and the brake engine torque measurements are propagated through the drivetrain in the direction of the tractive road load demand. To determine the torque delivered from component to component, the model utilizes a combination of measured dynamic drivetrain data and component efficiency maps.

Because real-world data is being used the user can be certain that chassis dynamometer driver met the intended driver's trace within a relatively narrow tolerance band. Also since the total fuel consumed is determined by emissions bench modal tests on a chassis dynamometer rolls, the results include dynamic vehicle effects and can be cross-checked with the accumulated CVS fuel economy results, the EPA's preferred method of measuring fuel economy, or other ECU parameters, such as injector pulse width. While some of the component models still rely on steady-state efficiency maps, measured drivetrain component speeds, such as turbine speed, are incorporated into the simulation. Thus, the energy consumption of the individual components becomes an energy balance based on the total fuel consumed and quantities directly measured in the vehicle.

Given that this approach is both analytical and empirical in nature, inherent advantages and disadvantages exist. One advantage is that the tool, where empirical speed and load data exists, can determine individual effects on fuel economy in much more detail. Proposed subsystem changes that may only account for a fraction of the total energy consumed can be analyzed with far more accuracy compared to the measurement variation inherent in current available fuel economy testing. Moreover, assuming only small measurement error, the empirical results can be more relied upon

since they accurately reflect the energy use observed. The tool is well-suited to quantifying the relative energy savings that can be expected due to the implementation of various powertrain and component alternatives when compared to a baseline scenario. Yet while the tool offers the ability to model the effect of individual vehicle and component changes on fuel efficiency, due to its empirical nature, care must be taken in using the tool to predict vehicle system interaction effects that are not explicitly represented in the tool. Nonetheless, such an energy analysis tool offers the potential to help focus technology development efforts on areas that have the greatest impact on energy conservation.

1.4.2 Research Approach for Reverse Tractive Road Load Demand Model and Dynamic Optimization Methodology

For the development of the reverse tractive road load model, a strictly backward-looking approach is applied. The backward-looking approach has particular advantages to powertrain system integration analyses due to their fast run times and the fact they do not have the stability issues associated with more complex driver feedback models in forward-looking simulations. The backward-looking approach is also well suited for determining torque based requirements for advanced hardware design studies. Instead of acquiring empirical drive cycle data for this simulation approach, the wheel torque required is derived from the road load demand determined by the given speed and grade trace and propagated through the powertrain system. Then an optimization routine will be applied that iterates the required fuel flow for all possible states of the selected powertrain configuration and determines the best operating path over the cycle given the constraint that the required torque does not exceed the available engine torque. The

advantage of this reverse dynamic optimization approach over the state-of-the-art vehicle models is that the simulation tool automatically alters the powertrain control strategy for each vehicle configuration and drive cycle combination.

The reverse tractive road load demand model will be better suited for evaluating powertrain hardware configurations since current models usually require the control strategy, such as the shift schedule calibration, as an input into the simulation. Evaluating alternative hardware configurations with an optimized control strategy that exploits the full capability of the powertrain will yield less biased evaluations compared to the state-of-the-art vehicle simulations. The backward-looking approach coupled with dynamic optimization is unique to prior research in that using the propagated tractive road load demand, hardware design objectives can be established for future non-existing powertrain designs. Another advantage to this approach is the ability to investigate the optimal control strategy over different drive cycles. After the trade-off between different control strategies and their resulting fuel economy over different drive cycles is determined, decisions can be made as to which strategy makes the most sense given the customer base of the product.

1.5 Dissertation Outline

The first portion of this dissertation will detail the development and application of the energy analysis methodology. CHAPTER 2 will describe how each subsystem is modeled and the basic physics and thermodynamics equations that are incorporated in the MATLAB®/Simulink® tool. The process of identifying the system and subsystem behavior by collecting the chassis dynamometer rolls data and individual component

efficiency surfaces will be explained briefly in CHAPTER 2. CHAPTER 3 will demonstrate potential applications of the energy analysis tool and the types of conclusions that can be drawn from a comprehensive vehicle energy analysis. CHAPTER 4 will detail the development of a new torque-based modeling methodology and reverse predictive simulation methodology for optimizing powertrain system configurations and control strategies. CHAPTER 5 will discuss how the reverse dynamic optimization technique can be used to assess and assist in developing engine, transmission shift, torque converter lock-up, and pedal control strategies. The reverse tractive road load demand model and dynamic optimization technique will be extended to engine cylinder deactivation in CHAPTER 6. CHAPTER 7 will reveal how the reverse dynamic optimization methodology and tool facilities more efficient design of advanced powertrain hardware configurations. The dissertation will conclude in CHAPTER 8 with a summary of the scientific contributions and suggested future work.

CHAPTER 2

DEVELOPMENT OF VEHICLE ENERGY ANALYSIS MODEL

2.1 Introduction

A better understanding of where fuel energy is being demanded from a vehicle system standpoint is necessary for developing more fuel efficient vehicles. It is difficult for existing state-of-the-art vehicle simulation models to accurately predict individual component speeds and loads and account for detailed energy demand in real-world driving. Consequently, opportunities for fuel economy savings within vehicle systems are often overlooked since their potential benefits are difficult to quantify. Only a fraction of the fuel energy supplied to the vehicle system is converted into useful work. In order to develop more fuel efficient vehicles, an increased understanding of the parasitic losses within the vehicle system is essential. Considering the energy demand at a vehicle subsystem level will expose the effect of individual component design and system integration decisions on the fuel economy of the vehicle system. Developing a hybrid semi-empirical and analytical approach by using measured component speed and load data will produce a detailed understanding of where the actual fuel energy supplied to the vehicle system is being demanded. To accomplish this, an energy analysis tool based on MATLAB®/Simulink® was developed to determine energy demand from a vehicle subsystem perspective over different drive cycles.

The primary objective of the vehicle energy analysis tool is to account for where the fuel energy supplied over a drive cycle is demanded. The simulation calculates how much fuel energy is initially released and how power is passed from one vehicle subsystem to another. As the energy is passed from one subsystem to another, parasitic losses occur and only a portion of the initial energy supplied constitutes the energy required to propel the vehicle down the road. Depending on the vehicle configuration (e.g., front-wheel versus four-wheel drive), the model attempts to account for losses in numerous vehicle subsystems as summarized in Figure 2-1. The direction of energy transfer and where the losses occur are shown in Figure 2-2. The simulation tool provides the user with instantaneous and accumulated vehicle subsystem energy usage versus drive cycle time in megajoules. The energy analysis methodology and tool will be used to investigate vehicle system energy requirements, prevailing fuel economy factors, and incremental hypothetical fuel saving scenarios that could not otherwise be measured due to inherent test to test variability. The development and application of the vehicle system energy analysis methodology is also described in Baglione, *et al.* (2007a).

2.2 Energy Analysis

The following is a description of the energy analysis that takes place in the vehicle subsystems that were modeled in Simulink®. The energy analysis tool simulates the various vehicle subsystem speeds and loads and calculates the power passed from one component to another using physics and thermodynamic relationships, measured component efficiencies, and basic vehicle and drive cycle data. The mathematical relationships for the different subsystems in the tool are described here.

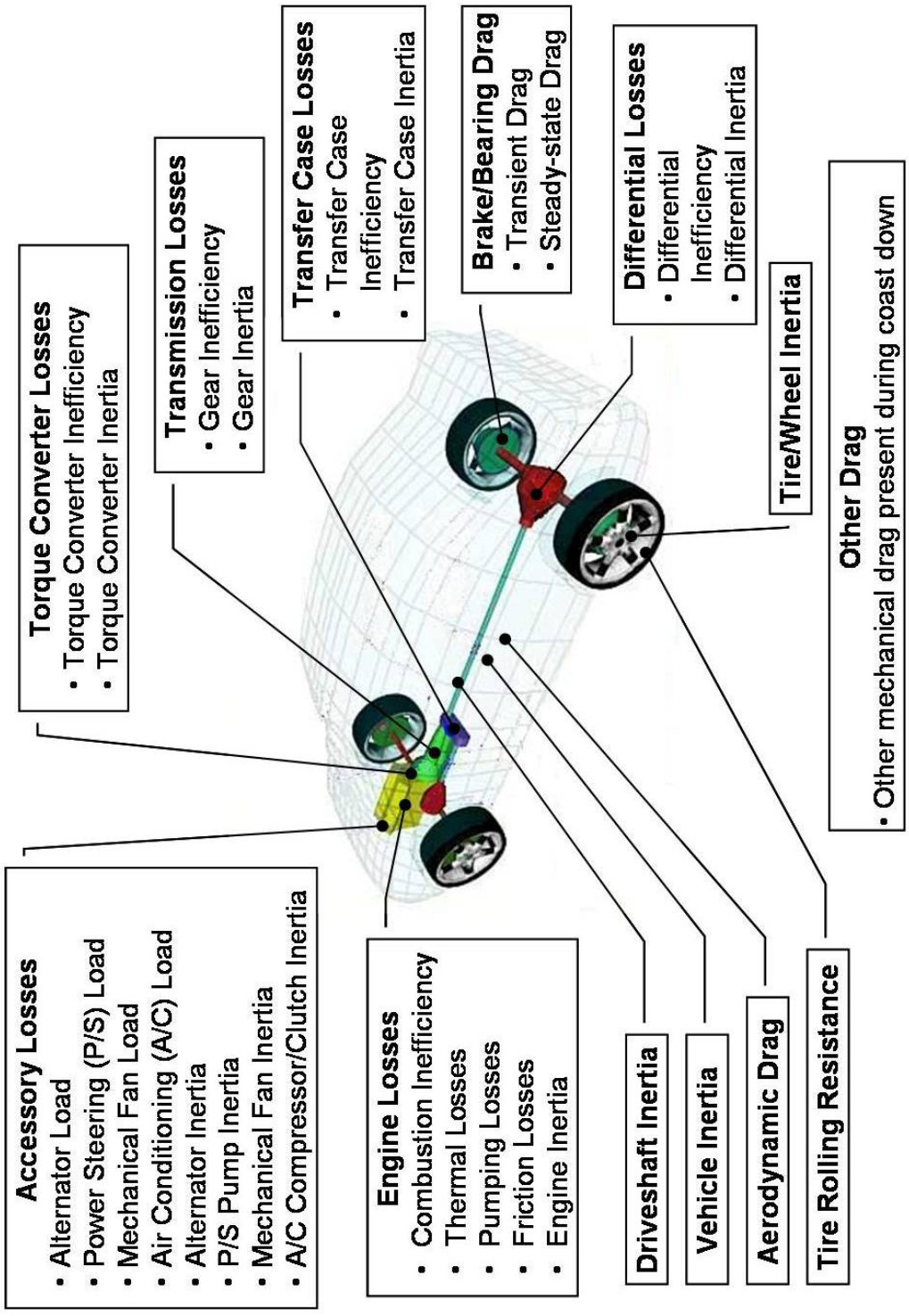

Figure 2-1 Energy Analysis Subsystems

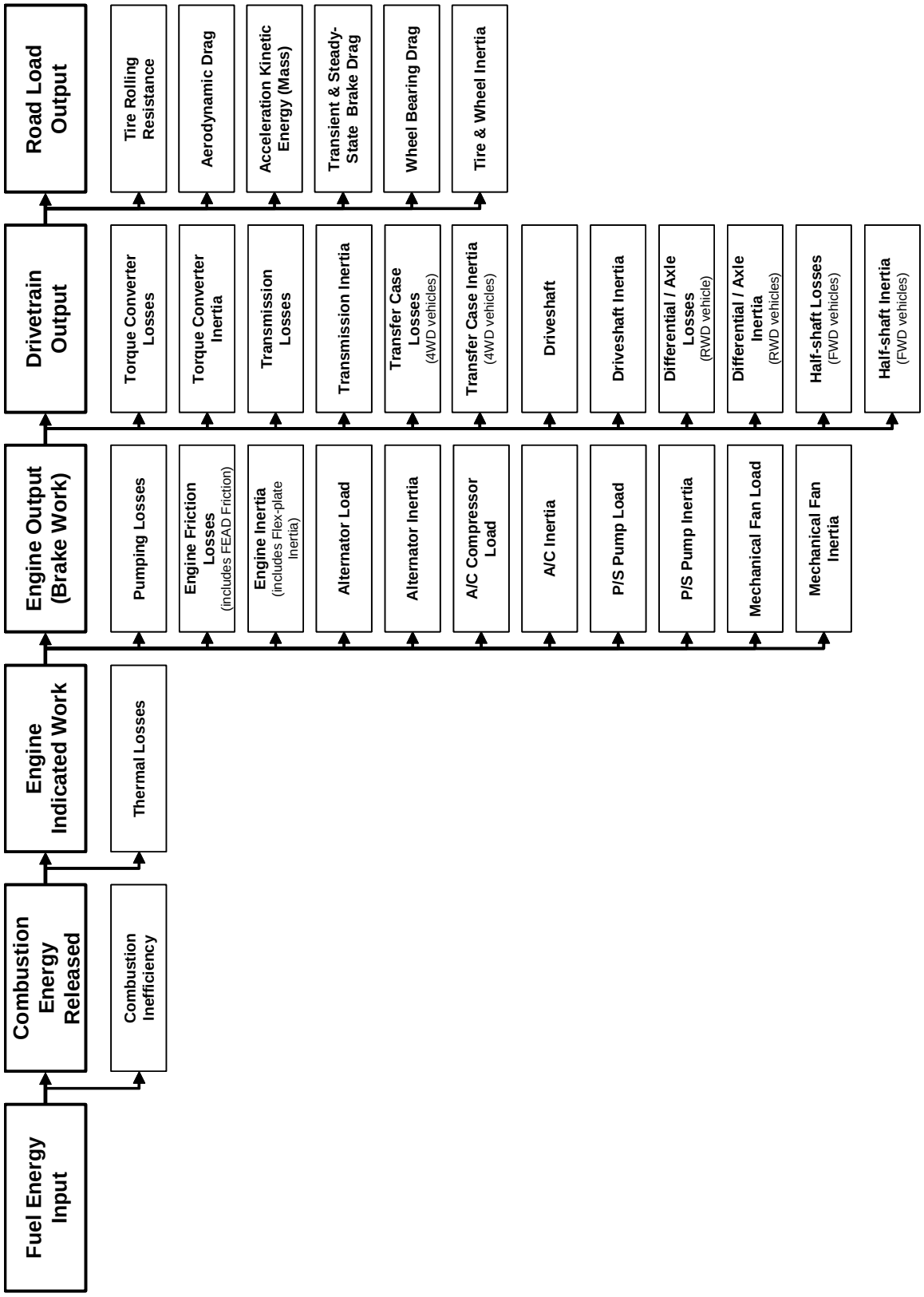

Figure 2-2 Energy Transfer and Energy Loss Subsystem Elements

2.2.1 Total Fuel Energy

To develop ways of better using fuel energy the first step is to understand how much fuel energy is being supplied to the engine over a given drive cycle. The first law of thermodynamics relates changes in internal energy or enthalpy to heat and work transfer. The total fuel energy can be quantified as the amount of fuel heat energy supplied to the control volume around the engine. Given the fuel flow, the rate of fuel energy supplied can be determined by multiplying by the net heating value, Q_{NHV} (Heywood 1988),

$$\dot{Q} = \dot{m}_f Q_{NHV} \tag{2-1}$$

The total energy supplied is the time integral of the energy rate:

$$Q = Q_{NHV} \int \dot{m}_f dt \tag{2-2}$$

where,

$\dot{Q}$	rate of energy or power (kW).
Q_{NHV}	net heating value of fuel (kJ/kg)
$\dot{m}_f$	mass flow rate of fuel (kg/s)
Q	energy (kJ).

2.2.2 Combustion Inefficiency

Combustion inefficiency is a measure of the fraction of total energy that is not completely released during the combustion process. Incomplete combustion products, consisting of CO, H_2, unburned hydrocarbons, soot, etc., in the exhaust product represent chemical energy not released during combustion.

The net chemical energy released during combustion can be quantified as the difference in enthalpies of the products and reactants,

$$Q_{r-p} = H'_p - H'_r \tag{2-3}$$

where H'_p and H'_r are the enthalpies of the products and reactants, respectively. The combustion efficiency is the fraction of the fuel energy supplied which is released in the combustion process and is given by:

$$\eta_c = 1 - \frac{\sum_i \chi_i Q_{HV,i}}{\chi_f Q_{HV,f}} \tag{2-4}$$

where χ_i are the mass fractions of exhaust constituents and χ_f is the mass fraction of the fuel. Thus,

$$\eta_c = 1 - N\left[(CO)\frac{h_{CO}MW_{CO}}{h_f MW_f} + (H_2)\frac{h_{H_2}MW_{H_2}}{h_{H_2}MW_{H_2}} + 3(C_3H_{3y})\right] \tag{2-5}$$

where CO, H_2, and C_3H_{3y} represent the respective constituent volume percent on a dry basis, h represents the respective mass lower heating values and N is the exhaust carbon count defined by:

$$N = \frac{1}{(CO) + (CO_2) + 3(C_3H_{3y})} \tag{2-6}$$

The molecular weight, MW, of the fuel can be determined from the fuel H/C ratio, y, and the molecular weights of carbon and hydrogen.

$$MW_f = MW_C + MW_H y \tag{2-7}$$

In order to protect the emission bench analyzers, water in the exhaust gas is typically removed by passing the exhaust gas through a cooler. Consequently to determine accurate species concentrations, the amount of moisture removed from the bench sample must be calculated.

$$(H_2O) = \frac{\frac{y}{2}\frac{100}{N} - \frac{3y}{2}(C_3H_{3y})}{\frac{(CO)}{K(CO_2)} + 1} \tag{2-8}$$

The incomplete combustion species in the exhaust gas primarily consist of unburned fuel, carbon monoxide, and hydrogen. Since the hydrogen concentration is not directly measured, it can be calculated using:

$$(H_2) = \frac{y}{2}\frac{100}{N} - (H_2O) - \frac{3y}{2}(C_3H_{3y}) \tag{2-9}$$

The aforementioned equations along with the measured exhaust species can be used to determine the combustion inefficiency (Asmus 2005; Heywood 1988). The exhaust gas concentrations used to populate the energy analysis tool are from modal exhaust gas analyzers. To further validate the drive cycle exhaust gas species and overall combustion efficiency, the modal exhaust gas analyzer measurements are cross-checked with constant volume sampling (CVS) emissions measurements.

2.2.3 Engine Thermal Losses

The thermal efficiency is the ratio of net work of the cycle to the heat added after combustion inefficiency is taken into account. The second law of thermodynamics limits the maximum thermal efficiency that any heat engine can attain. All real heat engines lose some heat to the environment and are limited by the Carnot efficiency, the maximum efficiency that can be obtained between two heat reservoirs (Moran and Shapiro 1995).

$$\eta_{carnot} = \frac{W}{Q_H} = \frac{Q_H - Q_C}{Q_H} \tag{2-10}$$

Adapting the Carnot efficiency above to the ideal Otto cycle reveals the effect of compression ratio on the maximum obtainable thermal efficiency:

$$\eta_{carnot,ottocycle} = 1 - \varepsilon^{1-\gamma} \tag{2-11}$$

where the compression ratio, ε, is the clearance volume over the volume displaced and γ is the isentropic expansion and compression ratio. It is important to note that the Otto cycle Carnot efficiency suggests that it is advantageous for combustion engines to have high compression ratios. While this is generally the case, the likelihood of knock places an upper limit on increasing compression ratio.

Coolant heat loss and exhaust energy heat loss account for most of the thermal losses. The thermal efficiency is further reduced since standard Otto cycle assumptions do not occur in reality. The Otto cycle is an ideal cycle that assumes combustion heat is added instantaneously at top dead center and that compression and expansion processes are reversible. Moreover, the ideal Otto cycle efficiency does not take into account blowdown losses, blow-by, and other real-world losses.

While heat rejection and exhaust enthalpy studies could be performed to further classify thermal losses, such an extensive analysis is considered out-of-scope for the purpose of this research. The difference in chemical fuel energy released and the indicated work done by the combustion gas on the piston (which will be determined by in-cylinder pressure data) will be the extent to which engine thermal losses are considered.

2.2.4 Engine Pumping Losses

Pumping losses comprise the net work per cycle done by the piston on the in-cylinder gases during the intake and the exhaust strokes. Cylinder pressure data can be

used to calculate the work transfer between the gas and the piston. The work per cycle, $W_{c,i}$, can be obtained by integrating around the cylinder pressure curve over volume displaced:

$$W_{c,i} = \oint pdV \tag{2-12}$$

As shown in the *p-V* diagram in Figure 2-3, the gross indicated work per cycle, W_{ig}, is (area A + area C) and the net indicated work per cycle, W_{in}, is (area A - area B), where area B represents the pumping work, W_p.

A useful parameter in describing engine performance is the mean effective pressure (*mep*), which is obtained by dividing the work per cycle, $W_{c,i}$, by the volume displaced, V_d,

$$mep = \frac{W_{c,i}}{V_d} \tag{2-13}$$

When considering the *p-V* diagram again:

$$W_p = W_{ig} - W_{in} \tag{2-14}$$

Or similarly,

$$pmep = imep - nmep \tag{2-15}$$

where,

pmep	pumping mean effective pressure (kPa)
imep	indicated mean effective pressure (kPa)
nmep	net mean effective pressure (kPa).

To calculate the power per cylinder:

$$P_i = \frac{W_{c,i} N_e}{n_R} \tag{2-16}$$

Thus the power loss due to pumping can be determined by:

$$P_i = \frac{pmep\, V_d N_e}{n_R} \tag{2-17}$$

where N_e is the engine speed in revolutions per minute and n_R is the number of crank revolutions for each power stroke (e.g., n_R is two for a four stroke engine). Once the power loss is obtained, the energy can be determined as the time integral of power.

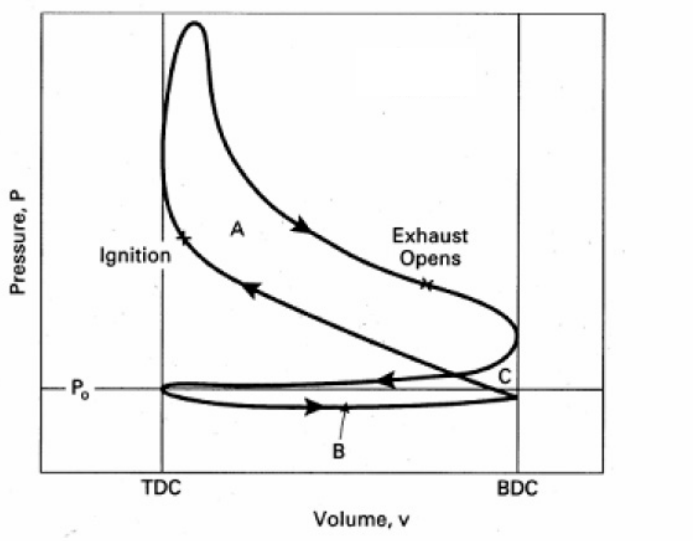

Figure 2-3 p-V diagram

Alternatively, the mean effective pressure can be described as a constant pressure that would produce the same power per cycle if it acted on the piston for the power stroke. Hence the pumping mean effective pressure can be described as:

$$pmep = p_e - p_i \tag{2-18}$$

where p_e is the average cylinder pressure over the exhaust stroke and p_i is the average cylinder pressure over the intake stroke.

Considering the aforementioned equation, where high speed cylinder pressure measurements cannot be obtained, *pmep* can be approximated by assuming the average

exhaust stroke cylinder pressure is that of barometric pressure, p_{baro}, and the average intake stroke pressure is taken as the average manifold air pressure (*map*).

$$pmep_{estimated} = p_{baro} - map \tag{2-19}$$

2.2.5 Engine Friction, Accessory, and Inertial Losses

Engine friction losses consist of the difference in the net indicated work delivered by the working fluid to the piston and the usable work delivered to the flywheel or flex-plate, i.e., brake work, W_b.

$$W_f = W_{in} - W_b \tag{2-20}$$

The engine friction losses include the work done to overcome the resistance to relative motion of all of the moving parts of the engine. This includes the friction between the piston rings, piston skirt and cylinder wall; friction in the wrist pin, crankshaft bearings, crankshaft endplay, and camshaft bearings; friction in the valve train; friction in the gears, pulleys and/or belts that drive the camshaft and front-end accessory drive (FEAD). The coolant water pump and oil pump are accessories that are built into the engine and are also considered part of the basic engine friction.

The engine output is further reduced by accessory loads. The model includes accessory losses for the alternator, air conditioning (A/C) compressor, power steering (P/S) pump, and mechanical fan (if equipped). The A/C load is calculated given the A/C head pressure, engine speed, and A/C pulley ratio. Once the A/C clutch is engaged, the model looks up the required A/C compressor torque as a function of A/C head pressure and compressor speed. The power steering load component of the model works in a similar fashion. Given the P/S pump pressure, engine rpm, and P/S pulley ratio, the P/S torque demand can be found as a function of P/S pump pressure and pump speed. The

alternator load is a function of current and alternator speed. Given the alternator duty cycle which determines the current, engine speed, and alternator pulley ratio, the alternator torque demand can be determined. If the vehicle is equipped with a mechanical fan, then the mechanical fan torque demand must also be included (electric fan loads are included in the alternator load). The mechanical fan load must account for the torque demand while the fan is disengaged and acting like a viscous couple as well as when the fan clutch is fully engaged.

In addition to the engine friction and accessory losses, the actual torque delivered to the drivetrain is further reduced by the inertial effects of the engine components and accessories. Since engine torque is normally measured at steady-state on an engine dynamometer, actual torque delivered to the drivetrain is reduced by the amount necessary to accelerate the rotating and reciprocating engine components. The energy required to overcome the inertia of the following engine components are included in the model: crankshaft, piston and connecting rod assembly, flex-plate or flywheel, valve train, and damper. The energy required to overcome the inertia of the following accessories are also included: alternator, A/C compressor and clutch, power steering pump, and mechanical fan and clutch (if equipped). Equation (2-21) expresses how the engine dynamometer torque is further reduced by the sum of the torque demand of all the accessories, the inertial loads of all of the rotating and reciprocating engine components, and the inertial loads of all of the accessories.

$$\tau_{engine,output} = \tau_{brake} - \Sigma \tau_{accessory\,loads} - \Sigma I_{engine\,components} \alpha_{engine\,components} - \Sigma I_{accessory} \alpha_{accessory} \qquad (2\text{-}21)$$

where I represents the moment of inertia and α represents the angular acceleration of the individual components. Once the individual torque losses are obtained, the power losses can be calculated and integrated to determine the energy losses.

$$P_{loss} = \tau_{loss}\omega \tag{2-22}$$

Currently the model only considers the positive inertial energy required. This overestimates the inertial effects as some of the inertial energy is recouped. More extensive component analysis would be required to determine the drag characteristics of the rotating inertia components to determine the net inertial parasitic losses.

2.2.6 Drivetrain Losses

The flywheel or flex-plate torque is further reduced by the inefficiency of the drivetrain. Most automatic transmissions today are equipped with torque converters, a type of fluid coupling that uses hydrodynamic principles to amplify the input torque at the expense of input speed and allows the engine to spin somewhat independently of the transmission. A typical torque converter, as shown in Figure 2-4, consists of an impeller, which is the driving component connected to the flex-plate, a turbine, which is driven and connected to the input of the transmission, and a stator that redirects the hydrodynamic fluid from the turbine back to the impeller resulting in torque multiplication at lower speed ratios.

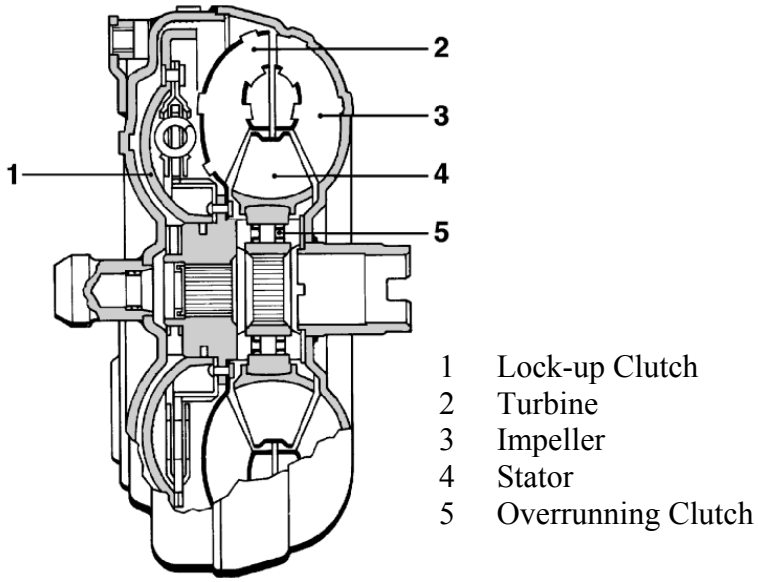

Figure 2-4 Typical Torque Converter (Bosch 1999)

Significant losses occur with automatic transmission drivetrains due to slippage of the torque converter. Thus torque converters are typically equipped with a lock-up clutch that provides a friction coupling between the impeller and turbine to avoid the efficiency losses associated with slip during conditions in which torque multiplication and damping are not required. The torque converter is characterized in the model by dynamometer data including, its corresponding torque ratio, efficiency, and capacity factor (K-factor) curve, where K-factor is defined by:

$$K - factor = \frac{N_e}{\sqrt{\tau_e}} \tag{2-23}$$

where τ_e is the engine torque and the K-factor is a function of the speed ratio which is defined as the turbine speed, N_t, over the engine speed:

$$K - factor = f(\frac{N_t}{N_e}) \tag{2-24}$$

Typical torque converter characteristics are shown in Figure 2-5. Given the speed ratio, the corresponding torque converter efficiency and losses can be obtained.

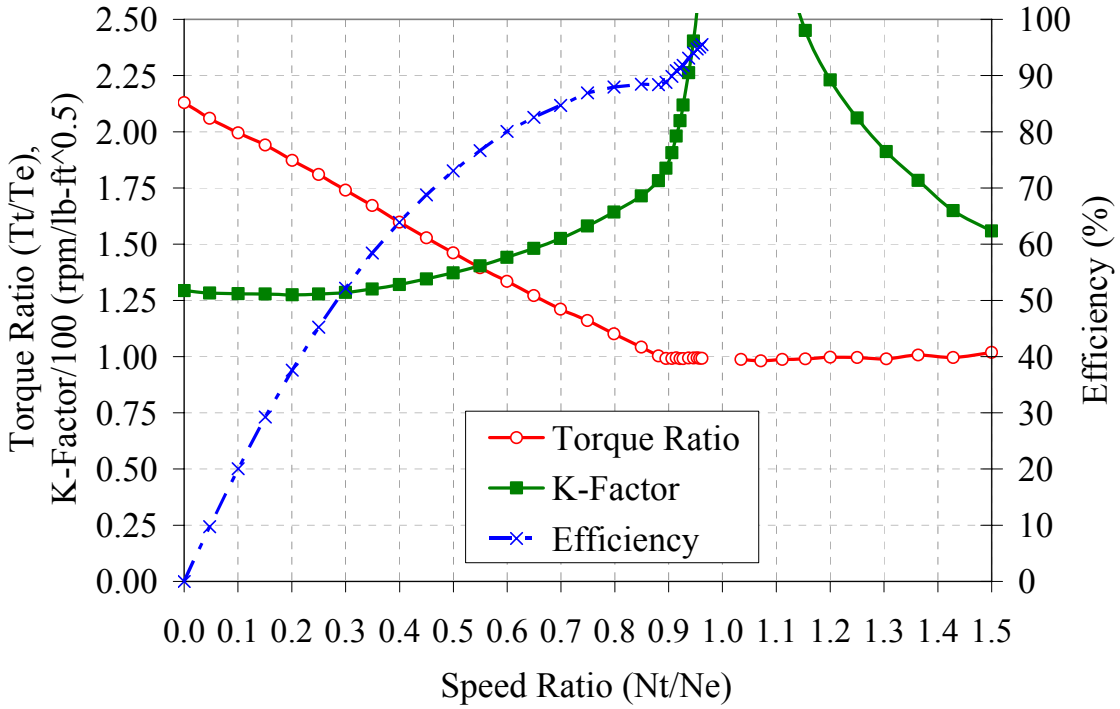

Figure 2-5 Typical Torque Converter Characteristics

The transmission model not only includes the transfer of speed and torque corresponding to the current gear ratio, but also includes spin losses, inertia losses and loaded gear inefficiency. Typical automatic transmission efficiencies are described in Kluger and Long (1999). If the vehicle is 4WD equipped, the corresponding transfer case spin loss and inertia loss is also considered. The inertia of the driveshaft is included and the speed and torque transfer due to the axle ratio, also known as the final drive ratio, as well as the respective inefficiency of the differential.

2.2.7 Road Load Losses

Only a fraction of the initial fuel energy goes into propelling the vehicle down the road. The propulsion load for a vehicle, also known as road load, is comprised of rolling resistance, aerodynamic drag, and grade forces (if present).

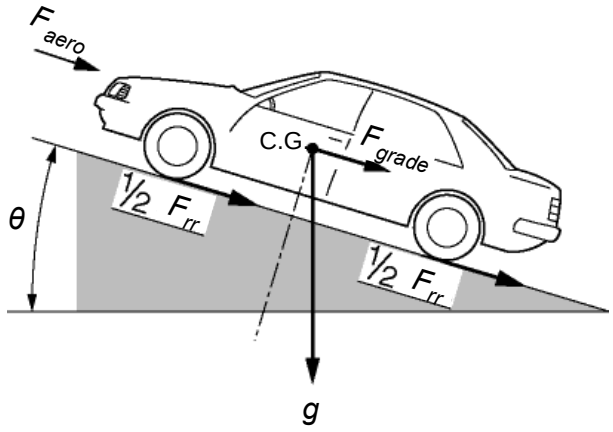

Figure 2-6 Road Load Forces (Bosch 1999)

Per federal regulations automotive manufacturers are required to certify vehicle fuel economy on a chassis dynamometer. The following force equation is used to determine the appropriate dynamometer load settings.

$$F_{RL} = A + Bv + Cv^2 + mg\sin\theta + m\frac{dv}{dt} \tag{2-25}$$

where:

A,B,C	road load coefficients
v	vehicle velocity
m	vehicle mass
θ	angle the road makes with the horizontal

Vehicle coastdown testing is performed to determine the A, B, and C coefficients for the force versus speed equation, $F = A + Bv + Cv^2$. Typical values of the coefficients are shown in Table 2-1. The 3-term force includes aerodynamic drag and tire rolling

resistance as well as additional mechanical drag present in the vehicle during the coastdown, such as the unloaded transmission spin losses, steady-state brake drag, and wheel bearing losses. In order to further subdivide the energy required due to the 3-term *ABC*-force, the required energy is further subdivided as described in this section. The remainder of the 3-term energy due to the *ABC* force that cannot be specifically accounted for is categorized as "other drag" in the energy analysis.

Table 2-1 Typical Passenger Vehicle Road Load Coefficients and Units

Coefficient	Typical Values	Units
A	100-10	lbf
B	1.0-0.1	lbf/mph
C	0.1-0.01	$lbf/(mph)^2$

A significant portion of the vehicle drag is due to the rolling resistance of the tires, which is a resistive force resulting from several mechanisms (Gillespie 1992):

- Energy loss due to deflection of the tire sidewall near the contact area
- Energy loss due to tread elements
- Scrubbing in the contact patch
- Tire slip in the longitudinal and lateral directions
- Deflection of the road surface
- Energy loss on the bumps

Because many factors influence tire rolling resistance, such as tire temperature, tire inflation pressure, load, speed, tire material and design, tire slip, etc., it is impossible to devise a single formula that takes all variables into account. Nevertheless, several equations for estimating rolling resistance have been developed. The following rolling resistance equation was selected for the model as the equation takes into account tire

inflation pressure, tire load, and vehicle speed and uses coefficients determined from experimental rolling resistance data (Kelly 2002).

$$F_{rr} = P^{\alpha} L^{\beta} (a + bv + cv^2) \tag{2-26}$$

where:

F_{rr}	rolling resistance force (N)
P	tire pressure (MPa)
L	tire load (kg)
α,β,a,b,c	coefficients used to fit experimental rolling resistance data

Other factors such as tire slip and temperature will be ignored and should not sacrifice the accuracy of the energy analysis to any significant extent.

Aerodynamic forces on a vehicle arise from two sources, namely pressure drag and viscous friction (Gillespie 1992). Since air flow over a vehicle is very complicated, a semi-empirical formula is commonly used to represent this effect:

$$F_{aero} = \frac{1}{2} \rho C_d A v^2 \tag{2-27}$$

where:

ρ	air density (kg/ m^3)
C_d	aerodynamic drag coefficient
A	vehicle frontal area (m^2)

Once the road load forces are obtained, their contribution to the total energy loss in megajoules can be determined by finding and taking the time integral of the required road load power, $P_{RL.}$

$$P = F v \tag{2-28}$$

Energy is also required to accelerate a vehicle. While some of the kinetic energy or energy due to vehicle inertia is regained when the vehicle coasts down, a portion of the

kinetic energy may be lost in engine braking, driveline drag or in mechanical braking depending on the rate of deceleration.

Figure 2-7 illustrates how the losses due to road load and vehicle inertia are determined. The figure depicts the road load power required to overcome rolling resistance, aerodynamic and other drag from the 3-term *ABC*-force and the kinetic power required to accelerate and decelerate the vehicle. The summation of these two yields the net road load and kinetic power. During decelerations the road load helps to decelerate the vehicle, yet if additional deceleration is required, some of the kinetic energy is lost during braking represented by the hatched area in Figure 2-7. This kinetic energy represents the energy that is absorbed by the brakes to decelerate the vehicle (this is the energy available for regeneration in hybrid vehicles).

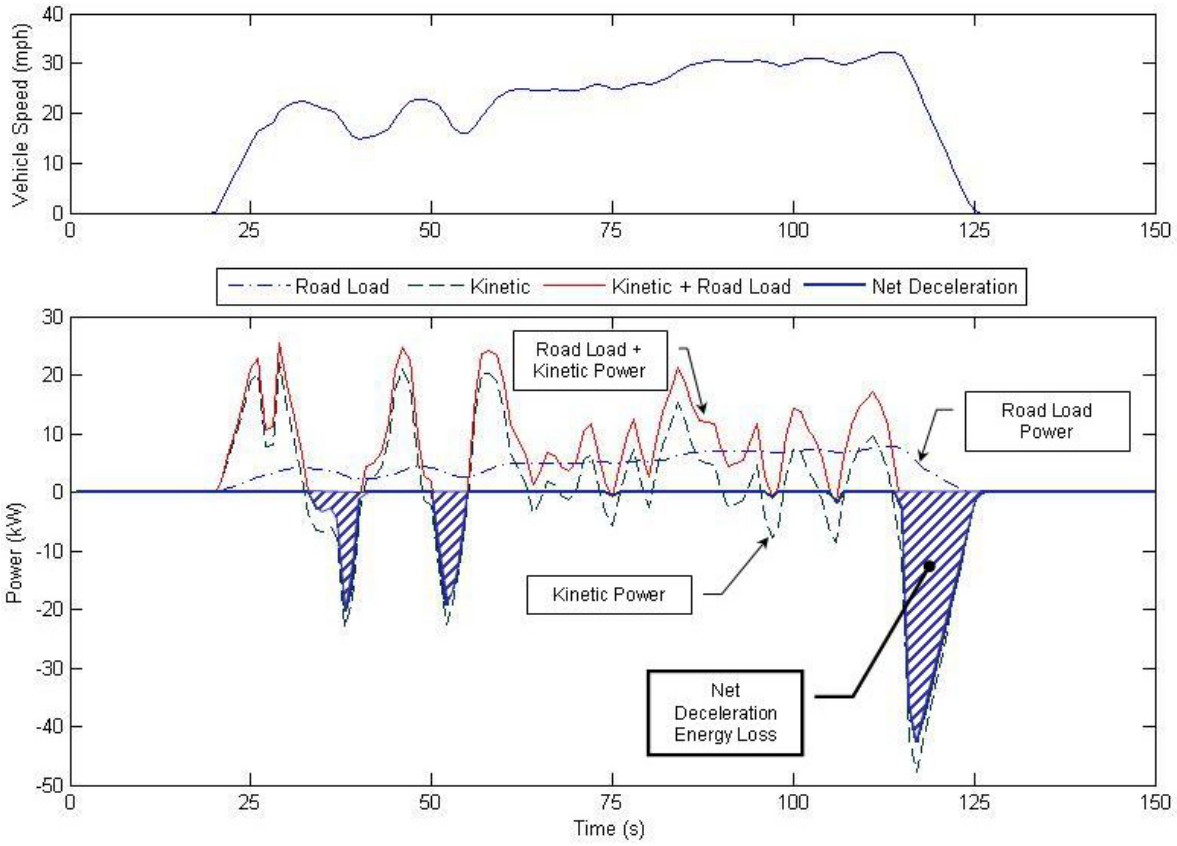

Figure 2-7 Road Load, Kinetic and Net Deceleration Power

After the brake pedal is deactivated, some transient brake drag as well as steady-state brake drag exists. This is represented in model using data from a mechanical brake test bench by moderating applying and disengaging the brakes to determine the transient drag associated with the brake pads not disengaging instantaneously. To achieve a responsive brake feel, some steady-state brake drag is designed into the vehicle system, which is also assumed in the model to be a constant resistive torque applied to the wheel. In actual driving conditions, the transient and steady-state brake drag would vary depending on the actual brake line pressure and the rate and force applied as well as other environmental factors.

2.3 Test Based Methods and Energy Analysis Model Structure

Section 2.2 described the vehicle subsystems under investigation in the energy analysis and their mathematical relationships. In order to construct the model, observed data from a series of measurements is necessary to identify the vehicle and subsystem behavior. The energy analysis tool consists of three components: (1) real-time vehicle schedule data from a chassis dynamometer rolls to determine fuel consumed, combustion efficiency and the actual vehicle and component states over a given drive cycle, (2) subsystem bench measurements to identify component performance and efficiency, and (3) the construction of the subsystem mathematical relationships into MATLAB®/Simulink® block diagrams where they are joined to obtain a model of the entire vehicle system.

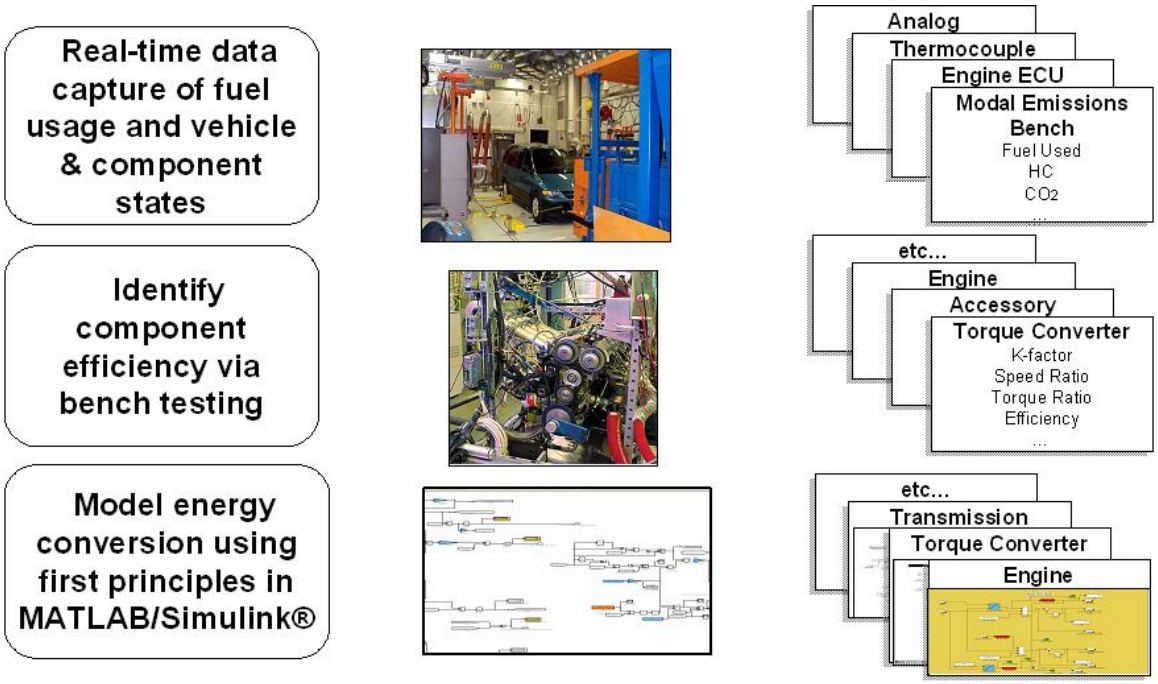

Figure 2-8 Identification of Vehicle System Energy Analysis Model

2.3.1 Drive Cycle Fuel Consumption and Vehicle State Determination

The fuel used over a given vehicle drive cycle is measured in an emissions chassis dynamometer test cell under standardized conditions. The test vehicle is parked with its wheels resting on rollers that adjust to simulate the road load force. Speed-sensitive loads are applied to the vehicle via the rollers representing the vehicular inertia, rolling resistance, aerodynamic drag, and other resistive forces that the vehicle must overcome during the pre-defined cycle.

Exhaust emissions analyzer modal data is measured during the drive cycle and used to determine the total fuel consumption and combustion inefficiency. The simulation uses the one hertz modal exhaust gas analyzer emissions bench HC, CO, CO_2, and exhaust flow volume results to determine combustion efficiency (refer to Section 2.2.2) and the volume of fuel used.

$$v_{fuel} = \frac{\rho_{H_2O} \cdot CWF \cdot SG_{fuel}}{CWF \cdot HC + 0.429CO + 0.273CO_2} \tag{2-29}$$

where:

CWF	carbon weight fraction of fuel
SG_{fuel}	specific gravity of fuel
ρ_{H_2O}	density of water

Once the fuel flow is obtained, the fuel economy can then be determined and validated using the exhaust concentrations in the CVS bag.

While the chassis dynamometer testing takes place, various parameters are collected from the engine and transmission controllers to determine the exact vehicle state. Engine speed and manifold air pressure determine the engine operating state. The alternator duty cycle is captured to determine alternator load (i.e., current). The transmission gear, torque converter turbine speed, and lock-up status determine the drivetrain state. Additional parameters, such as injector pulse width, can be collected to verify the fuel consumption determined by the emissions bench. Additional analog and thermocouple measurements are taken during vehicle testing to quantify energy consumption of the various subsystems under investigation. Power steering head pressure, A/C line pressure, and mechanical fan speed are acquired to determine their respective parasitic losses.

2.3.2 Test Based Methods and Model Structure

The vehicle subsystem behavior must be identified through a series of experiments to accurately simulate the subsystem energy consumption in the vehicle system model. Empirical data is collected as described in Section 2.3.1 and used to determine actual states of all of the components modeled in the energy analysis over the

tested drive cycles. Bench tests in the form of steady-state efficiency mapping or parasitic loss testing are performed for each modeled subsystem to determine their responses to the input conditions. The data is then used to build models of subsystem behavior in MATLAB®/Simulink®. In addition to extensive bench testing, computer-aided engineering (CAE) models were used to determine moments of inertia for individual components in order to calculate inertial energy required for each vehicle component during the various drive cycles studied. The subsystem data requirements necessary to populate the model are shown in Table 2-2.

To determine the drag characteristics of the vehicle, coastdown testing is performed per the Society of Automotive Engineer (SAE) Standard J1263, by allowing a vehicle to coastdown in neutral and measuring the elapsed time from 70 to 10 miles per hour. The 3-term *ABC*-coefficients in Equation (2-25) are then determined by curve fitting. Tire rolling resistance is measured at multiple loads, inflation pressures, and speeds per SAE Standard J2452. A similar curve fitting analysis is performed on the experimental tire rolling resistance data to find the α, β, a, b, and c-coefficients from Equation (2-26) and the C_dA values for aerodynamic drag in Equation (2-27).

The engine response for the torque and fuel flow are determined using linear interpolation between discrete steady-state engine dynamometer data points in terms of engine speed and load (i.e., manifold air pressure, MAP) as shown in Figure 2-9. The mean effective pressure data is acquired with in-cylinder pressure probes either via steady-state engine dynamometer mapping or via in-vehicle testing.

Table 2-2 Energy Analysis Subsystem Data Requirements

Component	Information	Data Format
Vehicle	Test Weight	lbs
Vehicle	Weight Distribution front-to-rear	% front axle or % rear axle
Vehicle	Roadload targets	A (lbf), B (lbf/mph), C (lbf/mph^2)
Vehicle	CdA	m^2
Vehicle	Tire Parameters	alpha, beta, a, b, c
Vehicle	Tire Size	rev/mi (calculated using dynamic tire radius)
Vehicle	Rated Tire Pressure	kPa
Vehicle	Wheel and Tire Inertia	constant in kg-m^2
Engine	Compression Ratio	constant
Engine	Engine Displacement	constant in L
Engine	Engine Inertia	constant in kg-m^2
Engine	Torque	Torque in ft-lbs = f (Engine RPM, MAP in kPa)
Engine	NMEP, IMEP, PMEP	MEP in psi = f (Engine RPM, MAP in kPa)
Engine	Fuel Flow	Fuel Flow in kg/hr = f (Engine RPM, MAP in kPa)
Engine	HC, CO, CO2	HC in ppm, CO %, CO2 % = f (Engine RPM, MAP in kPa)
Engine	FEAD Inertia	constant in kg-m^2
Transmission	Gear Ratios	-
Transmission	Trans Inertia	constant in kg-m^2 for each Gear
Transmission	Trans Efficiency	Efficiency in Each Gear = f (Input Torque in ft-lbs, Input Speed in RPM)
Torque Converter	Torque Converter Inertia	constant in kg-m^2
Torque Converter	Flexplate Inertia	constant in kg-m^2
Torque Converter	K-factor Data	K-factor in rpm/(ft-lb)^0.5 = f (Speed Ratio)
Torque Converter	K-factor Data (overrunning, i.e. speed ratios greater than one)	K-factor in rpm/(ft-lb)^0.5 = f (Speed Ratio)
Torque Converter	TC Torque Ratio	TC Torque Ratio = f (Speed Ratio)
Torque Converter	TC Efficiency	TC Efficiency = f (Speed Ratio)
Transfer Case (if equipped)	Transfer Case Inertia	constant in kg-m^2
Transfer Case (if equipped)	Transfer Case Efficiency	Efficiency = f (Input Torque in ft-lbs, Input Speed in RPM)
Powertrain	Driveshaft Inertia	constant in kg-m^2
Powertrain	Half-shaft Inertia	constant in kg-m^2
P/S	P/S Inertia	constant in kg-m^2
P/S	P/S Drive Ratio	-
P/S	P/S Load	P/S Load in N/m = f (Delta Pressure in psi, Input Speed in RPM)
Mech Fan (if equipped)	Mech Fan Clutch Inertia	constant in kg-m^2
Mech Fan (if equipped)	Mech Fan Inertia	constant in kg-m^2
Mech Fan (if equipped)	Mech Fan Drive Ratio	Fan Torque in ft-lbs = f (Fan Clutch Speed in RPM)
Differential	Final Drive Ratio	-
Differential	Differential Efficiency	Efficiency = f (Input Speed in RPM, Input Torque in ft-lbs)
Differential	Differential Inertia	constant in kg-m^2
Brake Drag	Brake Drag	Brake Drag (ft-lbs) = f (Disengage Time)
Wheel Bearing	Wheel Bearing Loss	Torque Loss (N-m) = f (Axle RPM)
Alternator	Alternator Load	Load (N-m) = f (Alternator RPM, Alternator DC)
Alternator	Alternator Current	Current (Amps) = f (Alternator RPM, Alternator DC)
Alternator	Alternator Pully Ratio	-
Alternator	Alternator Inertia	constant in kg-m^2
A/C	A/C Load	A/C Load (N-m) = f (A/C RPM, A/C Delta P)

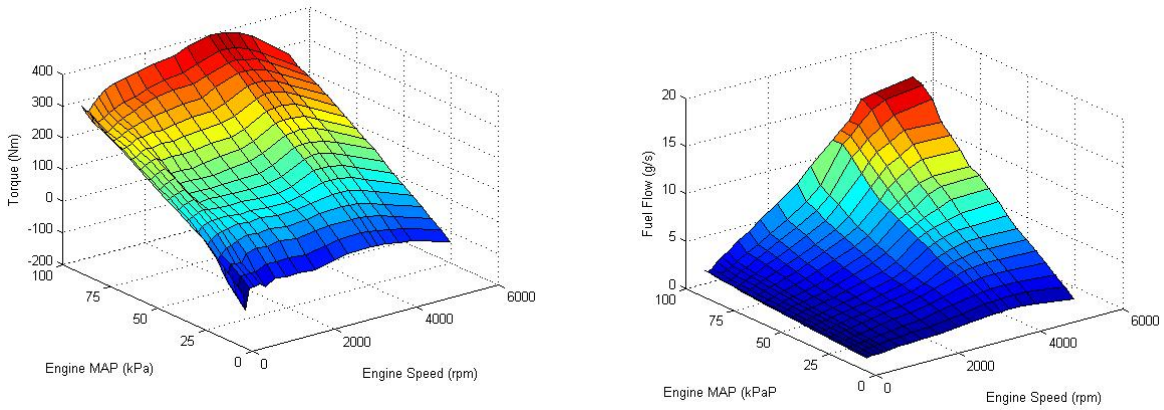

Figure 2-9 Example of Engine Torque and Fuel Flow Response Characterization

The efficiency and K-factor characteristics of the torque converter as shown in Figure 2-5 are also collected on a dynamometer for various input speeds. The transmission loaded efficiency as a function of input speed and load is determined on a doubled-ended dynamometer. The parasitic losses as a function of speed and load for the accessory components are also determined by special bench tests.

Once the individual subsystem behavior is identified, MATLAB®/Simulink® block diagrams are constructed to represent the subsystems. Mathematical relationships, including basic physics and thermodynamics equations, are included in the block diagrams such that the energy consumption contribution of each subsystem can be determined in the simulation. An example of one of the subsystem models, specifically the power steering model, is shown in Figure 2-10. Finally the block diagrams are joined to obtain a model of the entire vehicle system where the power passed from one component to another is simulated over the entire drive cycle. A diagram of the overall model structure is shown in Figure 2-11.

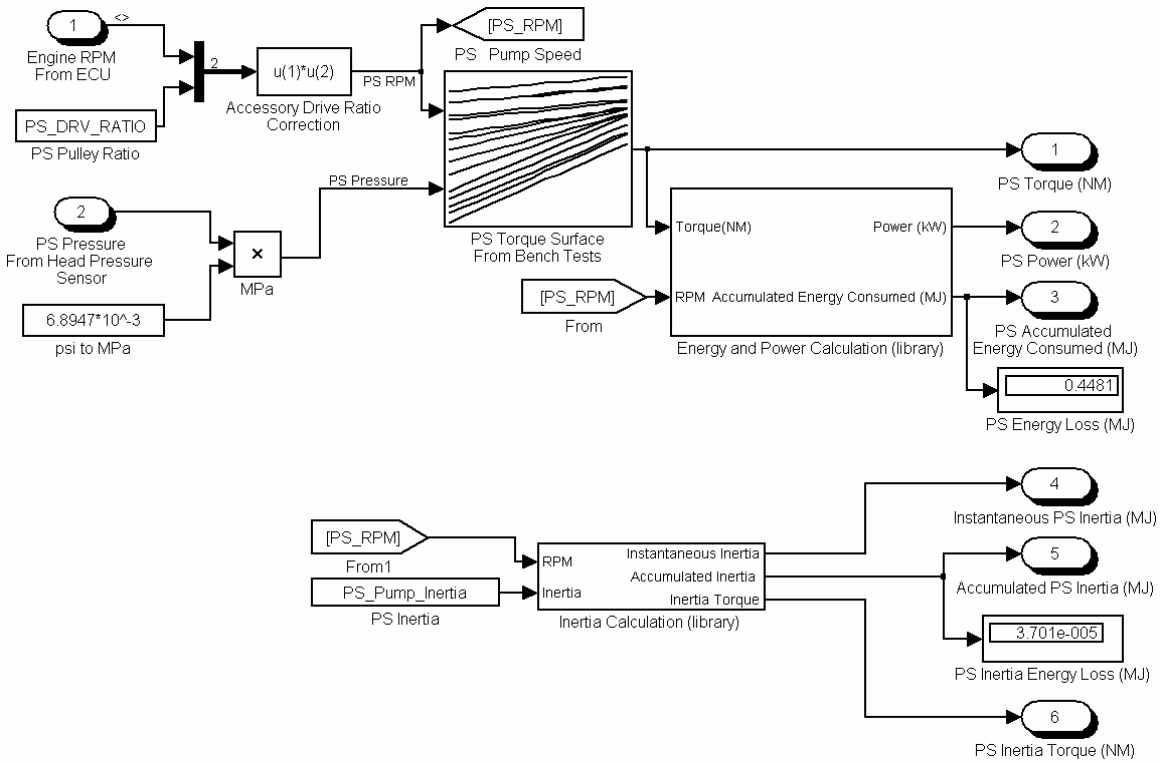

Figure 2-10 Energy Analysis Power Steering Subsystem Simulink® Model

The user first identifies the vehicle to be investigated and loads the corresponding subsystem data files to populate the subsystem models. Next the user selects the drive cycle schedule files which are loaded into the model. The simulation is run using a simple first-order Euler-based integration routine at one hertz and outputs a summary file of the total and instantaneous energy consumed for each subsystem in the model. Additional plots of efficiency and performance characteristics can be obtained in the model. The user can then vary the individual subsystems to determine their individual impact of fuel economy.

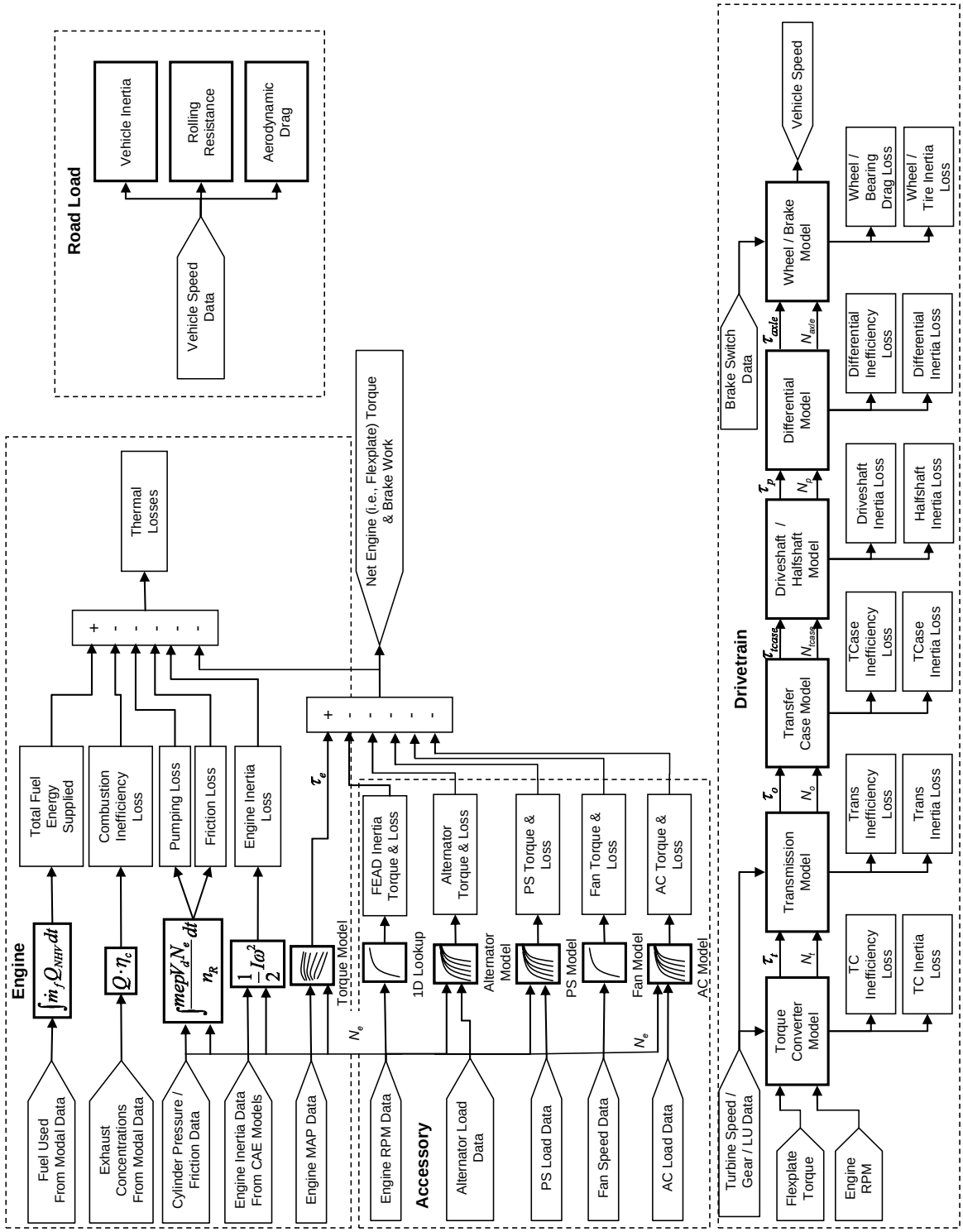

Figure 2-11 Diagram of Energy Analysis Model Structure

2.4 Energy Analysis Methodology Utility

The energy analysis methodology has many benefits including mitigating the effect of test to test and driver variation on the fuel economy evaluation process. Some potential fuel savings fall within the bandwidth of current fuel economy test variation. Standard deviations of the CVS bag chassis dynamometer fuel economy results with the same driver and the same test cell in this study were observed to be around 0.2 miles per gallon. Another variation study that included variability in test cells, drivers and vehicles revealed that a minimum of 15 tests would be necessary to measure a 0.5 mpg change with 90% confidence (Wong and Clemens 1979). Although a degree of variability exists because the energy analysis model relies on empirical data, there is still significant advantage to using this approach when making A-B comparisons since the tool is populated with data from a single chassis dynamometer test. Hence, the methodology eliminates some of the major sources of fuel economy test to test variability. CHAPTER 3 will demonstrate how the energy analysis methodology can be used to investigate the energy demand for a typical vehicle and to estimate potential incremental fuel saving scenarios.

CHAPTER 3

INVESTIGATION OF VEHICLE SYSTEM ENERGY EFFICIENCY

Once the energy analysis tool is populated with the necessary vehicle data, the energy usage of vehicle and powertrain subsystems can be simulated in order to highlight areas that have potential for fuel efficiency improvements. The energy analysis methodology and tool can be used to study predominate fuel economy factors over various drive cycles or quantify potential incremental subsystem fuel economy improvements that would otherwise be difficult to measure with experimental fuel economy testing due to inherent test variability. Although a degree of variability is inevitable since parts of the analytical tool are populated with empirical data, the energy analysis methodology and tool mitigates the effect of many external noise factors that exist when trying to compare design alternatives using purely empirical methods.

3.1 Investigation of Engine Energy Supply for a Typical Vehicle

To demonstrate the usefulness of the tool, an energy analysis will be presented for a 2700 kilogram full-size 4x4 pick-up truck with a V8 engine and 5-speed transmission in two-wheel drive operation over the FTP urban drive cycle, also commonly referred to as the FTP74 cycle (refer to Figure 3-1). Of the fuel energy supplied to the system, the tool results show that 63.5% of the losses are due to engine thermal losses. The second law of

thermodynamics limits the maximum thermal efficiency that any combustion engine can attain. Most of the thermal losses in a spark-ignition ICE are due to heat loss to the coolant or to the exhaust.

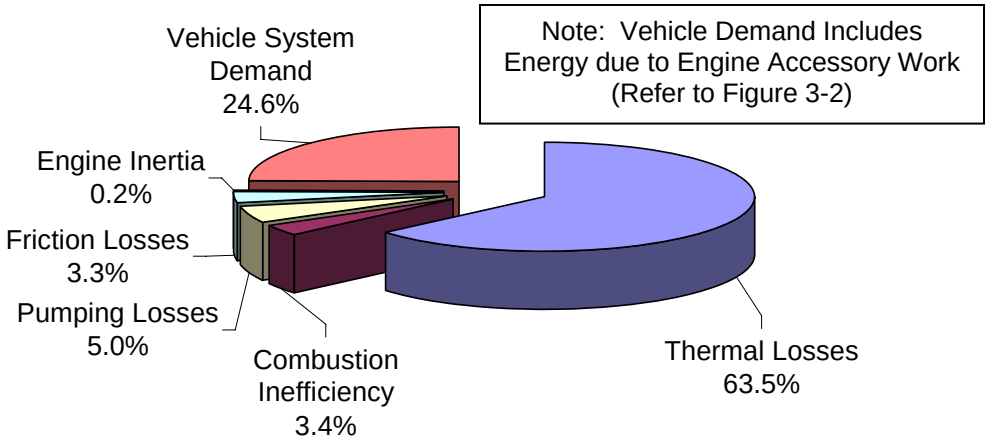

Figure 3-1 Analysis of Engine Energy Supply

Unavoidable combustion inefficiency losses occur since not all of chemical energy supplied is released during the combustion process. Incomplete combustion products in the exhaust representing chemical energy not released during combustion accounted for 3.4% of the total fuel energy losses.

Pumping losses are also inevitable with any spark-ignition ICE. Pumping losses account for 5% of the losses in this study. The losses due to pumping work can be influenced by the engine design and control strategy as well as with the implementation of advanced engine technology, such as variable valve timing (VVT), variable lift, and/or cylinder deactivation concepts.

Engine friction losses accounted for 3.3% of the losses. The type of valvetrain configuration (e.g., overhead cams versus pushrod) plays a major role in the extent of engine mechanical friction losses. Additional attenuation of friction losses can be

achieved during the design process with the inclusion of low-friction components, such as low-tension compression rings.

Of the total fuel energy supplied, only 24.6% of the energy satisfies the vehicle demand. That is, 75.4% of the total energy supplied is consumed to overcome the fuel conversion inefficiency (Note that accessory losses further reduce the flywheel output torque but will be considered part of the vehicle demand to be discussed in Section 3.2).

While careful design and advanced technology offer the potential to improve engine efficiency to some extent, engine efficiency is still limited to a great degree by the laws of thermodynamics. With regards to engine efficiency, the focus of this vehicle energy analysis is mainly to quantify how efficiently the energy supplied to the engine is being converted to useful work demanded downstream. In other words, during vehicle system and component design, it is useful to remember that state-of-the-art spark ignition engines generally require a supply of fuel energy three to four times the energy demand to overcome inherent fuel conversion inefficiencies. In addition to improving engine efficiency as much as feasibly possible, minimizing the demand of downstream vehicle subsystems is essential to designing efficient vehicle systems. For every joule of energy demand or parasitic loss downstream, the engine requires three to four joules of fuel energy.

3.2 Comparison of Vehicle Energy Demand for City and Highway Drive Cycles

Determining which vehicle subsystem elements account for the 24.6% vehicle system energy demand in Figure 3-1 is crucial to understanding where fuel efficiency opportunities exist. Figure 3-2 depicts the breakdown of how the 24.6% of vehicle

system demand is sub-divided by the vehicle subsystems. It is important to note here that the percentages in Figure 3-2 are percentages of the total vehicle system demand, i.e., rolling resistance accounts for 15.5% percent of the vehicle system energy demand but 3.8% of the total energy supplied.

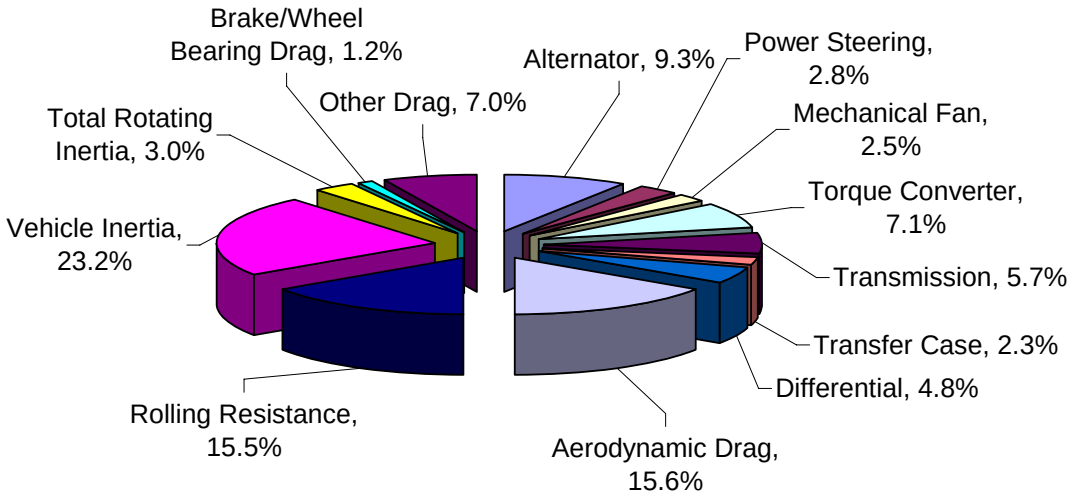

Figure 3-2 Analysis of Percent Vehicle System Energy Demand

Figure 3-3 illustrates the accumulated vehicle system energy over the drive cycle in megajoules. The results reveal that the majority of the vehicle energy demand losses during urban driving, 23.2% in this case, are due to vehicle inertia in the form of kinetic energy dissipated by the brakes.

The prevailing fuel economy factors are different during highway driving. A comparison of both the EPA FTP urban and highway drive cycles is shown in Figure 3-4. Figure 3-5 illustrates a comparison of the total energy demand rankings for the various subsystems over both of these cycles. While the majority of vehicle energy during urban driving is needed to overcome the vehicle inertia, aerodynamic drag predominates during highway driving. In addition to road load effects, the figures depict that drivetrain inefficiency and accessory load compose a significant portion of the vehicle system demand.

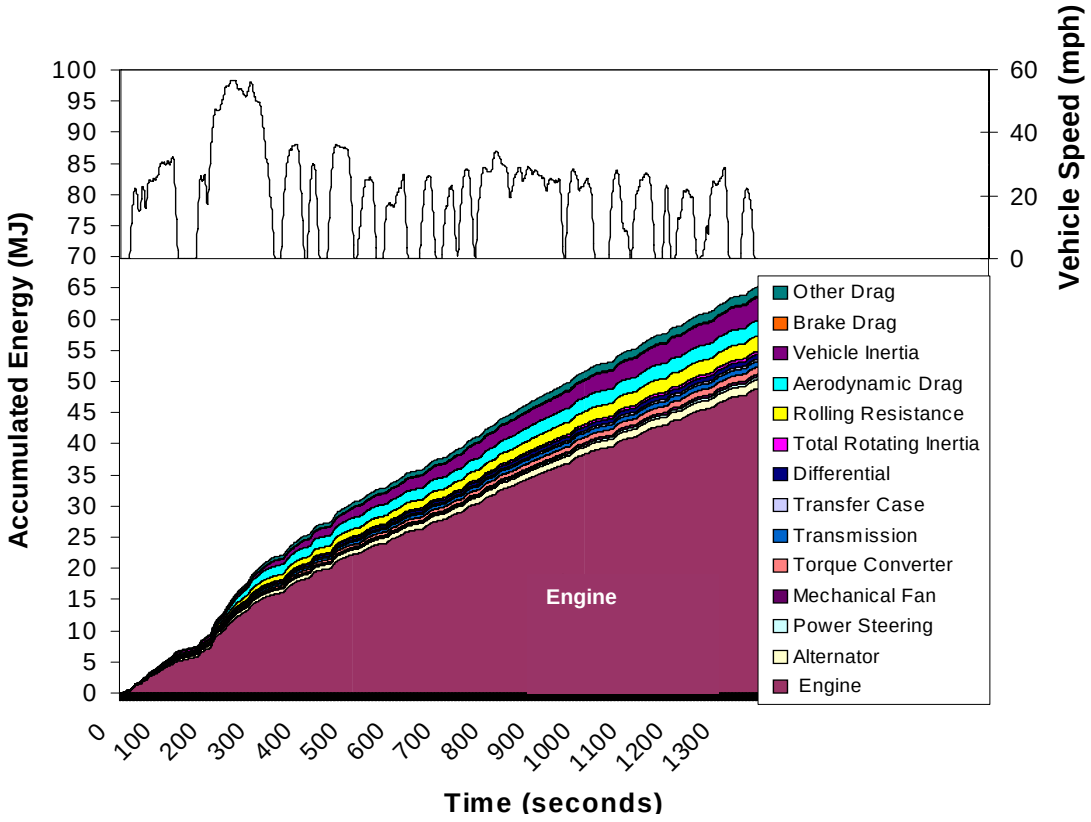

Figure 3-3 Accumulated Vehicle System Energy Demand vs. Vehicle Speed

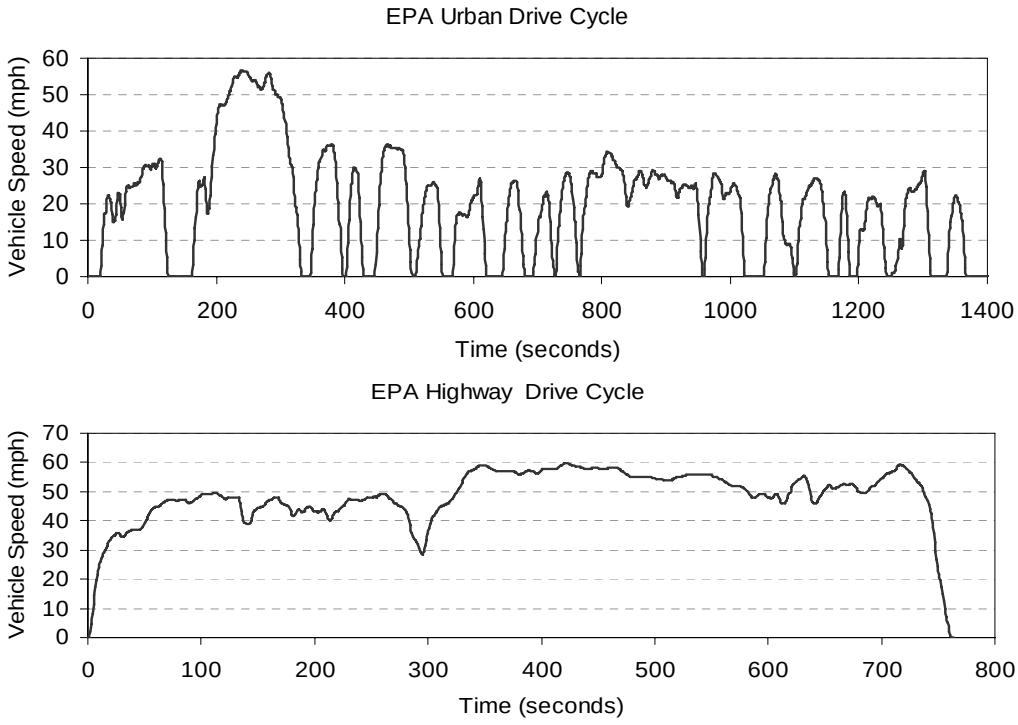

Figure 3-4 EPA FTP Urban and Highway Drive Cycles

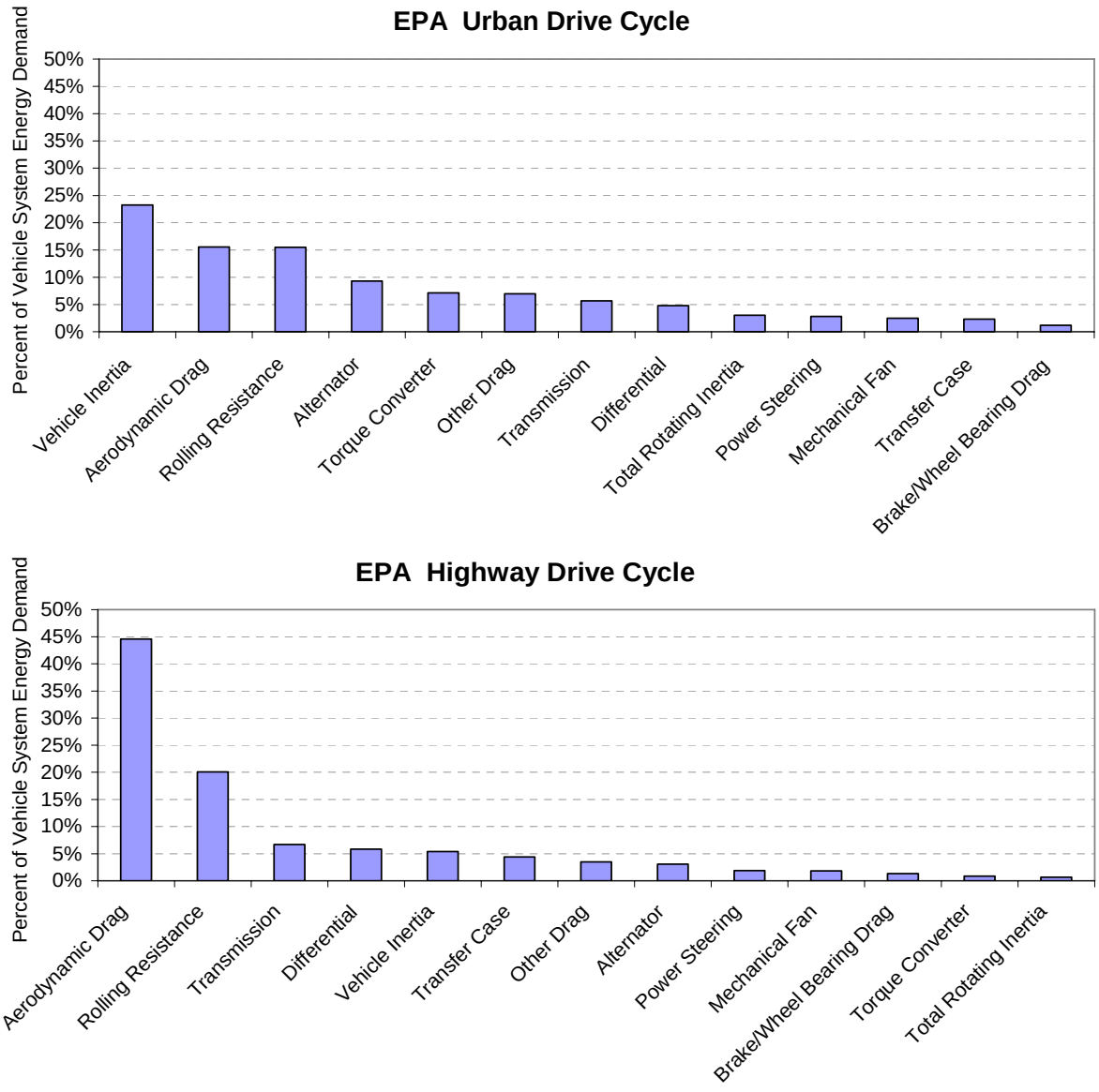

Figure 3-5 Comparison of Percent Vehicle System Energy Demand by Subsystem for FTP Urban and Highway Drive Cycles

The energy analysis methodology helps to focus development efforts on vehicle and subsystem attributes that have the potential to impact the downstream energy demand.

3.3 Investigation of Potential Fuel Saving Hypothetical Scenarios

Once the energy analysis tool is populated with component speed and load data, the tool can be used to estimate the change in energy demand for incremental hypothetical subsystem changes. The hypothetical fuel savings are estimated by determining the change in subsystem energy required in megajoules for a given scenario. Once the subsystem energy delta is determined the energy conversion efficiency is taken into account to determine the overall energy delta. The change in fuel economy in miles per gallon can be calculated from the overall energy delta in megajoules using the net heating value and density of the fuel used:

$$MPG = \frac{3.785 \cdot x \cdot \rho_{H_2O} \cdot SG_{fuel} \cdot Q_{NHV}}{Q} \tag{3-1}$$

where:

MPG	fuel economy in miles per gallon
3.785	conversion factor to gallons from liters
x	distance traveled over a given cycle in miles
SG_{fuel}	specific gravity of fuel
Q_{NHV}	net heating value of fuel in kJ/kg
Q	total energy consumed in kJ.

For demonstration purposes, the effects of various accessory drive changes will be analyzed. Figure 3-6 shows energy analysis estimates of the fuel economy effects of the following changes: (1) reduction in power steering (P/S) pump speed by reducing P/S pulley ratio by 0.1, (2) reduction in P/S pump volume by 3 cc/rev, and (3) reduction in alternator load by 4 amps. Even though the fuel economy benefits may only be incremental, such changes may add little or no cost to a vehicle system design. Often such ideas are not considered or disregarded since the potential benefits cannot be measured due to variation inherent in experimental fuel economy testing. Yet when

designing vehicles for fuel economy, it is necessary to consider even incremental fuel economy improvements.

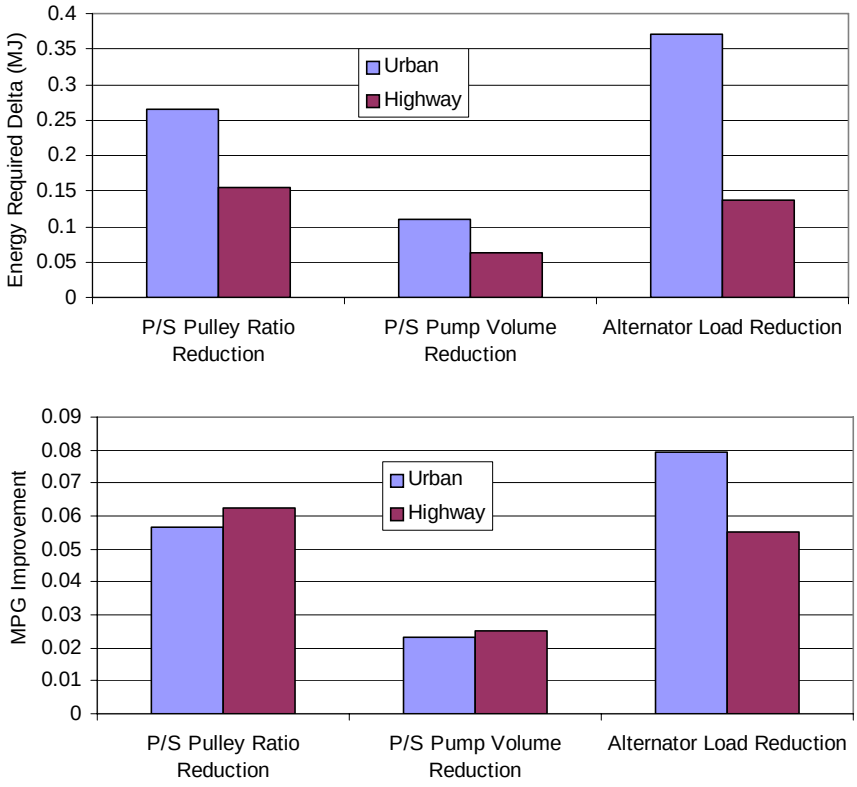

Figure 3-6 Predictions for Change in Overall Required Energy and Fuel Economy Improvement for Various Accessory Drive Hypothetical Scenarios over FTP Drive Cycles

When testing these or similar incremental changes on a chassis dynamometer, also commonly referred to as a chassis rolls, the potential benefit could fall within the bandwidth of external noise factors, which includes:

- Driver to driver variability
- Test cell to test cell differences
- Human deviation or error (for same driver)
- Measurement system variability (e.g., instrumentation)
- Dynamometer warm-up and vehicle soak time influences

- Vehicle to vehicle differences (break-in, tolerances, tire pressure, etc.)
- Throttle movement and ECU calibration sensitivity
- Ambient conditions (Flor and Karell 1997).

Figure 3-7 depicts a pareto of the results of a study to determine the sources of fuel economy measurement system variation.

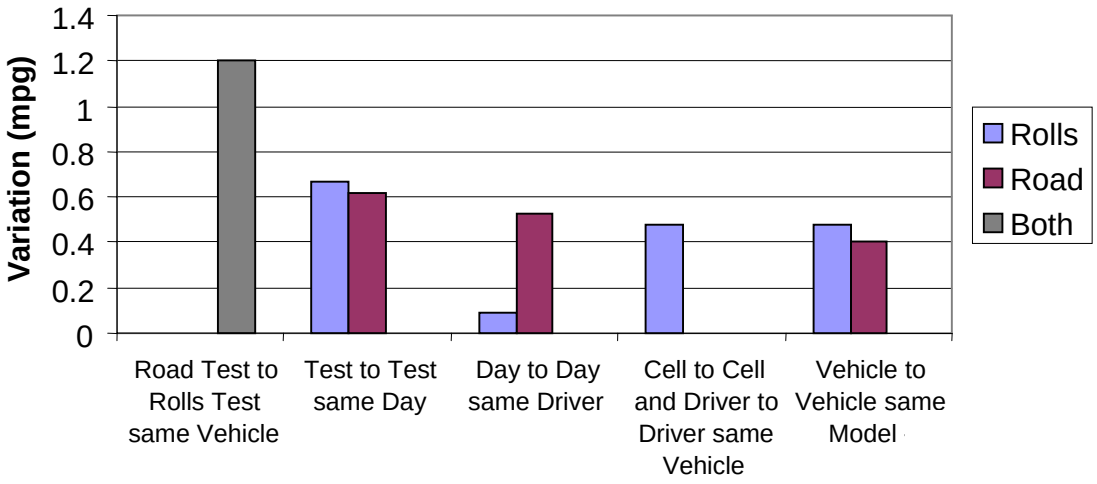

Figure 3-7 Fuel Economy Measurement System Sources of Variation (McGregor 2005)

The actual test environment precludes changing one variable at a time while holding the other variables constant. The energy analysis methodology is able to mitigate some of the largest sources of variability, which include driver to driver variability and other test to test variation. By populating the analytical tool with measurements from a single dynamometer test, the difference in energy demand can be calculated for various hypothetical scenarios without obscuring the results by running additional tests that compound the sources of variability.

The baseline vehicle and a vehicle with both the P/S pulley ratio and pump volume changes were tested on a chassis dynamometer and compared to the energy analysis estimates of the combined changes. In an attempt to obtain a statistical sample,

the generally accepted practice is to run three of each FTP urban and highway cycles. Figure 3-8 depicts both the energy analysis estimates and measured CVS measured fuel economy improvements of the combined power steering pump changes. The mean of the difference between the measured baseline and alternative P/S configuration compared to the energy analysis estimate are both approximately 0.08 miles per gallon. However, the highway results are more ambiguous due to inherent test variation. The figure also shows the 95% confidence interval for the difference of the measured dynamometer results revealing that any potential benefit is within test to test variation. Given the test to test variation in standard chassis dynamometer fuel economy testing, over 100 tests would be necessary to measure a 0.08 mpg difference with 80% confidence. Seeing as such extensive testing is impractical, the energy analysis methodology is a far better alternative to estimating incremental fuel economy improvements.

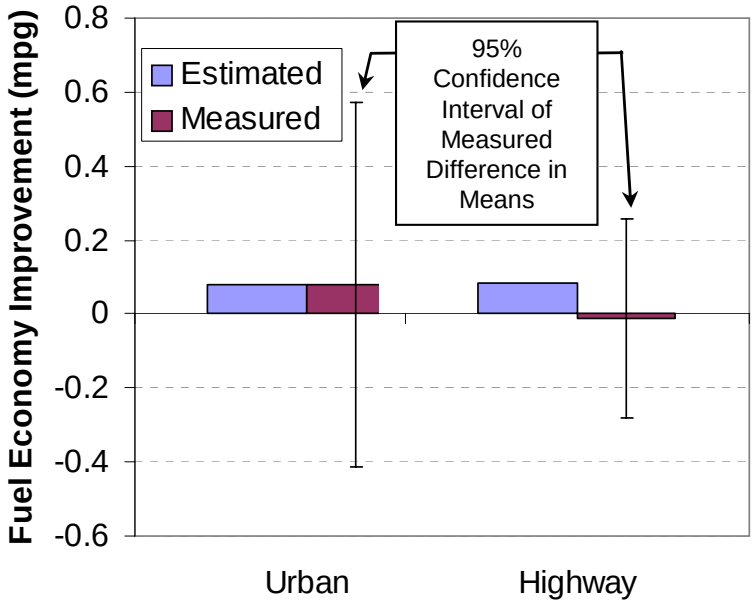

Figure 3-8 Comparison of Measured CVS and Energy Analysis Estimates of Fuel Economy Improvement for Combined Power Steering Pulley Ratio and Pump Volume Reductions

The energy analysis results in Figure 3-8 suggest that reducing the P/S pump pulley ratio and reducing the alternator load yields higher fuel economy benefits. However, it is important to consider that the P/S pump is not actuated on a standard FTP dynamometer test; therefore the steady-state chassis dynamometer P/S pump energy usage does not reflect "real-world" energy usage.

One advantage of the energy analysis methodology is that the tool can be populated with speed and load and fuel consumption data from a vehicle test track or on-road testing to reflect more real-world speeds and loads observed. Consequently the P/S pump was instrumented with a pressure transducer to capture the P/S pump load over a one mile dynamic steering vehicle test track. Figure 3-9 shows the measured power steering head pressure over the test. The P/S pump pressure and efficiency over the speed and loads encountered during the one mile test track was incorporated into the energy analysis tool and the changes in energy demand for the same accessory drive scenarios were analyzed. Figure 3-10 depicts how actuating the P/S pump influences the energy analysis results. While reducing the P/S pump ratio results in a higher percent increase in fuel economy during steady-state test conditions, reducing the displacement of the pump is a far better P/S alternative in real-world driving conditions. This example demonstrates the usefulness of using the energy analysis methodology in evaluating incremental vehicle system technologies that have the potential to improve real-world fuel economy.

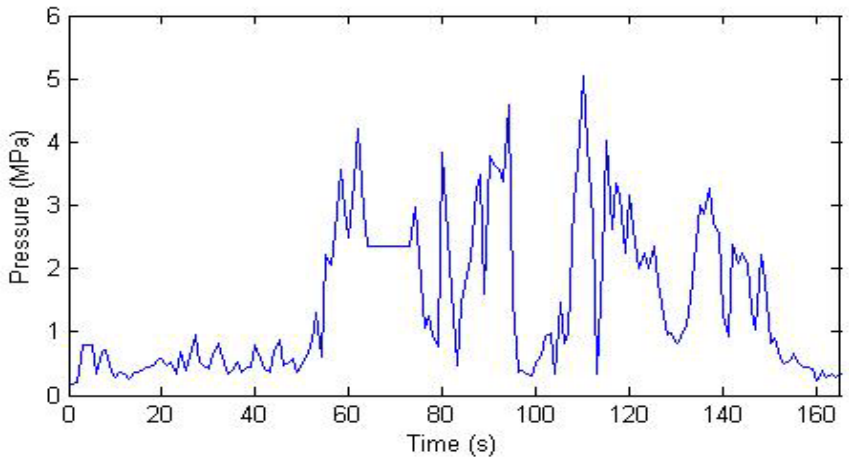

Figure 3-9 Measured Power Steering Head Pressure over Dynamic One Mile Test Track

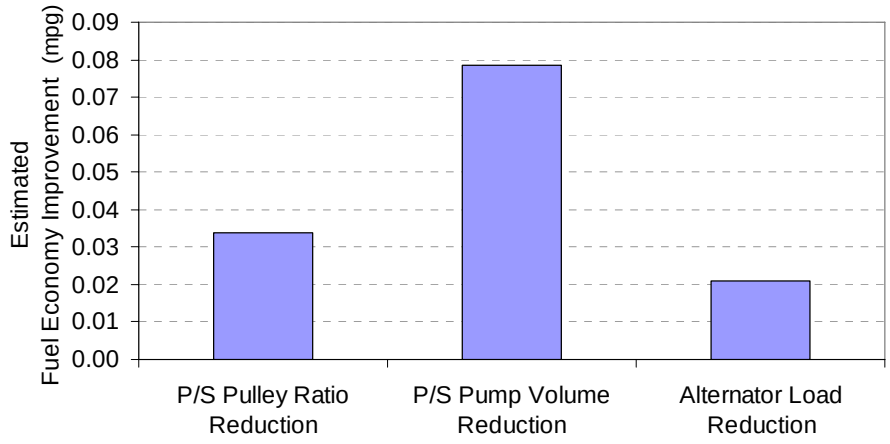

Figure 3-10 Predicted Fuel Economy Improvement for Various Accessory Drive Hypothetical Scenarios over Dynamic One Mile Test Track

3.4 Advantages and Limitations of Energy Analysis Methodology

Given that the energy analysis approach is both analytical and empirical in nature, advantages and disadvantages exist. Since the tool is populated with empirical data, the results can be more relied upon because they reflect the actual energy use and speeds and loads observed, whereas virtual vehicle simulations could potentially yield inaccurate results which could lead to false conclusions. Another benefit of the hybrid semi-empirical and analytical approach is that the measurements used in the energy analysis

tool can be cross-checked with alternate means of data acquisition to verify the accuracy of the results.

One current limitation is that the energy analysis tool assumes standard operating temperatures of all components and does not take into account warm-up temperature effects. Even though it is known that the efficiency of drivetrain components heavily depends on operating temperature, often detailed efficiency data as a function of speed, load and temperature does not exist. As more temperature dependent data becomes available, the tool could be easily modified to include such effects.

Another advantage is that the tool can estimate individual effects on fuel economy in more detail given that some potential fuel economy improvements fall within standard fuel economy test to test variation. The energy analysis methodology mitigates the effects of some external sources of variation and can therefore evaluate design alternatives that yield only small changes in fuel economy. Proposed subsystem changes that account for a fraction of the total energy demand, as in accessory drive changes, can be analyzed without extensive testing.

On the other hand, while the tool offers the ability to model the effect of individual vehicle and component changes on fuel economy, due to its empirical nature, the tool should not be used to predict vehicle system interaction effects that are not explicitly represented in the tool unless empirical data is acquired. For instance, while the tool can determine the hypothetical vehicle inertia and road load energy savings due to a 5% vehicle weight reduction, any corresponding system level effects that might occur, such as the ability to operate in a higher gear ratio with a lower engine speed, would not be reflected unless a vehicle of the hypothetical weight and new shift

calibration were actually tested on a chassis dynamometer and the test measurements incorporated into the tool. This limitation illustrates the need for a predictive simulation methodology that has the ability to take system level effects into account when evaluating hypothetical vehicle system configurations. CHAPTER 4 will explore the development of such a methodology.

Nonetheless, the energy analysis tool offers the potential to quickly evaluate possible fuel saving subsystem design alternatives and can be used to explore the prevailing fuel economy effects for different drive cycles or different classes of vehicles. Ultimately performing a comprehensive vehicle system energy analysis can assist in focusing technology development efforts on areas that have the greatest potential for improving vehicle system energy efficiency.

CHAPTER 4

DEVELOPMENT OF REVERSE DYNAMIC OPTIMIZATION METHODOLOGY FOR OPTIMAL POWERTRAIN INTEGRATION AND CONTROL DESIGN

4.1 Introduction

While new technology offers the potential to significantly improve fuel economy, adding multiple degrees of freedom to powertrain systems introduces the challenge of optimal hardware integration and control design. Current vehicle system models have the ability to predict fuel economy yet they lack the ability to effectively evaluate powertrain hardware since optimal hardware selection is related to control design. For example, it is insufficient to evaluate two different torque converters based on simulation results without re-designing the powertrain control system to operate each torque converter *coupled* with their respective drivetrain components in their most efficient operating states. In addition, optimal powertrain hardware and control design depends on the driver application. Often the interrelationship between hardware and control design and their dependence on driver application is overlooked. A reverse tractive road load demand model for optimal powertrain integration and control is being developed to address the challenge of quickly optimizing the hardware configuration and control design early in the design process. The development of this reverse dynamic optimization methodology

and application to optimizing control and maximizing powertrain system efficiency are also described in Baglione, *et al.* (2007b).

4.2 Model Approach and Development

The reverse dynamic optimization approach combines a backward-looking model that simulates the powertrain in every possible state with a dynamic programming algorithm that finds the optimal control strategy.

4.2.1 Benefits of Backward-Looking Modeling Approach

A backward-looking approach was selected for the reverse tractive road load demand model since a main objective of this research is to quickly evaluate multiple design alternatives early in the design process. Backward-looking models are well suited for fuel economy predictions and for providing trends related to component sizing, sensitivity analyses, and optimal powertrain matching.

One major advantage of backward-looking models compared to forward-looking models is the significant simulation time savings. In order to produce accurate results, forward models require higher order integration routines with small time steps. As discussed in Section 1.3.1, backward models have been shown to simulate 2.6 to 8.0 times faster than representative forward models (Wipke, *et al.* 1999). The Rapid Automotive Performance Simulator (RAPTOR) has the capability of performing both backward- and forward-looking simulations. A study was performed with RAPTOR using the same 180 kilobyte vehicle model and inputs to compare both approaches. The backward-looking model was run with a one second fixed time step and the forward-looking model was run with the maximum variable time step of 0.09 seconds. Table 4-1

reveals the forward model was more accurate than the backward model for the Consumer Reports (CR) city cycle albeit with a much slower run time. However, even with a larger post simulation model, the forward model was less accurate for the CR highway cycle. Due to the slower run times and potential stability issues, forward models are impractical for studying numerous design alternatives and for establishing direction early on in the design process. A significant benefit of the backward-looking approach is that the reverse model will be run with Euler integration routines that yield faster run times with relatively large sample times which will be necessary as additional degrees of freedom as well as optimization routines are added to the reverse dynamic simulation.

Table 4-1 Comparison of RAPTOR Backward-Looking versus Forward-Looking Models

	Backward-Looking Model			**Forward-Looking Model**			**Test Vehicle Results (mpg)**
	Simulation Result (mpg)	CPU Run Time (sec)	Post Simulation Vehicle Model Size (kb)	Simulation Result (mpg)	CPU Run Time (sec)	Post Simulation Vehicle Model Size (kb)	
CR City Cycle	9.647	0.554	370	10.098	29.23	960	9.96
CR Highway Cycle	20.453	0.702	770	18.468	35.211	6180	20.61

Backward-looking models have a further advantage when comparing design alternatives since they follow the drive cycle trace exactly. On the other hand, while forward-looking models are theoretically more representative and allow for the development of control strategies that can be utilized in hardware-in-the-loop (HIL) simulators, stability issues can result. Forward models rely on the calibration or tuning of a driver feedback model, which can be difficult and time-consuming. Also unique tuning might be necessary for different configurations, e.g., different power to weight ratios, adding an additional source of variability to the simulations. Furthermore, due to the

driver feedback loop, forward models have less ability to compare small changes in hardware because they do not follow the drive cycle trace exactly.

To demonstrate the differences, a baseline torque converter was compared to a torque converter with stator and turbine design changes that yield a flat characteristic K-factor curve (refer to Figure 4-1). The fuel efficiency benefits of a flat torque converter design are discussed in Ochi, *et al.* (2006).

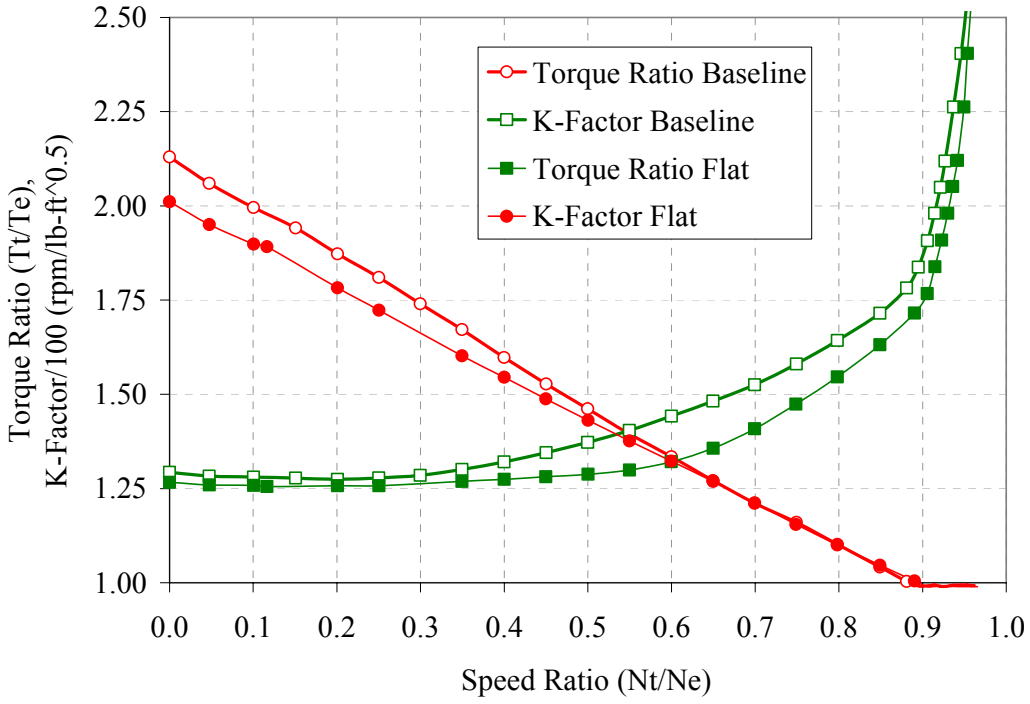

Figure 4-1 Comparison of Flat Torque Converter Curve

Both converters were simulated over the CR city cycle using a proprietary dSPACE HIL simulator (http://www.dspaceinc.com) as well as using the reverse dynamic approach proposed in this dissertation. The simulation results compared to actual powertrain dynamometer test measurements including the 95% confidence interval for the difference in the means are shown in Table 4-2. The results prove that the HIL simulator does not perform well at estimating incremental fuel economy improvements

due to significant test to test variation that results from the controller in the loop adapting and the driver model's response varying. The reverse dynamic optimization methodology ultimately removes major external sources of noise when evaluating incremental changes. It should also be noted that the HIL simulator runs at real time while the reverse dynamic methodology runs 40 times faster than real time.

Table 4-2 Comparison of HIL, Reverse Dynamic Optimization, and Measured Fuel Economy for Flat Torque Converter Design

	Fuel Economy Difference (mpg)	95% Confidence Interval for Difference in Means (mpg)
HIL Simulation	-0.062	(-0.222, 0.097)
Reverse Dynamic Optimization Simulation	0.138	N/A
Dynamometer CVS Test Measurement	0.095	(0.020, 0.169)
Dynamometer Modal Test Measurement	0.054	(-0.084, 0.192)
Dynamometer Fuel Flow Meter Test Measurement	0.158	(0.049, 0.267)

Another key benefit to the backward approach is the ability to perform concept studies and establish hardware design objectives for future non-existing powertrain designs. Once a vehicle concept is established, the reverse model can be used to study how each component must perform to achieve optimal vehicle system performance. By translating the required road load force into a wheel torque "requirement" and propagating the required torque backwards through the powertrain system, targets can be more easily established for non-existing designs. Often when designing a new engine program, for example, peak torque and peak power targets are set based on marketing, but it is difficult to ascertain what will be required of the engine under part load conditions. The reverse model will facilitate determining part throttle torque requirements that are constraint driven and drive cycle based given target vehicle attributes to achieve optimal system performance.

4.2.2 Reverse Tractive Road Load Demand Model

The reverse tractive road load demand model developed here is quasi-static, derivative based with inverted physical causality in that the force required to achieve the corresponding acceleration is iteratively calculated from the desired speed trace.

$$a = \frac{dV}{dt} = \frac{V_k - V_{k-1}}{t_k - t_{k-1}} \tag{4-1}$$

$$F = ma \tag{4-2}$$

The required tractive road load force is derived from the 3-term *ABC* rolling resistance, vehicle inertia, and given road grade as described in Section 2.2.7 and in Equation (2-25). The power required to overcome the vehicle propulsion force required at a given vehicle velocity, *v*, is then derived:

$$P = Fv \tag{4-3}$$

The torque required at the wheel is then calculated given the corresponding rotational wheel velocity:

$$\tau = \frac{P}{\omega} \tag{4-4}$$

where,

$$\omega = \frac{2\pi vT}{3600} \tag{4-5}$$

where T is the number of tire revolutions per mile.

An assumption is made during decelerations as to the magnitude of the mechanical braking force applied. It is assumed that a mechanical braking force is applied to achieve a deceleration force greater than a given deceleration. This assumption and its implications will be discussed further in Section 4.3.1.3.

The required wheel torque and rotational speed is then propagated in reverse direction throughout the drivetrain. The vehicle subsystems modeled and the direction of power flow are shown in Figure 4-2:

Figure 4-2 Reverse Tractive Road Load Demand Model Subsystems and Direction of Power Flow

The torque at the axle includes the required propulsion torque as well as the inertia of the wheels:

$$\tau_{axle,k} = \tau_{wheel,k} + I_{wheel} \frac{\omega_{wheel,k} - \omega_{wheel,k}}{t_k - t_{k-1}} \tag{4-6}$$

The torque at the differential pinion, i.e., axle or final drive input, must overcome the inefficiency and rotational inertia of the final drive:

$$\tau_{pinion,k} = \frac{1}{\eta_{final\,drive}(\tau_{pinion,k-1}, \omega_{pinion,k-1}) R_a} \tau_{axle,k} + I_{final\,drive} \frac{\omega_{pinion,k} - \omega_{pinion,k-1}}{t_k - t_{k-1}} \tag{4-7}$$

where,

$$\omega_{pinion,k} = R_a \omega_{axle,k} \tag{4-8}$$

and,

$$\omega_{axle,k} = \omega_{wheel,k} \tag{4-9}$$

The torque required at the driveshaft or transmission output must overcome the driveshaft inertia:

$$\tau_{driveshaft,k} = \tau_{pinion,k} + I_{driveshaft} \frac{\omega_{pinion,k} - \omega_{pinion,k-1}}{t_k - t_{k-1}} \tag{4-10}$$

If the vehicle is four-wheel drive equipped the losses and inertia of the transfer case need to be included:

$$\tau_{o,k} = \frac{1}{\eta_{transfer\ case}(\tau_{o,k-1}, \omega_{o,k-1}) R_{transfer\ case}} \tau_{driveshaft,k} + I_{transfer\ case} \frac{\omega_{o,k} - \omega_{o,k-1}}{t_k - t_{k-1}} \tag{4-11}$$

where τ_o and ω_o are the transmission output torque and rotational speed, respectively,

$$\omega_{o,k} = R_{transfer\ case} \omega_{driveshaft,k} \tag{4-12}$$

and the transfer case ratio, $R_{transfer\ case}$, is usually one.

The transmission model differs from the state-of-the-art vehicle models in that the required transmission input torque and rotational speed for all of the possible transmission gears is calculated given the efficiency, $\eta_{Gx,}$ and rotational inertia of each gear, I_{Gx}:

$$\tau_{t,k} = \frac{1}{\eta_{G_x}(\tau_{t,k-1}, \omega_{t,k-1}) R_{G_x}} \tau_{o,k} + I_{G_x} \frac{\omega_{t,k} - \omega_{t,k-1}}{t_k - t_{k-1}} \tag{4-13}$$

where τ_t and ω_t are the transmission input, i.e., turbine, torque and rotational speed for each corresponding gear, G_x, with gear ratio, R_{Gx}.

$$\omega_{t,k} = R_{G_x} \omega_{o,k} \tag{4-14}$$

Similarly the required torque converter input, i.e., impeller, torque and rotational speed for a plurality of states is considered to meet the transmission input torque and speed demand. When the torque converter is in the open state, the corresponding engine and impeller speed and torque are influenced by the torque converter design characteristics. The parameters used to describe the characteristics of a torque converter are depicted in Figure 2-5 for a typical torque converter. The causality of torque converter K-factor relationship needs to be inverted due to the reverse modeling

approach. A similar K-factor relationship for the torque converter turbine is derived from Equation (2-23), the speed ratio, and torque ratio to determine the torque converter speed ratio and torque ratio in the open state:

$$K - factor_{turbine} = \frac{N_t}{\sqrt{T_t}} \tag{4-15}$$

The torque required at the impeller must also overcome the torque converter turbine inertia. During decelerations where the turbine torque is negative, overrunning K-factor data where the speed ratio is greater than one, i.e., turbine drives the impeller, is used to characterize the torque converter.

When the torque converter clutch is fully engaged, the torque converter's input and output shafts are locked, effectively eliminating any power loss yet losing any of the converter torque multiplication at low speed ratios. In the locked state the engine torque is limited to the torque available at the required turbine speed, which may be insufficient to meet the torque requirements of the vehicle speed profile. In addition, during the locked state, noise, vibration and harshness (NVH) due to torque fluctuations produced by engine combustion are transmitted directly through the drivetrain which adds another constraint to enabling lock-up at low turbine speed conditions. For regions where torque fluctuation does not allow for full lock-up, partial duty cycle control can be applied to the torque converter clutch to allow for some slippage which incurs some power loss but no transmittal of torque fluctuations. The model currently determines whether clutch control should be disabled (LU_{state}=0), enabled (LU_{state}=1), or electronically modulated (LU_{state}=0.5), i.e. partial lock-up (PL), to control to a desired slip, s, where the slip can be input as a constant or as a function of turbine speed. The power loss in partial-lock mode is assumed to be a function of the desired slip and any torque loss is neglected. The

model currently does not have the ability to vary the amount of slip as a function of load but could be modified to include this feature. Clutch control enable mode is constrained by the minimum turbine speed to enable partial lock-up or full lock-up, usually determined by NVH characteristics.

$$if\ N_t < N_{t,LU\ enable},\quad LU_{state} \neq 1 \tag{4-16}$$

$$if\ N_t < N_{t,PL\ enable},\quad LU_{state} \neq 0.5 \tag{4-17}$$

The torque required at the engine must also overcome the torque converter impeller and flywheel inertias.

In the engine model, the required engine torque and rotational speed for each of the torque converter states is considered. The following constraint is added to ensure the engine speed does not fall below the calibrated engine idle speed:

$$N_{e,k} > N_{idle} \tag{4-18}$$

The engine inertia is taken into account as well as the accessory drive loads and inertias, including the power steering, alternator, air conditioning systems and mechanical cooling fan. To overcome one shortfall of the backward-looking modeling approach, a penalty is added to states where the engine torque required exceeds the maximum engine torque available at the corresponding engine speed:

$$\tau_{b,k}(N_{e,k}) < \tau_{e,k}(N_{e,k}) < \tau_{e-\max,k}(N_{e,k}) \tag{4-19}$$

This constraint guarantees that the drivetrain is always in a suitable gear and lock-up state that is capable of meeting the acceleration of the vehicle speed trace. States which do not meet this condition are penalized. For advanced hardware design studies, the user is automatically alerted to situations where the capabilities of the desired powertrain design

are exceeded. The minimum engine torque is determined by the available engine braking, τ_b, which will be discussed in Section 4.3.1.3.

A screen shot of the reverse tractive road load subsystem models can be seen in Figure 4-3. Once vectors of required fuel flows for all of the feasible gear and torque converter lock-up states for each time step are obtained, an optimization routine finds the optimal control path over the cycle that minimizes the accumulated fuel flow.

4.2.3 Dynamic Optimization of Powertrain State Problem Formulation

Once the required fuel flow for all of the powertrain states is determined, the control strategy is formulated as a multi-stage, multi-dimension decision process applied to a discrete time, non-linear dynamic system. The shift schedule and torque converter clutch control strategies have a significant effect on the efficiency and overall fuel economy of the powertrain system. In a stepped transmission, there may be a number of gear ratios with different corresponding transmission input shaft speeds that meet the road load demand at the prescribed wheel speed; the challenge is determining which gear operates the engine at the lowest fuel flow with acceptable drivability. Furthermore, since automatic transmissions are typically equipped with torque converters, the control decision is further complicated by the clutch control interaction effects. The torque converter can be controlled to operate in an open state, a fully-locked state, or a controlled slip state, which also has a considerable impact on the engine operating domain and the overall system efficiency losses.

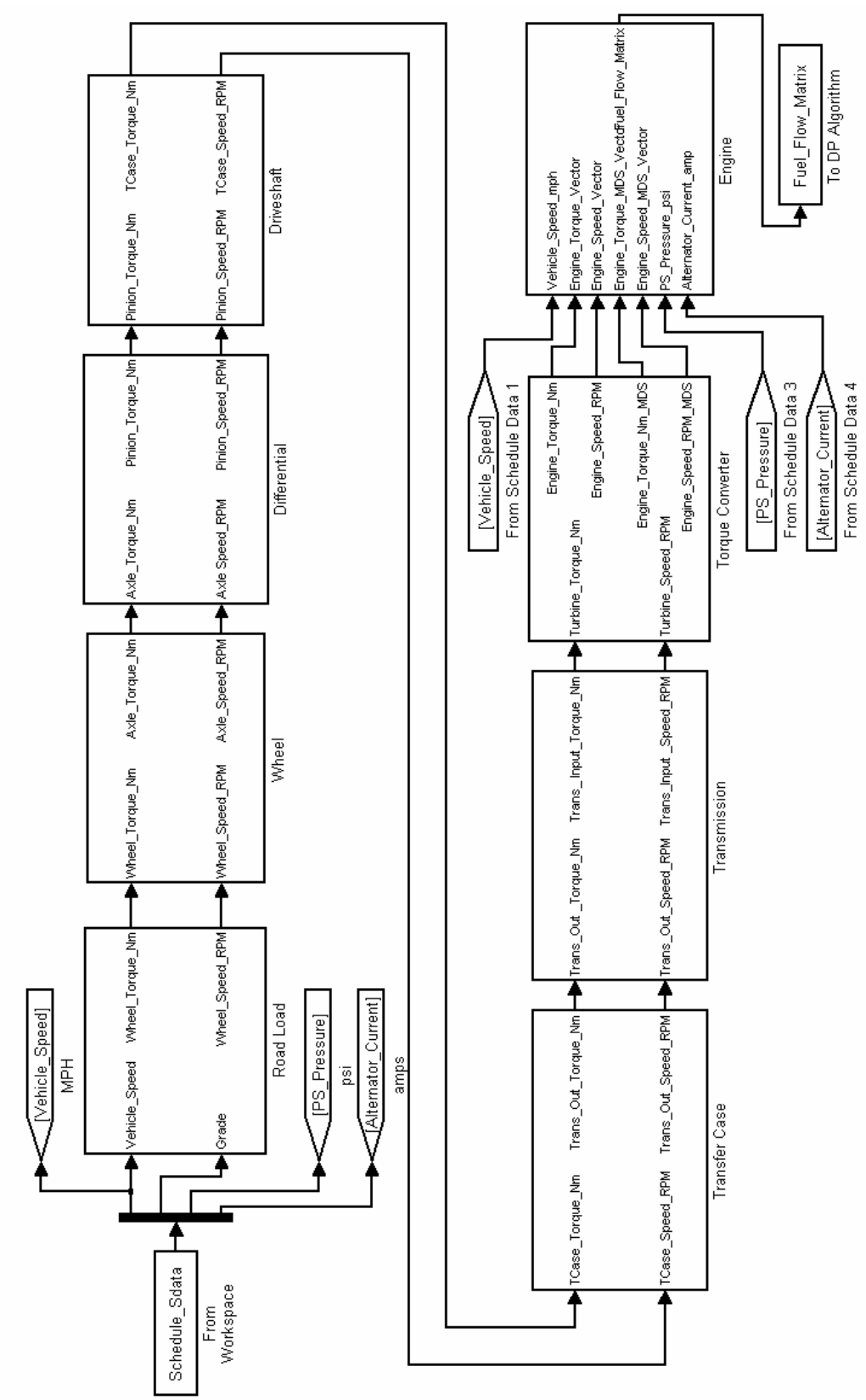

Figure 4-3 Reverse Tractive Road Load Demand Simulink® Model

As the intention is to develop a powertrain control strategy that minimizes the total fuel flow, the objective of the reverse simulation is to minimize the objective function:

$$J = \sum_{k=0}^{N-1} \dot{m}_f(k) \rightarrow \min \tag{4-20}$$

where N is the drive cycle duration and k is the time step. Gear shift scheduling is modeled as a discrete time dynamic system, where the gear state, $G_{x,k}$, is the gear number and the *shift* is constrained by mechanical limitations of the stepped transmission, such as *shift* values of -1, 0, 1 for downshift, no shift and upshift, respectively, or as operation of the specific transmission permits (Note that some transmissions permit some skip shifts, such as 3-1 kickdowns, where *shift* would be permitted to be -2. The tool could be modified to include such constraints).

$$G_{x,k+1} = \begin{cases} G_{x,k}, & no\,shift \\ G_{x+1,k}, & upshift \\ G_{x-1,k}, & downshift \end{cases} \tag{4-21}$$

where $G_{x,k}$ is constrained by:

$$G_{x-\min,k} \leq G_{x,k} \leq G_{x,k-\max} \tag{4-22}$$

In addition to the NVH turbine speed enable conditions described in Section 4.2.2, there are additional constraints imposed when optimizing torque converter state and gear simultaneously. Basic torque converter clutch control assumptions include (1) clutch engagement transient dynamics are ignored, (2) the clutch must engage partial lock-up before engaging full lock-up, (3) the clutch is released for all downshifts, (4) upshifts and clutch engagement cannot occur simultaneously, and (5) full lock-to-lock

upshifts are not permitted except in instances where the specific powertrain clutch hardware under consideration is capable of such maneuvers.

4.2.4 Discrete Deterministic Dynamic Programming

Discrete deterministic dynamic programming (DP) is applied as a model-based system design tool to find the control strategy that maximizes the powertrain efficiency over a desired drive cycle. Dynamic programming is based on Bellman's Principle of Optimality, which states:

> "An optimal policy has the property that whatever the initial state and initial decision are, the remaining decisions must constitute an optimal policy with regard to the state resulting from the first decision (Bellman 1972)."

Bellman's Principle of Optimality suggests that an optimal policy can be constructed in an iterative fashion by first solving the sub-problem at the last time step, *N*, then gradually extending the problem to include the last two time steps, and continuing in this fashion until the optimal policy for the entire problem is determined (Bellman 1972; Bertsekas 2000; Denardo 1982). Figure 4-4 illustrates the concept of dynamic programming using a simple shortest path example:

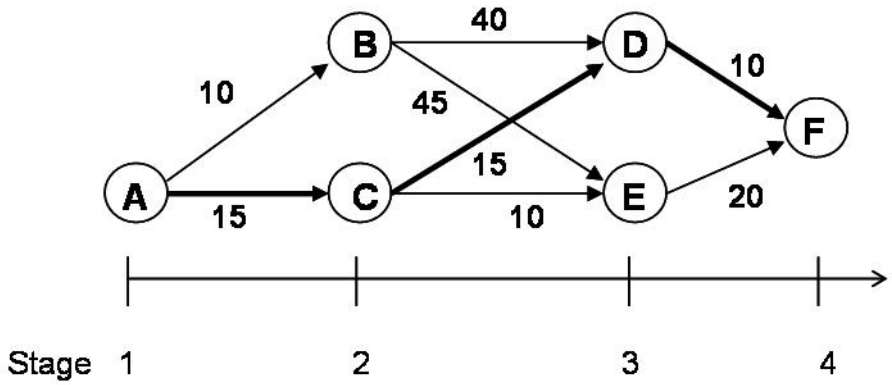

Figure 4-4 Dynamic Programming Shortest Path Example

The circles represent the feasible states and the arrows represent possible control decisions at each stage with an associated transition cost. When trying to determine the optimal path from state A to state F that minimizes the total cost, the problem can be subdivided into four stages. If the decision policy only took into account the subsequent transition cost, the optimal decision at stage one would appear to be to travel to state B since traveling from A to B has the least instantaneous transition cost of ten to arrive at stage two. However it is clear that to minimize the total cost to arrive at stage four the problem must anticipate the corresponding cost-to-go. Dynamic programming allows this problem to be solved numerically by computing a sequence of decisions in a series of computations, each of which has complexity on the order of the computation for a single decision. Thus, the total computation time required grows linearly with the number of stages (i.e., the number of decisions in the sequence), rather than exponentially, as would be the case with algorithms for computing these decisions simultaneously. The computations in Equations (4-23) illustrate how the problem is solved recursively by finding the optimal decision for each state that minimizes the sum of the instantaneous transition cost and corresponding cost-to-go associated with each stage. Upon arriving at the initial state at stage one, an optimal policy with the corresponding optimal path A-C-D-F and a minimum cost of 40 can be concluded.

$$
\begin{aligned}
f_3(D) &= 10 \\
f_3(E) &= 20 \\
f_2(B) &= \min\begin{cases} 40 + f_3(D) \\ 45 + f_3(E) \end{cases} = \min\begin{cases} 40 + 10 \\ 45 + 20 \end{cases} = 50 \\
f_2(C) &= \min\begin{cases} 15 + f_3(D) \\ 10 + f_3(E) \end{cases} = \min\begin{cases} 15 + 10 \\ 10 + 20 \end{cases} = 25 \\
f_1(A) &= \min\begin{cases} 10 + f_2(B) \\ 15 + f_2(C) \end{cases} = \min\begin{cases} 10 + 50 \\ 15 + 25 \end{cases} = 40
\end{aligned}
\tag{4-23}
$$

The advantage of dynamic programming is that the optimal control state at a given time step is not viewed in isolation since control decisions will be ranked against the sum of the present costs and future costs, where the "cost" is the required fuel flow to meet the tractive road load demand. The cost function is additive in the sense that the cost incurred in time, k, accumulates over time. The total cost to be minimized is:

$$J = g_N(x_N) + \sum_{k=0}^{N-1} L_k(x_k, u_k) \tag{4-24}$$

where g_N is the cost at time step N, L_k is the instantaneous transition cost at time step k, and the system is modeled as a discrete time non-linear system of the form,

$$x_{k+1} = f_k(x_k, u_k), \qquad k = 0,1,..., N-1 \tag{4-25}$$

where x_k is the state of the system and u_k is the control variable to be selected at time k. The state and control variables are stored in discrete grids and the optimal global solution is determined by solving for the minimum cost recursively. The first step is to determine the minimum cost to go, J^*, from state, $x_{N\text{-}1}$, at time step, N-1,

$$J^*_{N-1}(x_{N-1}) = \min_{u(N-1)}[g_N(x_N) + L(x_{N-1}, u_{N-1})] \tag{4-26}$$

given the instantaneous transition cost, L, for each decision, u, and continuing backwards in time from $0 \leq k < N$-1,

$$J^*_k(x_k) = \min_{u(k)}[J^*(x_{k+1}) + L(x_k, u_k)] \quad (4\text{-}27)$$

until the first step is reached and the optimal path and minimum accumulated cost for the entire cycle duration is determined.

A flow chart of the reverse dynamic methodology is shown in Figure 4-5. The possible system states, x_k, and control decisions, u_k, are shown in Table 4-3. Incorporating drivability constraints, such as shift busyness beta penalties, also shown in Table 4-3, will be discussed in Section 4.3.1.1. The reverse tractive road load demand model will be extended to cylinder deactivation, also known as Multi-Displacement System (MDS) in Chrysler vehicles and Active Fuel Management (AFM) in General Motors vehicles, in CHAPTER 6.

Table 4-3 Possible Dynamic Programming States and Control Decisions

Possible States, x(k)	Possible Decisions, u(k)	1	2	3	4	5	6	7	8	9	10	11	12	13	14	15	16	17	18	19	20	21	22	23	24
		1	2	3	4	5	6	7	8	1 PL	2 PL	3 PL	4 PL	5 PL	6 PL	7 PL	8 PL	1 LU	2 LU	3 LU	4 LU	5 LU	6 LU	7 LU	8 LU
1		x	Downshift (-1) β							x	Downshift Open (-1-8) β							x	Downshift Open (-1-16) β						
2		No Shift (0)								No Shift Open (0-8) β								No Shift Open (0-16) β							
3		Upshift (+1) β						x		Upshift Open (+1-8) β							x	Upshift Open (+1-16) β						x	
4		PL (+8)								No Shift PL (0)								No Shift PL (0-8) β							
5		MDS Open (+24)								Upshift PL (+1) β							x	Upshift PL (+1-8) β						x	
6		MDS PL (+32)								LU (+8)								No Shift LU (0)							
7		x								Upshift LU (+1+8) β							x	x (+1) *unless hardware permits							
8		x								MDS Open (+16) β								MDS Open (+8) β							
9		x								MDS PL (+24)								MDS PL (+16)							
10		x								MDS LU (+32)								MDS LU (+24)							
11		x								x								x							

Possible States, x(k)	Possible Decisions, u(k)	25	26	27	28	29	30	31	32	33	34	35	36	37	38	39	40	41	42	43	44	45	46	47	48
		1 MDS	2 MDS	3 MDS	4 MDS	5 MDS	6 MDS	7 MDS	8 MDS	1 MDS PL	2 MDS PL	3 MDS PL	4 MDS PL	5 MDS PL	6 MDS PL	7 MDS PL	8 MDS PL	1 MDS LU	2 MDS LU	3 MDS LU	4 MDS LU	5 MDS LU	6 MDS LU	7 MDS LU	8 MDS LU
1		x	Downshift Non-MDS Open (-1-24) β							x	Downshift Non-MDS Open (-1-32) β							x	Downshift non-MDS Open (-1-40) β						
2		No Shift Non-MDS Open (-24)								No Shift Non-MDS Open (-32) β								No Shift Non-MDS Open (-40) β							
3		No Shift Non-MDS PL (-16)								No Shift Non-MDS PL (-24)								No Shift Non-MDS PL (-32) β							
4	x	Downshift MDS Open (-1) β								No Shift Non-MDS LU (-16)								No Shift Non-MDS LU (-24)							
5		No Shift MDS Open (0)							x	Downshift MDS Open (-1-8) β							x	Downshift MDS Open (-1-16) β							
6		Upshift MDS Open (+1) β							x	No Shift MDS Open (-8) β								No Shift MDS Open (-16) β							
7		No Shift MDS PL (0+8)								Upshift MDS Open (+1-8) β							x	Upshift MDS Open (+1-16) β						x	
8		x								No Shift MDS PL (0)								No Shift MDS PL (-8) β							
9		x								Upshift MDS PL (+1) β							x	Upshift MDS PL (+1-8) β						x	
10		x								No Shift MDS LU (+8)								No Shift MDS LU (0)							
11		x								Upshift MDS LU (+1+8) β							x	x (+1) *unless hardware permits							

* x indicates penalty (decision not allowed)

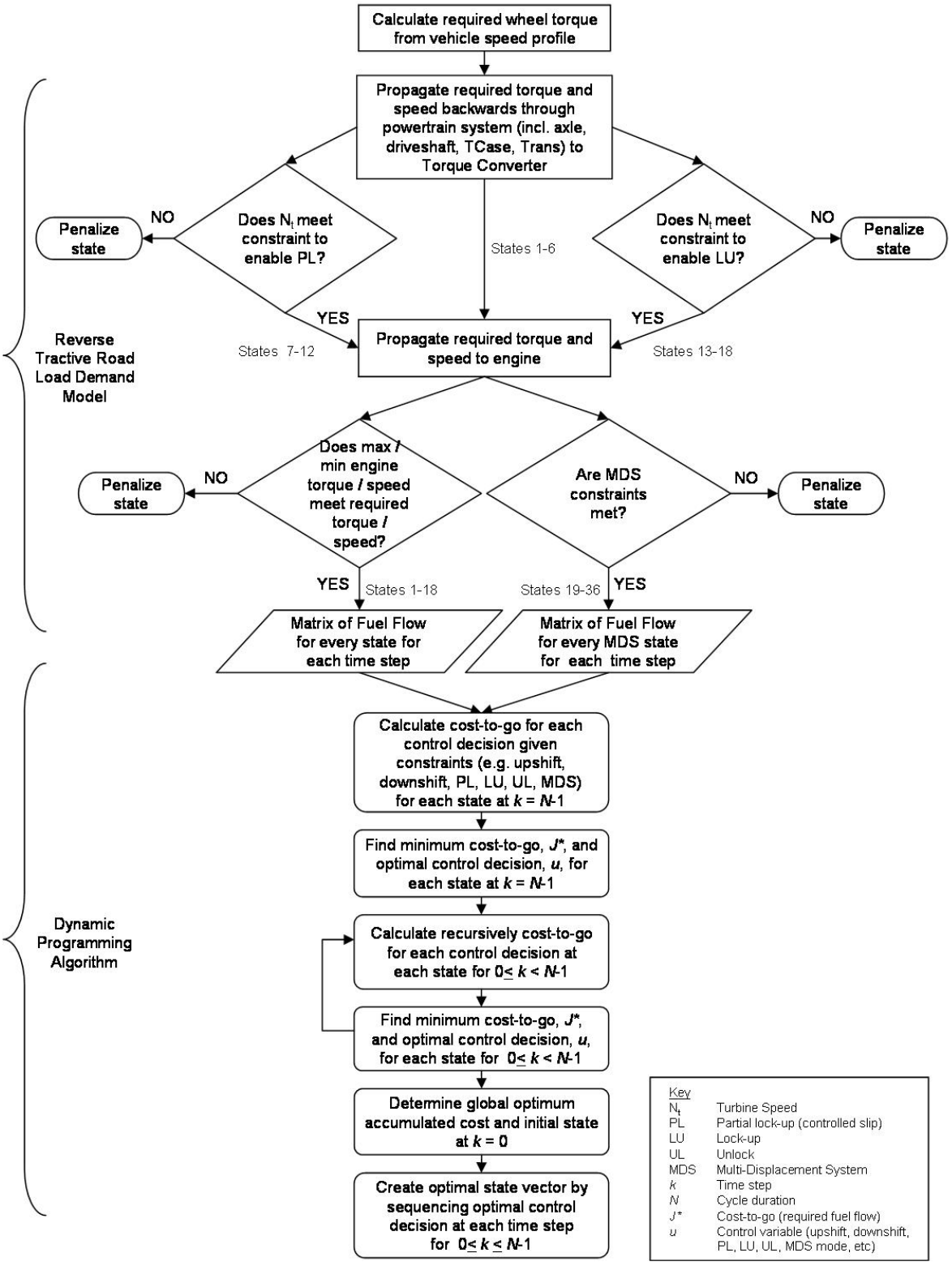

Figure 4-5 Reverse Dynamic Optimization Flow Chart

4.3 Model Correlation and Validation

While the dynamic programming (DP) simulation methodology is not intended to predict the same results as the control strategy implemented in the actual vehicle, it is important that under the same conditions (e.g., gear and lock-up state), the results correlate. To determine the validity of the model, the DP simulation results will be compared to the actual results from a 2700 kilogram full-size 4x4 pick-up truck with a V8 engine and 5-speed transmission in 2WD operation over the FTP urban drive cycle. The DP optimized gear and lock-up state are shown in Figure 4-6. The overall fuel economy measured using the CVS method and the DP fuel economy are shown in Table 4-4. Improvements to the initial simulation results will be discussed in the following sections.

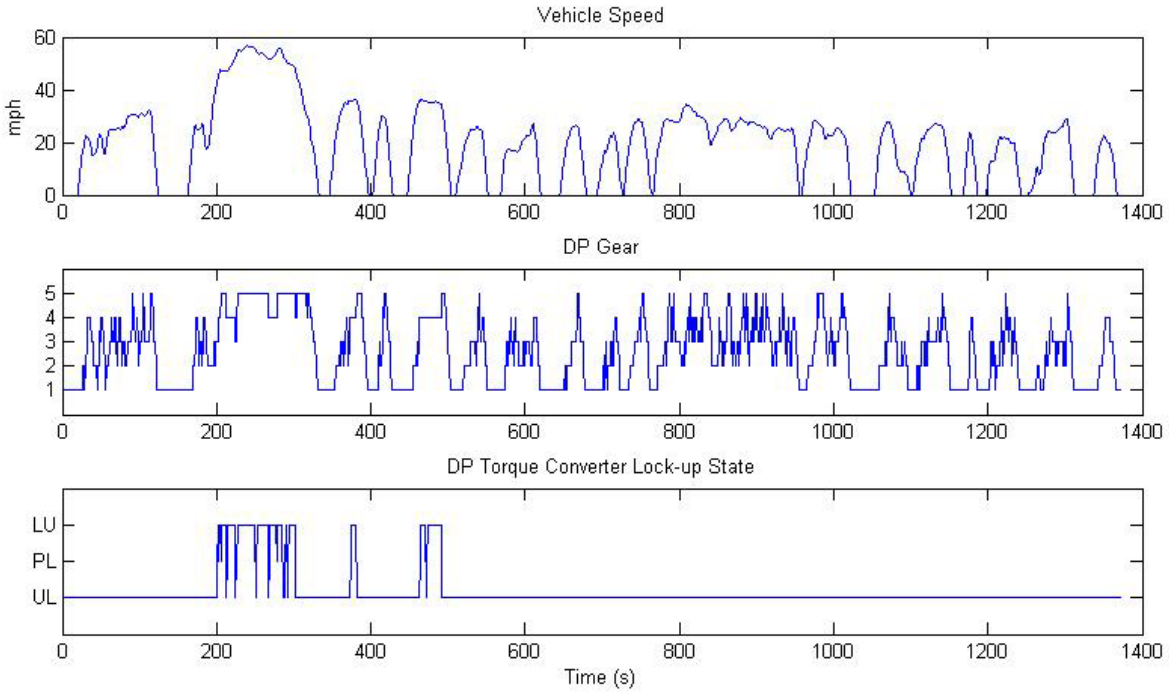

Figure 4-6 Unfiltered Dynamic Programming Optimal Gear and Lock-up State for FTP Urban Drive Cycle

Table 4-4 Actual Fuel Economy Test Measurements vs. Initial Dynamic Programming Simulation Results for FTP Urban Drive Cycle

FTP Urban Fuel Economy Results for 2700 kg Full-size Pick-up with V8 engine, 5-speed transmission	
Average CVS Measurement	14.61 mpg
Unfiltered Dynamic Programming Simulation	15.42 mpg

4.3.1 Drivability Constraints

Shift and torque converter clutch control strategies significantly influence driver perception of ride quality and NVH. A control strategy that is perceived as producing a good feeling is said to have good "drivability". An attempt to incorporate some more realistic driving constraints will be discussed here.

4.3.1.1 Busyness β-penalty

The initial DP results in Figure 4-6 yielded too frequent upshifting, downshifting and torque converter clutch engagements and unlocks, which in practice can yield a busy, disconcerting feeling to the driver. Thus a β-penalty was added to the DP cost function for upshift, downshift, and torque converter disengagements i.e., LU to PL and PL to open torque converter states. The states and control decisions that a β-penalty is specifically applied to can be referred to in Table 4-3.

$$J^*_k(x_k) = \min_{u(k)}[J^*(x_{k+1}) + L(x_k, u_k) + \beta(u_k)] \tag{4-28}$$

Initially the β-penalty was implemented as a constant. The DP results for constant β-penalty values of 0.25 and 0.5 can be seen in Figure 4-7:

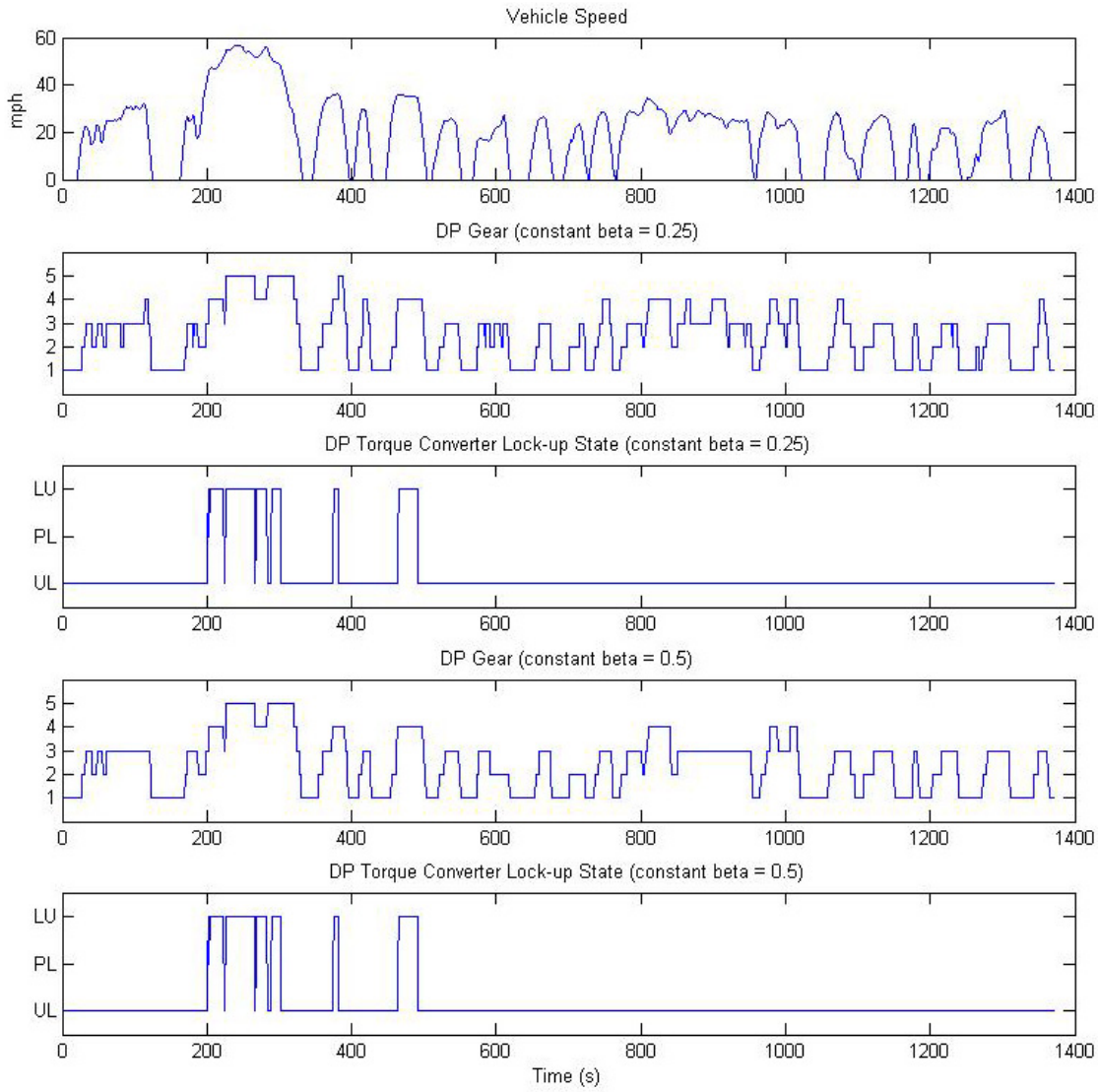

Figure 4-7 Dynamic Programming Optimal Gear and Lock-up State for FTP Urban Drive Cycle with Constant Busyness β-Penalties

After much consideration the β-penalty was changed to be a function of the fuel flow at the current state, x_k, so that the decision takes into account differences in changing states, such as the difference in transmission gear ratio spread. For instance, the β-penalty for a 1-2 upshift would be more than for a 4-5 upshift since the corresponding fuel flow delta between first and second gear is higher.

$$J^*_k(x_k) = \min_{u(k)}[J^*(x_{k+1}) + L(x_k, u_k) + \beta(u_k)L(x_k, u_k)] \quad (4\text{-}29)$$

where the β-penalty is a percent of the fuel flow associated with the instantaneous transition cost, $L(x_k, u_k)$.

Figure 4-7 shows the DP results where β is a percent of the instantaneous transition cost with values of 25% and 50%. The corresponding fuel economy for various penalties is shown in Table 4-5. It is important to note that a β-penalty of 0.5 and 50% are not equivalent since a 0.5 value represents a constant, whereas a 50% value represents a percentage of the fuel flow associated with transitioning states. The subsequent analyses will be performed with a β-penalty of 50% unless otherwise noted.

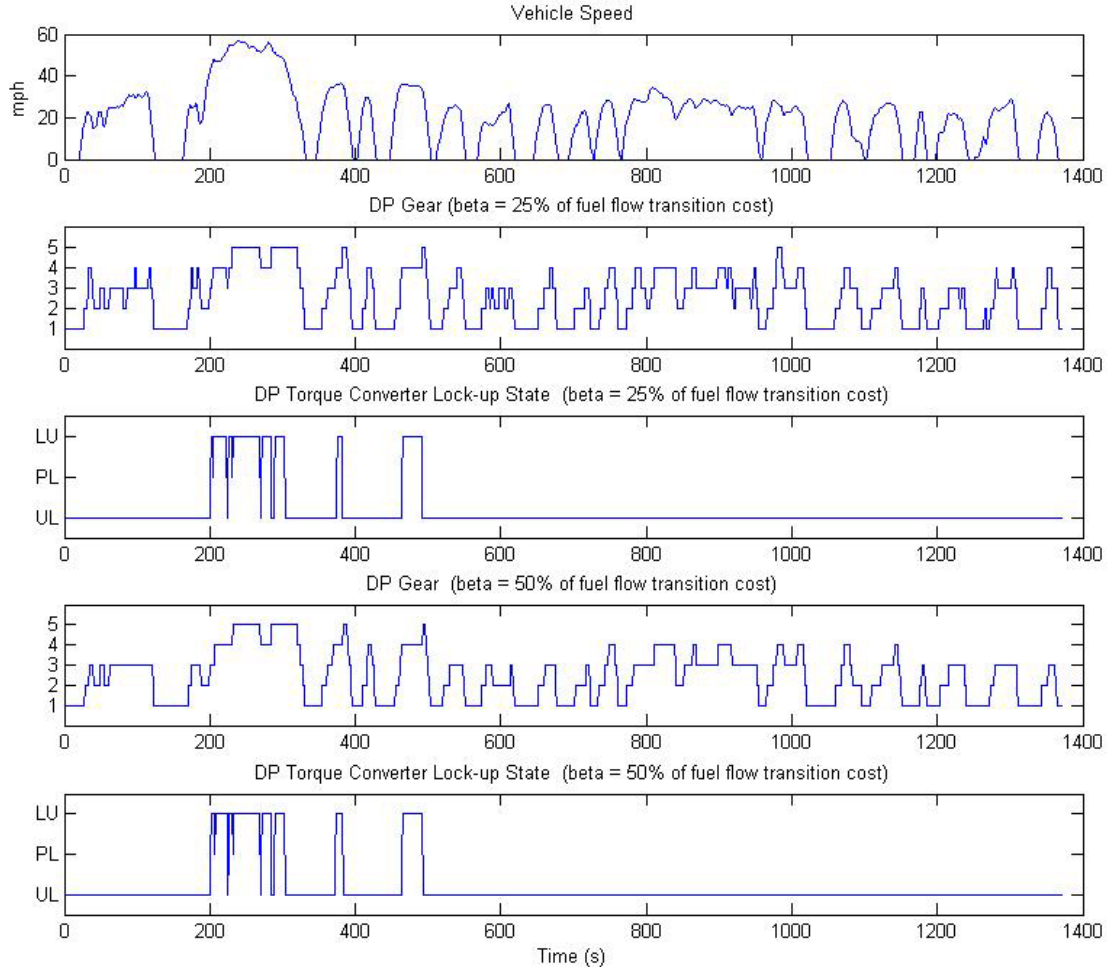

Figure 4-8 Dynamic Programming Optimal Gear and Lock-up State for FTP Urban Drive Cycle with Percent of Instantaneous Transition Cost Busyness β-Penalties

Table 4-5 Dynamic Programming Simulation Fuel Economy for Various Busyness β-Penalties

FTP Urban Fuel Economy Results for 2700 kg Full-size Pick-up with V8 engine, 5-speed transmission	
Dynamic Programming Simulation $\beta = 0.25$ (constant)	15.22 mpg
Dynamic Programming Simulation $\beta = 0.5$ (constant)	15.07 mpg
Dynamic Programming Simulation $\beta = 25\%$ (percent of fuel flow transition cost)	15.22 mpg
Dynamic Programming Simulation $\beta = 50\%$ (percent of fuel flow transition cost)	15.02 mpg

4.3.1.2 Minimum Engine Speed After Upshift

Upshifting too early can produce a disturbing feeling that the vehicle is malfunctioning or is underpowered. An example of this occurs when a driver of a manual transmission upshifts too early and senses the engine is lugging. Consequently a lug limit or minimum engine speed after upshift (MESAU) constraint is incorporated into the DP algorithm to avoid this situation. Figure 4-9 depicts the DP simulation results for a portion of FTP urban drive cycle and indicates how incorporating a MESAU constraint delays upshifting.

Table 4-6 reveals that incorporating a MESAU constraint only minimally affects the fuel economy on an automatic transmission with a lock-up clutch. The reason the fuel economy is barely affected is due to the fact the torque converter lock-up is constrained to not enable until a minimum turbine speed of 1100 rpm is reached. Thus the DP control policy tends to not upshift until a high enough turbine speed is obtained to enable lock-up since lock-up generally results in a lower fuel flow. In other words, the torque converter minimum turbine speeds to enable lock-up already indirectly serve as a MESAU constraint.

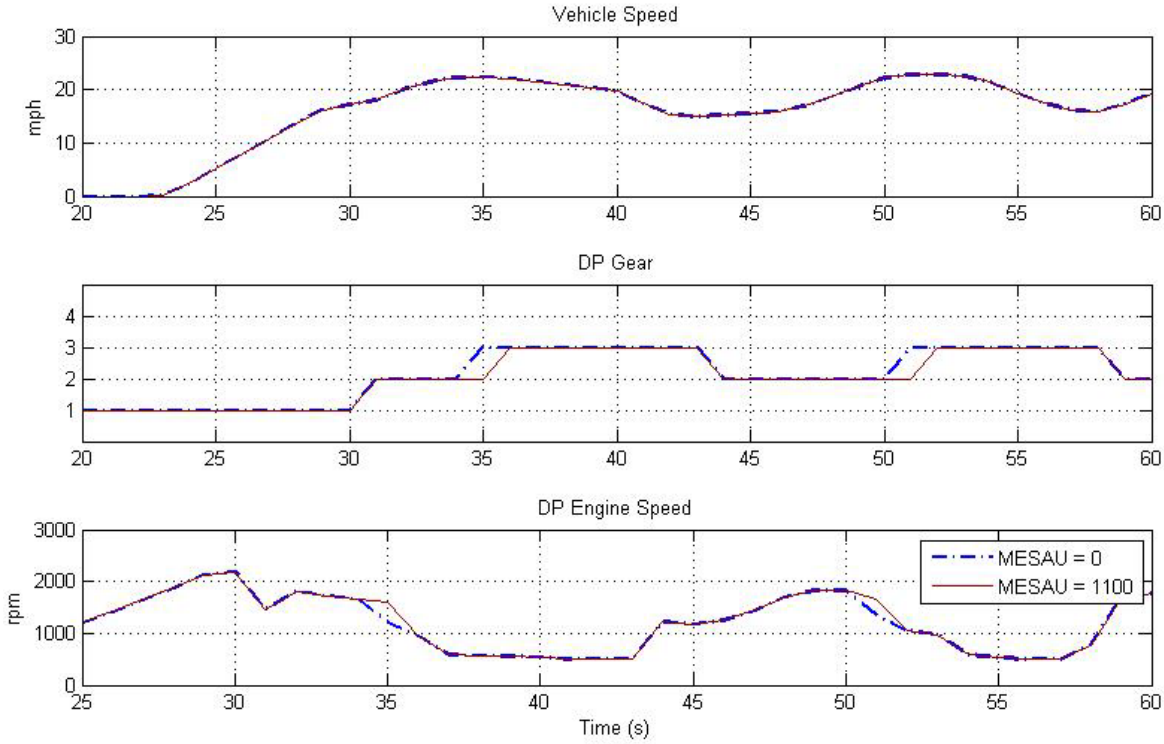

Figure 4-9 Comparison of DP Simulation Results with Minimum Engine Speed After Upshift (MESAU) Constraint

Table 4-6 DP Simulation Fuel Economy with Minimum Engine Speed After Upshift (MESAU) Constraint

FTP Urban Fuel Economy Results for 2700 kg Full-size Pick-up with V8 engine, 5-speed transmission	
Dynamic Programming Simulation β = 50%, MESAU = 0	15.02 mpg
Dynamic Programming Simulation β = 50%, MESAU = 1100	15.00 mpg

The importance of a MESAU constraint becomes more evident when low-speed lock-up is enabled or when the reverse model and DP algorithm are extended to dual clutch transmissions (DCT), also known as automated manual transmissions, in Section 7.4. Since in a DCT there is continuous flow of power from the engine to the wheels, the engine often delivers enough torque to the wheels and could theoretically deliver better fuel flow by upshifting much earlier compared to a conventional automatic transmission with a torque converter due to its inherent viscous coupling losses. However a MESAU

constraint must be incorporated when modeling a DCT since minimum turbine lock-up speeds do not apply when modeling a DCT and since too early upshifts are unreasonable and would give a feeling to the driver that the vehicle is lugging or does not have significant acceleration capability.

4.3.1.3 Engine Braking

During decelerations, road load, driveline drag and calibrated engine braking are all forces that help to slow a vehicle down subsequently requiring less driver mechanical braking (i.e., the driver depressing the brake pedal). The contribution of the road load and neutral driveline drag is incorporated in the model via the force due to the *A*, *B*, and *C*-coefficients in Equation (2-25). However, if the deceleration force is greater than what is available due to the road load, additional braking must come in the form of either mechanical braking or calibrated engine braking.

Figure 2-7 depicts the power required to decelerate a vehicle after taking the road load into account during the first portion of the FTP urban cycle. Engine braking can be calibrated by reducing the airflow to the engine, either via closing the throttle for electronic throttle engines or closing the idle air control valve for manual throttle engines, until the engine undergoes a negative torque or motoring condition. The amount of engine braking calibrated is a trade-off between brake pad wear, fuel economy, and deceleration feel when the driver lifts his or her foot off the accelerator pedal.

Due to the backward-looking approach of the model, it becomes challenging to determine the contribution of mechanical braking and calibrated engine braking since the amount of engine braking in terms of deceleration force at the wheel depends on the engine speed, i.e., powertrain state, and the optimal state is not determined until dynamic

programming algorithm is executed. The initial reverse optimization simulation results assumed that the equivalent newtons of deceleration force required to decelerate one mile per hour per second or faster would be compensated with mechanical braking and any equivalent deceleration force less than that would be propagated through the reverse model as required engine braking. It was assumed that the engine could provide the necessary engine braking to decelerate at a rate less than one mile per hour per second. This assumption did not reflect reality since the resulting required braking force could be greater than the engine braking torque available under a given engine speed condition. In other words, the initial simulation results often assumed the engine could provide more braking than physically possible since there was no feedback as to how much engine braking is actually available.

Consequently, the engine braking available was included in the reverse model in the form of a minimum manifold air pressure constraint for manual throttle engines and a minimum torque request for electronic throttle engines. The required engine speed, N_e for all the possible states is determined in the torque converter model and used to determine the amount of engine braking torque, τ_b, available in each state at the subsequent time step (refer to Figure 4-10) .

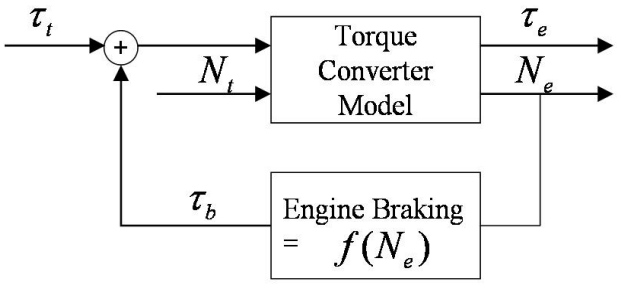

Figure 4-10 Calibrated Engine Braking Torque Feedback

The simulated results both with and without engine braking feedback are shown in Figure 4-11. The figure depicts the simulation parameters both with and without incorporating a minimum manifold air pressure (MAP) constraint. The dotted trace represents the model with no engine braking feedback and thus assumes a more negative engine torque and torque converter slip compared to the improved engine braking model. The improved engine braking model better reflects reality. The corresponding fuel economy with engine braking feedback is shown in Table 4-7.

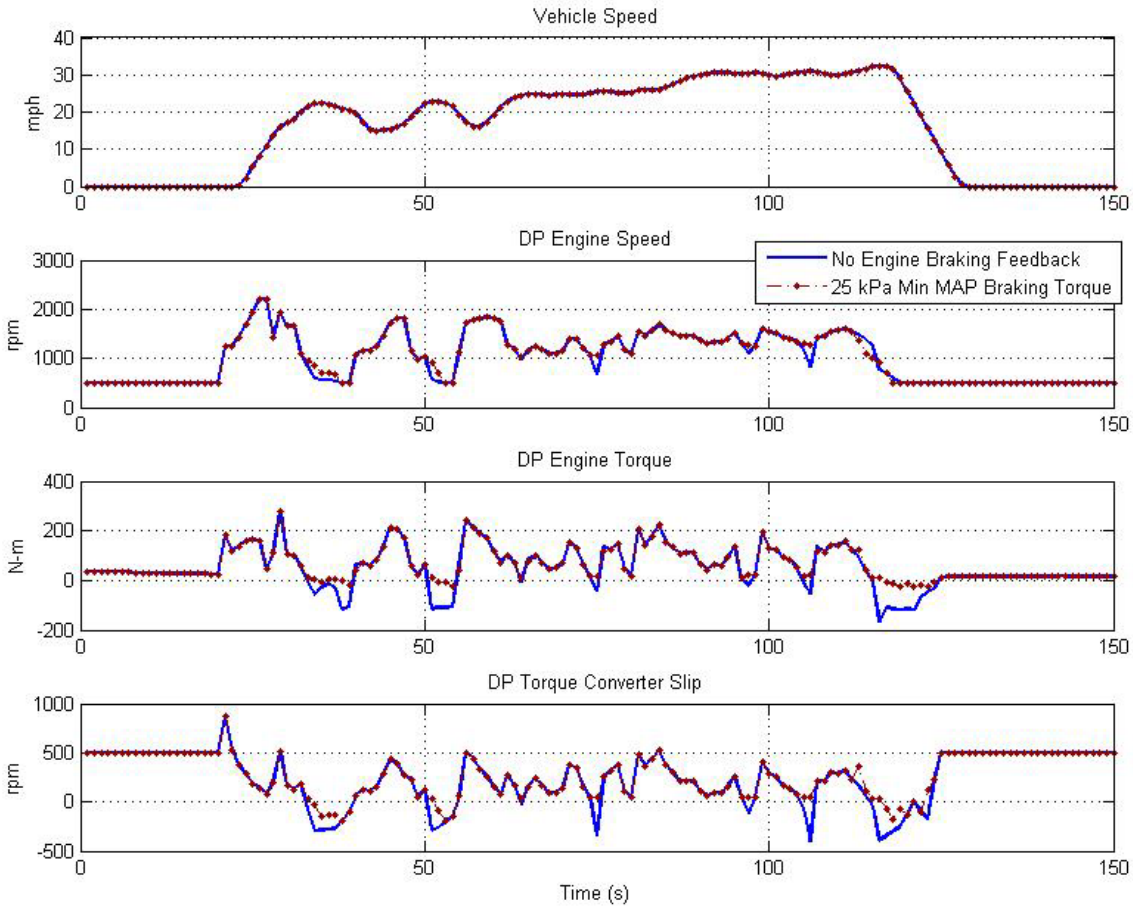

Figure 4-11 Comparison of DP Simulation Results with Engine Braking Feedback

As expected, the results in Table 4-7 reveal that as the calibrated engine braking is increased, i.e., the minimum MAP constraint is decreased by closing the idle air control valve or throttle, the fuel economy improves. This occurs since closing the throttle

results in a lower air flow corresponding to less fuel flow required. This phenomenon only occurs with engines that are not calibrated to shut off the fuel during decelerations. Currently deceleration fuel shut off is not considered in the reverse model and dynamic optimization algorithm.

Table 4-7 DP Simulation Fuel Economy with Minimum Manifold Air Pressure (MAP) Constraint

FTP Urban Fuel Economy Results for 2700 kg Full-size Pick-up with V8 engine, 5-speed transmission	
Dynamic Programming Simulation β = 50%, MESAU = 1100, No Engine Braking Feedback	15.00 mpg
Dynamic Programming Simulation β = 50%, MESAU = 1100, **Min MAP = 30 kPa**	14.62 mpg
Dynamic Programming Simulation β = 50%, MESAU = 1100, **Min MAP = 25 kPa**	14.90 mpg

A minimum MAP constraint of 25 kPa is consistent with the calibration strategy for the engine in this study and will be used for the remainder of the simulations. The DP simulation results that take into account the aforementioned drivability constraints will be compared to actual chassis dynamometer data in Sections 4.3.2 and 4.3.3.

4.3.2 Simulation Comparison to FTP Chassis Dynamometer Results

The DP simulation results from the reverse tractive road load demand model demonstrate its predictive capability and optimization potential. It is important to reiterate that the dynamic optimization simulation is not intended to predict the same results as the control strategy implemented in an actual vehicle; instead, a sequence of gear and lock-up control decisions is selected that minimizes the accumulated fuel flow over the cycle. Nevertheless, it is important that under the same gear and lock-up conditions the results correlate.

The DP simulation gear and lock-up states for the FTP urban drive cycle for a full-size loaded pick-up with a 5-speed automatic transmission are shown in Figure 4-12.

A similar vehicle with the identical turbine speed constraints for fourth and fifth gear lock-up was tested on a chassis dynamometer rolls using the CVS method, the EPA's preferred method of measuring fuel economy, and the modal exhaust bench. A comparison of the simulation versus measurements for a portion of the urban cycle is shown in Figure 4-13.

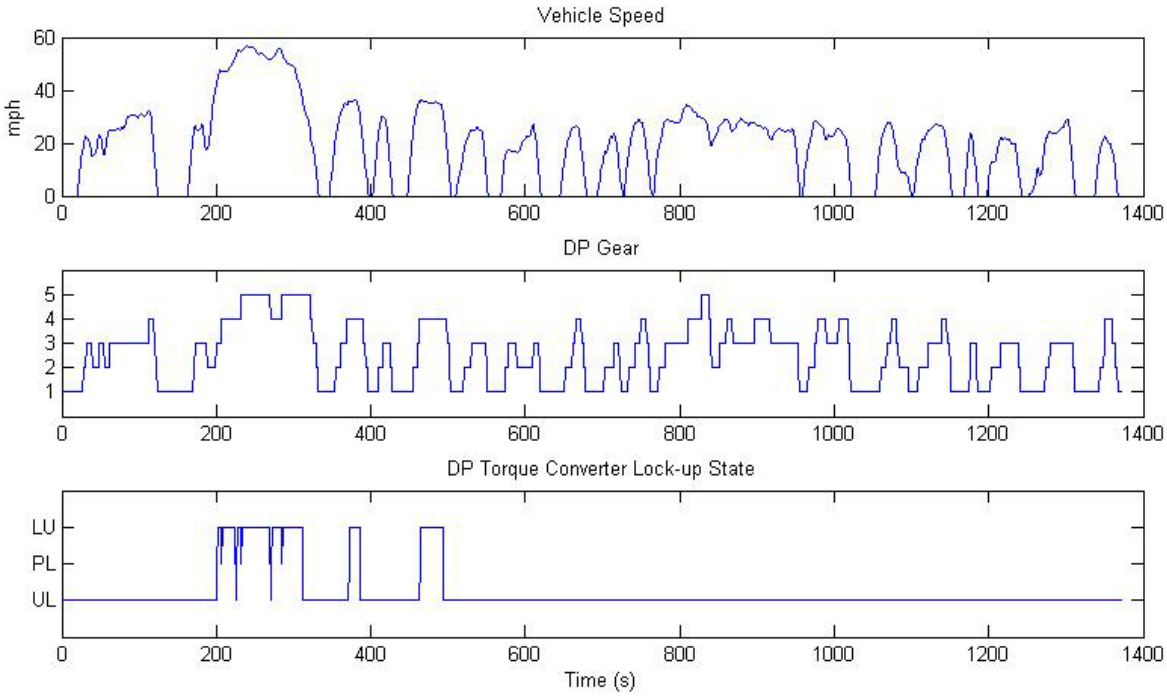

Figure 4-12 FTP Urban DP Gear and Torque Converter Lock-up States

Figure 4-14 depicts a comparison of the highway results. Table 4-8 compares the DP simulated fuel economy versus the measured constant volume sampling (CVS) and modal exhaust fuel economy. Table 4-8 also shows the standard deviations of the measured results revealing that a considerable degree of variability is inherent with chassis dynamometer fuel economy measurements. Some of the simulation discrepancies can be attributed to the fact that transient effects and calibrations such as deceleration fuel shut off and rolling idle speeds are not represented in the DP results. Certain

discrepancies in the torque converter slip exist since the K-factor is assumed to be solely a function of speed while in actuality the K-factor also depends on torque at low speed ratios. Also it is sometimes difficult to control to the desired slip during actual driving conditions. Even so, given that the standard deviation of chassis dynamometer test measurements is typically between 0.2 and 0.5 miles per gallon, the DP method can reliably predict the potential fuel economy of different powertrain system designs.

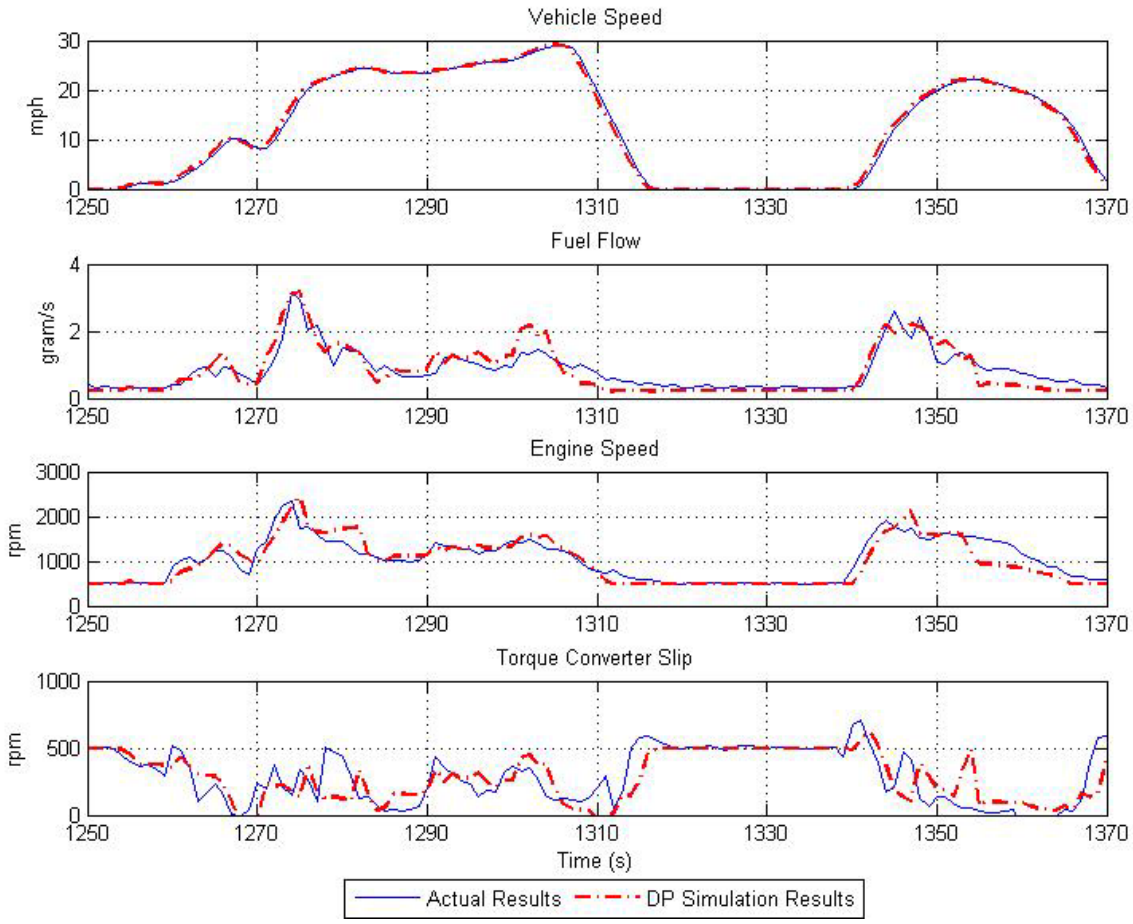

Figure 4-13 FTP Urban Test Measurements vs. DP Simulation Results

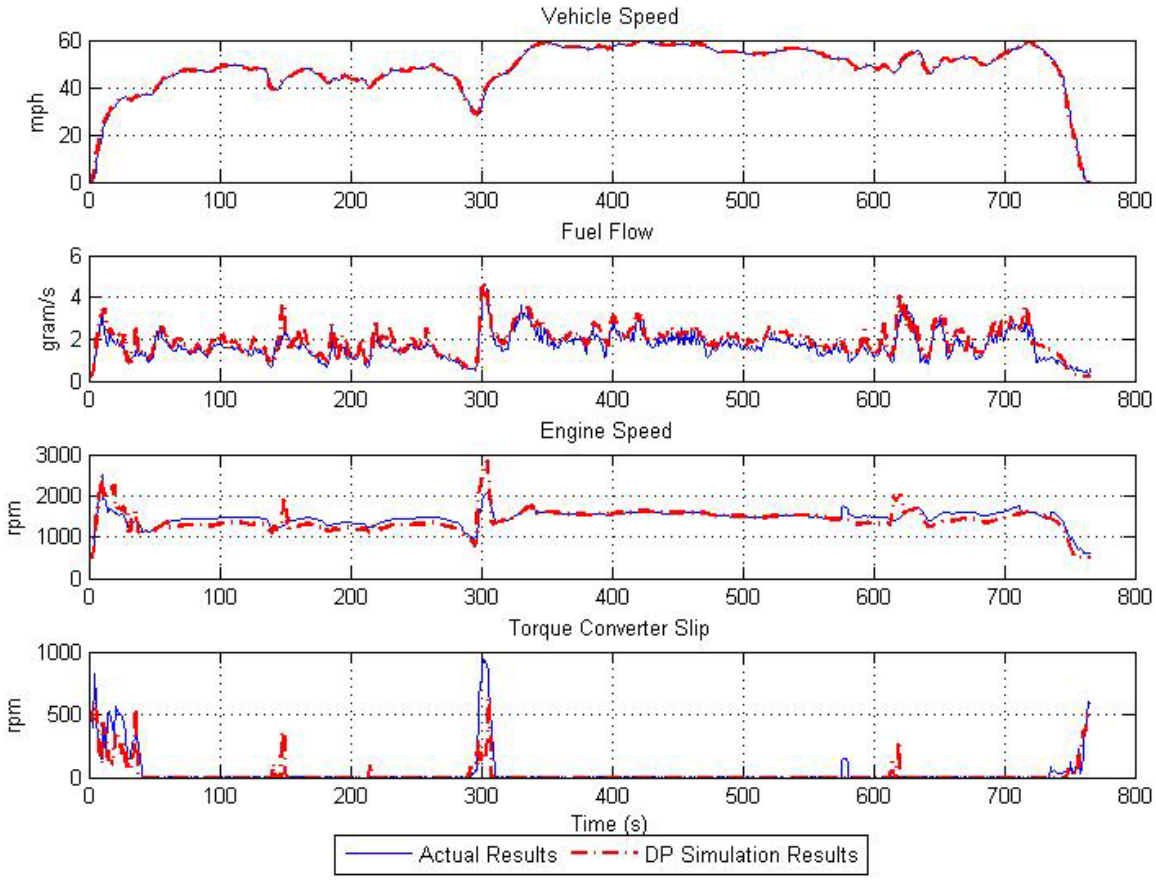

Figure 4-14 FTP Highway Test Measurements vs. DP Simulation Results

Table 4-8 DP Simulation Fuel Economy Results vs. CVS and Modal Measurements

Drive Cycle	DP Simulation	CVS Measurement / (Standard Deviation)	Modal Measurement / (Standard Deviation)
FTP Urban	14.90 mpg	14.61 (0.34) mpg	14.32 (0.57) mpg
FTP Highway	20.90 mpg	21.23 (0.15) mpg	21.66 (0.24) mpg

4.3.3 Simulation Comparison to Consumer Drive Cycles

The FTP urban and highway drive cycles have acceleration rates and driving speeds that are generally seen as lower than those experienced by drivers in the real world and for some drivers the federal fuel economy rating is very difficult to achieve. For this reason, the reverse model and dynamic programming algorithm will be compared

to more aggressive consumer cycles. Recently many consumers rely on the Consumer Reports® (CR) magazine ratings to evaluate fuel economy (http://www.consumerreports.org). Consumer Reports measures fuel economy on road and on their test track using pre-defined driving cycles. A comparison of the CR cycles versus the FTP cycles is shown in Table 4-9.

Table 4-9 Comparison of FTP and Consumer Reports® Drive Cycles

	Maximum Speed	Maximum Acceleration	Maximum Deceleration	Maximum Grade
FTP Urban	56.7 mph (25.4 m/s)	3.3 mph/s (1.5 m/s²)	-3.3 mph/s (-1.5 m/s²)	0
FTP Highway	59.9 mph (26.8 m/s)	3.2 mph/s (1.4 m/s²)	-3.3 mph/s (-1.5 m/s²)	0
CR City	43.4 mph (19.4 m/s)	5.7 mph/s (2.5 m/s²)	-7.4 mph/s (-3.3 m/s²)	0
CR Highway	65 mph (29.1 m/s)	0	0	3 percent

Speed and road grade traces representing the CR city and highway fuel economy drive cycles were inputted into the DP simulation as well as tested on a chassis dynamometer. The CR city cycle consists of aggressive accelerations followed by aggressive braking maneuvers and the CR highway cycle consists of steady-state 65 mile per hour driving with rolling hills and a maximum road grade of three percent. A comparison of the DP simulation versus chassis dynamometer results for the CR cycles are shown in Figure 4-15 and Figure 4-17. The DP optimized gear and torque converter state are shown in Figure 4-16 and Figure 4-18. The CVS measurement and DP simulation fuel economy, as well as test standard deviation and simulation error are shown in Table 4-10.

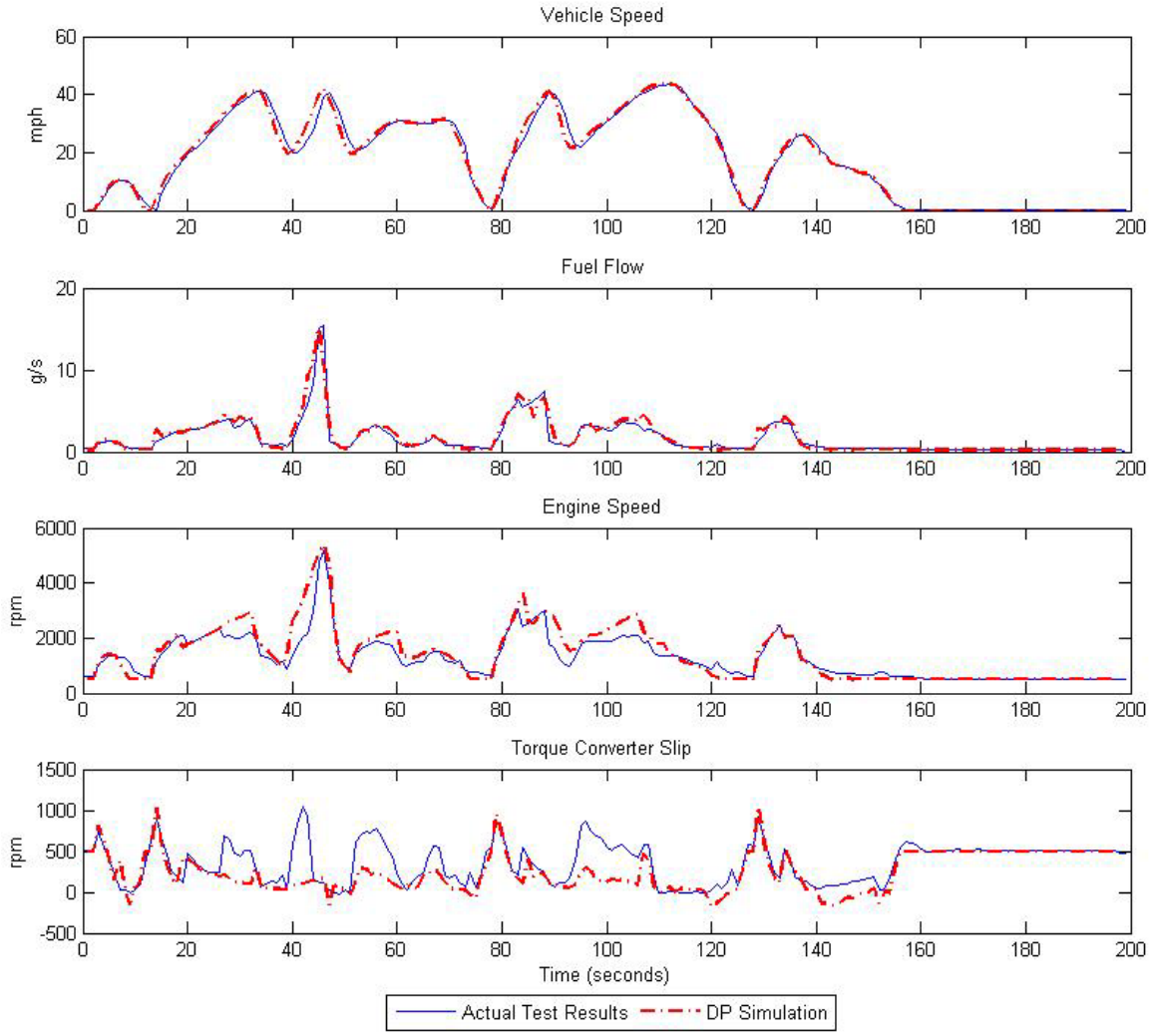

Figure 4-15 CR City Measurements vs. DP Simulation Results

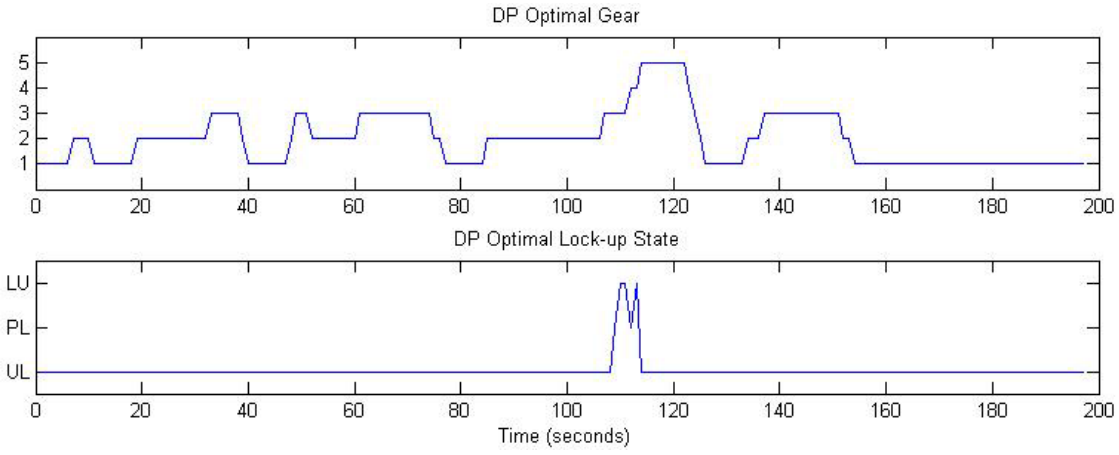

Figure 4-16 CR City DP Gear and Torque Converter Lock-up States

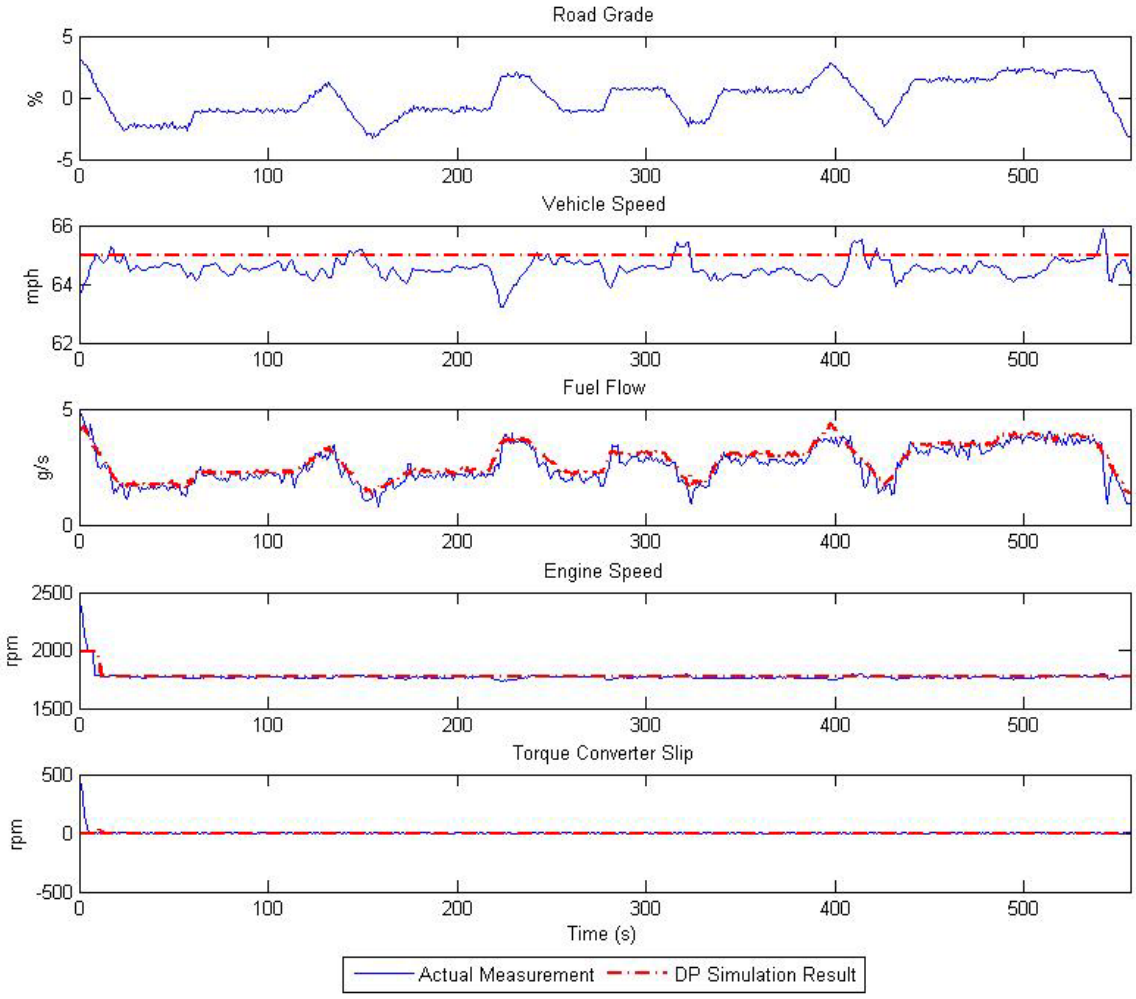

Figure 4-17 CR Highway Measurements vs. DP Simulation Results

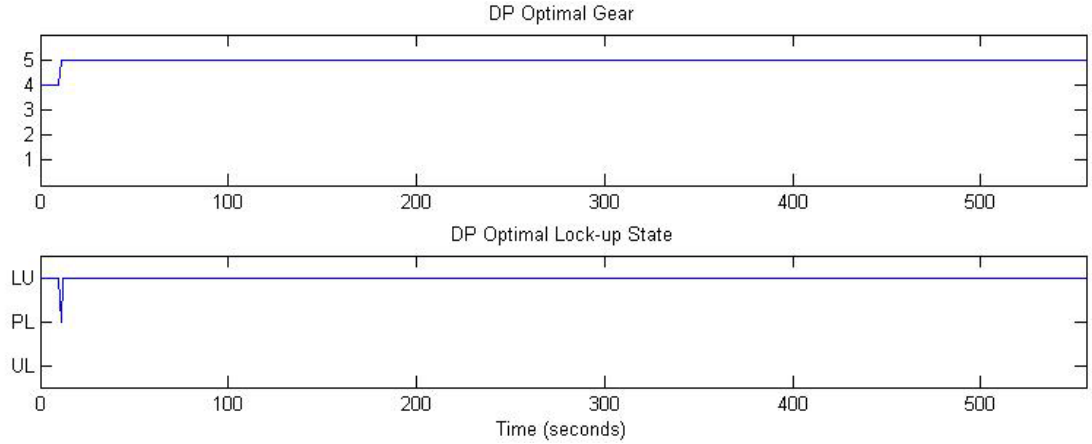

Figure 4-18 CR Highway DP Gear and Torque Converter Lock-up States

Table 4-10 CR Cycle CVS Measurements vs. DP Simulation Results

Drive Cycle	DP Simulation	CVS Measurement / (Standard Deviation)
CR City	8.32 mpg	8.81 (0.24) mpg
CR Highway	18.38 mpg	18.51 (0.17) mpg

Additional discrepancies occur in the data since the chassis dynamometer results consist of human error. Drivers often do not follow the vehicle speed trace precisely either due to anticipation or lagging behind the trace. For instance, the CR highway cycle includes steady-state 65 mile per hour driving with rolling hills. While the simulation can maintain 65 mile per hour even with grade disturbances, it is very difficult for the driver to precisely maintain constant speed. After close inspection of the measured driver speed on the dynamometer in Figure 4-17, the driver does not maintain 65 miles per hour as the road grade increases. Such driver deviation from the trace accounts for some of the simulation fuel economy discrepancy. Moreover driver error and variability makes it difficult to measure small changes in fuel economy on the chassis dynamometer. An attempt to model the driver influence on fuel economy is described in Section 4.3.4

4.3.4 Incorporation of Driver Filter

Figure 4-19 depicts a portion of the actual CR city drive cycle test trace that a chassis dynamometer driver, often referred to as a rolls driver, tries to follow with a cursor. Per federal standards, as long as the driver keeps the cursor within two miles per hour than highest and lowest point on the trace within one second, the test is considered valid. Speed variations greater than these limits, such as those that occur with gear changes or braking spikes, are acceptable provided they occur for less than 2 seconds (Federal Regulation 59 16296 1994). However, even if the driver meets these

specifications and produces a valid test, how closely the driver's cursor follows the trace can notably affect the fuel economy results. The actual vehicle velocity for two different rolls drivers is also shown in Figure 4-19. It can be seen that during aggressive accelerations the drivers lag behind the trace. It should also be noted that maximum speed at 45 seconds is not attained by either rolls driver.

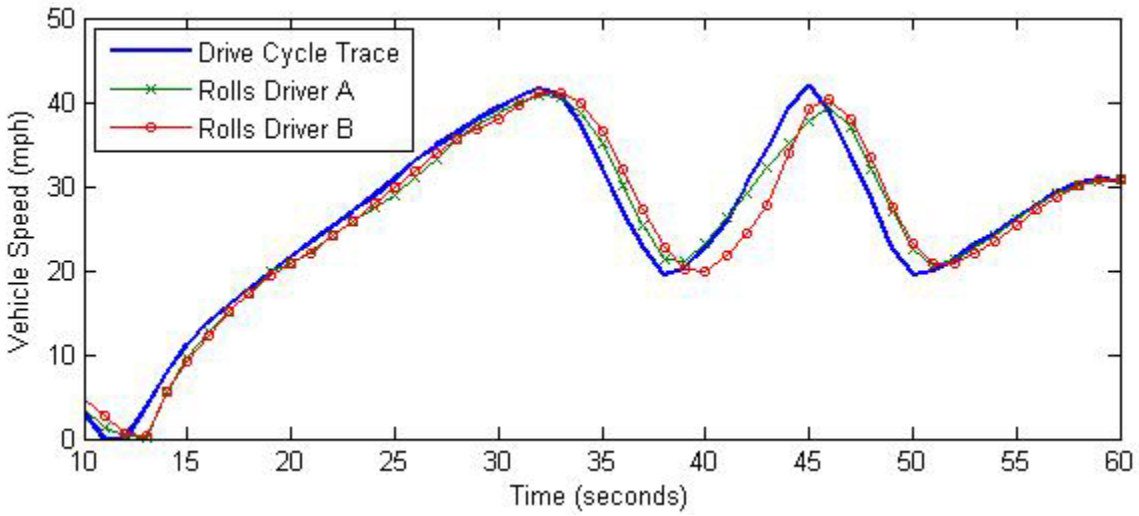

Figure 4-19 Comparison of Drive Cycle Trace and Chassis Dynamometer Drivers

Since it is impossible for a human driver to follow the trace exactly, a driver filter was added to the reverse model in an attempt to reflect the driver influence on the fuel economy results (refer to Figure 4-20). A driver filter constant was included as a parameter to simulate how much the driver lags behind the trace during the accelerations. A driver filter constant of one reflects cursor correct and the lesser the constant, the more the driver deviates from the drive cycle trace. Table 4-11 depicts that as the filter constant is reduced, the simulation driver velocity lags the drive cycle trace and the fuel economy improves. Figure 4-21 compares the cursor correct trace to a trace with a driver filter of 0.65, which produces a velocity profile similar to the actual rolls drivers in

Figure 4-19. Table 4-11 reveals that the fuel economy results for a driver filter value of 0.65 closely approaches the average of ten CVS chassis dynamometer test measurements.

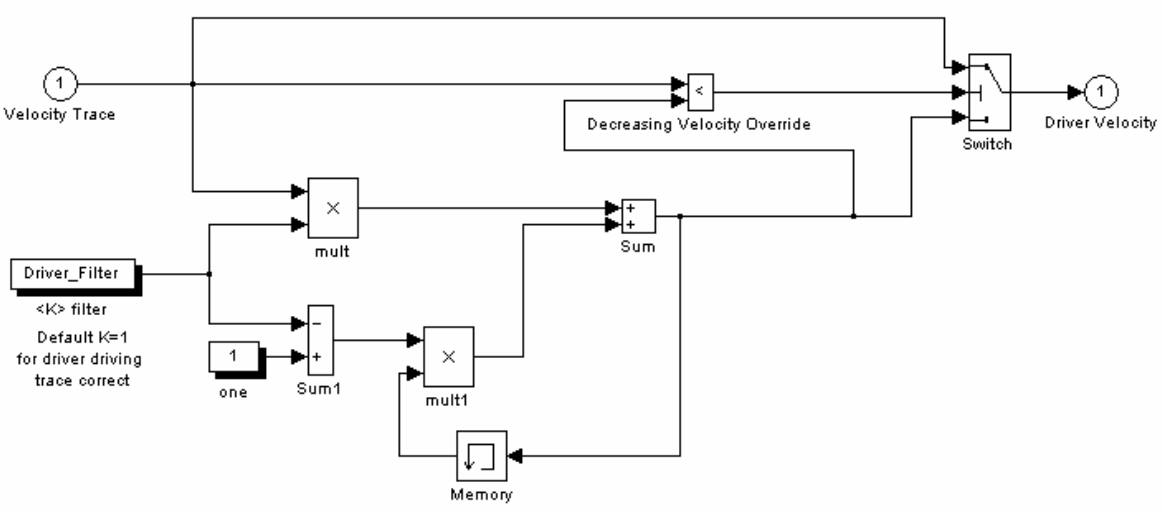

Figure 4-20 Driver Filter Model to Simulate Driver Lag during Accelerations

Table 4-11 Comparison of DP Simulation Results with and without Driver Filter

Consumer Reports® Fuel Economy Results for Full-size Pick-up with V8 Engine, 5-speed Transmission	
Average of 10 CVS Chassis Dynamometer Measurements	8.81 mpg
DP Simulation **No Driver Filter (i.e., Driver Filter = 1)**	8.32 mpg
DP Simulation **Driver Filter = 0.8**	8.66 mpg
DP Simulation **Driver Filter = 0.65**	8.87 mpg

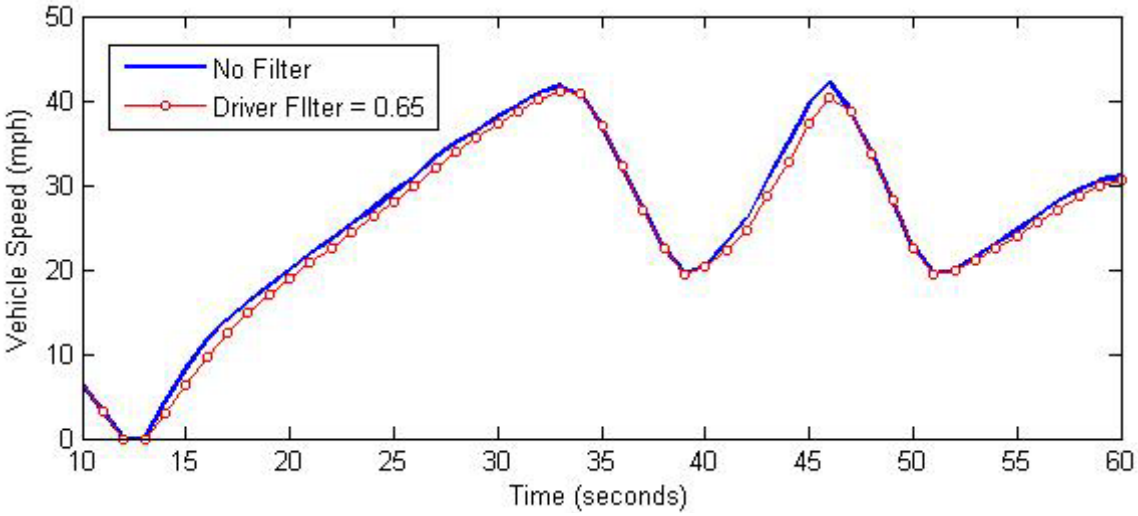

Figure 4-21 Simulation Driver Trace with and without Driver Filter

The driver filter analysis was included to demonstrate the variability in the fuel economy results due to driver error. One benefit of the simulation approach is that it eliminates driver variability and other test to test variation associated with evaluating potential powertrain control strategies and hardware configurations. Since the intention is for the driver to follow the trace precisely, subsequent simulations will be performed without a driver filter.

4.4 Reverse Dynamic Optimization Methodology Assumptions and Limitations

Since the tool is intended to rapidly study system level vehicle efficiency effects, some assumptions and limitations are included to simplify the simulation and reduce run times. Ignition and engine speed start-up flare that are included in some drive cycles, such as the EPA FTP75 cycle, are neglected. Currently the model assumes idle when vehicle speed is zero. Only fully warm cycles were considered to validate the model since the temperature effects are not taken into account. While powertrain efficiency and

optimal shift and lock-up control strategies may differ during warm-up because the efficiency of driveline and accessory components can heavily depend on operating temperature, the focus of this research will remain on the optimization of the powertrain system during standard operating temperatures since the majority of driving occurs during these conditions.

Some additional limitations are assumed insignificant considering the intended application of the tool is to evaluate powertrain system efficiency. Since the model operates at one second time steps and assumes quasi steady-state, transient effects are not represented. Given that the primary research objective is to investigate system level effects and overall fuel economy over a cycle, transient effects that occur much faster than one hertz can be ignored. Also seeing as the model is backward-looking and the component efficiency maps are a function of input speed and load, the efficiency is calculated with a one time step delay. This assumption can still produce reliable results since significant step changes in load do not typically occur.

Other limitations inherent to the backward-looking approach were specifically addressed during the development of this new reverse dynamic methodology. One weakness of traditional backward-looking models is the assumption that the drive cycle trace is met. As a result, they fall short when the accelerations of the speed trace exceed the capabilities of the powertrain. To address this shortfall, a penalty was added to states that exceed the maximum engine torque available (refer to Section 4.2.2). Another limitation arises with traditional backward-looking models since throttle and brake commands are not output from a driver model. Nevertheless, the required braking force was determined by implementing an engine braking feedback model as discussed in

Section 4.3.1.3. The required percent of maximum torque is also calculated for all possible states, such that the appropriate throttle and pedal commands to achieve the desired vehicle acceleration can be back calculated. This will be particularly useful when applying the reverse dynamic optimization methodology to optimal transmission control design in Section 5.2.

4.5 Advantages of Reverse Dynamic Optimization Methodology

Introducing a dynamic optimization algorithm that is capable of determining the most efficient powertrain control strategy over various drive cycles offers significant potential in the design of more efficient vehicle systems. The reverse dynamic optimization approach expedites consistent evaluation of hardware design alternatives early in the design process and significantly reduces the time to evaluate multiple design configurations. A primary advantage of this methodology over the state-of-the-art is that it allows high speed analysis of the vehicle design space and expedites multi-dimensional parametric studies and design optimization. The dynamic programming approach facilitates comparing advanced designs and technology in conjunction with optimized system control. The potential benefits of the reverse dynamic optimization methodology can be extended to develop better shift and lock-up control strategies. The advantage of this methodology over the state-of-the-art simulations is that the control strategy is catered to vehicle attributes and drive cycle characteristics while taking system interaction effects into account. Simulating the powertrain system in every possible state helps to ensure that no opportunities are missed to optimize the entire vehicle system.

CHAPTER 5 proposes using the DP simulation to assess and develop transmission gear shift, torque converter clutch, and pedal control strategies. The DP optimized results can serve as a benchmark for developing traditional rule-based control calibrations. Additionally, the methodology can assist in investigating how the optimal control strategy varies for different vehicle attributes and drive cycles, such as with the difference between FTP cycles versus the more aggressive Consumer Reports cycles.

The reverse dynamic optimization methodology will be extended to variable displacement engine technology in CHAPTER 6. Current methods to optimize variable displacement operation require extensive testing. Furthermore it is difficult to determine the effects of shift and lock-up control on optimal variable displacement operation. A benefit of the reverse dynamic optimization methodology is that control strategies for cylinder deactivation in conjunction with different drivetrain configurations and their interaction effects can be studied virtually. Also the DP approach allows investigation of the full potential benefit of variable displacement for vehicle systems early in the design process before prototype hardware is available.

The benefits of using the reverse dynamic optimization model to study advanced powertrain hardware designs will be discussed in CHAPTER 7. The backward-looking approach is well suited to establishing design criteria for future powertrain designs. By simulating all powertrain components in all feasible states, the reverse tractive road load demand model can be used to establish design targets. Since the dynamic programming algorithm caters the powertrain control strategy to the given hardware configuration, the methodology can more effectively evaluate hardware design alternatives. This approach is specifically advantageous when evaluating multiple design alternatives since the user

does not need to manually alter the control strategy for each configuration under consideration. Section 7.6 reveals the significant simulation time savings that result from using the reverse dynamic optimization methodology to evaluate multiple powertrain configurations.

CHAPTER 5

POWERTRAIN CONTROL STRATEGY ASSESSMENT

The dynamic programming (DP) optimized control strategy serves as a benchmark of the best performance achievable and can be used to assess the potential benefit of alternative control strategies. Also rules can be extracted from the DP simulation results for use in traditional rule-based control strategies. Using the proposed approach in this dissertation, fuel economy benefits of one to four percent have been measured relative to baseline production passenger vehicles with new shift, lock-up clutch, and pedal control strategies.

5.1 Torque Converter Lock-up Clutch Control Assessment

The reverse dynamic optimization simulation offers significant advantage in evaluating the potential fuel economy benefit of alternative powertrain control strategies. By determining the most efficient gear and torque converter state over various drive cycles, the simulation can be used to determine which conditions are better for operating in a lower gear in clutch control mode as opposed to in a higher gear in the open torque converter state. The simulation can also be used to estimate the trade-off between potential fuel economy improvements due to different clutch control strategies and the vehicle system hardware costs associated with expanding the low-speed lock-up region

(e.g., higher heat capacity friction clutch material, higher quality motor mounts, turbine dampers, etc.).

The vehicle considered in Section 4.3.2 was constrained to engage in torque converter lock-up in fourth and fifth gear only. The simulation can be applied to predict the fuel economy benefit of expanding clutch control to include partial lock-up in third gear. The DP simulation gear and lock-up states for the same vehicle allowing for third gear partial lock-up (PL) over the FTP urban cycle are depicted in Figure 5-1.

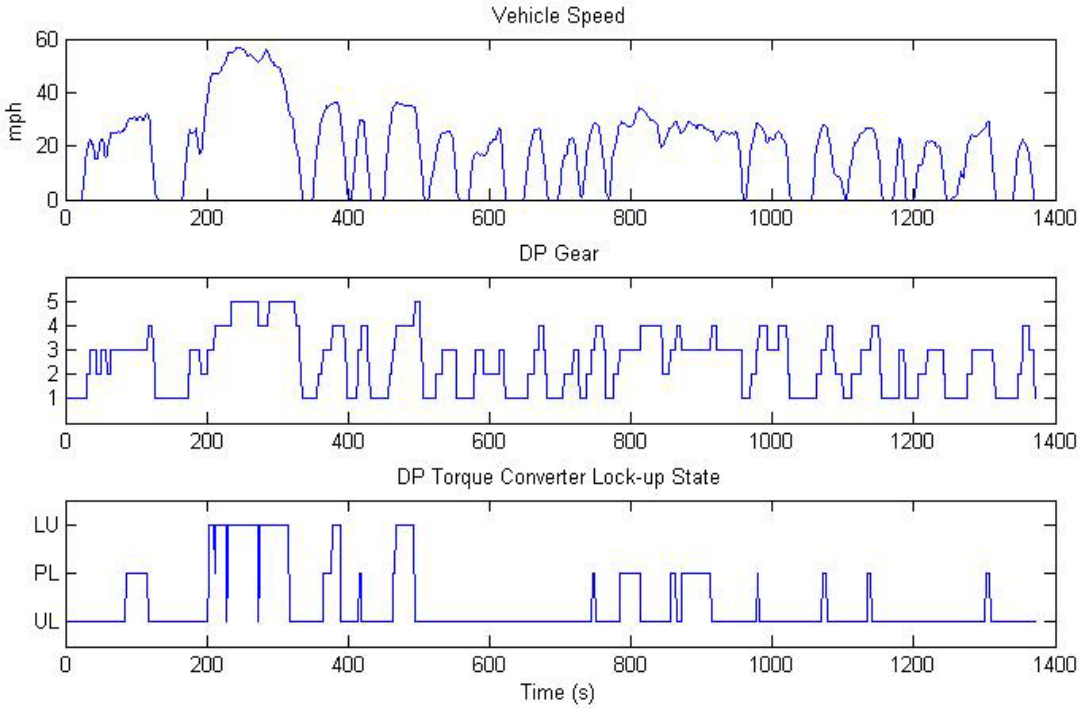

Figure 5-1 FTP Urban DP Gear and LU States with Third Gear PL

To verify the results, chassis dynamometer CVS measurements were compared to the simulation results. Both configurations were tested three times each on three different days to obtain a statistical sample for use in a two-sample t-test. A comparison of the simulation and the average measured fuel economy benefit is shown in Figure 5-2. The mean of the difference between the measured baseline and third gear PL configurations compared to the DP estimate over the FTP urban cycle were 0.30 and 0.32 miles per

gallon, respectively. The figure also shows the 95% confidence interval for the difference in means of the measured results with and without third gear PL. The measured highway results are more ambiguous due to inherent test variation and the fact that little time is spent in third gear yielding less benefit. Given a chassis dynamometer test standard deviation of 0.4 miles per gallon, over 60 tests would be necessary to measure a 0.2 mile per gallon difference with 80% confidence. Seeing as such extensive testing is impractical, the reverse dynamic optimization methodology is a practical alternative to estimating incremental fuel economy benefits of alternate hardware and control strategies.

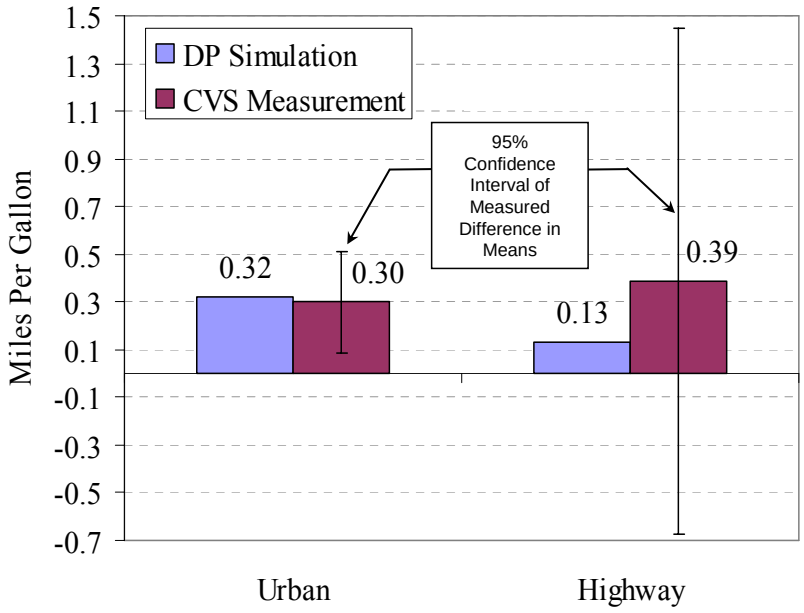

Figure 5-2 Simulated vs. Measured Fuel Economy Benefit of Third Gear PL

5.2 Transmission Control Optimization

The DP optimized states can be used to assist in developing transmission control strategies. The optimal powertrain states over dynamic cycles can be decomposed to determine rules to apply to traditional shift and lock-up control schedules. Once the

optimal states are determined, the corresponding engine torque and speed can be used to back calculate the appropriate driver request given a throttle map for a manual throttle engine or the pedal to throttle transfer function calibrations for an electronic throttle engine. Figure 5-3, Figure 5-4, Figure 5-5, and Figure 5-6 depict the DP optimized gear and clutch control (CC) states for both FTP and Consumer Reports (CR) city and highway cycles for a typical vehicle.

By analyzing the optimized time-in-gear in terms of pedal percent and transmission output speed, lines can be fitted to develop shift and lock-up schedules. The DP approach can be used to optimize the speeds and loads encountered over drive cycles of interest. When the driver pedal request is closer to wide open throttle, where maximum performance is of interest, the optimal shift points are determined using the method depicted in Figure 1-2.

Using the DP approach described here, a new shift map was proposed and the fuel economy was compared to a baseline production shift map for a 5-speed pick-up truck. The CVS measured percent fuel economy improvement from the proposed shift schedule changes can be seen in Figure 5-7. Since no changes were made to the lock-up schedule in this example, further improvement would be possible with additional lock-up schedule changes. The fuel economy improved for all cycles except for the CR city cycle. This is expected since the CR city cycle has far higher accelerations compared to the FTP cycle and often what can be done to improve the fuel economy on one cycle (e.g., early upshifts) can come at a detriment to another cycle. Section 5.3 will discuss possible solutions to this challenge.

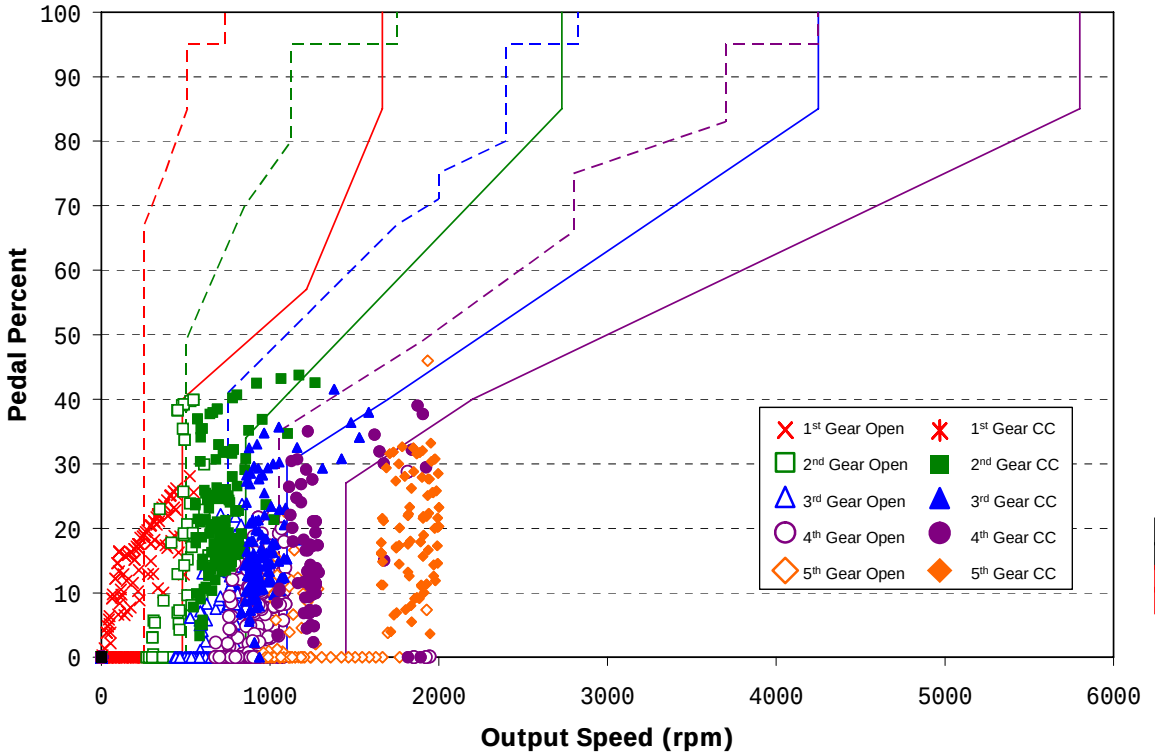

Figure 5-3 Example FTP Urban Optimized Time-in-Gear and Proposed Shift Schedule

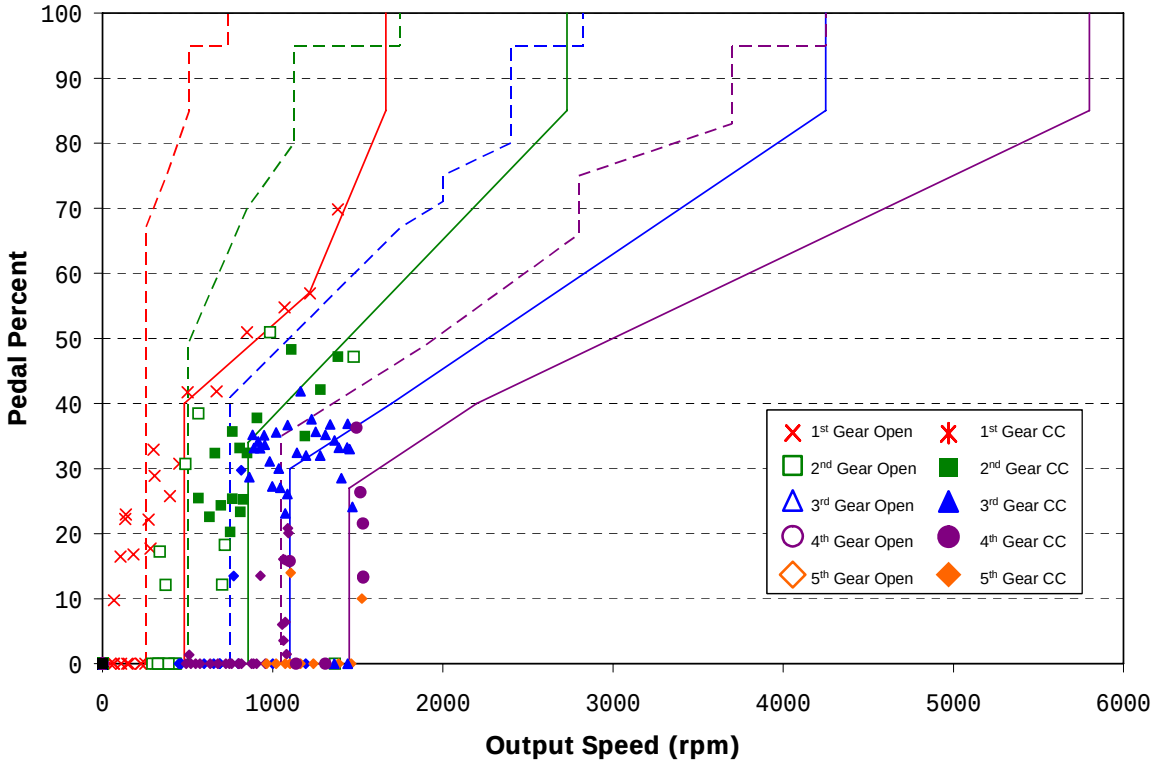

Figure 5-4 Example CR City Optimized Time-in-Gear and Proposed Shift Schedule

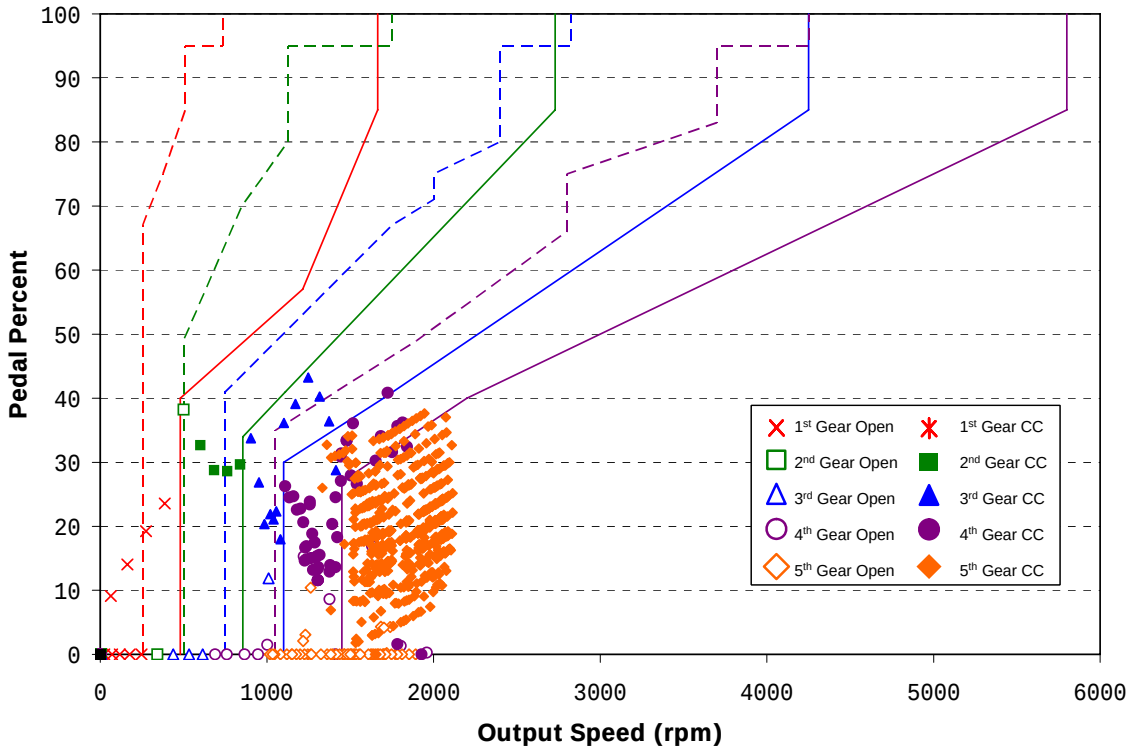

Figure 5-5 Example FTP Highway Optimized Time-in-Gear and Proposed Shift Schedule

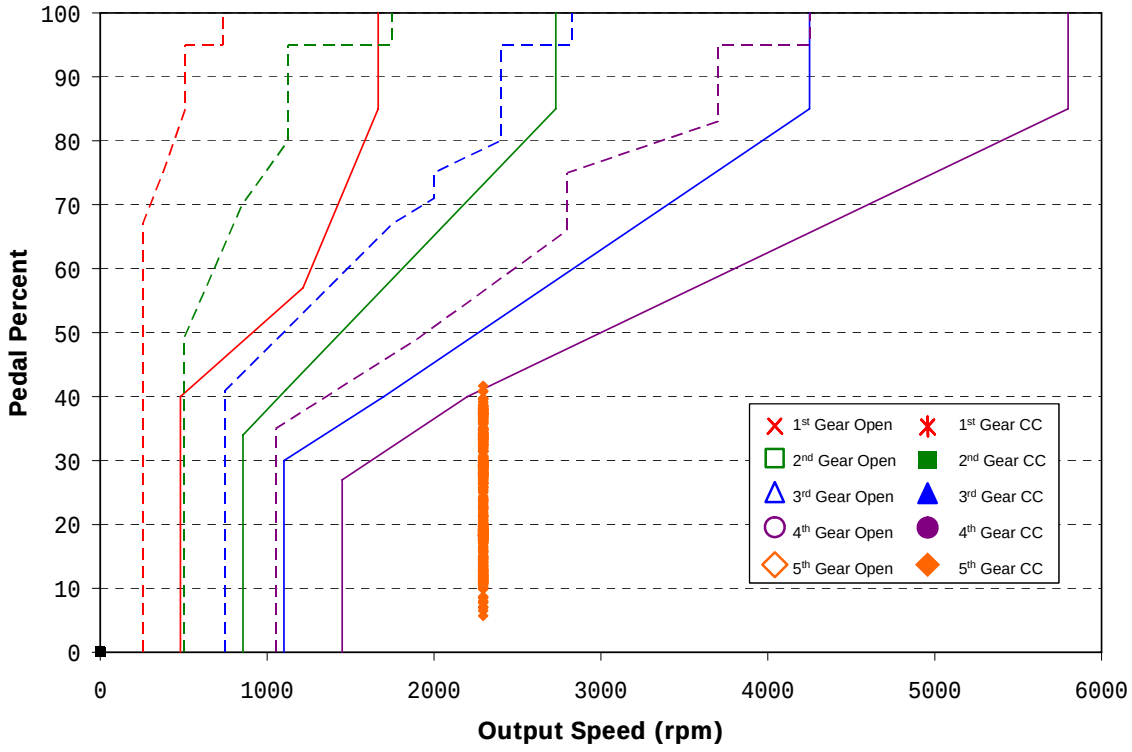

Figure 5-6 Example CR Highway Optimized Time-in-Gear and Proposed Shift Schedule

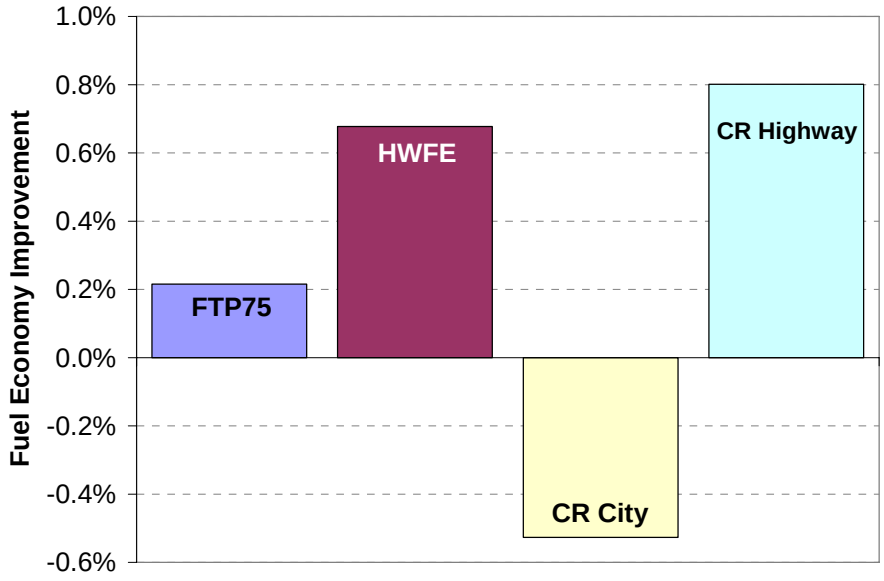

Figure 5-7 CVS Measured Fuel Economy Improvement Using DP Time-In-Gear to Develop Shift Schedule Calibration

It should also be noted that when evaluating any control strategy a subjective driving evaluation should be performed to assess whether excessive shift busyness, unacceptable drivability and/or objectionable NVH results. The proposed shift schedule was evaluated by different transmission calibrators as well as everyday drivers and regarded as acceptable.

5.3 Drive Cycle Influence on Optimal Control Strategy

The advantage of the deterministic DP approach is that the control strategy is catered to specific drive cycle characteristics. On the other hand, this poses a challenge since different drive cycle characteristics can yield conflicting optimal shift points. The optimal control strategy that yields the best fuel economy on one cycle may yield less than optimal performance on a more aggressive drive cycle. For instance, while early

upshift is generally thought of as good for fuel economy, it compromises performance and fuel economy for drive cycles with more rapid acceleration maneuvers. When comparing the FTP and Consumer Reports drive cycles in Table 4-9, the CR city consists of far higher accelerations that result in later upshifts compared to the earlier upshifts that result from the slower accelerations in the FTP cycle. Consequently, to realize the best possible fuel economy for all driving conditions, an optimization algorithm ultimately needs to be implemented that adjusts the shift and lock-up control strategies real-time based on the driver intent. Stochastic dynamic programming is one possible approach to real-time control and has been investigated by Kolmanovsky, *et al.* (2002), Lin, *et al.* (2004c), and Johannesson, *et al.* (2006).

The intent of this research is to develop design methodologies where rules can be extracted to assist in developing rule-based control strategies and to evaluate different powertrain configurations assuming an optimal control policy. Real-time control implementation is out of scope for this dissertation but online optimization is suggested future work. Nonetheless, the reverse dynamic optimization approach offers the ability to extract rules that are catered to drive cycles to assist in developing shift and lock-up schedules as demonstrated in Sections 5.2 and 5.5. In many instances engine controller units (ECUs) are not capable of real-time optimal control due to algorithm or processor limitations; thus the method proposed here can be particularly beneficial to the control design process. The results from this method can be used to develop a starting point shift and lock-up schedule for new vehicle platforms where no baseline exists saving considerable calibration time. Once optimal control strategies for a specific driving cycle are determined, the next step is to develop a shift and lock-up schedule that is tailored to

the driving styles of the intended customer base (e.g., performance oriented cars versus fuel economy oriented minivans versus load carrying heavy-duty trucks). Considering that the EPA passed new regulations that will require fuel economy labels for the 2008 model year to incorporate results from more aggressive drive cycles than today's FTP75 and highway cycles, such as the US06 (faster speeds and acceleration), SC03 (air conditioning use), and Cold FTP (colder outside temperatures), introducing a technique that captures the performance and fuel economy trade-off for multiple drive cycles can add considerable value in the design process.

5.4 Virtual Development of Engine Pedal Calibration

The reverse tractive road load demand model can also be used to help shape the pedal calibration for electronic throttle control vehicles. Figure 5-8 depicts the engine torque for lines of constant engine throttle for a typical engine. Electronic throttle control (ETC) gives the ability to tune the relationship between the driver pedal request and the engine throttle for different types of vehicles to yield a desired performance feel. The reverse tractive road load demand model facilities virtual calibration of the pedal curve. The reverse model can be used to determine the engine torque required for steady-state vehicle speeds for a defined "driving zone". Then depending on the vehicle attributes and desired pedal feel, the rate of change in torque per percent pedal can be defined. A reduced gain or low rate of change in torque with pedal movement will yield a soft pedal feel. On the other hand, a more aggressive pedal feel with increased rate of torque change may be desired at higher speeds. Figure 5-9 depicts the rate of change in engine throttle per percent change in pedal with respect to the simulated steady-state road load

torque required for 25 miles per hour to 85 miles per hours in 10 mile per hour increments (indicated by the dots and squares) for different pedal curve approaches.

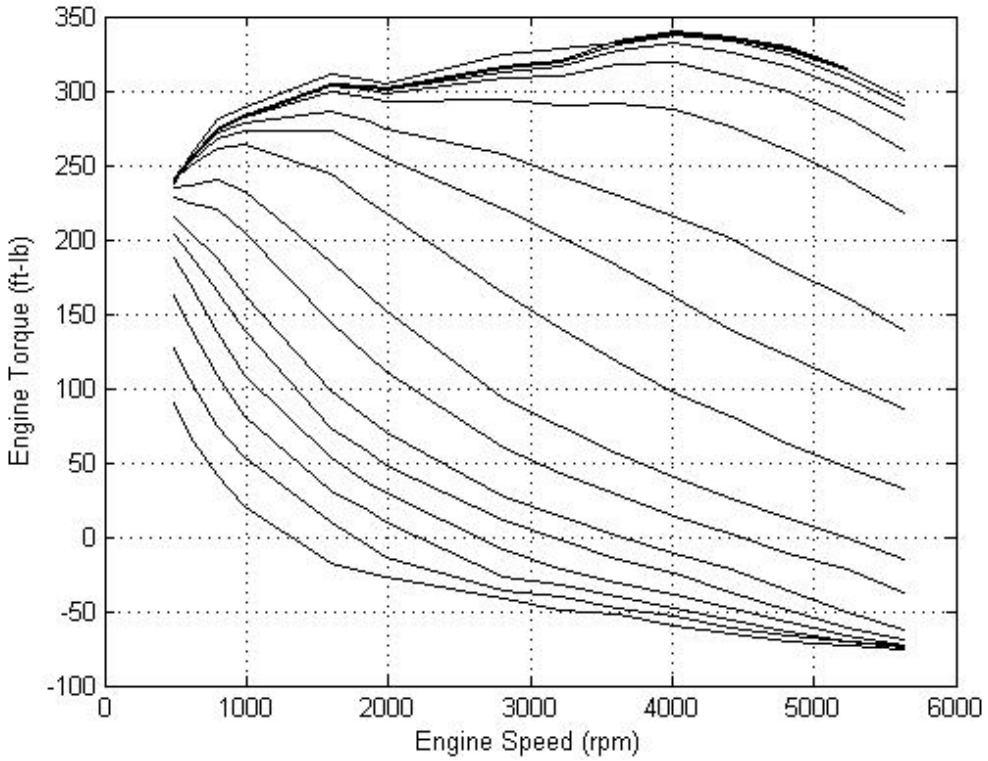

Figure 5-8 Lines of Constant Engine Throttle

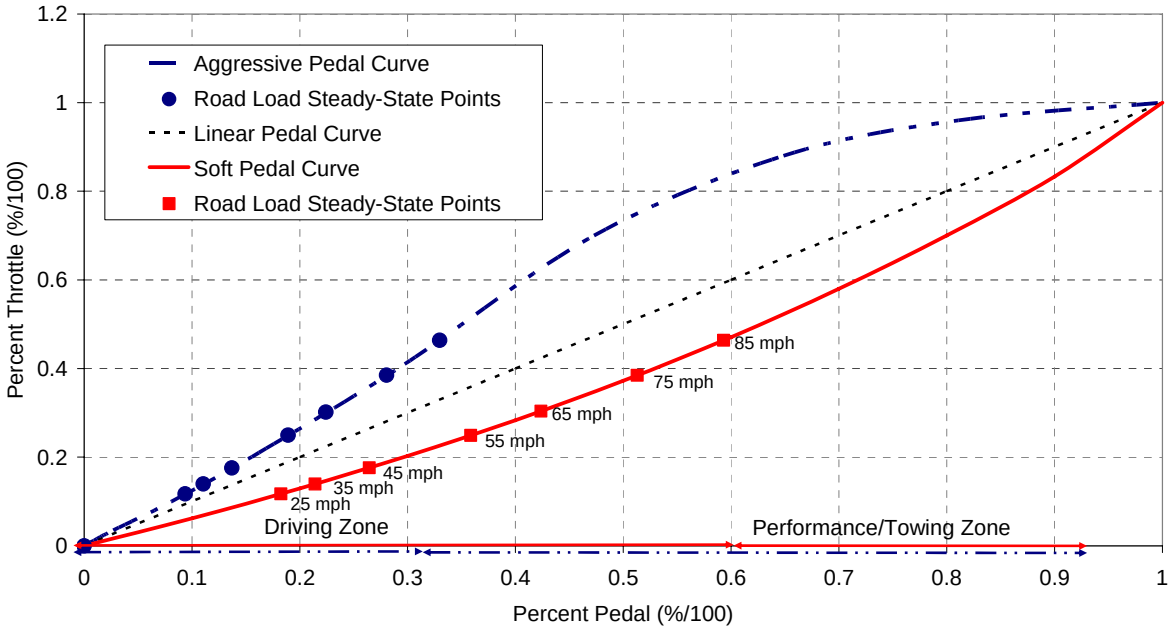

Figure 5-9 Example Pedal Curves

By using the reverse model to facilitate the pedal calibration process, engine calibrators can more rapidly develop pedal curves that improve the driver's ability to control the vehicle (e.g., maintain desired constant vehicle speed) and reduce the inertia losses from overly "touchy", i.e., too sensitive, pedal calibrations. Determining the appropriate gain for the pedal curve can also improve the resolution for scheduling shift and lock-up points for transmission control and decrease the "dead", i.e., unresponsive, pedal zones.

5.5 Combined Powertrain Control Fuel Economy Improvement

While the DP approach provides a simulated control strategy for a given drive cycle, it cannot be implemented under real driving conditions since it requires a priori knowledge of the vehicle drive cycle and corresponding future speed and load. Nonetheless, the results provide a benchmark against which other control strategies can be compared. One particular advantage of the DP optimization approach is that the control strategy is catered to specific vehicle and drive cycle characteristics while taking system interaction effects into account. The DP optimization approach can illustrate opportunities for improving traditional rule-based control strategies that may not have been apparent from engineering intuition.

Figure 5-10 depicts the combined measured fuel economy improvement with new shift, torque converter lock-up clutch, and pedal calibrations developed using the DP optimized results for a passenger vehicle equipped with variable displacement engine technology. Some of the improvement can be attributed to reducing the pedal gain, which results in fewer transitions in and out of cylinder deactivation mode with slight

pedal movements. Reducing the pedal gain improves the fuel economy by increasing the time in cylinder deactivation mode with no noticeable drivability effect. The improvements suggest that a system analysis approach to control design is essential to obtaining the highest fuel economy possible – the DP approach offers significant advantages in understanding where opportunities exist.

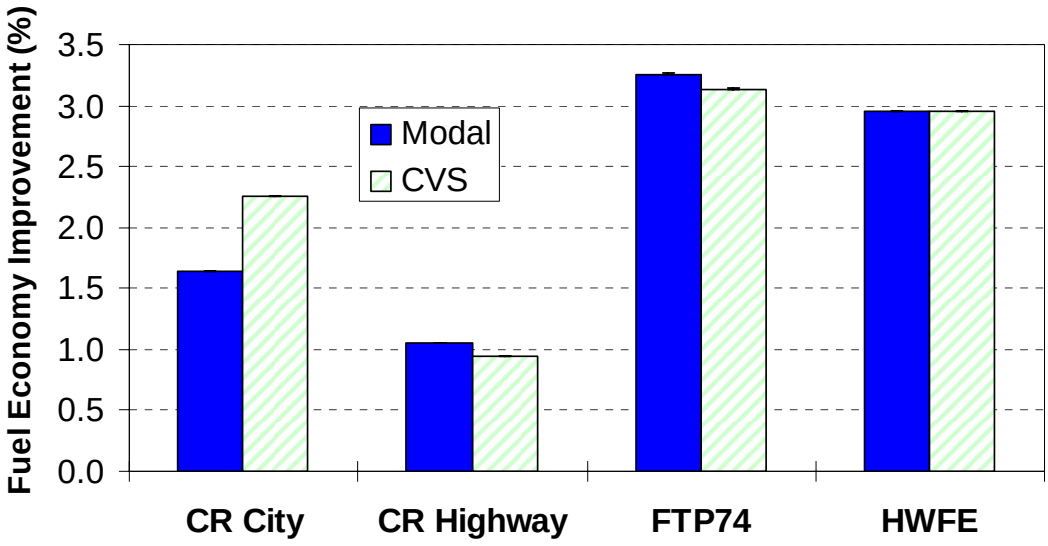

Figure 5-10 Fuel Economy Improvement with DP Optimized Shift, Clutch Control, and Pedal Calibrations

CHAPTER 6

DYNAMIC OPTIMIZATION OF VARIABLE DISPLACEMENT ENGINE OPERATION

6.1 Introduction and Motivation

A particular new engine technology capable of improving fuel economy without sacrificing performance is variable displacement, also known as cylinder deactivation. The technology delivers the fuel economy of a smaller displacement engine when the vehicle system is under part load, but also delivers the high horsepower and torque of a larger engine when demanded by the driver. To achieve the most benefit, variable displacement needs to be properly integrated into the vehicle system. Integrating variable displacement with the appropriate driveline configuration and calibration strategy can increase the engine's ability to operate with some of its cylinders deactivated.

Using the reverse dynamic optimization approach, control strategies for variable displacement engines in conjunction with different drivetrain configurations and their interaction effects will be studied virtually. The research described in this chapter will concentrate on optimizing variable displacement operation taking the powertrain hardware configuration as well as the gear shift and torque converter clutch control strategies for specific vehicle and drive cycle attributes into account.

6.2 Variable Displacement Background

The fuel economy advantage of cylinder deactivation has been well documented (Bates 1978; Fukui 1983; Leone 2001). Variable displacement functions by deactivating the intake and exhaust valves and shutting off fuel for some of the cylinders. For same torque demand, deactivating cylinders reduces pumping work, friction work, and heat transfer losses, which in turn improves fuel economy.

The additional degrees of freedom associated with implementing cylinder deactivation complicate calibration efforts. The ability to engage variable displacement mode is constrained by the ability of the engine to meet the driver torque demand with some of the cylinders disabled as well as other enable conditions, such as oil and coolant temperature, engine and vehicle speed. Operating in variable displacement mode and transitioning in and out of variable displacement mode results in torque fluctuations which introduce noise, vibration and harshness (NVH) challenges. Some of the control challenges associated with variable displacement operation and transitions as well as the associated NVH challenges are discussed in Michelini and Glugla (2003) and Falkowski, *et al.* (2004).

Operating the torque converter in controlled slip mode is one way of reducing the resulting engine vibrations, yet slipping the converter could potentially negate the fuel economy gained by deactivating some of the cylinders. The shift schedule also affects the amount of time in variable displacement mode. While operating in a higher gear at a lower engine speed is generally better for fuel economy for engines that are not equipped with variable displacement, operating in higher gears may decrease the amount of time the cylinders can be deactivated.

Current attempts to optimize variable displacement operation from the vehicle system perspective include steady-state powertrain dynamometer testing, where all of the possible states: (1) gear (2) torque converter, and (3) cylinder deactivation mode, as well as vehicle speed are manually dialed into the dynamometer and the corresponding fuel flow is measured. Not only is extensive testing required, the results must be interpreted in order to implement them into a control strategy. Another disadvantage is that the resulting fuel economy effect over a drive cycle cannot be easily determined using this experimental approach. Furthermore, testing alternative hardware configurations requires additional mechanical work and test time and in many instances prototype hardware does not exist early in the design process.

6.3 Engine Cylinder Deactivation Model Development

The reverse dynamic optimization methodology has been extended to incorporate virtual optimization of variable displacement operation. Vehicle simulations exist that are capable of modeling variable displacement but they only simulate a predefined region of operation and do not take system interaction effects into account, thus extensive testing is required to optimize variable displacement (Gale 2005; Trask, *et al*. 2003) . It will be shown that the ability to virtually optimize when the system is in cylinder deactivation mode taking the shift and torque converter lock-up control can further increase the potential benefits.

Operation in variable displacement mode is based upon the ability of the engine to satisfy the torque demand necessary to meet the drive cycle vehicle speed trace. Variable displacement is enabled if the torque required can be delivered with its cylinders

deactivated. While in variable displacement mode, if the torque required cannot be met, the system switches back to full cylinder operation.

Minimum and maximum engine and vehicle speed boundaries exist and are included in the model for operation of the cylinder deactivation system. To avoid excessive switching into and out of variable displacement mode, a hysteresis is incorporated. At certain speeds and loads, operation in variable displacement mode can result in unacceptable NVH. As a result, the system can be constrained to not operate in a given region also known as a "No Fly Zone", where the torque demand is met but subjective NVH criteria are not fulfilled. Figure 6-1 is a visual depiction of a generic region of variable displacement operation and constraints.

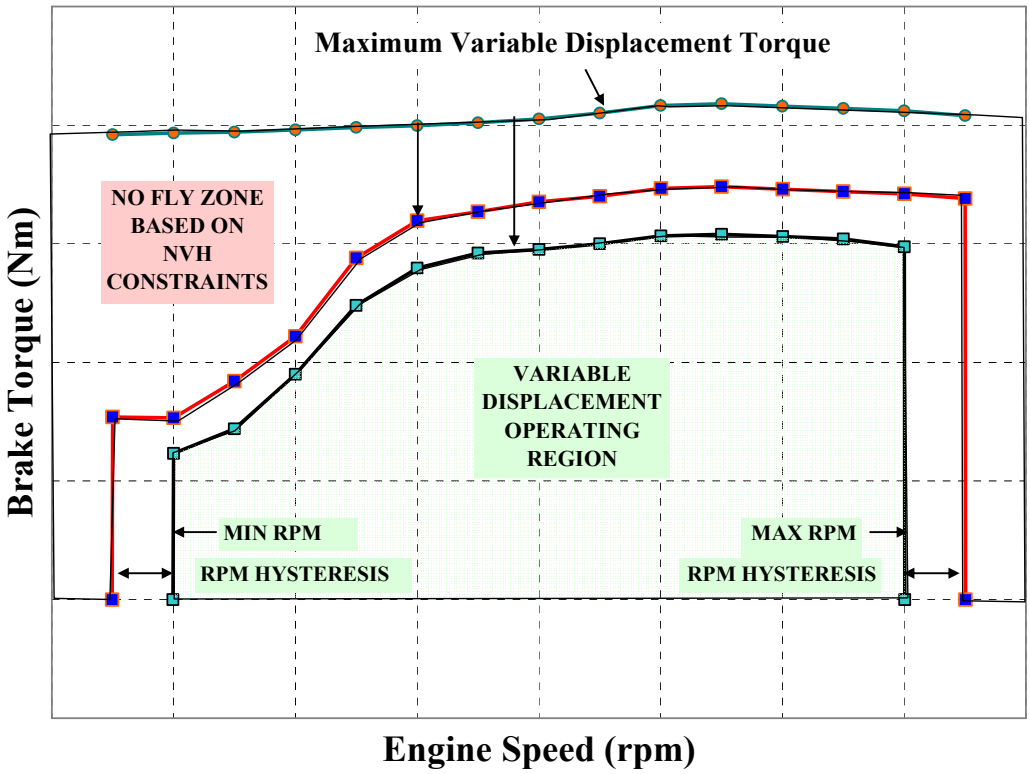

Figure 6-1 Variable Displacement Operation Region and Constraints

A block diagram depicting how the cylinder deactivation, otherwise known as Multi-Displacement System (MDS), constraints were implemented in Simulink® is shown in Figure 6-2.

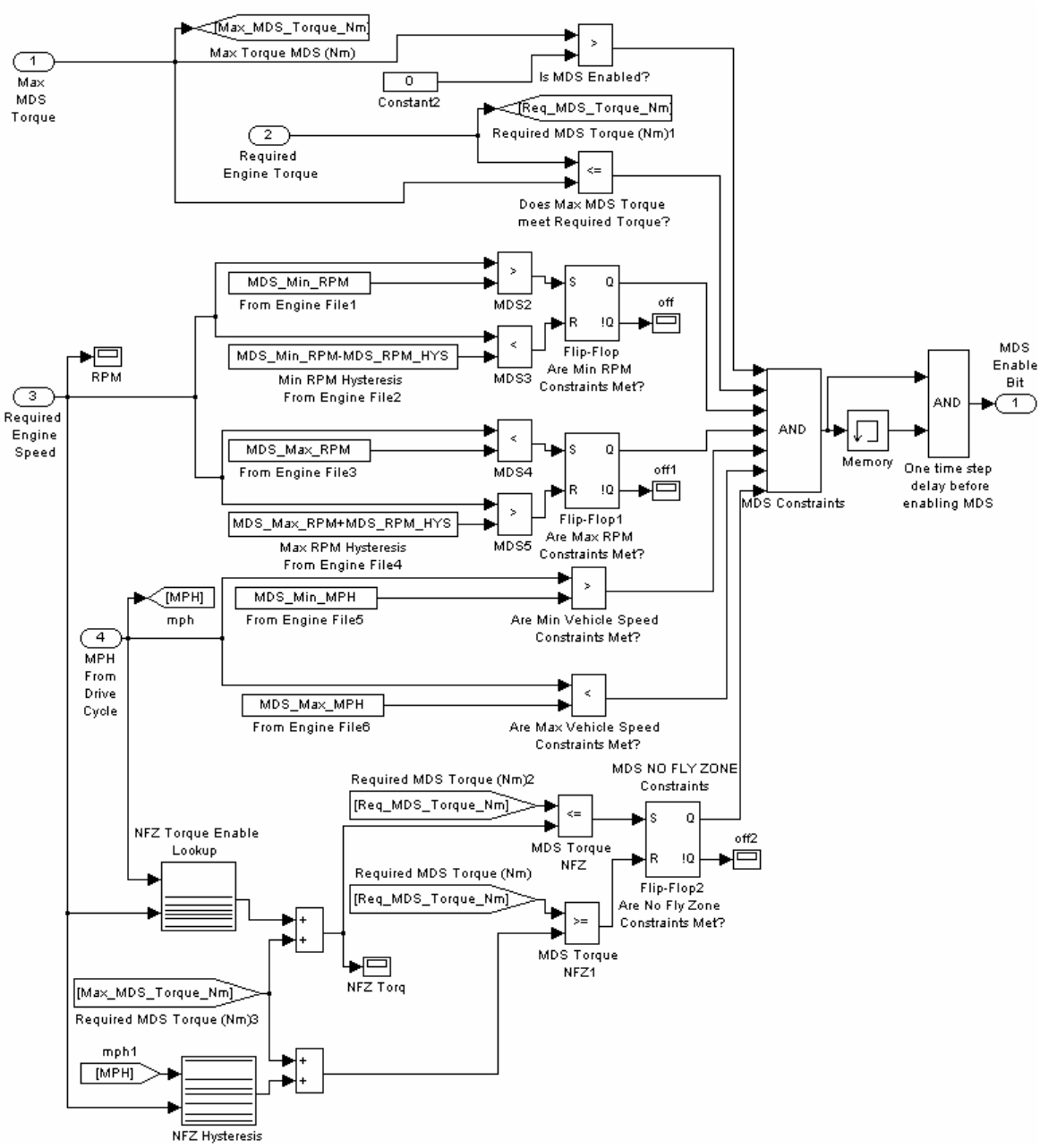

Figure 6-2 Multi-Displacement System Constraints Simulink® Block Diagram

The shift schedule and torque converter clutch control strategies have a significant effect on whether the system can operate in variable displacement mode. Often due to NVH limitations, a vehicle system equipped with variable displacement is not allowed to engage in full torque converter lock-up, thus lock-up must be specifically enabled in the simulation. Possible control variables during MDS are depicted in Table 4-3. Other engine oil and coolant temperature constraints exist but since the reverse model assumes fully-warmed conditions, temperature constraints are not modeled.

6.4 Model Correlation and Validation

To validate the accuracy of the variable displacement model, a sedan equipped with Multi-Displacement System (MDS) and a five speed transmission was simulated with the same shift, torque converter clutch control, and cylinder deactivation control commands as tested in an actual production vehicle on a chassis dynamometer rolls. Phase 2 of the FTP75 (Federal Test Procedure) cycle was selected to validate the model because the model assumes standard operating temperatures and does not take into account ignition or warm-up effects that are included in the cold start of phase 1. The vehicle speed trace and corresponding control parameters used in the testing and model validation are shown in Figure 6-3.

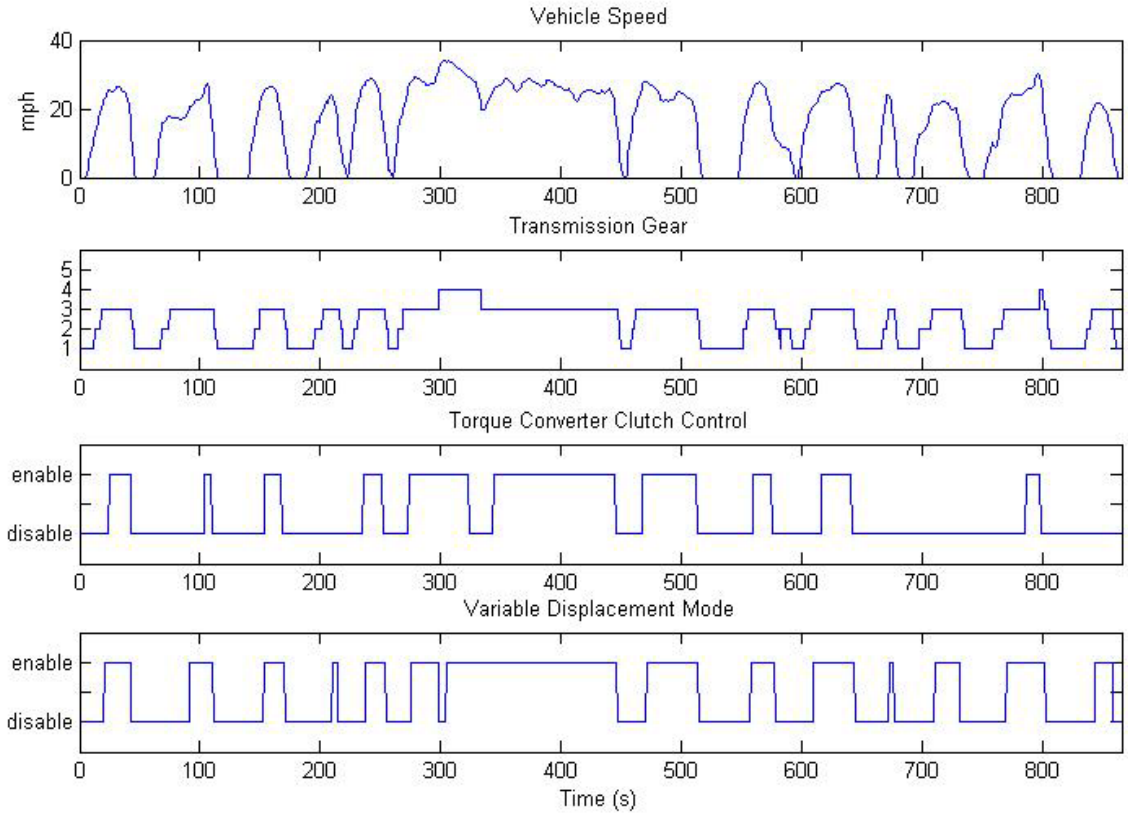

Figure 6-3 FTP75 Phase 2 Variable Displacement Control Parameters

A comparison of the simulation versus the actual engine controller unit measurements for a portion of the FTP75 cycle is shown in Figure 6-4. Table 6-1 compares the simulated fuel economy versus the measured constant volume sample (CVS) fuel economy. As the fuel economy difference is within one percent, it can be concluded that the variable displacement model is sufficiently accurate to investigate the potential fuel economy benefits of different variable displacement control strategies.

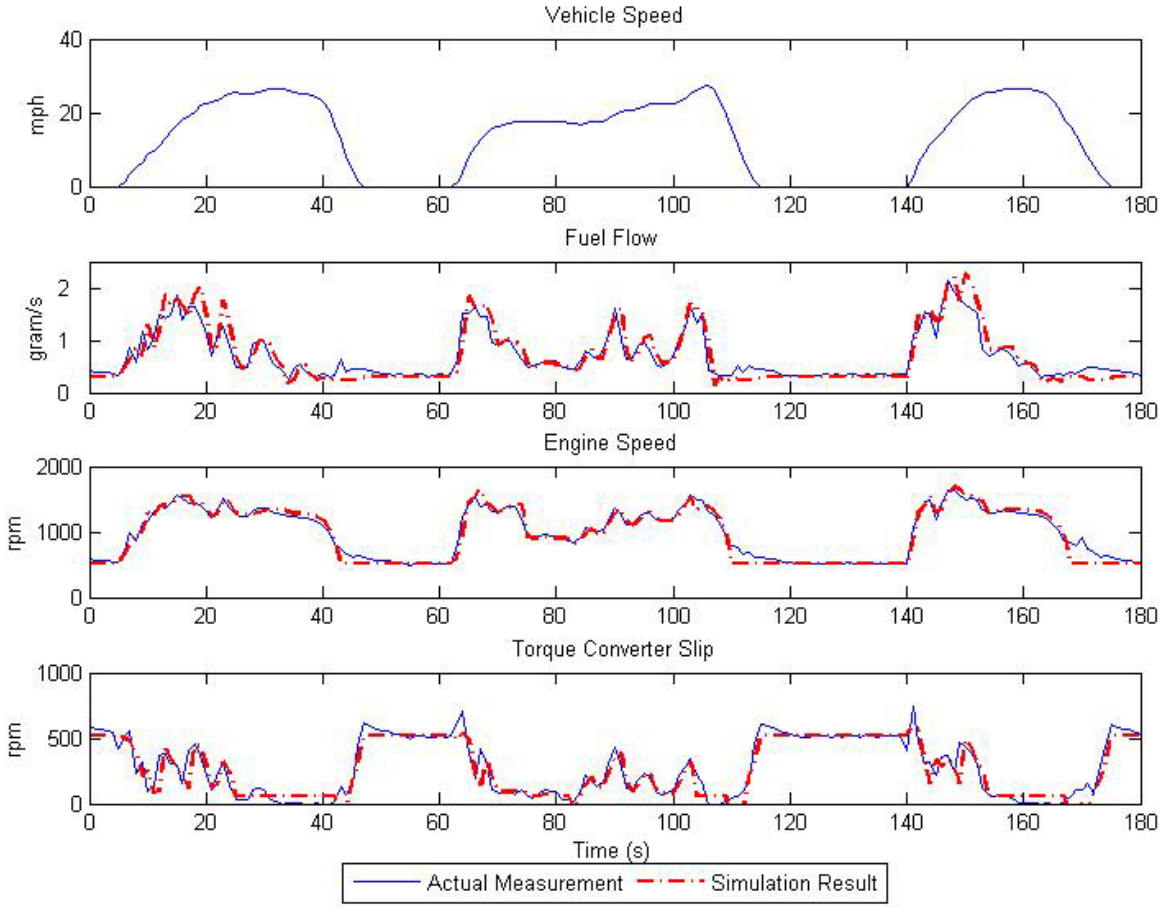

Figure 6-4 FTP75 Phase 2 Test Measurements vs. Simulation Results with Variable Displacement

Table 6-1 Variable Displacement FTP75 Phase 2 Fuel Economy Validation

Simulation Result	CVS Measurement
17.77 mpg	17.60 mpg

6.5 Multi-Displacement System Simulation Results

The reverse dynamic optimization technique was used to simulate the benefit of MDS operation by comparing the results to the same vehicle without MDS enabled. Figure 6-5 depicts the engine torque and speed operating points for phase 2 of the FTP75 cycle with and without MDS enabled. Comparing the simulation results without MDS

enabled to the simulated production control strategy resulted in an 8 percent (1.3 mile per gallon) improvement (refer to Table 6-2).

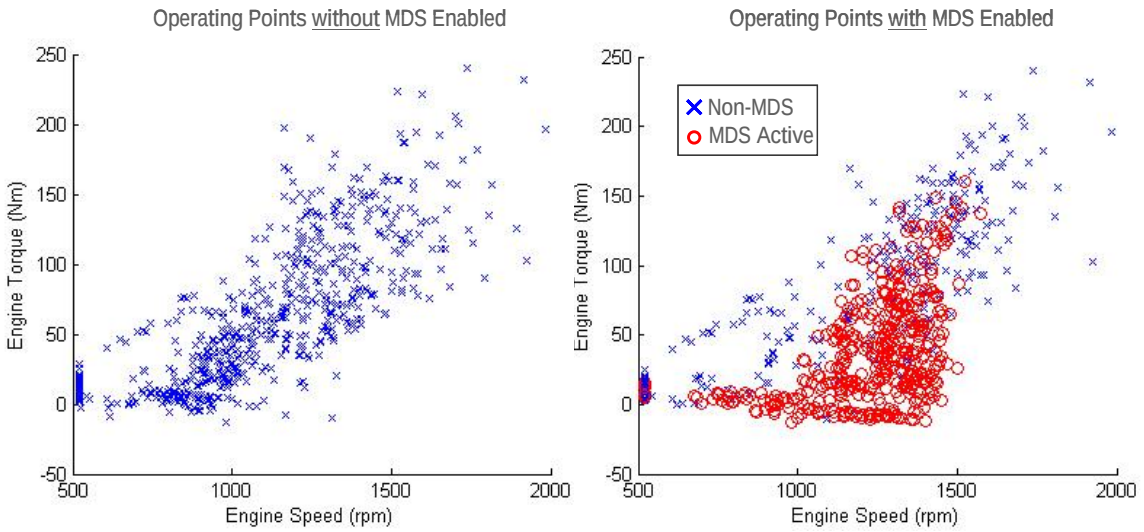

Figure 6-5 FTP75 Phase 2 Multi-Displacement System Operating Points

Table 6-2 FTP75 Phase 2 Simulated Fuel Economy Results with and without Multi-Displacement System Operation

Simulated Control Strategy	Fuel Economy (mpg)
No MDS	16.46
Baseline MDS Production Control	17.77
DP Optimized with Same Production No Fly Zone	17.93
DP Optimized with Open MDS Operating Region	19.52

Table 6-2 reveals that further opportunities exist to optimize the system control strategy when simulating the dynamic programming optimized variable displacement and torque converter clutch control strategies. One advantage over the state-of-the-art variable displacement simulation capabilities is that the DP algorithm approach optimizes variable displacement control while simultaneously taking into account torque converter clutch and transmission control interaction effects. A specific example of how DP

optimizes the system control will be discussed in Section 6.6. The DP simulation results are also shown for a vehicle simulated without a "No Fly Zone", in other words no engine speed, vehicle speed or torque constraints on MDS operation. The corresponding time in gear, clutch control (CC) mode, and MDS mode for each of the simulated control strategies is shown in Figure 6-6.

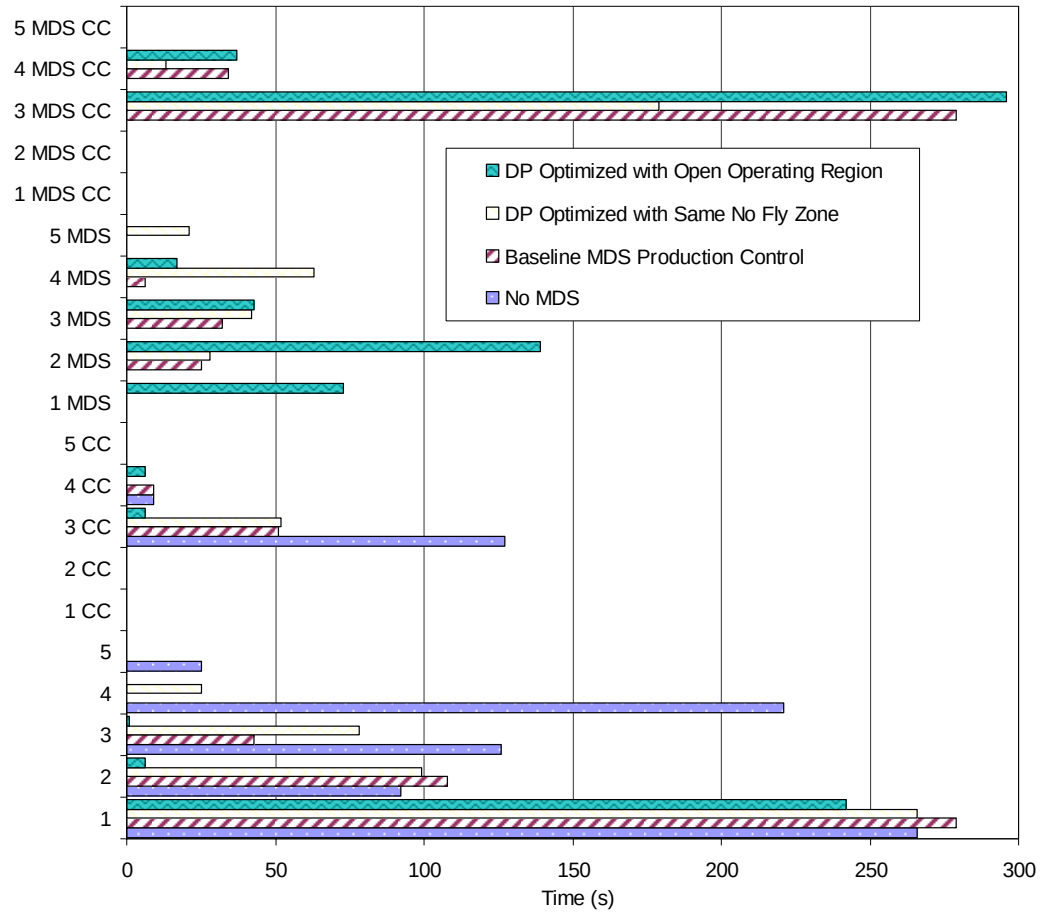

Figure 6-6 FTP75 Phase 2 Simulated Time-in-Gear, Clutch Control, and MDS Mode

Figure 6-6 reveals that as the MDS operating region is increased, it is beneficial to remain in a numerically lower gear to maintain MDS mode rather than upshift. The advantage of the DP optimization methodology is that the shift and lock-up control are automatically adjusted to take advantage of MDS operation whenever possible.

6.6 System Interaction Effects on Optimal Control Strategy

By determining the most efficient gear, torque converter, and variable displacement states over various drive cycles, the dynamic optimization simulation offers significant advantage in evaluating the potential fuel economy benefit of alternative control strategies. An example of the usefulness of the dynamic optimization tool can be demonstrated by analyzing the vehicle control strategy when cruising on the interstate at 65 miles per hour with the road grade varying between -3 and +3 percent, a drive cycle representing the Consumer Reports® (CR) highway cycle. Figure 6-7 and Figure 6-8 depict that when the road grade becomes too steep for the engine to maintain fifth gear in MDS mode, the production control strategy disengages MDS. However, the dynamic optimization results reveal that maintaining MDS and downshifting to fourth gear results in overall lower fuel flow even though there is a slight fuel economy penalty during the shift transition due to unlocking the converter (refer to Figure 6-8 and Table 6-3). The results prove the reverse dynamic optimization approach can yield insight into system control strategies that fully exploit variable displacement operation.

Table 6-3 CR Highway Cycle MDS Fuel Economy Simulation Results

Simulated Production Control Strategy	DP Optimized Control Strategy
25.21 mpg	25.47 mpg

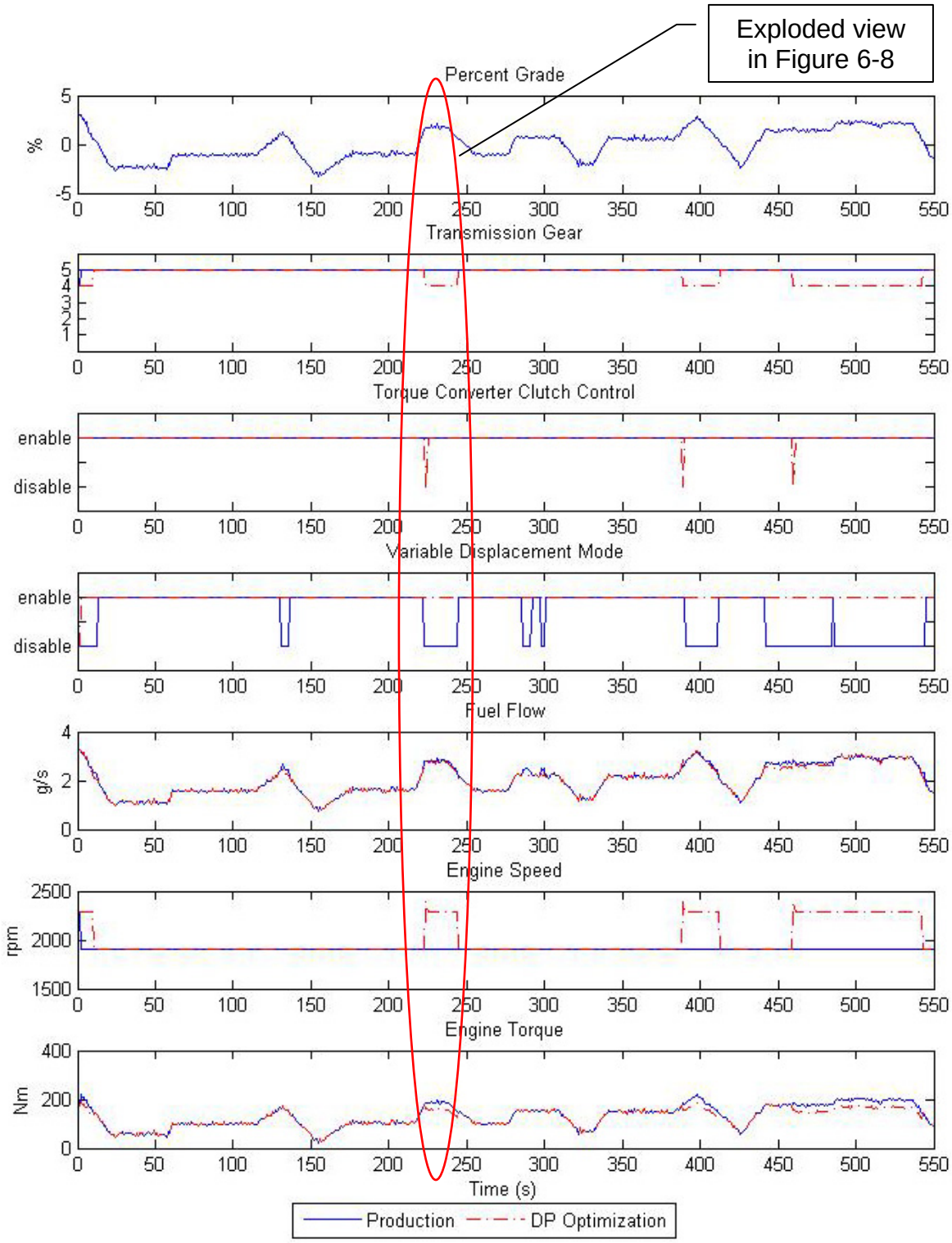

Figure 6-7 65 MPH Steady-state Interstate with Varying Road Grade MDS Control Strategy Comparison

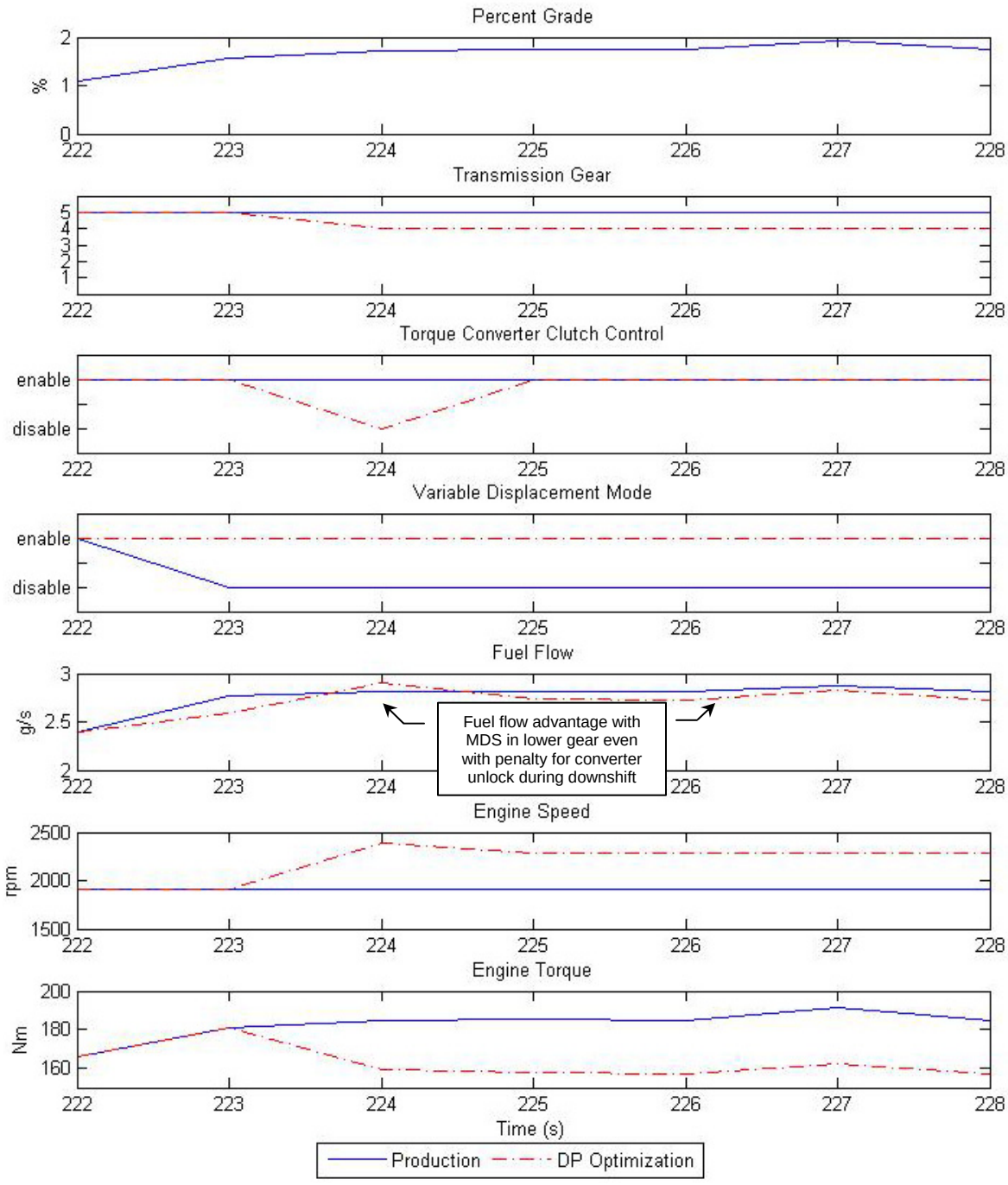

Figure 6-8 Exploded View of MDS Control Strategy Comparison during Road Grade Ascent

CHAPTER 7

ADVANCED POWERTRAIN HARDWARE DESIGN AND SYSTEM INTEGRATION

Besides dynamically optimizing the powertrain control strategy, the reverse tractive road load and dynamic optimization methodology can be used for advanced powertrain hardware design and system integration optimization. The systems analysis methodologies and tools described here have been implemented at a major automotive manufacturer and are being applied to optimize all new vehicle programs.

7.1 Establishing Design Criteria using Reverse Tractive Road Load Demand Model

The reverse tractive road load demand model can be used to establish performance criteria for the design of future new powertrain programs. Given vehicle attributes and drive cycle constraints, the simulation can be used to determine the program targets to achieve specific objectives. Since the model is backward-looking and simulates the powertrain in all possible states, the required speeds and loads to traverse desired drive cycles can be used as design criteria.

To illustrate how the model could be used to establish design criteria, consider what engine torque would be required of a 2700 kilogram full-size pick-up truck cruising steady-state at 65 mile per hour with the road grade varying from zero to three percent. Figure 7-1 depicts the engine torque and speeds required to maintain a constant gear with and without torque converter lock-up (LU). The sloping effect for gears 3, 4, and 5 represents the higher engine speeds required due to torque converter slip in the open state. The DP simulated fuel economy in a given gear at 65 miles per hour for a V8 engine is shown in Table 7-1. Table 7-1 clearly reveals that the ability to maintain lock-up in high gear is crucial to achieving higher fuel economy. Thus, the torque requirements to maintain lock-up in Figure 7-1 could be used as criteria for future engine designs.

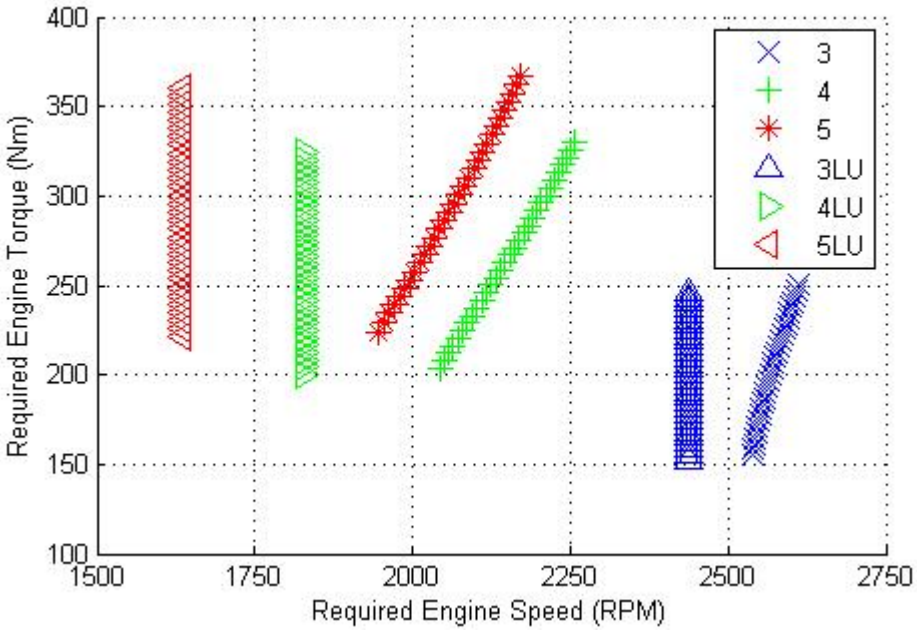

Figure 7-1 Engine Torque Required at 65 MPH with 0 to 3% Varying Grade

Table 7-1 65 MPH Steady-State Fuel Economy

Gear State	No Grade	+3% Grade
3	15.36 mpg	10.39 mpg
4	15.79 mpg	9.64 mpg
5	15.39 mpg	9.11 mpg
3 LU	16.20 mpg	11.32 mpg
4 LU	17.89 mpg	12.07 mpg
5 LU	18.62 mpg	12.29 mpg

The above example was selected for simplicity but other dynamic cycles such as the FTP or other customer-focused cycles could be analyzed and used to establish design requirements in a similar manner. The reverse tractive road load demand model was applied to set specific design targets for the development of a new V6 engine program using this approach. The model can be used to establish design criteria for numerous other vehicle applications and driving scenarios. The advantage of this approach is that the design criteria are specifically matched to the vehicle attributes and driver applications.

7.2 Powertrain Hardware Evaluation using Dynamic Optimization Technique

With shorter product development times, the capability of quickly evaluating potential hardware alternatives is becoming increasingly important. Since fuel economy testing requires significant hardware set-up and test time, simulations are often relied on in the decision process. Many existing vehicle simulations require control parameters, such as the shift map, as an input. Since a detailed control strategy rarely exists for powertrain configurations that are still in the design phase, simulations are often

performed on hypothetical hardware configurations with existing shift maps. Figure 7-2 depicts the predicted FTP urban and highway fuel economy improvements for a numerical reduction in final drive ratio (FDR) from 3.55 to 3.21 and different shift maps from RAPTOR, a commercially available vehicle simulation package that requires the shift map (SM) as an input (Gale 2005). The modified SM used in the simulation included earlier upshifts and delayed downshifts. It can be seen that using a shift map that is not optimized can lead to false conclusions since the resulting fuel economy improvement depends heavily on the shift map. Evaluating alternative hardware configurations with an optimized control strategy that exploits the full capability of the powertrain ensures unbiased assessment of the hardware's potential. The predicted DP fuel economy improvement for the reduced FDR is shown in Table 7-2.

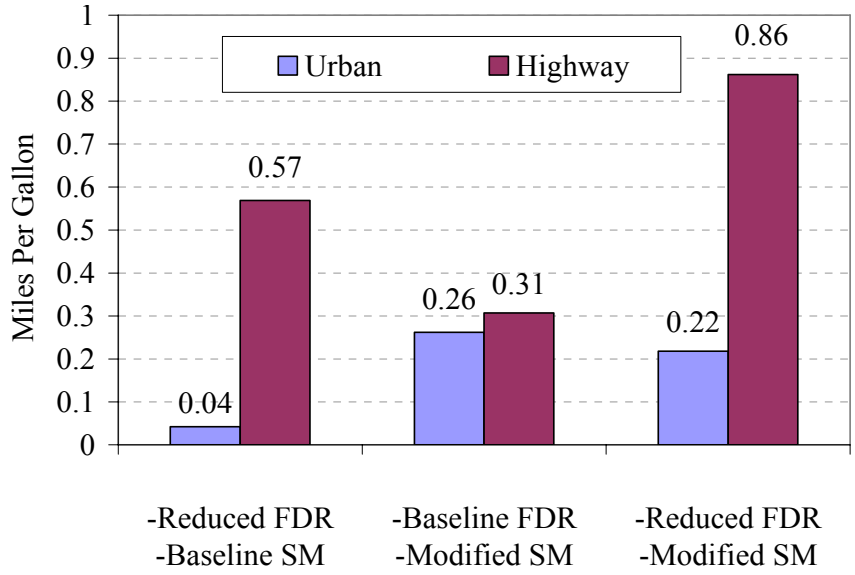

Figure 7-2 RAPTOR Fuel Economy Prediction Dependence on Shift Map

Table 7-2 DP Simulation Fuel Economy Improvement for Reduced Final Drive Ratio

Urban	Highway
-0.05 mpg	0.31 mpg

While the reduced FDR improves fuel economy for the highway drive cycle due to the reduction in engine speed, there is a slight fuel economy penalty for the urban drive cycle. Figure 7-3 shows a portion of the urban cycle and reveals that the numerically higher FDR enables earlier upshifts that yield far greater reductions in overall engine speed offsetting the steady-state reduction in engine speed benefit due to the reduced FDR.

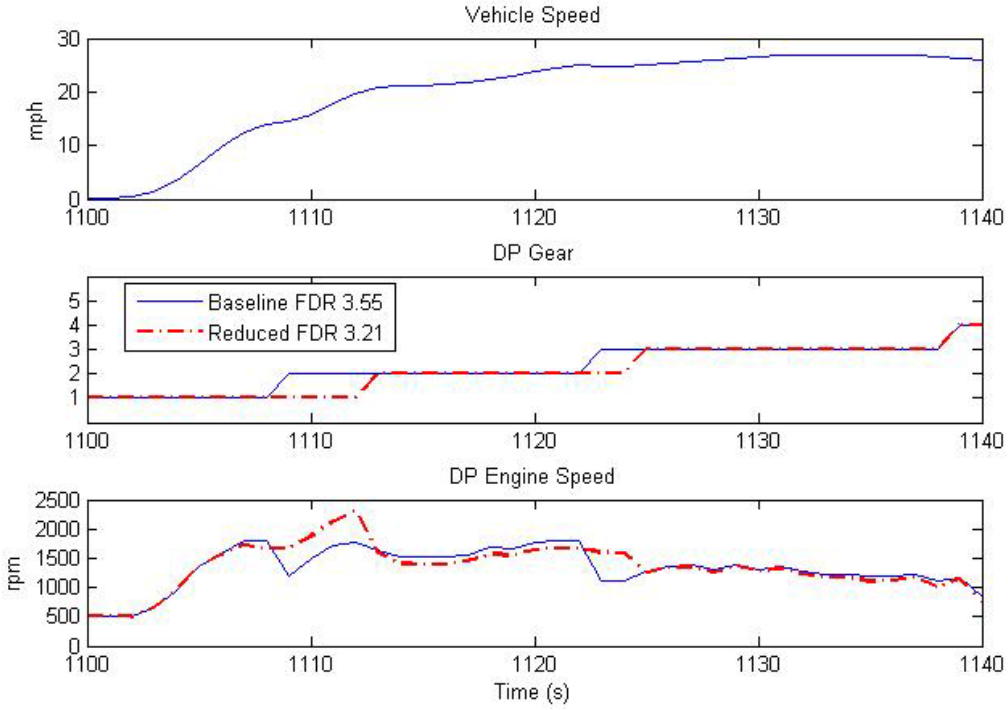

Figure 7-3 DP Simulation Comparison of Final Drive Ratios for FTP Urban Cycle

The DP technique facilitates quick evaluation of future hardware design alternatives in the absence of existing shift and lock-up schedules that are required for the state-of-the-art vehicle simulations. Even though the actual fuel economy results may not be entirely realistic given that the DP algorithm lacks some real life constraints, the technique supports timely and consistent assessment of how one powertrain configuration compares to another.

7.3 Performance Model Development

Modifying the powertrain system hardware design to improve fuel economy can come at a detriment to the acceleration performance. It is important to understand the trade-off between fuel economy and performance when evaluating multiple hardware configurations. Some performance measures of interest include:

- 0 to 60 mile per hour time (seconds)
- ¼ mile time (seconds)
- ¼ mile speed (mile per hour)

As a result, a performance model was integrated into the system analysis tools using the same reverse dynamic optimization inputs to quantify the corresponding performance trade-off of different design alternatives.

The objective of the performance simulation tool is to model the results of a vehicle wide open throttle (WOT) acceleration test for relative comparisons between different powertrain hardware configurations. Since a performance predictor requires the use of a forward-looking model (refer to Section 1.3.1), a new MATLAB®/Simulink® tool will be developed and proposed using the same inputs required in the reverse tractive road load demand model.

7.3.1 Linear Acceleration Dynamics

For translational motion the acceleration can be determined by the rate of change of velocity with respect to time, where the velocity is the rate of change of position, *s*, with respect to time:

$$\vec{a} = \frac{d\vec{v}}{dt} = \frac{d^2\vec{s}}{dt^2} \tag{7-1}$$

The acceleration can also be determined using Newton's Second Law:

$$\vec{a} = \frac{\vec{F}}{m} \tag{7-2}$$

The force on the vehicle can be summarized as the difference in the tractive effort and the road load forces:

$$F = F_{TE} - F_{RL} \tag{7-3}$$

The road load force is determined by the road load coefficients and vehicle speed as described in Section 2.2.7 and Equation (2-25). The inertia of all the rotating components further reduces the force available at the wheel:

$$F = F_{TE} - F_{RL} - F_{rot} \tag{7-4}$$

Inserting Equation (7-4) into (7-2) yields:

$$a = \frac{F_{TE} - F_{RL} - F_{rot}}{m} \tag{7-5}$$

The maximum longitudinal acceleration performance of a vehicle is determined by one of two limits – engine power limited or traction limited. In the traction-limited case, where there is adequate power from the engine, the acceleration is limited by the coefficient of friction between the tire and road (Gillespie 1992):

$$a_{\max} \le k \cdot g \cdot \mu_r \tag{7-6}$$

where k is the ratio between the driven axle load and the total vehicle mass (for all wheel drive, k=1) and μ_r is the peak coefficient of friction. For simplicity and since the performance predictor is only intended for comparing the relative performance between different powertrain configurations, the model does not consider dynamic axle loads nor tire slip.

7.3.2 Powertrain Model

Wide open throttle acceleration tests can either be performed from an idle start or a stall start, where the brake pedal and accelerator pedal are depressed until the engine reaches its stall torque speed. The model was developed to simulate either user-defined start conditions. If a stall start test is selected, the stall torque speed must first be determined.

A new parameter, inverse K-factor*, is defined to assist in determining the engine and turbine torque values:

$$inverse\,K-factor^{*}=\frac{1}{(K-factor)^{2}}\cdot\frac{1}{1+\left(\frac{N_t}{N_e}\right)^{2}} \tag{7-7}$$

An inverse K-factor* curve is created using the aforementioned equation and torque converter characteristic data similar to the data in Figure 2-5. The corresponding inverse K-factor* is a function of speed ratio, which can be determined from the initial idle or stall torque engine speed and an initial turbine speed of zero. Then by inserting Equation (2-23) into Equation (7-7), the engine flywheel torque, τ_e, can be determined:

$$\tau_e=(N_t^{\,2}+N_e^{\,2})\cdot(inverse\,K-factor^{*}) \tag{7-8}$$

Given the engine torque and determining the torque ratio from the speed ratio, the turbine torque can now be determined.

To determine the engine speed for the subsequent time step, the net torque available to accelerate the engine must be determined using the wide open throttle (WOT) torque from engine dynamometer testing and the corresponding accessory torque, including the power steering, alternator, A/C compressor, and mechanical fan loads:

$$\tau_{net} = \tau_{WOT} - \tau_{accessory} - \tau_e \tag{7-9}$$

Given the engine inertia, flywheel or flexplate inertia, and torque converter impeller inertia, the engine speed can then be determined.

$$\alpha_e = \frac{\tau_{net}}{\sum I_e} \tag{7-10}$$

$$N_e = \frac{60}{2\pi}\int \alpha_e dt = \frac{60}{2\pi}\omega_e \tag{7-11}$$

After the turbine torque is determined, the wheel output torque is determined from the drivetrain model taking into account the transmission gear ratio for the corresponding gear (the simulation requires the WOT upshift engine speed as an input), final drive ratio as well as all component inefficiencies and inertia losses as shown in Figure 7-4. The rotational inertia effects, including the engine, flex-plate, impeller, turbine, transmission gear, transfer case, driveshaft, final drive, wheel and tire, are calculated using the corresponding rotational acceleration and moment of inertia. :

$$\tau = I \cdot \alpha \tag{7-12}$$

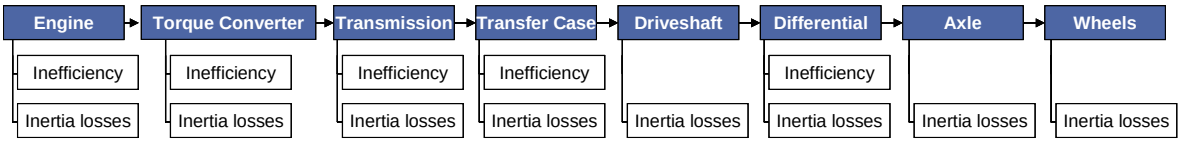

Figure 7-4 Performance Model Vehicle Subsystems, Losses and Direction of Power Flow

The net wheel torque after taking rotational inertia effects into account is translated into a tractive effort force, F_{TE}, using the tire radius, R_t.

$$F_{TE} = \frac{\tau_{wheel}}{R_t} = \frac{2\pi \cdot T \cdot \tau_{wheel}}{1609.35} \tag{7-13}$$

Combining the results from Equation (7-13) into Equation (7-5) yields the acceleration which can be integrated to determine the vehicle velocity and further integrated to solve for the distance traveled yielding the corresponding performance characteristics of interest (e.g., 0 to 60 time, ¼ mile time, etc.).

7.3.3 Performance Model Correlation and Validation

To validate the model, test track measurements from a sport utility vehicle with a V6 engine and 5-speed transmission were compared to the simulation parameters. Figure 7-5 shows a comparison of the test track and simulation engine speed, vehicle speed, and acceleration. The overall performance Simulink® model is shown in Figure 7-6. The areas requiring improvement, including the initial launch and gear shifting, are circled. Improvements to the simulation will be discussed in the subsequent sections.

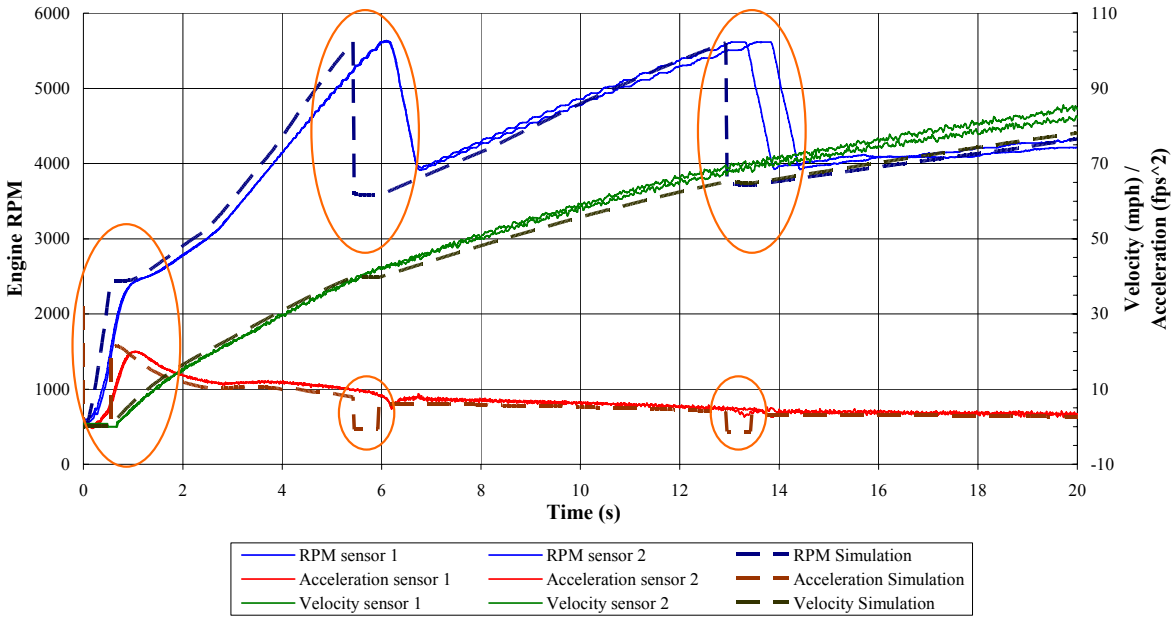

Figure 7-5 Initial Performance Simulation Results Compared to Test Track Measurements

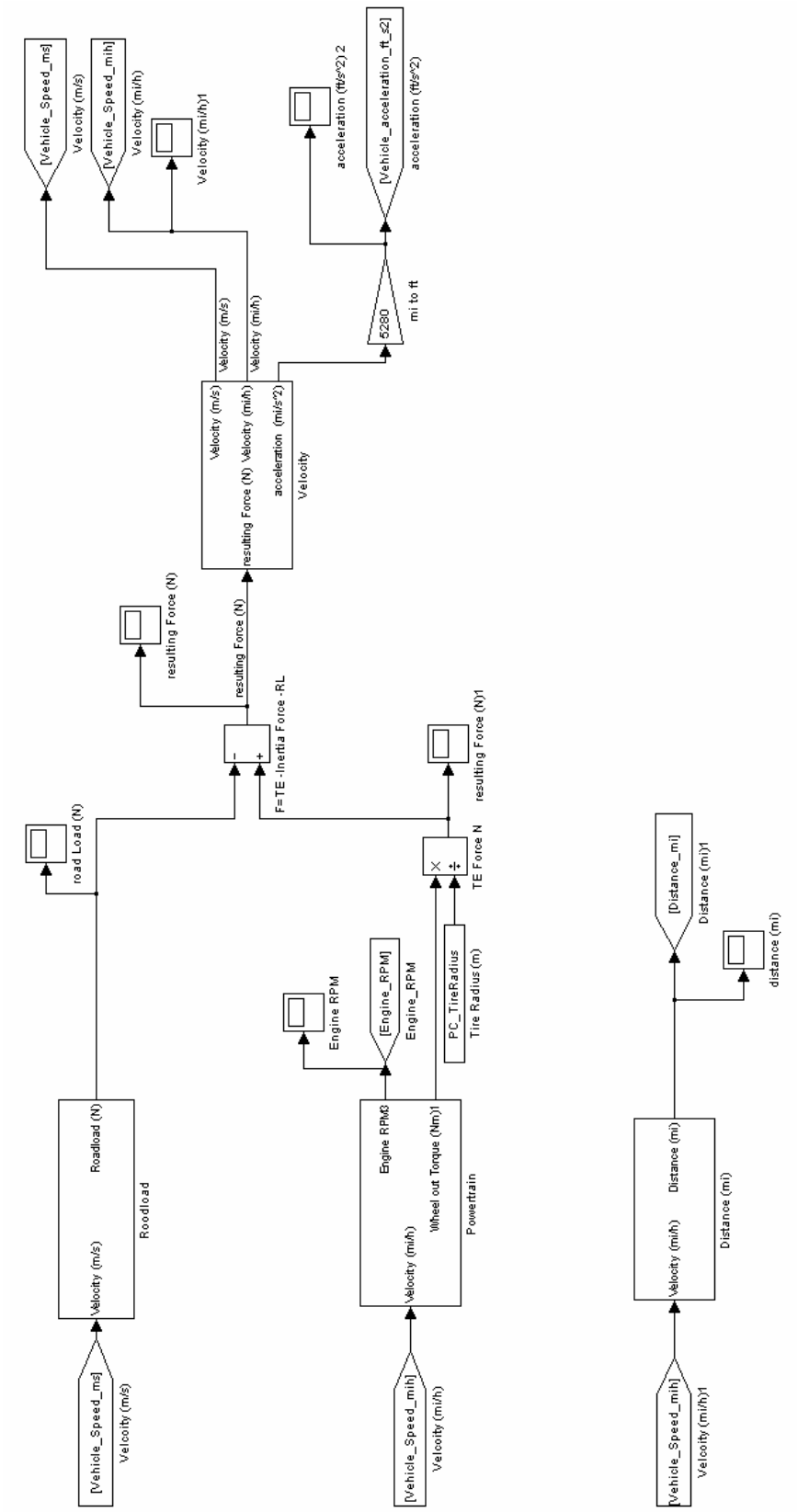

Figure 7-6 Performance Simulation Simulink® Model

7.3.3.1 Throttle Delay and Torque Blend Factor

The initial simulation results unrealistically assumed that the WOT torque was immediately achieved. In reality there is a time delay since the throttle cannot instantaneously open to 100 percent after the driver depresses the pedal to 100 percent. Also there is a transport delay due to the intake manifold filling. Therefore a WOT torque delay is assumed for a time period when the engine torque output is only the pre-determined idle torque due to the accessory loads. Then a first-order time delay is assumed by applying a torque factor to filter or blend the torque output from idle to WOT torque during manifold filling.

$$f(t) = e^{-\tau_d t} \tag{7-14}$$

The torque factor and how the WOT torque is blended is shown in Figure 7-7.

7.3.3.2 Shift Model

The initial simulation results also unrealistically assume that the transmission torque and speed change instantaneously during a gear shift. In reality it takes time to disengage and engage the appropriate transmission clutches to execute a shift. Therefore a shift time is assumed in which the transmission gear ratio is blended from the gear ratio before and after the shift as shown in Figure 7-8. Also shown in Figure 7-8 is a shift torque reduction factor that simulates the torque loss due to slip during the disengaging and engaging of the clutches. To more accurately represent the actual losses in the clutches, it is assumed that the time to release the clutches is less than the time to engage clutches.

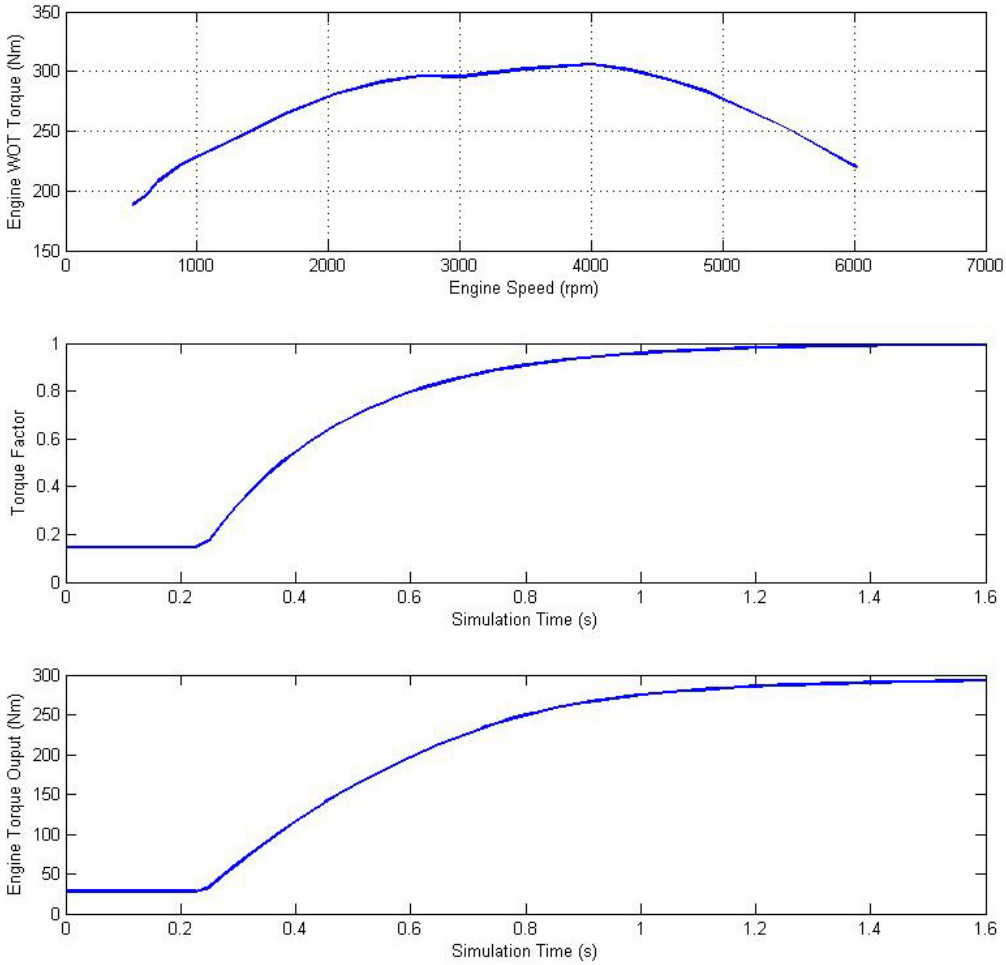

Figure 7-7 Engine WOT Torque, Torque Blend Factor and Engine Torque Output

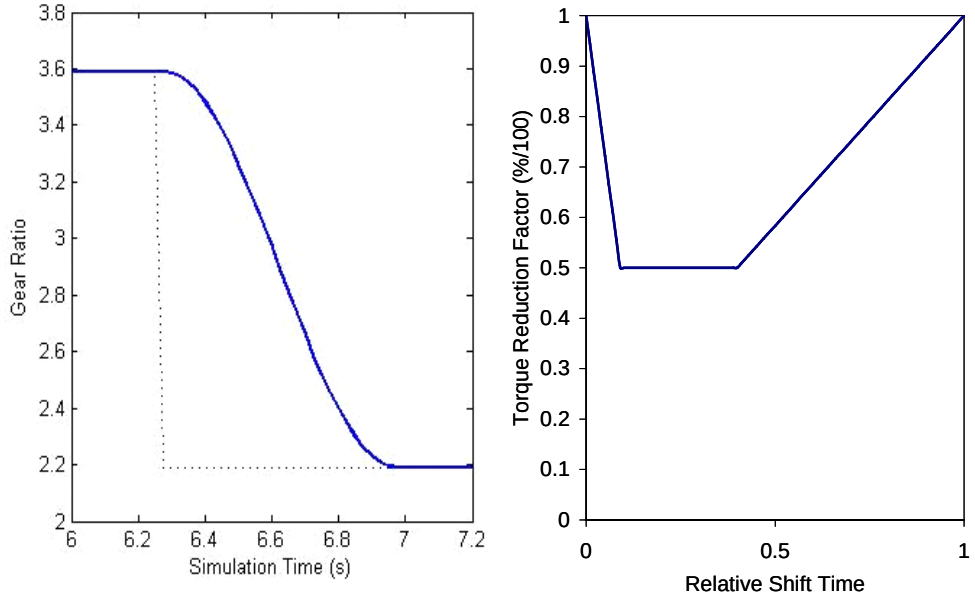

Figure 7-8 Transmission Gear Ratio Blend and Shift Torque Reduction Factor

After incorporating the performance model improvements the simulation results were compared to the test track results as shown in Figure 7-9.

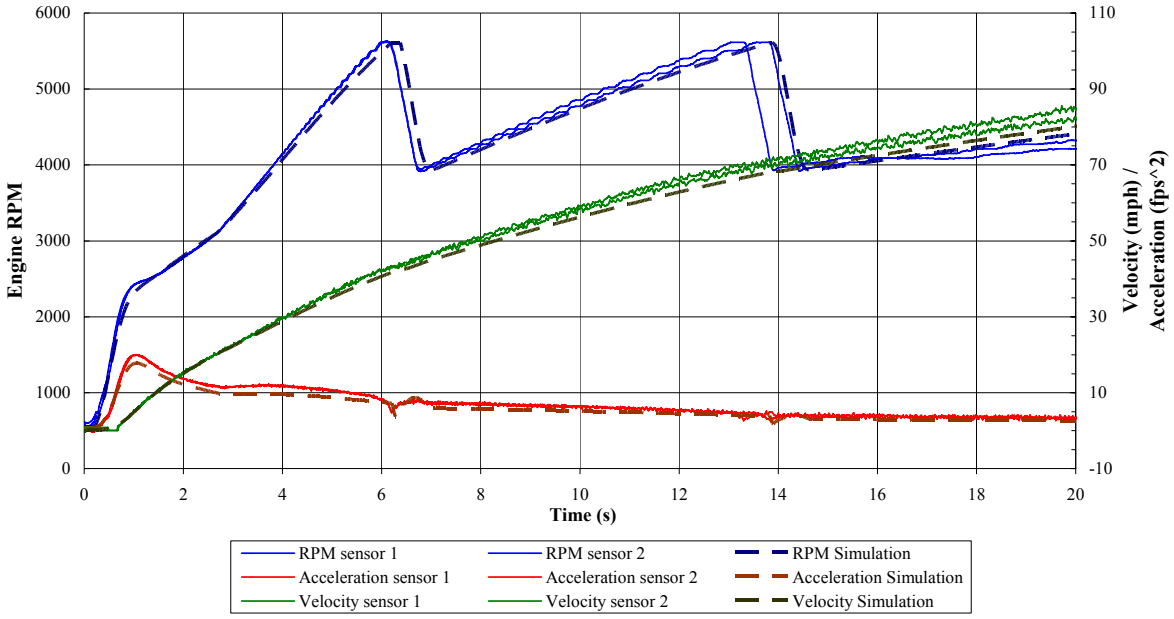

Figure 7-9 Final Performance Simulation Results Compared to Test Track Measurements

The performance measures of interest from both the simulation and test track are shown in Table 7-3 and Table 7-4, respectively. Note that the test track results are an average of six measurements each. Some of the discrepancies in the absolute values can be attributed to the fact that the component inertia and spin losses are accounted for in the individual powertrain component models but some of these effects are also indirectly factored in the overall road load coefficients resulting in slightly overall slower performance times as the vehicle speed increases. The individual inertia effects were intentionally included so that incremental changes in component inertias could be evaluated. Since the performance tool was developed to determine the relative performance between different powertrain configurations, two different final drive ratios (3.07 versus 3.55) were also simulated and the results were compared to the test

measurements. The simulation consistently predicted which final drive ratio performs better. The results validate that the tool can be used to effectively rank the relative performance of advanced powertrain hardware designs. The trade-off between acceleration performance and fuel economy will be studied in Section 7.5.

Table 7-3 Simulation Performance Prediction Results

	Performance Data Prediction Tool					
	FDR	3.07	FDR	3.55	Difference	
	Feet		Feet		Feet	
5 SEC DISTANCE	**125.57**		**130.20**		**4.63**	
20 SEC DISTANCE	1485.34		1498.37		13.03	
	Seconds	Feet	Seconds	Feet	Seconds	Feet
0-10 MPH	1.52	6.81	1.47	6.60	-0.05	-0.21
0-20 MPH	2.72	33.89	2.66	33.39	-0.06	-0.50
0-30 MPH	4.25	89.81	4.06	84.87	-0.18	-4.94
0-40 MPH	5.94	177.41	5.88	179.05	-0.06	1.64
0-50 MPH	8.37	337.79	8.16	330.03	-0.20	-7.76
0-60 MPH	**11.17**	**564.50**	**11.05**	**564.82**	**-0.12**	**0.32**
0-70 MPH	14.84	916.32	14.92	933.96	0.08	17.64
0-80 MPH	19.97	1481.57	19.49	1438.02	-0.48	-43.54
40-60 MPH	5.22		5.17		-0.05	
50-70 MPH	6.47		6.75		0.28	
	Seconds	MPH	Seconds	MPH	Seconds	MPH
1/4 MILE	**18.57**	**77.41**	**18.47**	**77.94**	**-0.10**	**0.53**

Table 7-4 Test Track Performance Results

	Performance Data Test Measurements					
	FDR	3.07	FDR	3.55	Difference	
	Feet		Feet			
5 SEC DISTANCE	**128.53**		**133.18**		**4.65**	
20 SEC DISTANCE	1525.21		1531.15		5.94	
	Seconds	Feet	Seconds	Feet	Seconds	Feet
0-10 MPH	1.54	9.85	1.50	9.30	-0.04	-0.55
0-20 MPH	2.76	37.23	2.65	35.55	-0.11	-1.68
0-30 MPH	4.23	90.37	4.03	85.62	-0.20	-4.75
0-40 MPH	5.89	178.42	5.82	180.10	-0.07	1.68
0-50 MPH	8.21	333.01	8.02	326.28	-0.19	-6.73
0-60 MPH	**10.90**	**552.50**	**10.72**	**547.35**	**-0.18**	**-5.15**
0-70 MPH	14.29	881.35	14.47	907.89	0.18	26.54
0-80 MPH	19.05	1410.82	18.80	1390.29	-0.25	-20.53
40-60 MPH	5.00		4.90		-0.10	
50-70 MPH	6.10		6.50		0.40	
	Seconds	MPH	Seconds	MPH	Seconds	MPH
1/4 MILE	**18.27**	**79.38**	**18.19**	**79.60**	**-0.08**	**0.22**

7.4 Advanced Dual Clutch Transmission Modeling

The reverse dynamic optimization methodology was extended to dual clutch transmission technology to study the potential of advanced powertrain design alternatives.

7.4.1 Dual Clutch Transmission Background

A dual clutch transmission (DCT) is an automated "clutchless" manual type transmission and is a relatively new technology in production passenger car vehicles. A conventional manual transmission requires the driver to operate a clutch that disconnects the engine from the transmission and then use the stick shift to select a new gear. A DCT, however, has a two-part transmission shaft with two clutches and uses automated electronics and hydraulics to control the clutches. Since there are two clutches, one controlling the even gears and one controlling the odd gears, gears can be changed sequentially without interrupting the power flow from the engine to the transmission. Figure 7-10 shows a typical five-speed DCT with one clutch controlling second and fourth gears, while another, independent clutch controls first, third and fifth gears. Instead of using a torque converter, DCTs generally use a wet or dry multi-plate clutch to drive the gears. One of the advantages of DCTs is the ability to quickly execute a shift. Also DCT technology has the potential to improve fuel efficiency given that the power flow from the engine to the transmission is not interrupted. Still, the potential fuel economy benefit is highly dependent on the clutch slip during the launch of the vehicle and during shift transitions.

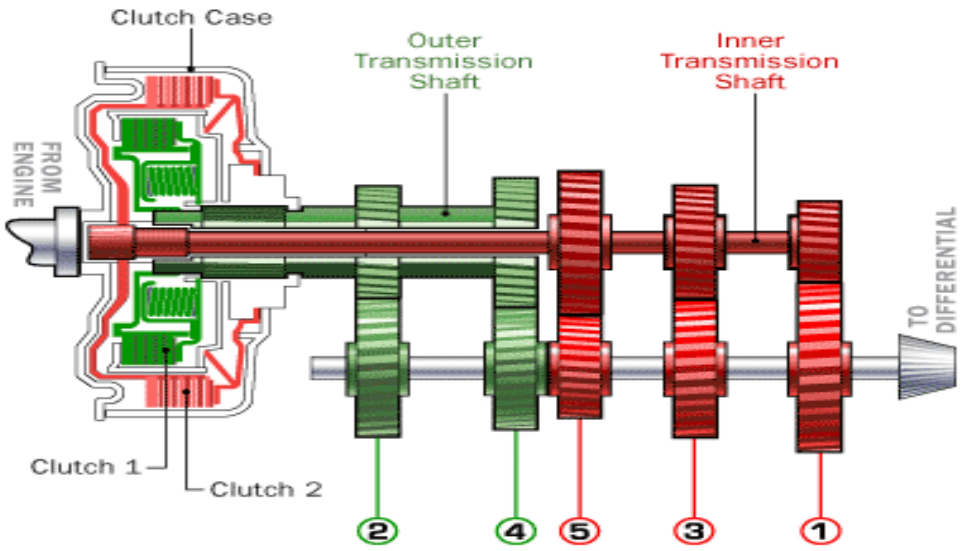

Figure 7-10 Typical Dual Clutch Transmission (Harris 2006)

7.4.2 Dual Clutch Transmission Model Development

The reverse tractive road load demand model was modified to accommodate DCT technology. The component models are similar to those described in Section 4.2 except those related to the torque converter. To accommodate DCT technology, the reverse model had to be modified to model the slip of a DCT launch device. In order to launch the vehicle there is considerable slip between the clutch and the transmission input to allow the engine to rev up to speed. In addition there is some degree of slip when one clutch is disengaged and the other clutch engages during shift transitions. The launch device is modeled such that during first gear the amount of clutch slip is determined as a function of the output speed. Clutch slip is also modeled as a function of the output speed during shift transitions for a minimum of one second.

7.4.2.1 Launch Clutch Slip Model Correlation

To correlate the DCT slip model, testing was performed to determine the amount of clutch slip on a production 6-speed DCT equipped sports coupe and entered into the model vehicle configuration files. Actual clutch speed was acquired via ECU data collected from the Controller Area Network (CAN) bus via the CANape measurement data acquisition system (http://www.vector-informatik.com.html). The measured clutch slip values used for the correlation vehicle are shown in Figure 7-11.

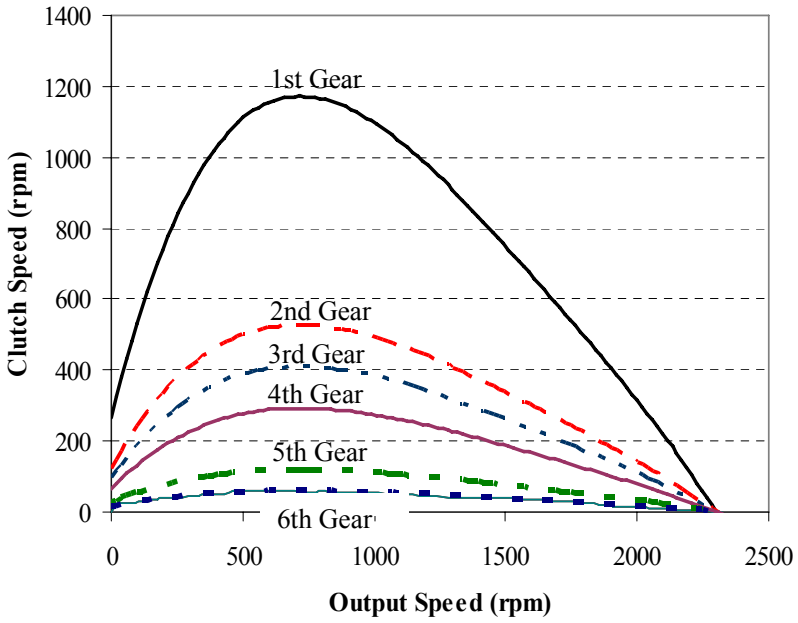

Figure 7-11 DCT Slip Assumptions for First Gear and During Shift Transitions

7.4.2.2 DCT Drivability Constraints

The initial dynamic programming (DP) simulation results with the aforementioned slip assumptions are shown in Figure 7-12. The DP optimization results reveal that the ideal shift strategy would be to launch the vehicle in second gear similar to how a manual transmission driver could choose to launch in second gear if sufficient torque is available to overcome the vehicle inertia and accelerate the vehicle. A

constraint was added to the DP algorithm such that the vehicle must launch in first gear. The simulation results with the first gear launch constraint and the corresponding fuel economy for a simulated CR city cycle are shown in Figure 7-12 and Table 7-5

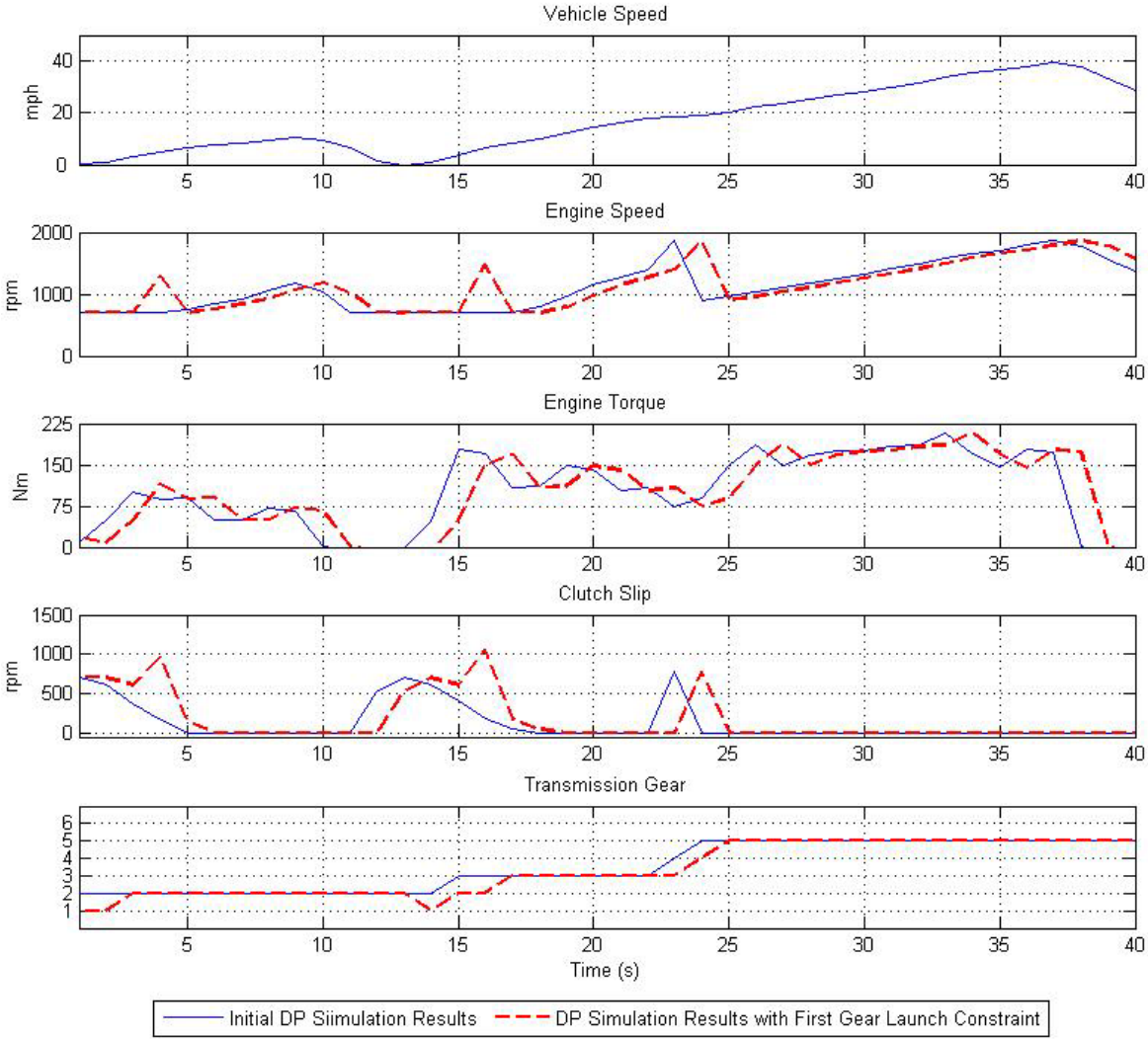

Figure 7-12 DCT Launch Constraint DP Simulation Results

As discussed in Section 4.3.1.2, selecting a minimum engine speed after upshift (MESAU) constraint is critical to properly modeling a DCT. A MESAU constraint of 1100 rpm was added to the simulation parameters to ensure sufficient acceleration capability and avoid giving the driver the feeling that the engine is lugging. Figure 7-13

depicts the simulation results with and without a MESAU constraint. Adding the MESAU constraint delays the upshift points yielding higher engine speeds during accelerations. The significant decrease in the simulated fuel economy by adding a MESAU constraint is shown in Table 7-5.

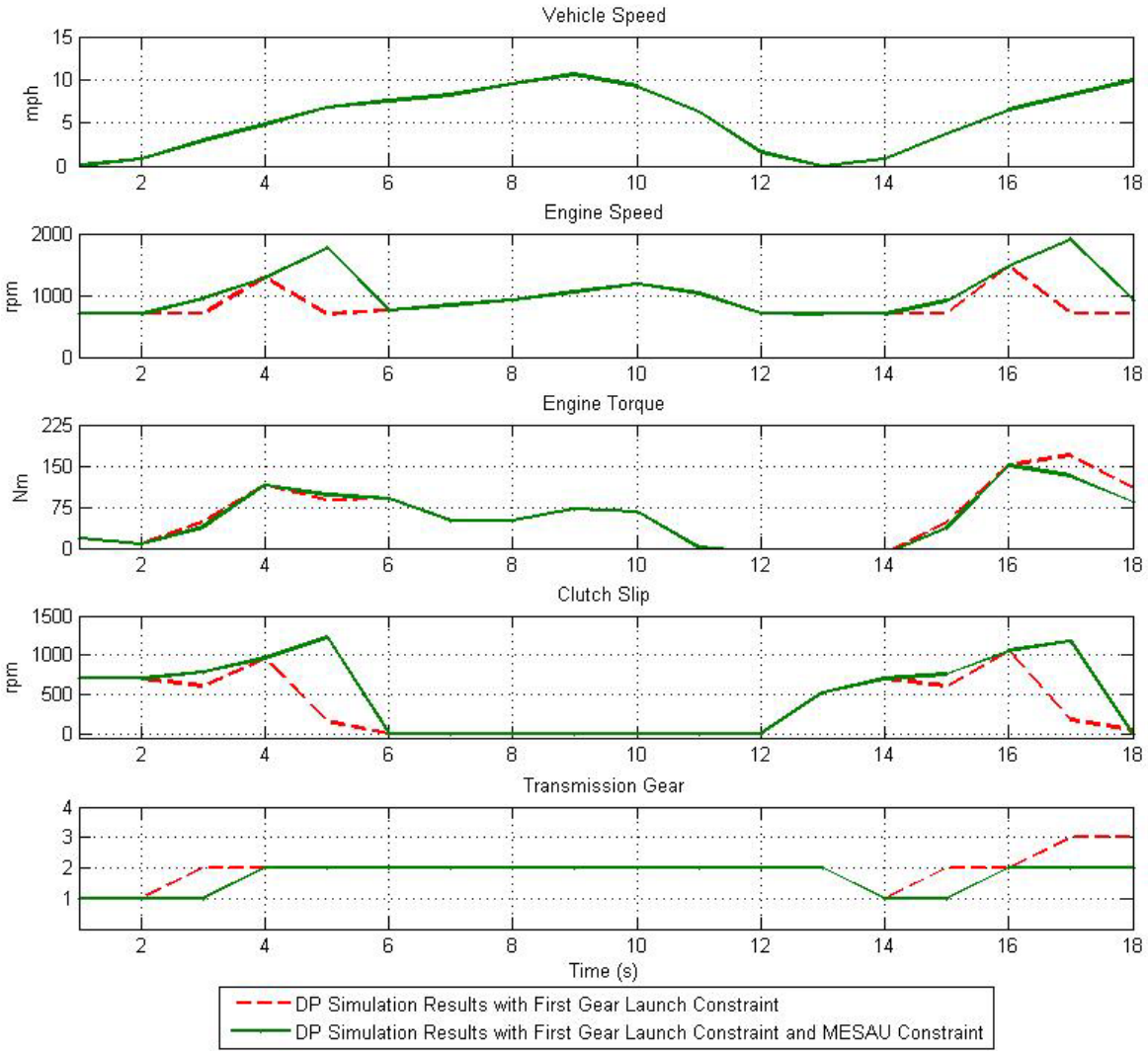

Figure 7-13 DCT MESAU Constraint DP Simulation Results

Table 7-5 DP Simulation Dual Clutch Transmission Fuel Economy Results with and without Drivability Constraints

Initial DCT DP Simulation Results	14.95 mpg
DP Simulation Results with First Gear Launch Constraint	14.58 mpg
DP Simulation Results with First Gear Launch and Minimum Engine Speed After Upshift (MESAU) Constraints	14.11 mpg

7.4.3 Dual Clutch Transmission Model Validation

The correlation vehicle measurements from test track results are compared to the DP simulation results in Figure 7-14. Some simulation discrepancies result since the DP algorithm does not result in the same shift control as the actual correlation vehicle. The correlation vehicle under consideration is biased towards a sporty shift feel while DP results are biased towards fuel economy. Also the data acquisition rate of the sensors is higher than the one second sample rate of the simulation. The clutch speed sensors appear to be noisy as well. Nonetheless, the DP simulation reasonably models the clutch slip at launch and during shift transitions and yields an engine speed and torque profile that closely models the DCT drivetrain.

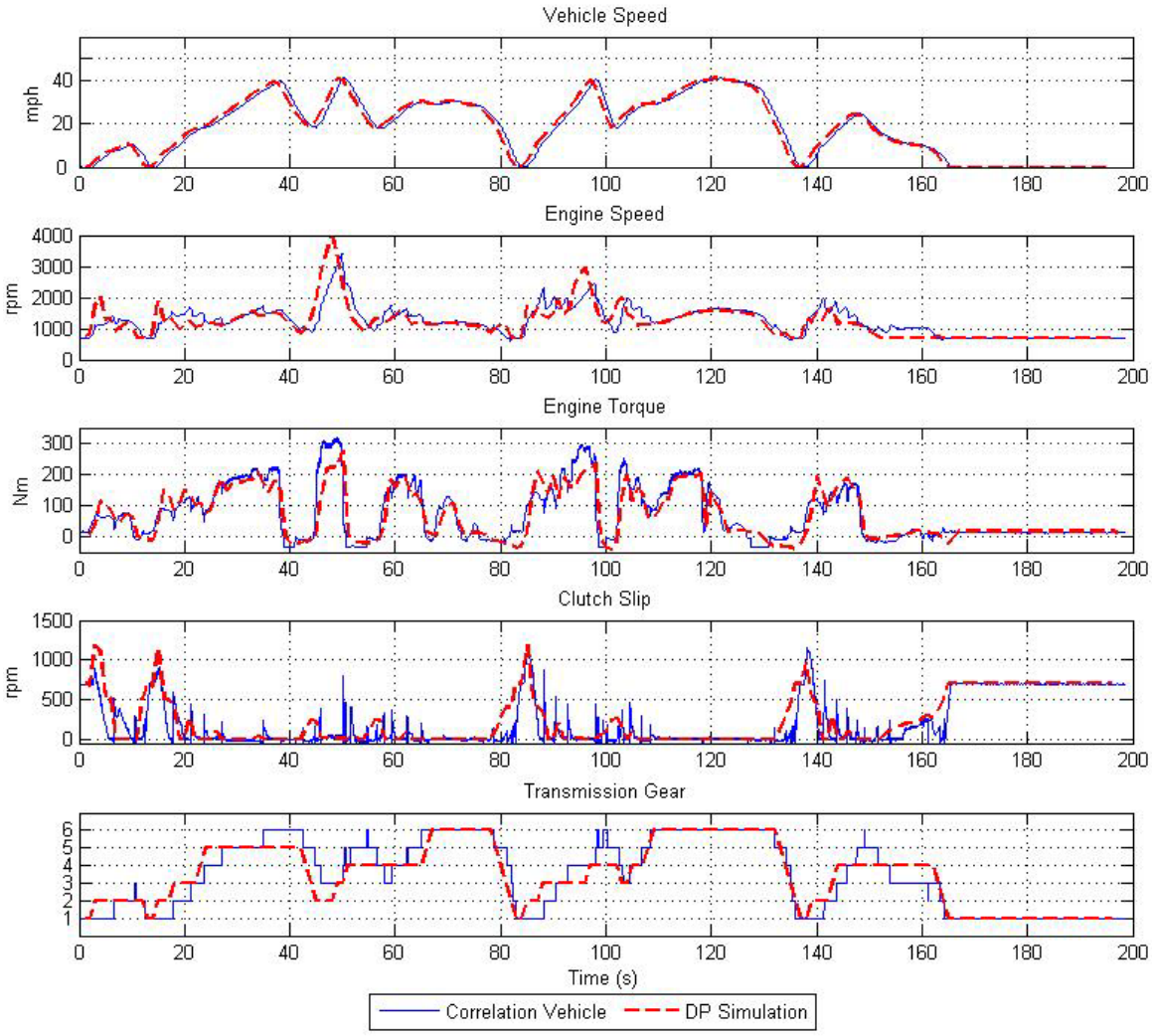

Figure 7-14 Dual Clutch Transmission Model Correlation

7.5 Powertrain Matching Analyses

Optimizing fuel economy requires a "systems analysis" approach and the methodologies and tools developed in this dissertation facilitate rapid and systematic assessment of advanced design alternatives relative to both vehicle attributes and performance. The primary advantages of the reverse dynamic optimization simulation methodology over the state-of-the-art are as follows:

- Expedites consistent evaluation of hardware design alternatives early in the design process (Reduces time to simulate multiple design configurations from weeks to hours)
- Compares advanced designs and technology in conjunction with optimized system control
- Facilities control design that is catered to vehicle and drive cycle characteristics taking system interaction effects into account

The following are examples of the type of analyses that can be performed using the reverse dynamic optimization and performance simulation tools.

7.5.1 Fuel Economy Sensitivity to Vehicle Attributes

Fuel economy is highly sensitive to vehicle attributes. Hence establishing vehicle targets to reduce vehicle weight, aerodynamic drag, tire rolling resistance, and brake and bearing drag are essential to attaining fuel economy improvements. It is important to reiterate the conclusions drawn in Section 3.1 that reducing road load power and other system parasitic losses not only has a direct benefit on fuel economy but also yields a further benefit by reducing the demand requirements of the engine. One advantage of the reverse dynamic optimization tool over other vehicle models is that when vehicle parameters are changed, the dynamic programming algorithm automatically takes corresponding system level effects into account. For instance, if the vehicle weight is reduced, the transmission control strategy is automatically adjusted to upshift earlier so the engine can operate at a lower engine speed with less energy demand. The reverse dynamic approach was applied to illustrate the sensitivity of changes in vehicle weight

and road load demand (via changes to the road load coefficients described in Section 2.2.7) to fuel economy in Figure 7-15.

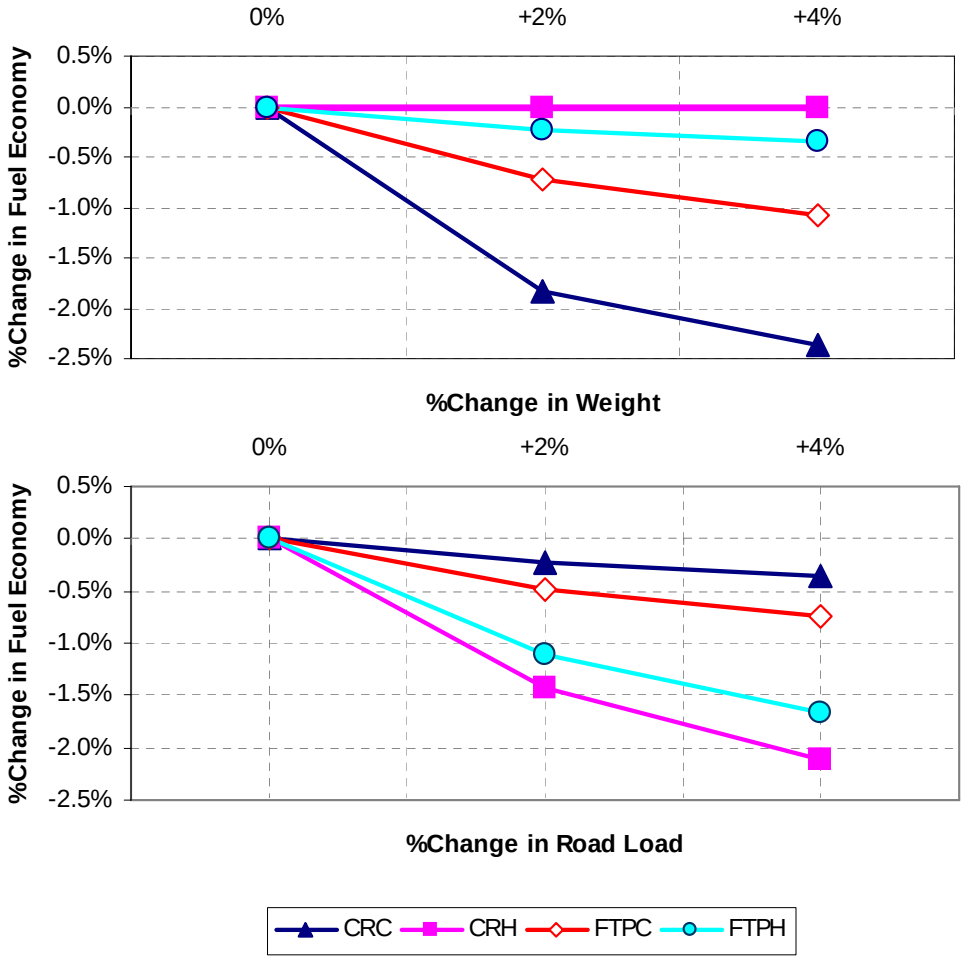

Figure 7-15 Fuel Economy Sensitivity to Vehicle Weight and Road Load Demand

Both Consumer Reports city (CRC) and the FTP city (FTPC) cycles are very sensitive to increasing weight since city driving is dominated by the inertial effects of changes in velocity. The Consumer Report highway (CRH) and FTP highway (FTPH) fuel economy are very sensitive to increases in aerodynamic drag and rolling resistance as reflected in the road load coefficients.

Further reductions in vehicle weight and road load could potentially yield further benefits by enabling engine downsizing for the same performance level. Therefore it is imperative that practical targets are set before further powertrain matching analyses can be performed.

To quantify the trade-off in performance and fuel economy, ranking criteria are established. The fuel economy ranking used here is based on the harmonic average of the simulation results for the Consumer Reports city, Consumer Reports highway, and FTP combined fuel economy, where the FTP combined is a weighted harmonic average:

$$FTP\ \ Combined = \frac{1}{\frac{0.55}{FTP\ City} + \frac{0.45}{FTP\ Highway}} \tag{7-15}$$

The performance ranking, defined as the average of the 0 to 30 mile per hour, 0 to 60 mile per hour, and ¼ mile times, is held constant for purposes of this study. Figure 7-16 reveals how reducing vehicle weight combined with engine displacement downsizing can lead to substantial fuel economy benefit with similar performance rankings.

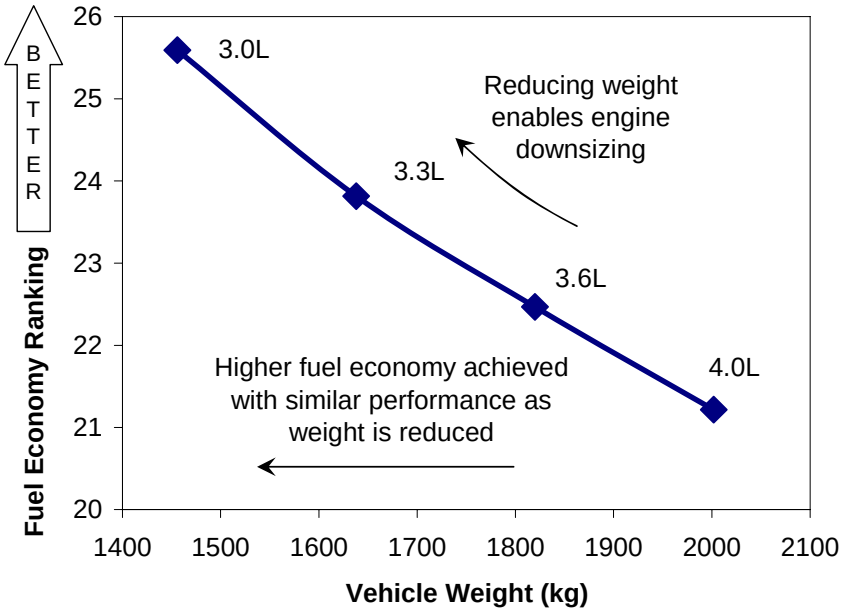

Figure 7-16 Effect of Vehicle Weight Reduction and Downsizing on Fuel Economy

7.5.2 Optimal Engine Displacement, Transmission, and Final Drive Ratio Selection

To minimize fuel usage, the vehicle subsystem components must be made to operate as efficiently as possible. However, it is equally important that each component interact with the system so as to maximize the efficiency as a whole. For advanced vehicle designs, it is crucial that the engine displacement, torque converter characteristics, transmission and final drive ratio match the vehicle system. Once the target vehicle attributes, such as weight, aerodynamic drag and rolling resistance are established, the reverse dynamic optimization and performance evaluation tools can be used to match the powertrain to specific vehicle attributes.

Various speed transmissions with different overall ratio spreads were analyzed with varying engine displacements for a target sedan. Descriptions of the three transmissions considered in this study can be found in Greiner, *et al.* (2004) and Wagner, *et al.* (2007). To reflect the transmission inefficiencies in the analysis, theoretical gear efficiencies were assumed based on the gear ratio and clutch configuration. Spin losses (i.e., losses in open running clutches) were assumed based on the number of discs, clutch diameter, gear, geometry, and engine speed. For purposes of this study, brake specific fuel consumption data was scaled to determine the torque and fuel flow characteristics of different displacement engines. The results in Figure 7-17 indicate that more transmission gears and a wider ratio spread is desirable since it enables the reduction of engine displacement to achieve higher fuel economy with constant or better performance.

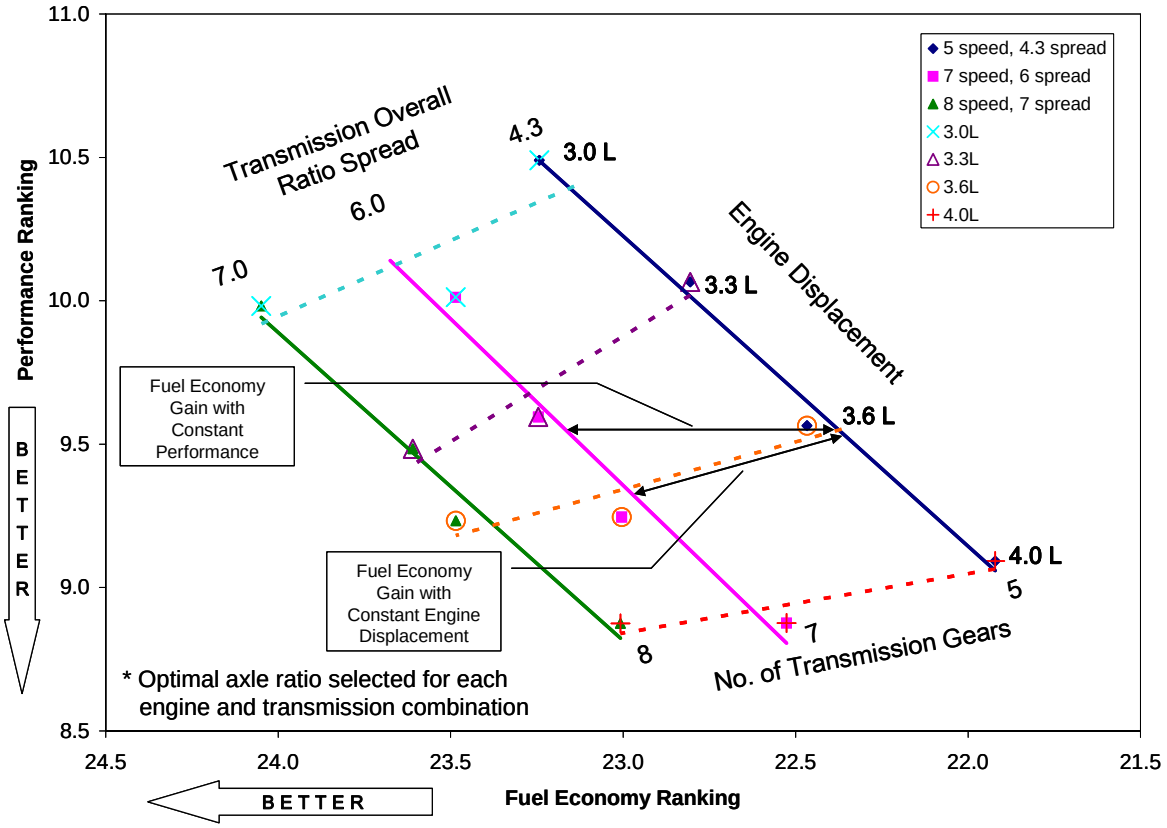

Figure 7-17 Effect of Engine Displacement, Transmission Gears and Ratio Spread on Performance and Fuel Economy

Final drive ratios (i.e., axle ratios) were selected for each configuration by sweeping a number of ratios and creating a performance/fuel economy "hook" similar to Figure 7-18. Although the "hooks" can vary somewhat, a near optimum final drive ratio is selected such that lower numerical ratios yield no appreciable gain in fuel economy for a loss in performance and higher ratios produce no appreciable performance gain for a small or no gain in fuel economy. To simplify the study in Figure 7-18 similar axle efficiencies were assumed, although in practice slight increase in efficiency may result by lowering the axle ratio.

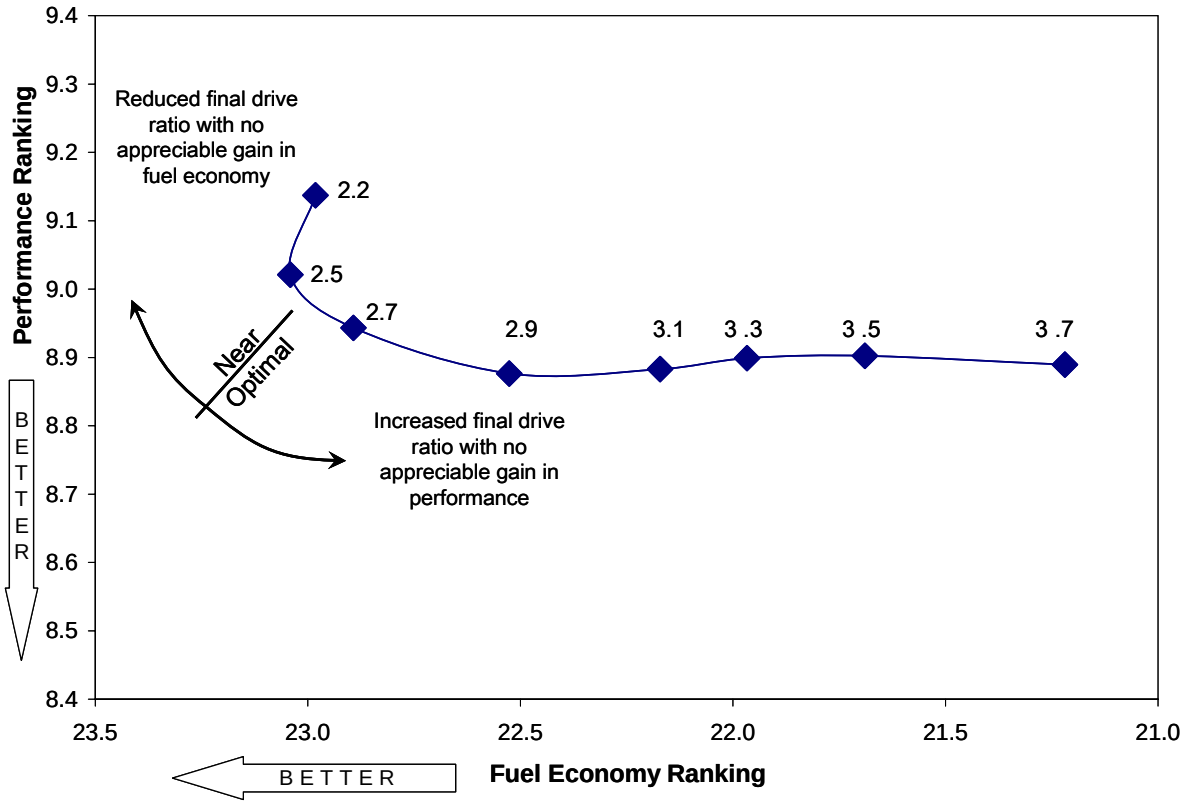

Figure 7-18 Near Optimal Final Drive Ratio Selection

7.5.3 Variable Displacement Effect on Powertrain Matching

Introducing variable displacement technology to a new vehicle system influences the optimal powertrain configuration. Figure 7-19 demonstrates the effect on fuel economy of adding Multi-Displacement System (MDS) technology to the same engine and transmission combinations from Section 7.5.2.

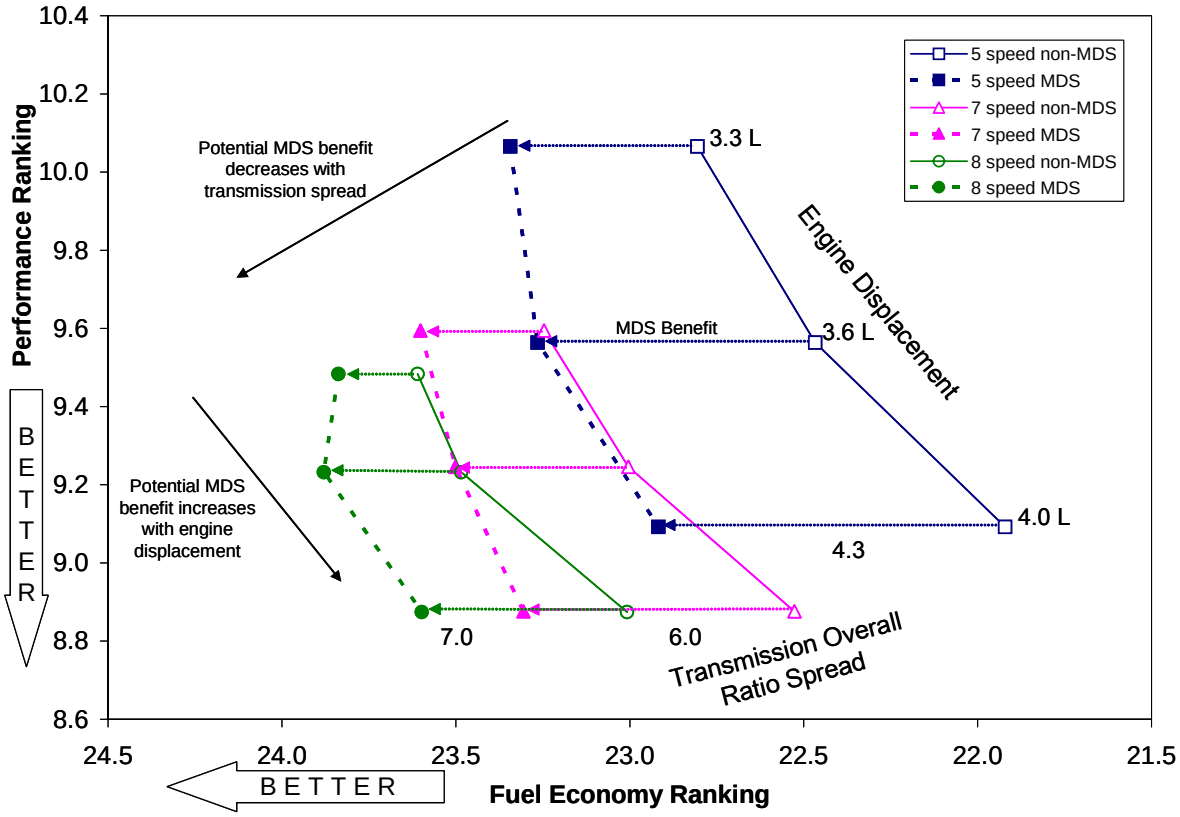

Figure 7-19 Multi-Displacement System (MDS) Effect on Optimal Powertrain Configuration

It is clear that MDS technology achieves higher fuel economy while maintaining the same performance. Given that variable displacement functions by reducing pumping work by deactivating half of the engine cylinders under part load conditions, the percent fuel economy benefit is reduced as the engine displacement is reduced. Smaller displacement engines have less torque available with some of their cylinders deactivated and maintain less MDS active time while traversing the drive cycles. Increasing the number of transmission gears and ratio spread enables the engine to operate in a more efficient region such that the percent benefit of MDS is less significant. This analysis suggests that achieving higher fuel economy requires the appropriate combination of new technology as adding many powertrain features that all attempt to reduce the same losses

(e.g., pumping work) will not result in additive fuel economy benefits. In other words, when estimating the fuel economy potential of a new vehicle system, the individual measured fuel economy benefit of different technologies, such as higher speed transmissions, MDS, or variable valve timing, cannot be added together when combined. This further demonstrates the advantage of the reverse dynamic optimization approach since the interaction effects of individual technologies are taken into account to determine the combined effect.

Another consideration when adding MDS technology to a vehicle design is its impact on noise, vibration and harshness (NVH) as previously described in Section 6.2. The torque converter can be controlled to operate in slip mode to reduce the resulting engine vibrations in MDS, but slipping the converter could potentially negate the fuel economy benefit of deactivating cylinders. Figure 7-20 depicts the cycle-based fuel economy sensitivity to slipping the converter while in MDS mode. Previously the only way to determine whether operating in MDS was a benefit was to run steady-state points on a powertrain dynamometer both in and out of MDS while measuring fuel flow to determine if slipping the converter negated the benefit. The previous method was not only time consuming, it is not possible to run tests on theoretical system designs and it is very difficult to determine the fuel economy impact on drive cycles. The reverse dynamic optimization simulation approach is advantageous since it automatically determines whether being in MDS at the prescribed slip is a benefit and corresponding adjusts the MDS control strategy to achieve the highest fuel economy. Likewise the dynamic programming algorithm automatically modifies the MDS-equipped gear shift strategy to maintain MDS if there is a fuel economy benefit. The end result is that the

reverse dynamic optimization methodology facilitates quick evaluation of the full MDS potential on a system design early in the design process.

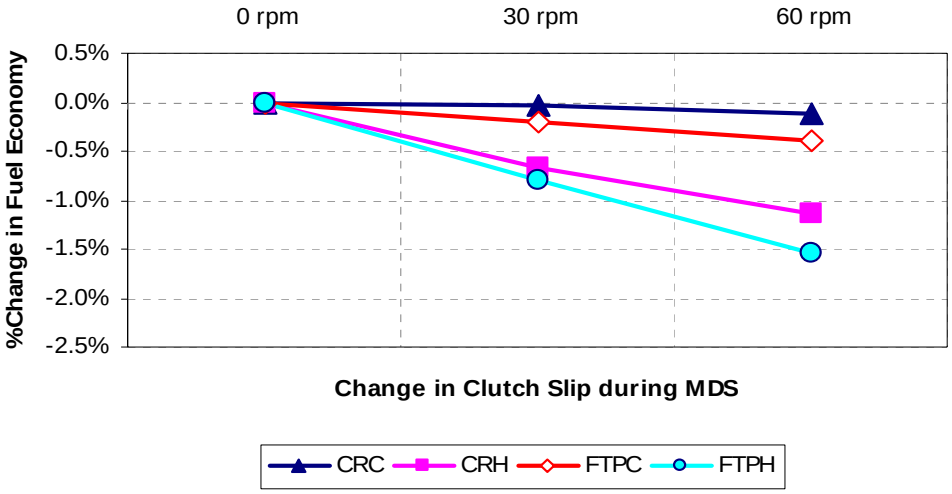

Figure 7-20 Effect of Clutch Slip during MDS Mode on Fuel Economy

7.6 Simulation Time Advantage

One primary advantage of the new reverse dynamic simulation approach is the significant time savings to evaluate a plurality of powertrain design alternatives. The analysis in Figure 7-17 and Figure 7-18 required simulations for a total of 96 powertrain configurations (4 engines × 3 transmissions × 8 final drive ratios). A script was developed that automatically changes the input parameters for the powertrain configurations of interest and loops the simulations thereby expediting the total simulation time. The total simulation time for the 96 configurations was just 2 hours and 15 minutes, approximately 40 times faster than real time, as shown in Table 7-6. In addition to computation time savings, additional time savings result by using the dynamic programming algorithm since new powertrain control inputs (e.g., new shift maps for each configuration) do not need to be developed offline when changing the powertrain

configuration. Between the additional computation time, control development and input time, performing such an extensive analysis using existing the state-of-the-art vehicle simulations would have required a number of days to weeks.

Table 7-6 Reverse Dynamic Optimization and Performance Simulation Times

Number of Powertrain Configurations	Simulation Cycles	Total Cycle Time (sec)	Simulation Time Step (sec)	Total Simulation Time (hr:min:sec)
1	FTPC, FTPH, CRC, CRH, WOT Acceleration	3396 (FE), 100 (WOT)	1 (FE), 0.025 (WOT)	1 min : 30 sec
96	376 fuel economy cycles, 96 performance cycles	326,016 (FE), 960 (WOT)	1 (FE), 0.025 (WOT)	2 hr : 15 min

CHAPTER 8

CONCLUSION AND FUTURE WORK

New system analysis methodologies and tools are proposed to improve current methods of evaluating and optimizing the interaction and control of automotive powertrain components and subsystems for improved overall vehicle efficiency. Current state-of-the-art vehicle system models lack true optimization capabilities since they disregard the interdependence between hardware design and control strategy and their further dependence on drive cycle characteristics and vehicle attributes. The proposed model-based engineering approach combines optimal hardware design and optimal control and facilitates rapid investigation of the potential benefits of given powertrain system configurations early in the design process while taking driver application into account.

8.1 Scientific Contributions

The scientific contributions of this dissertation are summarized as follows:

- Developed a vehicle system energy analysis methodology and tool using hybrid semi-empirical and analytical approach with detailed component speed and load data;

- Developed a reverse tractive road load demand model and introduced dynamic optimization methodology as a predictive technique for objectively evaluating vehicle system efficiency assuming minimum accumulated fuel consumption over a given drive cycle;
- Proposed a dynamic optimization technique for transmission gear shift, torque converter lock-up clutch, pedal control design and evaluation employing the reverse tractive road load demand model and dynamic programming algorithm;
- Extended the reverse tractive road load demand model to variable displacement engine technology and proposed dynamic optimization approach to virtually optimize variable displacement system-level control strategies (including gear shift and clutch control) in conjunction with different drivetrain configurations and their interaction effects;
- Integrated a performance model to the reverse dynamic optimization simulation approach to quantify the trade-off in fuel economy and performance for advanced powertrain hardware and system integration; and
- Demonstrated advantages of the reverse dynamic optimization methodology by performing powertrain matching analyses and revealing key system integration concepts for improving fuel economy (i.e., sensitivity to vehicle attributes; optimal engine, transmission and final drive ratio selection; and effect of variable displacement).

8.2 Recommendations for Future Work

The proposed reverse dynamic optimization methodology has been successfully applied to powertrain systems with conventional automatic transmissions, advanced dual clutch transmissions as well as manual and electronic throttle engines including engines with variable displacement technology. Possible future work includes extending the reverse tractive road load model and dynamic optimization capabilities to include other advanced vehicular technology, such as hybrid electric or fuel cell drivetrains. Hybrid electric and fuel cell vehicles have been studied using both the forward- and backward-looking approaches (Markel, et al. 2002; Lin 2004b). Further work to optimize these vehicle systems for maximum system efficiency in terms of power management (e.g., engine versus fuel cell versus battery pack), component sizing, driveline configuration, and cost while addressing the interdependence of hardware and control design needs to be explored.

The optimization methods applied in this dissertation involved powertrain components with discrete states. To incorporate control of continuous types of powertrain components, such as continuously variable transmissions, the dynamic programming algorithm needs to be modified. After formulating a sequential decision process for the continuous decision variables, a grid can be placed at each stage on each decision set to interpolate in the state space to find the optimal control policy (Denardo 1982).

Both adding new powertrain technologies and/or continuous systems complicates calibration efforts and increases the number of possible states and control variables to be computed. As the degrees of freedom associated with complex advanced powertrain

systems increases, the curse of dimensionality prevails and methods to reduce the dynamic programming computational burden need further investigation. Possible methods investigated by Larson (1967) and de Madrid (1999) could be applied to reduce the computational burden of the dynamic programming algorithm.

The objective of the cost function for this research was to minimize the accumulated fuel flow over a drive cycle. Depending on the vehicle application, a multi-objective dynamic optimization problem could be formulated to incorporate additional criteria, such as emissions, drivability, trailer tow performance, etc. In order to simulate emissions as a function of speed and load with the backward-looking approach, the engine model would need to be populated with steady-state dynamometer engine-out and tailpipe emissions data. If only engine-out emissions data were to be populated in the model, a catalyst model would need to calculate the conversion efficiency to determine the tailpipe emissions. Since steady-state dynamometer emissions data is usually acquired at fully warm conditions, temperature correction factors would need to be included. Thus, the reverse model and the corresponded subsystem models and input data would need to be expanded to take temperature effects into account. The effect of design decisions on drivability or trailer tow performance could be incorporated into the model by including acceleration capability or a torque reserve into the cost function and/or model constraints.

In addition, new novel methods for presenting and implementing the DP optimization results merit further study. For example, the DP simulation results were formulated into traditional look-up tables by fitting a line to the optimized shift and lock-up points over a drive cycle. Additional criteria could be established to evaluate the

significance of the individual shift and lock-up points in terms of fuel economy versus drivability. Given the significance of the individual shift and lock-up points, an optimal control policy could be determined by assigning weighting factors based on the control decision significance on the overall cost function.

Another consideration when optimizing the powertrain hardware configuration and control design is the impact on noise, vibration, and harshness (NVH). Currently little work is done early in the vehicle design process to assess the consequence of hardware and control design decisions on NVH. The dynamic optimization results could be presented in a format that reveals the complete envelope of speed and load conditions encountered over a drive cycle and used as an input to traditional finite element (FE) models. By incorporating a higher fidelity engine model, the predicted or measured peak cylinder pressure versus crank angle can be determined which can subsequently be generated into a combustion force. Corresponding equations of motion can then be solved to calculate the bearing and engine mount force and used as inputs to a FE solver to reveal the time history and frequency spectrum of the loads (Inagaki, *et al.* 2000; Sumi, *et al.* 2002). Understanding the complex interactions between the engine, transmission, and driveline as it relates to a vehicle's NVH behavior could facilitate early consideration of the NVH impact and requirements before prototype hardware is available.

While this doctoral work concentrated on optimizing powertrain hardware configurations and control design early in the design process, the natural progression is to extend this research to real-time powertrain system control. As new technologies increase the degrees of freedom associated with vehicle systems, interactive and robust real-time optimization and control capabilities need to be developed. Online optimization

using stochastic dynamic programming has been studied by Kolmanovsky, *et al.* (2002), Lin, *et al.* (2004c), and Johannesson, *et al.* (2006). Many other approaches to model-based calibration that rely on Design of Experiments, Response Surface Modeling, or the use of Artificial Neural Networks and online optimization using gradient based search methods, simulated annealing, or genetic algorithms have been investigated (Wu, *et al.* 2004; Rask and Sellnau 2004; Hiroyasu, *et al.* 2003). Much of this work has concentrated on engine optimization, yet there is considerable opportunity to improve vehicle system efficiency further with online interactive engine and transmission control optimization. One possible approach is to use feedback parameters such as driver pedal rate to bias the engine and transmission control strategy towards fuel economy or performance (Ohl, *et al.* 2004). The development of a real-time adaptive and interactive torque-based powertrain control system which minimizes fuel flow while taking driver intent into account offers significant potential to further improving the overall efficiency of future vehicle systems.

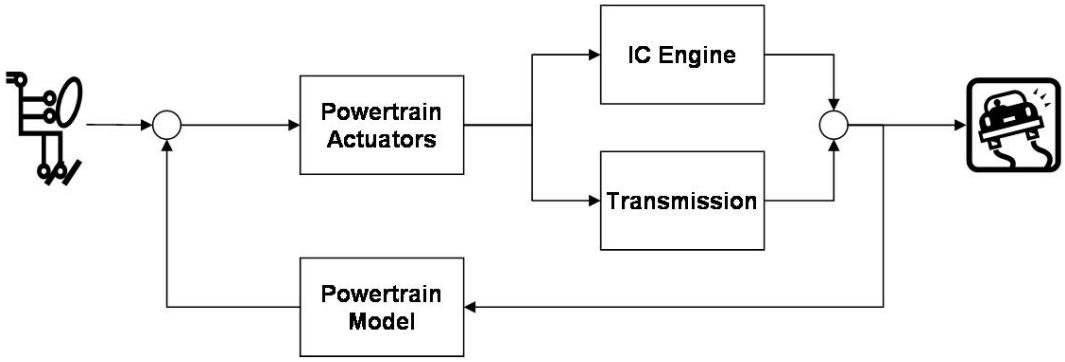

Figure 8-1 Real-Time Interactive Model-Based Control

APPENDIX

Dynamic Programming Algorithm Matlab® Code

```
%*************************************************************************
% Dynamic Programming Algorithm for Reverse Tractive Road Load Demand Model
%                       Version 4.0
% ************************************************************************
%  Developed By:  Melody Baglione    07/04/06
%                       Revision History
%  ------------------------------------------------------------------------
%  Revised By      Date              Revision
%  M.Baglione   09/13/06    Modified for PL and MDS
%  M.Baglione   10/04/06    Included MDS LU and proper MDS and LU decisions
%  M.Baglione   10/31/05    Modified to include MESAU constraint
%  M.Baglione   11/21/06    Penalize all non-1st gear states when MPH=0 for DCT
%  M.Baglione   12/07/06    Modified to incorporate 8 speed transmission capability
%  M.Baglione   12/15/06    Modified to include shift busyness penalty
%  M.Baglione   01/05/07    Added MDS_DS_Enable bit to allow downshift while in MDS
%  M.Baglione   01/05/07    Modified to include MDS busyness penalty
%  M.Baglione   01/14/07    Modified to include UL/PL busyness penalty
%  M.Baglione   03/26/07    Modified to remove MDS busyness penalty
%  M.Baglione   03/30/07    Modified to beta_percent of fuel flow
%  M.Baglione   05/02/07    Removed beta_percent from LU to MDS LU
%  ------------------------------------------------------------------------

% Penalize all non-1st gear states when MPH=0
% Ensures DCT does not launch in non-first gears
L=Fuel_Flow_Matrix; % Table of fuel flow vectors for each time step
i=1;
for i=1:sim_time/step+1;
    if MPH(i)==0;
        j=1;
        for j=2:24;
            L(i,j)=100;
        end
         for j=26:48;
            L(i,j)=100;
         end
    end
end

% Determine possible number of states at each discrete time step, k
num_states=length(L(1,:));
k=1;

% Determine cost-to-go, J, for k=N-1 and each possible control variable, u
i=1;
j=1;
% States 1-8 (Gears 1-8 Open)
for x=1:8;
    % DS
    if x==1;  % Penalize DS when g=g-min
        J{k}(1,x)=step*L(sim_time/step+1-k,x)+10000;
    else
        J{k}(1,x)=step*L(sim_time/step+1-k,x)+step*L(sim_time/step+2-k,x-1)+...
            beta_percent/100*step*L(sim_time/step+1-k,x);
    end
    % NS
    J{k}(2,x)=step*L(sim_time/step+1-k,x)+step*L(sim_time/step+2-k,x+0);
    % US
    if x==8 || Engine_Speed_Matrix(sim_time/step+2-k,1+x+1)<MESAU;
        % Penalize US when g=g-max or if MESAU constraint not met
        J{k}(3,x)=step*L(sim_time/step+1-k,x)+10000;
    else
        J{k}(3,x)=step*L(sim_time/step+1-k,x)+step*L(sim_time/step+2-k,x+1)+...
            beta_percent/100*step*L(sim_time/step+1-k,x);
    end
    % PL
    J{k}(4,x)=step*L(sim_time/step+1-k,x)+step*L(sim_time/step+2-k,x+8);
    % Transition to MDS Open
    J{k}(5,x)=step*L(sim_time/step+1-k,x)+step*L(sim_time/step+2-k,x+24);
    % Transition to MDS PL
    J{k}(6,x)=step*L(sim_time/step+1-k,x)+step*L(sim_time/step+2-k,x+32);
    % Penalize
    J{k}(7,x)=step*L(sim_time/step+1-k,x)+10000;
    J{k}(8,x)=step*L(sim_time/step+1-k,x)+10000;
    J{k}(9,x)=step*L(sim_time/step+1-k,x)+10000;
```

```
    J{k}(10,x)=step*L(sim_time/step+1-k,x)+10000;
    J{k}(11,x)=step*L(sim_time/step+1-k,x)+10000;
end

% Determine cost-to-go, J, for k=N-1 and each possible control variable, u
i=1;
% States 9-16 (Gears 1-8 PL)
for x=9:16;
    % DS Open
    if x==9;  % Penalize DS when g=g-min
        J{k}(1,x)=step*L(sim_time/step+1-k,x)+10000;
    else
        J{k}(1,x)=step*L(sim_time/step+1-k,x)+step*L(sim_time/step+2-k,x-1-8)+...
            beta_percent/100*step*L(sim_time/step+1-k,x);
    end
    % NS Open
    J{k}(2,x)=step*L(sim_time/step+1-k,x)+step*L(sim_time/step+2-k,x+0-8)+...
        beta_percent/100*step*L(sim_time/step+1-k,x);
    % US Open
    if x==16 || Engine_Speed_Matrix(sim_time/step+2-k,1+x+1-8)<MESAU;
        % Penalize US when g=g-max or if MESAU constraint not met
        J{k}(3,x)=step*L(sim_time/step+1-k,x)+10000;
    else
        J{k}(3,x)=step*L(sim_time/step+1-k,x)+step*L(sim_time/step+2-k,x+1-8)+...
            beta_percent/100*step*L(sim_time/step+1-k,x);
    end
    % NS stay PL
    J{k}(4,x)=step*L(sim_time/step+1-k,x)+step*L(sim_time/step+2-k,x+0);
    % US stay PL
    if x==16 || Engine_Speed_Matrix(sim_time/step+2-k,1+x+1)<MESAU;
        % Penalize US when g=g-max or if MESAU constraint not met
        J{k}(5,x)=step*L(sim_time/step+1-k,x)+10000;
    else
        J{k}(5,x)=step*L(sim_time/step+1-k,x)+step*L(sim_time/step+2-k,x+1)+...
            beta_percent/100*step*L(sim_time/step+1-k,x);
    end
    % NS and LU
    J{k}(6,x)=step*L(sim_time/step+1-k,x)+step*L(sim_time/step+2-k,x+0+8);
    % US and transition to LU
    if x==16 || Engine_Speed_Matrix(sim_time/step+2-k,1+x+1+8)<MESAU;
        % Penalize US when g=g-max or if MESAU constraint not met
        J{k}(7,x)=step*L(sim_time/step+1-k,x)+10000;
    else
        J{k}(7,x)=step*L(sim_time/step+1-k,x)+step*L(sim_time/step+2-k,x+1+8)+...
            beta_percent/100*step*L(sim_time/step+1-k,x);
    end
    % NS and MDS Open
    J{k}(8,x)=step*L(sim_time/step+1-k,x)+step*L(sim_time/step+2-k,x+16)+...
        beta_percent/100*step*L(sim_time/step+1-k,x);
    % NS and MDS PL
    J{k}(9,x)=step*L(sim_time/step+1-k,x)+step*L(sim_time/step+2-k,x+24);
    % NS and MDS LU
    J{k}(10,x)=step*L(sim_time/step+1-k,x)+step*L(sim_time/step+2-k,x+32);
    % Penalize
    J{k}(11,x)=step*L(sim_time/step+1-k,x)+10000;
end

% Determine cost-to-go, J, for k=N-1 and each possible control variable, u
i=1;
% States 17-24 (Gears 1-8 LU)
for x=17:24;
    % DS Open
    if x==17;  % Penalize DS when g=g-min
        J{k}(1,x)=step*L(sim_time/step+1-k,x)+10000;
    else
        J{k}(1,x)=step*L(sim_time/step+1-k,x)+step*L(sim_time/step+2-k,x-1-16)+...
            beta_percent/100*step*L(sim_time/step+1-k,x);
    end
    % NS Open
    J{k}(2,x)=step*L(sim_time/step+1-k,x)+step*L(sim_time/step+2-k,x+0-16)+...
        beta_percent/100*step*L(sim_time/step+1-k,x);
    % US Open
    if x==24 || Engine_Speed_Matrix(sim_time/step+2-k,1+x+1-16)<MESAU;
        % Penalize US when g=g-max or if MESAU constraint not met
        J{k}(3,x)=step*L(sim_time/step+1-k,x)+10000;
    else
        J{k}(3,x)=step*L(sim_time/step+1-k,x)+step*L(sim_time/step+2-k,x+1-16)+...
            beta_percent/100*step*L(sim_time/step+1-k,x);
    end
    % NS PL
    J{k}(4,x)=step*L(sim_time/step+1-k,x)+step*L(sim_time/step+2-k,x+0-8)+...
```

```
        beta_percent/100*step*L(sim_time/step+1-k,x);
    % US stay PL
    if x==24 || Engine_Speed_Matrix(sim_time/step+2-k,1+x+1-8)<MESAU;
        % Penalize US when g=g-max or if MESAU constraint not met
        J{k}(5,x)=step*L(sim_time/step+1-k,x)+10000;
    else
        J{k}(5,x)=step*L(sim_time/step+1-k,x)+step*L(sim_time/step+2-k,x+1-8)+...
            beta_percent/100*step*L(sim_time/step+1-k,x);
    end
    % NS and LU
    J{k}(6,x)=step*L(sim_time/step+1-k,x)+step*L(sim_time/step+2-k,x);
    % If Enable_45LU=1 then allow lock-to-lock US otherwise penalize
    if Enable_45LU==1 && x==20 && Engine_Speed_Matrix(sim_time/step+2-k,1+x+1)>=MESAU;
        J{k}(7,x)=step*L(sim_time/step+1-k,x)+step*L(sim_time/step+2-k,x+1)+...
            beta_percent/100*step*L(sim_time/step+1-k,x);
    else
        J{k}(7,x)=step*L(sim_time/step+1-k,x)+10000;
    end
    % MDS Open
        J{k}(8,x)=step*L(sim_time/step+1-k,x)+step*L(sim_time/step+2-k,x+8)+...
            beta_percent/100*step*L(sim_time/step+1-k,x);
    % MDS PL
        J{k}(9,x)=step*L(sim_time/step+1-k,x)+step*L(sim_time/step+2-k,x+16);
    % MDS LU
        J{k}(10,x)=step*L(sim_time/step+1-k,x)+step*L(sim_time/step+2-k,x+24);
    % Penalize
        J{k}(11,x)=step*L(sim_time/step+1-k,x)+10000;
end

% Determine cost-to-go, J, for k=N-1 and each possible control variable, u
i=1;
% States 25-32 (Gears 1-8 MDS Open)
for x=25:32;
    %  DS and non-MDS Open
    if x==25;  % Penalize DS when g=g-min
        J{k}(1,x)=step*L(sim_time/step+1-k,x)+10000;
    else
        J{k}(1,x)=step*L(sim_time/step+1-k,x)+step*L(sim_time/step+2-k,x-1-24)+...
            beta_percent/100*step*L(sim_time/step+1-k,x);
    end
    % NS non-MDS Open
    J{k}(2,x)=step*L(sim_time/step+1-k,x)+step*L(sim_time/step+2-k,x-24);
    % NS non-MDS PL
    J{k}(3,x)=step*L(sim_time/step+1-k,x)+step*L(sim_time/step+2-k,x-16);
    %  DS and MDS Open
    if x==25 || MDS_DS_Enable==0;  % Penalize DS when g=g-min
        J{k}(4,x)=step*L(sim_time/step+1-k,x)+10000;
    else
        J{k}(4,x)=step*L(sim_time/step+1-k,x)+step*L(sim_time/step+2-k,x-1)+...
            beta_percent/100*step*L(sim_time/step+1-k,x);
    end
    % NS stay MDS Open
    J{k}(5,x)=step*L(sim_time/step+1-k,x)+step*L(sim_time/step+2-k,x+0);
    % US MDS Open
    if x==32 || Engine_Speed_Matrix(sim_time/step+2-k,1+x+1)<MESAU;
        % Penalize US when g=g-max or if MESAU constraint not met
        J{k}(6,x)=step*L(sim_time/step+1-k,x)+10000;
    else
        J{k}(6,x)=step*L(sim_time/step+1-k,x)+step*L(sim_time/step+2-k,x+1)+...
            beta_percent/100*step*L(sim_time/step+1-k,x);
    end
    % NS MDS PL
    J{k}(7,x)=step*L(sim_time/step+1-k,x)+step*L(sim_time/step+2-k,x+0+8);
    % Penalize
    J{k}(8,x)=step*L(sim_time/step+1-k,x)+10000;
    J{k}(9,x)=step*L(sim_time/step+1-k,x)+10000;
    J{k}(10,x)=step*L(sim_time/step+1-k,x)+10000;
    J{k}(11,x)=step*L(sim_time/step+1-k,x)+10000;
end


% Determine cost-to-go, J, for k=N-1 and each possible control variable, u
i=1;
% States 33-40 (Gears 1-8 MDS PL)
for x=33:40;
    % DS non-MDS Open
    if x==33;  % Penalize DS when g=g-min
        J{k}(1,x)=step*L(sim_time/step+1-k,x)+10000;
    else
        J{k}(1,x)=step*L(sim_time/step+1-k,x)+step*L(sim_time/step+2-k,x-1-32)+...
            beta_percent/100*step*L(sim_time/step+1-k,x);
```

```
    end
    % NS non-MDS Open
    J{k}(2,x)=step*L(sim_time/step+1-k,x)+step*L(sim_time/step+2-k,x-32)+...
        beta_percent/100*step*L(sim_time/step+1-k,x);
    % NS non-MDS PL
    J{k}(3,x)=step*L(sim_time/step+1-k,x)+step*L(sim_time/step+2-k,x-24);
    % NS non-MDS LU
    J{k}(4,x)=step*L(sim_time/step+1-k,x)+step*L(sim_time/step+2-k,x-16);
    % DS MDS Open
    if x==33 || MDS_DS_Enable==0;  % Penalize DS when g=g-min
        J{k}(5,x)=step*L(sim_time/step+1-k,x)+10000;
    else
        J{k}(5,x)=step*L(sim_time/step+1-k,x)+step*L(sim_time/step+2-k,x-1-8)+...
            beta_percent/100*step*L(sim_time/step+1-k,x);
    end
    % NS MDS Open
    J{k}(6,x)=step*L(sim_time/step+1-k,x)+step*L(sim_time/step+2-k,x-8)+...
        beta_percent/100*step*L(sim_time/step+1-k,x);
    % US MDS Open
    if x==40 || Engine_Speed_Matrix(sim_time/step+2-k,1+x+1-8)<MESAU;
        % Penalize US when g=g-max or if MESAU constraint not met
        J{k}(7,x)=step*L(sim_time/step+1-k,x)+10000;
    else
        J{k}(7,x)=step*L(sim_time/step+1-k,x)+step*L(sim_time/step+2-k,x+1-8)+...
            beta_percent/100*step*L(sim_time/step+1-k,x);
    end
    % NS stay MDS PL
    J{k}(8,x)=step*L(sim_time/step+1-k,x)+step*L(sim_time/step+2-k,x+0); %
    % US and MDS PL
    if x==40 || Engine_Speed_Matrix(sim_time/step+2-k,1+x+1)<MESAU;
        % Penalize US when g=g-max or if MESAU constraint not met
        J{k}(9,x)=step*L(sim_time/step+1-k,x)+10000;
    else
        J{k}(9,x)=step*L(sim_time/step+1-k,x)+step*L(sim_time/step+2-k,x+1)+...
            beta_percent/100*step*L(sim_time/step+1-k,x);
    end
    % NS and LU
    J{k}(10,x)=step*L(sim_time/step+1-k,x)+step*L(sim_time/step+2-k,x+8);
    % US and MDS LU
    if x==40 || Engine_Speed_Matrix(sim_time/step+2-k,1+x+1+8)<MESAU;
        % Penalize US when g=g-max or if MESAU constraint not met
        J{k}(11,x)=step*L(sim_time/step+1-k,x)+10000;
    else
        J{k}(11,x)=step*L(sim_time/step+1-k,x)+step*L(sim_time/step+2-k,x+1+8)+...
            beta_percent/100*step*L(sim_time/step+1-k,x);
    end
end

% Determine cost-to-go, J, for k=N-1 and each possible control variable, u
i=1;
% States 41-48 (Gears 1-8 MDS LU - if enabled by Enable_MDS_LU=1)
for x=41:48;
    % DS non-MDS Open
    if x==41;  % Penalize DS when g=g-min
        J{k}(1,x)=step*L(sim_time/step+1-k,x)+10000;
    else
        J{k}(1,x)=step*L(sim_time/step+1-k,x)+step*L(sim_time/step+2-k,x-1-40)+...
            beta_percent/100*step*L(sim_time/step+1-k,x);
    end
    % NS non-MDS Open
    J{k}(2,x)=step*L(sim_time/step+1-k,x)+step*L(sim_time/step+2-k,x-40)+...
        beta_percent/100*step*L(sim_time/step+1-k,x);
    % NS non-MDS PL
    J{k}(3,x)=step*L(sim_time/step+1-k,x)+step*L(sim_time/step+2-k,x-32)+...
        beta_percent/100*step*L(sim_time/step+1-k,x);
    % NS non-MDS LU
    J{k}(4,x)=step*L(sim_time/step+1-k,x)+step*L(sim_time/step+2-k,x-24);
    % DS MDS Open
    if x==41 || MDS_DS_Enable==0;  % Penalize DS when g=g-min
        J{k}(5,x)=step*L(sim_time/step+1-k,x)+10000;
    else
        J{k}(5,x)=step*L(sim_time/step+1-k,x)+step*L(sim_time/step+2-k,x-1-16)+...
            beta_percent/100*step*L(sim_time/step+1-k,x);
    end
    % NS MDS Open
    J{k}(6,x)=step*L(sim_time/step+1-k,x)+step*L(sim_time/step+2-k,x-16)+...
        beta_percent/100*step*L(sim_time/step+1-k,x);
    % US MDS Open
    if x==48 || Engine_Speed_Matrix(sim_time/step+2-k,1+x+1-16)<MESAU;
        % Penalize US when g=g-max or if MESAU constraint not met
        J{k}(7,x)=step*L(sim_time/step+1-k,x)+10000;
```

```
    else
        J{k}(7,x)=step*L(sim_time/step+1-k,x)+step*L(sim_time/step+2-k,x+1-16)+...
            beta_percent/100*step*L(sim_time/step+1-k,x);
    end
    % NS MDS PL
    J{k}(8,x)=step*L(sim_time/step+1-k,x)+step*L(sim_time/step+2-k,x-8)+...
        beta_percent/100*step*L(sim_time/step+1-k,x); %
    % US and MDS PL
    if x==48 || Engine_Speed_Matrix(sim_time/step+2-k,1+x+1-8)<MESAU;
        % Penalize US when g=g-max or if MESAU constraint not met
        J{k}(9,x)=step*L(sim_time/step+1-k,x)+10000;
    else
        J{k}(9,x)=step*L(sim_time/step+1-k,x)+step*L(sim_time/step+2-k,x+1-8)+...
            beta_percent/100*step*L(sim_time/step+1-k,x);
    end
    % NS and LU
    J{k}(10,x)=step*L(sim_time/step+1-k,x)+step*L(sim_time/step+2-k,x+0);
    % If Enable_45LU=1 then allow lock-to-lock US otherwise penalize
    if Enable_45LU==1 && x==44 && Engine_Speed_Matrix(sim_time/step+2-k,1+x+1)>=MESAU;
        J{k}(11,x)=step*L(sim_time/step+1-k,x)+step*L(sim_time/step+2-k,x+1)+...
            beta_percent/100*step*L(sim_time/step+1-k,x);
    else
        J{k}(11,x)=step*L(sim_time/step+1-k,x)+10000;
    end
end

% Find min cost, J*, for each state x(N-1)
for m=1:num_states;
    [min_J(k,:),u(k,:)]=min(J{k}) ;
end

%  Determine cost-to-go for k=1:N-2 recursively
for k=2:sim_time/step;
    % States 1-8 (Gears 1-8 Open)
    for x=1:8;
    % DS
        if x==1;  % Penalize DS when g=g-min
            J{k}(1,x)=step*L(sim_time/step+1-k,x)+10000;
        else
            J{k}(1,x)=step*L(sim_time/step+1-k,x)+min_J(k-1,x-1)+...
                beta_percent/100*step*L(sim_time/step+1-k,x);
        end
        % NS
        J{k}(2,x)=step*L(sim_time/step+1-k,x)+min_J(k-1,x+0);
        % US
        if x==8 || Engine_Speed_Matrix(sim_time/step+2-k,1+x+1)<MESAU;
           % Penalize US when g=g-max or if MESAU constraint not met
            J{k}(3,x)=step*L(sim_time/step+1-k,x)+10000;
        else
            J{k}(3,x)=step*L(sim_time/step+1-k,x)+min_J(k-1,x+1)+...
                beta_percent/100*step*L(sim_time/step+1-k,x);
        end
        % NS and PL
        J{k}(4,x)=step*L(sim_time/step+1-k,x)+min_J(k-1,x+8);
        % MDS Open
        J{k}(5,x)=step*L(sim_time/step+1-k,x)+min_J(k-1,x+24);
        % MDS PL
        J{k}(6,x)=step*L(sim_time/step+1-k,x)+min_J(k-1,x+32);
        % Penalize
        J{k}(7,x)=step*L(sim_time/step+1-k,x)+10000;
        J{k}(8,x)=step*L(sim_time/step+1-k,x)+10000;
        J{k}(9,x)=step*L(sim_time/step+1-k,x)+10000;
        J{k}(10,x)=step*L(sim_time/step+1-k,x)+10000;
        J{k}(11,x)=step*L(sim_time/step+1-k,x)+10000;
    end

    % States 9-16 (Gears 1-8 PL)
    for x=9:16;
    % DS Open
    if x==9;  % Penalize DS when g=g-min
        J{k}(1,x)=step*L(sim_time/step+1-k,x)+10000;
    else
        J{k}(1,x)=step*L(sim_time/step+1-k,x)+min_J(k-1,x-1-8)+...
            beta_percent/100*step*L(sim_time/step+1-k,x);
    end
    % NS Open
    J{k}(2,x)=step*L(sim_time/step+1-k,x)+min_J(k-1,x-8)+...
        beta_percent/100*step*L(sim_time/step+1-k,x);
    % US Open
    if x==16 || Engine_Speed_Matrix(sim_time/step+2-k,1+x+1-8)<MESAU;
        % Penalize US when g=g-max or if MESAU constraint not met
```

```
    J{k}(3,x)=step*L(sim_time/step+1-k,x)+10000;
else
    J{k}(3,x)=step*L(sim_time/step+1-k,x)+min_J(k-1,x+1-8)+...
        beta_percent/100*step*L(sim_time/step+1-k,x);
end
% NS stay PL
J{k}(4,x)=step*L(sim_time/step+1-k,x)+min_J(k-1,x);
% US stay PL
if x==16 || Engine_Speed_Matrix(sim_time/step+2-k,1+x+1)<MESAU;
    % Penalize US when g=g-max or if MESAU constraint not met
    J{k}(5,x)=step*L(sim_time/step+1-k,x)+10000;
else
    J{k}(5,x)=step*L(sim_time/step+1-k,x)+min_J(k-1,x+1)+...
        beta_percent/100*step*L(sim_time/step+1-k,x);
end
% NS and LU
J{k}(6,x)=step*L(sim_time/step+1-k,x)+min_J(k-1,x+8);
% US LU
if x==16 || Engine_Speed_Matrix(sim_time/step+2-k,1+x+1+8)<MESAU;
    % Penalize US when g=g-max or if MESAU constraint not met
    J{k}(7,x)=step*L(sim_time/step+1-k,x)+10000;
else
    J{k}(7,x)=step*L(sim_time/step+1-k,x)+min_J(k-1,x+1+8)+...
        beta_percent/100*step*L(sim_time/step+1-k,x);
end
% NS and MDS Open
J{k}(8,x)=step*L(sim_time/step+1-k,x)+min_J(k-1,x+16)+...
    beta_percent/100*step*L(sim_time/step+1-k,x);
% NS and MDS PL
J{k}(9,x)=step*L(sim_time/step+1-k,x)+min_J(k-1,x+24);
% NS and MDS LU
J{k}(10,x)=step*L(sim_time/step+1-k,x)+min_J(k-1,x+32);
% Penalize
J{k}(11,x)=step*L(sim_time/step+1-k,x)+10000;
end

i=1;
% States 17-24 (Gears 1-8 LU)
for x=17:24;
% DS Open
if x==17;  % Penalize DS when g=g-min
    J{k}(1,x)=step*L(sim_time/step+1-k,x)+10000;
else
    J{k}(1,x)=step*L(sim_time/step+1-k,x)+min_J(k-1,x-1-16)+...
        beta_percent/100*step*L(sim_time/step+1-k,x);
end
% NS Open
J{k}(2,x)=step*L(sim_time/step+1-k,x)+min_J(k-1,x-16)+...
    beta_percent/100*step*L(sim_time/step+1-k,x);
% US Open
if x==24 || Engine_Speed_Matrix(sim_time/step+2-k,1+x+1-16)<MESAU;
    % Penalize US when g=g-max or if MESAU constraint not met
    J{k}(3,x)=step*L(sim_time/step+1-k,x)+10000;
else
    J{k}(3,x)=step*L(sim_time/step+1-k,x)+min_J(k-1,x+1-16)+...
        beta_percent/100*step*L(sim_time/step+1-k,x);
end
% NS PL
J{k}(4,x)=step*L(sim_time/step+1-k,x)+min_J(k-1,x-8)+...
    beta_percent/100*step*L(sim_time/step+1-k,x);
% US stay PL
if x==24 || Engine_Speed_Matrix(sim_time/step+2-k,1+x+1-8)<MESAU;
    % Penalize US when g=g-max or if MESAU constraint not met
    J{k}(5,x)=step*L(sim_time/step+1-k,x)+10000;
else
    J{k}(5,x)=step*L(sim_time/step+1-k,x)+min_J(k-1,x+1-8)+...
        beta_percent/100*step*L(sim_time/step+1-k,x);
end
% NS LU
J{k}(6,x)=step*L(sim_time/step+1-k,x)+min_J(k-1,x+0);
% If Enable_45LU=1 then allow lock-to-lock US otherwise penalize
if Enable_45LU==1 && x==20 && Engine_Speed_Matrix(sim_time/step+2-k,1+x+1)>=MESAU;
    J{k}(7,x)=step*L(sim_time/step+1-k,x)+min_J(k-1,x+1)+...
        beta_percent/100*step*L(sim_time/step+1-k,x);
else
    J{k}(7,x)=step*L(sim_time/step+1-k,x)+10000;
end
% NS and MDS
J{k}(8,x)=step*L(sim_time/step+1-k,x)+min_J(k-1,x+8)+...
    beta_percent/100*step*L(sim_time/step+1-k,x);
% NS and MDS PL
```

```
J{k}(9,x)=step*L(sim_time/step+1-k,x)+min_J(k-1,x+16)+...
    beta_percent/100*step*L(sim_time/step+1-k,x);
% NS and MDS LU
J{k}(10,x)=step*L(sim_time/step+1-k,x)+min_J(k-1,x+24);
% Penalize
J{k}(11,x)=step*L(sim_time/step+1-k,x)+10000;
end

% States 25-32 (Gears 1-8 MDS Open)
for x=25:32;
% DS non-MDS Open
if x==25;  % Penalize DS when g=g-min
    J{k}(1,x)=step*L(sim_time/step+1-k,x)+10000;
else
    J{k}(1,x)=step*L(sim_time/step+1-k,x)+min_J(k-1,x-1-24)+...
        beta_percent/100*step*L(sim_time/step+1-k,x);
end
% NS non-MDS Open
J{k}(2,x)=step*L(sim_time/step+1-k,x)+min_J(k-1,x-24);
% NS non-MDS PL
J{k}(3,x)=step*L(sim_time/step+1-k,x)+min_J(k-1,x-16);
% DS MDS Open
if x==25 || MDS_DS_Enable==0;  % Penalize DS when g=g-min
    J{k}(4,x)=step*L(sim_time/step+1-k,x)+10000;
else
    J{k}(4,x)=step*L(sim_time/step+1-k,x)+min_J(k-1,x-1)+...
        beta_percent/100*step*L(sim_time/step+1-k,x);
end
% NS stay MDS Open
J{k}(5,x)=step*L(sim_time/step+1-k,x)+min_J(k-1,x);
% US MDS Open
if x==32 || Engine_Speed_Matrix(sim_time/step+2-k,1+x+1)<MESAU;
    % Penalize US when g=g-max or if MESAU constraint not met
    J{k}(6,x)=step*L(sim_time/step+1-k,x)+10000;
else
    J{k}(6,x)=step*L(sim_time/step+1-k,x)+min_J(k-1,x+1)+...
        beta_percent/100*step*L(sim_time/step+1-k,x);
end
% NS MDS PL
J{k}(7,x)=step*L(sim_time/step+1-k,x)+min_J(k-1,x+8);
% Penalize
J{k}(8,x)=step*L(sim_time/step+1-k,x)+10000;
J{k}(9,x)=step*L(sim_time/step+1-k,x)+10000;
J{k}(10,x)=step*L(sim_time/step+1-k,x)+10000;
J{k}(11,x)=step*L(sim_time/step+1-k,x)+10000;
end

% States 33-40 (Gears 1-6 MDS PL)
for x=33:40;
% DS non-MDS Open
if x==33;  % Penalize DS when g=g-min
    J{k}(1,x)=step*L(sim_time/step+1-k,x)+10000;
else
    J{k}(1,x)=step*L(sim_time/step+1-k,x)+min_J(k-1,x-1-32)+...
        beta_percent/100*step*L(sim_time/step+1-k,x);
end
% NS non-MDS Open
J{k}(2,x)=step*L(sim_time/step+1-k,x)+min_J(k-1,x-32)+...
    beta_percent/100*step*L(sim_time/step+1-k,x);
% NS non-MDS PL
J{k}(3,x)=step*L(sim_time/step+1-k,x)+min_J(k-1,x-24);
% NS non-MDS LU
J{k}(4,x)=step*L(sim_time/step+1-k,x)+min_J(k-1,x-16);
% DS MDS Open
if x==33 || MDS_DS_Enable==0;  % Penalize DS when g=g-min
    J{k}(5,x)=step*L(sim_time/step+1-k,x)+10000;
else
    J{k}(5,x)=step*L(sim_time/step+1-k,x)+min_J(k-1,x-1-8)+...
        beta_percent/100*step*L(sim_time/step+1-k,x);
end
% NS MDS Open
J{k}(6,x)=step*L(sim_time/step+1-k,x)+min_J(k-1,x-8)+...
    beta_percent/100*step*L(sim_time/step+1-k,x);
% US MDS Open
if x==40 || Engine_Speed_Matrix(sim_time/step+2-k,1+x+1-8)<MESAU;
    % Penalize US when g=g-max or if MESAU constraint not met
    J{k}(7,x)=step*L(sim_time/step+1-k,x)+10000;
else
    J{k}(7,x)=step*L(sim_time/step+1-k,x)+min_J(k-1,x+1-8)+...
        beta_percent/100*step*L(sim_time/step+1-k,x);
end
```

```
    % NS stay MDS PL
    J{k}(8,x)=step*L(sim_time/step+1-k,x)+min_J(k-1,x+0); %
    % US and MDS PL
    if x==40 || Engine_Speed_Matrix(sim_time/step+2-k,1+x+1)<MESAU;
        % Penalize US when g=g-max or if MESAU constraint not met
        J{k}(9,x)=step*L(sim_time/step+1-k,x)+10000;
    else
        J{k}(9,x)=step*L(sim_time/step+1-k,x)+min_J(k-1,x+1)+...
            beta_percent/100*step*L(sim_time/step+1-k,x);
    end
    % NS and MDS LU
    J{k}(10,x)=step*L(sim_time/step+1-k,x)+min_J(k-1,x+8);
    % US and MDS LU
    if x==40 || Engine_Speed_Matrix(sim_time/step+2-k,1+x+1+8)<MESAU;
        J{k}(11,x)=step*L(sim_time/step+1-k,x)+10000;
    else
        J{k}(11,x)=step*L(sim_time/step+1-k,x)+min_J(k-1,x+1+8)+...
            beta_percent/100*step*L(sim_time/step+1-k,x);
    end
end

i=1;
% States 41-48 (Gears 1-6 MDS LU - if enabled by Enable_MDS_LU=1)
for x=41:48;
    % DS non-MDS Open
    if x==41;  % Penalize DS when g=g-min
        J{k}(1,x)=step*L(sim_time/step+1-k,x)+10000;
    else
        J{k}(1,x)=step*L(sim_time/step+1-k,x)+min_J(k-1,x-1-40)+...
            beta_percent/100*step*L(sim_time/step+1-k,x);
    end
    % NS non-MDS Open
    J{k}(2,x)=step*L(sim_time/step+1-k,x)+min_J(k-1,x-40)+...
        beta_percent/100*step*L(sim_time/step+1-k,x);
    % NS non-MDS PL
    J{k}(3,x)=step*L(sim_time/step+1-k,x)+min_J(k-1,x-32)+...
        beta_percent/100*step*L(sim_time/step+1-k,x);
    % NS non-MDS LU
    J{k}(4,x)=step*L(sim_time/step+1-k,x)+min_J(k-1,x-24);
    % DS MDS Open
    if x==41 || MDS_DS_Enable==0;  % Penalize DS when g=g-min
        J{k}(5,x)=step*L(sim_time/step+1-k,x)+10000;
    else
        J{k}(5,x)=step*L(sim_time/step+1-k,x)+min_J(k-1,x-1-16)+...
            beta_percent/100*step*L(sim_time/step+1-k,x);
    end
    % NS MDS Open
    J{k}(6,x)=step*L(sim_time/step+1-k,x)+min_J(k-1,x-16)+...
        beta_percent/100*step*L(sim_time/step+1-k,x);
    % US MDS Open
    if x==48 || Engine_Speed_Matrix(sim_time/step+2-k,1+x+1-16)<MESAU;
        % Penalize US when g=g-max or if MESAU constraint not met
        J{k}(7,x)=step*L(sim_time/step+1-k,x)+10000;
    else
        J{k}(7,x)=step*L(sim_time/step+1-k,x)+min_J(k-1,x+1-16)+...
            beta_percent/100*step*L(sim_time/step+1-k,x);
    end
    % NS MDS PL
    J{k}(8,x)=step*L(sim_time/step+1-k,x)+min_J(k-1,x-8)+...
        beta_percent/100*step*L(sim_time/step+1-k,x); %
    % US and MDS PL
    if x==48 || Engine_Speed_Matrix(sim_time/step+2-k,1+x+1-8)<MESAU;
        % Penalize US when g=g-max or if MESAU constraint not met
        J{k}(9,x)=step*L(sim_time/step+1-k,x)+10000;
    else
        J{k}(9,x)=step*L(sim_time/step+1-k,x)+min_J(k-1,x+1-8)+...
            beta_percent/100*step*L(sim_time/step+1-k,x);
    end
    % NS and LU
    J{k}(10,x)=step*L(sim_time/step+1-k,x)+min_J(k-1,x+0);
    % If Enable_45LU=1 then allow lock-to-lock US otherwise penalize
    if Enable_45LU==1 && x==44 && Engine_Speed_Matrix(sim_time/step+2-k,1+x+1)>=MESAU;
        J{k}(11,x)=step*L(sim_time/step+1-k,x)+min_J(k-1,x+1)+...
            beta_percent/100*step*L(sim_time/step+1-k,x);
    else
        J{k}(11,x)=step*L(sim_time/step+1-k,x)+10000;
    end
end

% Find min cost, J*, for each initial state x(0)
   for m=1:num_states;
```

```
        [min_J(k,:),u(k,:)]=min(J{k});
    end
end

% Find global optimum accumulated fuel and initial state
% Penalize initial states that do not meet MESAU
if MPH(1)==0;
    [global_min_J,initial_x]=min(min_J(sim_time/step,:));
else
    [global_min_J,initial_x]=min(min_J(sim_time/step,:));
    while Engine_Speed_Matrix(1,initial_x+1)<MESAU
        min_J(sim_time/step,initial_x)=Inf;
        [global_min_J,initial_x]=min(min_J(sim_time/step,:));
    end
end

% Create optimal state vector from optimal control variables, u, for DP simulation
n=1;
opt_x(n,1)=initial_x;
for n=1:sim_time/step;
    % if current state is unlocked
    if (u(sim_time/step+1-n,opt_x(n))==1) && (opt_x(n)<9);
        opt_x(n+1,1)=opt_x(n)-1;
    elseif (u(sim_time/step+1-n,opt_x(n))==2) && (opt_x(n)<9);
        opt_x(n+1,1)=opt_x(n)+0;
    elseif (u(sim_time/step+1-n,opt_x(n))==3) && (opt_x(n)<9);
        opt_x(n+1,1)=opt_x(n)+1;
    elseif (u(sim_time/step+1-n,opt_x(n))==4) && (opt_x(n)<9);
        opt_x(n+1,1)=opt_x(n)+8;
    elseif (u(sim_time/step+1-n,opt_x(n))==5) && (opt_x(n)<9);
        opt_x(n+1,1)=opt_x(n)+24;
    elseif (u(sim_time/step+1-n,opt_x(n))==6) && (opt_x(n)<9);
        opt_x(n+1,1)=opt_x(n)+32;
     % if current state is PL
    elseif (u(sim_time/step+1-n,opt_x(n))==1) && (opt_x(n)>8) && (opt_x(n)<17) ;
        opt_x(n+1,1)=opt_x(n)-1-8;
    elseif (u(sim_time/step+1-n,opt_x(n))==2) && (opt_x(n)>8) && (opt_x(n)<17);
        opt_x(n+1,1)=opt_x(n)+0-8;
    elseif (u(sim_time/step+1-n,opt_x(n))==3) && (opt_x(n)>8) && (opt_x(n)<17);
        opt_x(n+1,1)=opt_x(n)+1-8;
    elseif (u(sim_time/step+1-n,opt_x(n))==4) && (opt_x(n)>8) && (opt_x(n)<17);
        opt_x(n+1,1)=opt_x(n)+0;
    elseif (u(sim_time/step+1-n,opt_x(n))==5) && (opt_x(n)>8) && (opt_x(n)<17);
        opt_x(n+1,1)=opt_x(n)+1;
    elseif (u(sim_time/step+1-n,opt_x(n))==6) && (opt_x(n)>8) && (opt_x(n)<17);
        opt_x(n+1,1)=opt_x(n)+8;
    elseif (u(sim_time/step+1-n,opt_x(n))==7) && (opt_x(n)>8) && (opt_x(n)<17);
        opt_x(n+1,1)=opt_x(n)+1+8;
    elseif (u(sim_time/step+1-n,opt_x(n))==8) && (opt_x(n)>8) && (opt_x(n)<17);
        opt_x(n+1,1)=opt_x(n)+16;
    elseif (u(sim_time/step+1-n,opt_x(n))==9) && (opt_x(n)>8) && (opt_x(n)<17);
        opt_x(n+1,1)=opt_x(n)+24;
    elseif (u(sim_time/step+1-n,opt_x(n))==10) && (opt_x(n)>8) && (opt_x(n)<17);
        opt_x(n+1,1)=opt_x(n)+32;
        % if current state is LU
    elseif (u(sim_time/step+1-n,opt_x(n))==1) && (opt_x(n)>16) && (opt_x(n)<25) ;
        opt_x(n+1,1)=opt_x(n)-1-16;
    elseif (u(sim_time/step+1-n,opt_x(n))==2) && (opt_x(n)>16) && (opt_x(n)<25);
        opt_x(n+1,1)=opt_x(n)+0-16;
    elseif (u(sim_time/step+1-n,opt_x(n))==3) && (opt_x(n)>16) && (opt_x(n)<25);
        opt_x(n+1,1)=opt_x(n)+1-16;
    elseif (u(sim_time/step+1-n,opt_x(n))==4) && (opt_x(n)>16) && (opt_x(n)<25);
        opt_x(n+1,1)=opt_x(n)+0-8;
    elseif (u(sim_time/step+1-n,opt_x(n))==5) && (opt_x(n)>16) && (opt_x(n)<25);
        opt_x(n+1,1)=opt_x(n)+1-8;
    elseif (u(sim_time/step+1-n,opt_x(n))==6) && (opt_x(n)>16) && (opt_x(n)<25);
        opt_x(n+1,1)=opt_x(n)+0;
    elseif (u(sim_time/step+1-n,opt_x(n))==7) && (opt_x(n)>16) && (opt_x(n)<25);
        opt_x(n+1,1)=opt_x(n)+1;
    elseif (u(sim_time/step+1-n,opt_x(n))==8) && (opt_x(n)>16) && (opt_x(n)<25);
        opt_x(n+1,1)=opt_x(n)+8;
    elseif (u(sim_time/step+1-n,opt_x(n))==9) && (opt_x(n)>16) && (opt_x(n)<25);
        opt_x(n+1,1)=opt_x(n)+16;
    elseif (u(sim_time/step+1-n,opt_x(n))==10) && (opt_x(n)>16) && (opt_x(n)<25);
        opt_x(n+1,1)=opt_x(n)+24;
        % if current state is MDS Open
    elseif (u(sim_time/step+1-n,opt_x(n))==1) && (opt_x(n)>24) && (opt_x(n)<33) ;
        opt_x(n+1,1)=opt_x(n)-1-24;
    elseif (u(sim_time/step+1-n,opt_x(n))==2) && (opt_x(n)>24) && (opt_x(n)<33);
        opt_x(n+1,1)=opt_x(n)-24;
    elseif (u(sim_time/step+1-n,opt_x(n))==3) && (opt_x(n)>24) && (opt_x(n)<33);
```

```
        opt_x(n+1,1)=opt_x(n)-16;
    elseif (u(sim_time/step+1-n,opt_x(n))==4) && (opt_x(n)>24) && (opt_x(n)<33);
        opt_x(n+1,1)=opt_x(n)-1;
    elseif (u(sim_time/step+1-n,opt_x(n))==5) && (opt_x(n)>24) && (opt_x(n)<33);
        opt_x(n+1,1)=opt_x(n)+0;
    elseif (u(sim_time/step+1-n,opt_x(n))==6) && (opt_x(n)>24) && (opt_x(n)<33);
        opt_x(n+1,1)=opt_x(n)+1;
    elseif (u(sim_time/step+1-n,opt_x(n))==7) && (opt_x(n)>24) && (opt_x(n)<33);
        opt_x(n+1,1)=opt_x(n)+0+8;
    % if current state is MDS PL
    elseif (u(sim_time/step+1-n,opt_x(n))==1) && (opt_x(n)>32) && (opt_x(n)<41);
        opt_x(n+1,1)=opt_x(n)-1-32;
    elseif (u(sim_time/step+1-n,opt_x(n))==2) && (opt_x(n)>32) && (opt_x(n)<41);
        opt_x(n+1,1)=opt_x(n)-32;
    elseif (u(sim_time/step+1-n,opt_x(n))==3) && (opt_x(n)>32) && (opt_x(n)<41);
        opt_x(n+1,1)=opt_x(n)-24;
    elseif (u(sim_time/step+1-n,opt_x(n))==4) && (opt_x(n)>32) && (opt_x(n)<41);
        opt_x(n+1,1)=opt_x(n)-16;
    elseif (u(sim_time/step+1-n,opt_x(n))==5) && (opt_x(n)>32) && (opt_x(n)<41);
        opt_x(n+1,1)=opt_x(n)-1-8;
    elseif (u(sim_time/step+1-n,opt_x(n))==6) && (opt_x(n)>32) && (opt_x(n)<41);
        opt_x(n+1,1)=opt_x(n)-8;
    elseif (u(sim_time/step+1-n,opt_x(n))==7) && (opt_x(n)>32) && (opt_x(n)<41);
        opt_x(n+1,1)=opt_x(n)+1-8;
    elseif (u(sim_time/step+1-n,opt_x(n))==8) && (opt_x(n)>32) && (opt_x(n)<41);
        opt_x(n+1,1)=opt_x(n)+0;
    elseif (u(sim_time/step+1-n,opt_x(n))==9) && (opt_x(n)>32) && (opt_x(n)<41);
        opt_x(n+1,1)=opt_x(n)+1;
    elseif (u(sim_time/step+1-n,opt_x(n))==10) && (opt_x(n)>32) && (opt_x(n)<41);
        opt_x(n+1,1)=opt_x(n)+8;
    elseif (u(sim_time/step+1-n,opt_x(n))==11) && (opt_x(n)>32) && (opt_x(n)<41);
        opt_x(n+1,1)=opt_x(n)+1+8;
        % if current state is MDS LU
    elseif (u(sim_time/step+1-n,opt_x(n))==1) && (opt_x(n)>40);
        opt_x(n+1,1)=opt_x(n)-1-40;
    elseif (u(sim_time/step+1-n,opt_x(n))==2) && (opt_x(n)>40);
        opt_x(n+1,1)=opt_x(n)-40;
    elseif (u(sim_time/step+1-n,opt_x(n))==3) && (opt_x(n)>40);
        opt_x(n+1,1)=opt_x(n)-32;
    elseif (u(sim_time/step+1-n,opt_x(n))==4) && (opt_x(n)>40);
        opt_x(n+1,1)=opt_x(n)-24;
    elseif (u(sim_time/step+1-n,opt_x(n))==5) && (opt_x(n)>40);
        opt_x(n+1,1)=opt_x(n)-1-16;
    elseif (u(sim_time/step+1-n,opt_x(n))==6) && (opt_x(n)>40);
        opt_x(n+1,1)=opt_x(n)-16;
    elseif (u(sim_time/step+1-n,opt_x(n))==7) && (opt_x(n)>40);
        opt_x(n+1,1)=opt_x(n)+1-16;
    elseif (u(sim_time/step+1-n,opt_x(n))==8) && (opt_x(n)>40);
        opt_x(n+1,1)=opt_x(n)-8;
    elseif (u(sim_time/step+1-n,opt_x(n))==9) && (opt_x(n)>40);
        opt_x(n+1,1)=opt_x(n)+1-8;
    elseif (u(sim_time/step+1-n,opt_x(n))==10) && (opt_x(n)>40);
        opt_x(n+1,1)=opt_x(n)+0;
    elseif (u(sim_time/step+1-n,opt_x(n))==11) && (opt_x(n)>40);
        opt_x(n+1,1)=opt_x(n)+1;
    end
end
```

REFERENCES

Abenavoli, R.I., Carlini, M., Kormanski, H., Rudzinska, K. (1999) "Fuel Economy Improvement by Vehicle Control Optimization." *SAE Paper 1999-01-2473*.

Akucewich, E.S., O'Conner, B.M. Vinci, J.N., Schenkenberger, C. (2003) "Developing Next Generation Axle Fluids, Part III: Laboratory CAFE Simulation Test as Key Fluid Development Tool." *SAE Paper 2003-01-3235*.

Assanis, D., Filipi, Z., Gravante, S., Grohnke, S., Gui, X., Louca, L., Rideout, G., Stein, J., Wang, Y. (2000) "Validation and Use of SIMULINK Integrated, High Fidelity, Engine-In-Vehicle Simulation of the International Class VI Truck." *SAE Paper 2000-01-0288.*

Asmus, T. (2005) "Advanced Internal Combustion Engines." *ME538 Course Notes*, University of Michigan.

Auiler, J.E., Zbrozek, J.D., Blumberg, P.N. (1977) "Optimization of Automotive Engine Calibration for Better Fuel Economy – Methods and Applications." SAE Paper 770076.

Baglione, M., Duty, M., Pannone, G. (2007a) "Vehicle System Energy Analysis Methodology and Tool for Determining Vehicle Subsystem Energy Supply and Demand." *SAE Paper 2007-01-0398*.

Baglione, M., Duty, M., Ni, J., Assanis, D. (2007b) "Reverse Dynamic Optimization Methodology for Maximizing Powertrain System Efficiency." *Proceedings of the Fifth IFAC Symposium on Advances in Automotive Control*, 1, 17-24.

Bates, B., Dosdall, J.M., Smith, D.H. (1978) "Variable Displacement by Engine Valve Control." *SAE Paper 780145*.

Beck, R., Richert, F., Bollig, A., Abel, D., Saenger, S., Neil, K., Scholt, T.,Noreikat, K.E. (2005) "Model Predictive Control of a Parallel Hybrid Vehicle Drivetrain." *IEEE European Conference on Decision and Control*, 1, 2670- 2675.

Bellman, R. (1972). *Dynamic Programming*, 6th Ed. Princeton University Press, New Jersey.

Berry, A., Blissett, M., Steiber, J., Tobin, A., McBroom, S. (2002) "A New Approach to Improving Fuel Economy and Performance Prediction through Coupled Thermal Systems Simulation." *SAE Paper 2002-01-1208*.

Bertsekas, D.P. (2000) *Dynamic Programming and Optimal Control*, Athena Scientific, Boston, MA.

Blumberg, P.N. (1976) "Powertrain Simulation: A Tool for the Design and Evaluation of Engine Control Strategies in Vehicles." *SAE Paper 760158*.

BOSCH. (1999) *Gasoline-engine management*, Robert Bosch GmbH., Stuttgart.

Brahma, A., B. Glenn, Y. Guezennec, T. Miller, G. Rizzoni, G. Washington (1999) "Modeling, Performance Analysis and Control Design of a Hybrid, Sport-Utility Vehicle." *Proceedings of the 1999 IEEE International Conference on Control Applications.*

Buckley, F. (1995) "ABCD – An Improved Coast Down Test and Analysis Method." *SAE Paper 950626*.

Camacho, E.F., Bordons, C. (2004) *Model Predictive Control*, Springer, London.

Consumer Reports. (2007) http://www.consumerreports.org.

Cook, J.A., Sun, J., Grizzle, J.W. (2002) "Opportunities in automotive control applications." *Proceedings of the 2002 International Conference on Control Applications*, 1,

de Madrid, A.P., Dormido, S., Morilla, F. (1999) "Reduction of the Dimensionality of Dynamic Programming: A Case Study." *Proceedings of the 1999 IEEE American Control Conference*, 4, 2852-2856.

Denardo, E.V. (1982) *Dynamic Programming: Models and Applications*, Prentice-Hall, New Jersey.

Falkowski, A., McElwee, M., Bonne, M. (2004) "Design and Development of the Chrysler 5.7L HEMI® Engine Multi-Displacement Cylinder Deactivation System." *SAE Paper 2004-01-2106*.

Farzaneh, H.; Saboohi, Y. (2005) "Model for analysis of energy flow from tank-to-wheel in a passenger vehicle." *Proceedings of the 2005 IEEE Conference on Vehicle Power and Propulsion*, 7-9 Sept. 2005.

Federal Regulations, Code of. (1996)"§ 86.115-00 EPA Urban Dynamometer Driving Schedule." 59 FR 16296, 6 Apr. 1996.

Feng, A., A. Rousseau. (2001) "Integration of a Modal Energy and Emissions Model into a PNGV Vehicle Simulation Model, PSAT." SAE Paper 2001-01-0954.

Filipi, Z., Loucas, L., Daran, B., Lin, C-C., Yildir, U., Wu, B., Kokkolaras, M., Assanis, D., Peng, H., Papalambros, P., Stein, J., Szkubiel, D., Chapp, R. (2004) "Combined Optimization of Design and Power Management of the Hydraulic Hybrid Propulsion System for the 6x6 Medium Truck." *International Journal of Heavy Vehicle Systems*, 11 (3/4), 371-401.

Filipi, Z., Fathy, H., Hagena, J., Knafl, A., Ahlawat, R., Liu, J., Jung, D., Assanis, D., Peng, H., Stein, J. (2006) "Engine-in-the-Loop Testing for Evaluating Hybrid Propulsion Concepts and Transient Emissions – HMMWV Case Study." *SAE Paper 2006-01-0443*.

Flor, R.A., Karell, M.K. (1997) "Emissions and Fuel Economy Certification Testing and Corporate Cross Check: Variability Studies." *Chrysler Inter Company Correspondence.* 23 Dec. 1997.

Fredriksson, F., Egbert, B. (2000) "Nonlinear Control applied to Gearshifting in Automated Manual Transmissions." *Proceedings of the 39th IEEE Conference on Decision and Control*, 1, 444–449.

Fukui, T., Nakagmai, T., Endo, H. (1983) "Mitsubishi Orion-MD – A New Variable Displacement Engine." *SAE Paper 831007*.

Gale, N. (2005) "Road-to-lab-to-math: a new path to improved product." *Automotive Engineering International,* May 2005, 78-79.

Gao, W., Porandla, S.K. (2005) "Design Optimization of a Parallel Hybrid Electric Powertrain." *Proceedings of the 2005 IEEE Conference on Vehicle Power and Propulsion*, 7-9 Sept.

Gao, W., Mi, C. (2007) "Hybrid vehicle design using global optimization algorithms." *International Journal of Electric and Hybrid Vehicles*, 1 (1), 57-70.

Garofalo, F., Glielmo, L., Iannelli, L., Vasca, F. (2001) "Smooth engagement for automotive dry clutch." *Proceedings of the 40th IEEE Conference on Decision and Control*, 1, 529-534.

Geist, B. (2004) "ShiftMaster: New Tool for Automatic Transmission Shift and Lock-up Scheduling." *Chrysler Internal Technical Report PCTR7341*, 17 Sept. 2004.

Gillespie, T.D. (1992) *Fundamentals of Vehicle Dynamics*, Society of Automotive Engineers, Inc. Warrendale, PA.

Giorgetti, N., Ripaccioli, G., Bemporad, A., Kolmanovsky, I.V., Hrovat, D. (2006) "Hybrid Model Predictive Control of Direct Injection Stratified Charge Engines." *IEEE/ASME Transactions on Mechatronics*, 11 (5), 499- 506.

Greiner, J., Doerr, C., Nauerz, H., Graeve, M. (2004) "The New 7G-TRONICof Mercedes-Benz: Innovative Transmission Technology for Better Driving Performance, Comfort, and Fuel Economy." *SAE Paper 2004-01-0649.*

Harris, B. (2006) "How Dual-clutch Transmissions Work." http://auto.howstuffworks.com/dual-clutch-transmission.htm.

Heywood, J.B. (1988) *Internal Combustion Engine Fundamentals*, McGraw-Hill, Inc. New York.

Hiroyasu, H., Miao, H., Hiroyasu, T., Miki, M., Kamiura, J., Watanabe, S. (2003) "Genetic Algorithms Optimization of Diesel Engine Emissions, Fuel Efficiency with Air Swirl, EGR, Injection Timing, and Multiple Injections." *SAE Paper 2003-01-1853.*

Hoff, C., Davis, G. (2003) "Performance Selection for Fuel Economy and Acceleration Performance." SAE Course ID #C0243 Material, Warrendale, PA.

Inagaki, M., KawamotoA., Aoyama, T., Yamamoto, K. (2000) "Prediction of Structural and Kinematic Coupled Vibration on Internal Combustion Engine." *Proceedings of ISMA25, Noise and Vibration Engineering.*

Jankovic, M., Magner, S. (2004) "Optimization and scheduling for automotive powertrains." *Proceedings of the American Control Conference*, Boston, MA.

Johannesson, L., Asbogard, M., Egardt, B. (2006). "Assessing the Potential of Predictive Control for Hybrid Vehicle Powertrains Using Stochastic Dynamic Programming." *IEEE Transactions on Intelligent Transportation Systems*, 8 (1), 71-83.

Kang, J.M., Kolmanovsky, I, Grizzle, J.W. (2001) "Approximate dynamic programming solutions for lean burn engine aftertreatment." *Journal of Dynamic Systems, Measurement and Control*, 123, 153–160.

Kelly, K. (2002) "Modeling Tool for Predicting the Impact of Rolling Resistance on Energy Usage and Fuel Efficiency for Realistic Driving Cycles." *International Tire Exhibition and Conference Paper* #31C.

Kheir, N.A., Salman, M.A., Schouten, N.J. (2004) "Emissions and fuel economy trade-off for hybrid vehicles using fuzzy logic." *Mathematics and Computers in Simulation*, 66, 155-172.

Kluger, M., Long, D. (1999) "An Overview of Current Automatic, Manual and Continuously Variable Transmission Efficiencies and Their Projected Future Improvements." *SAE Paper 1999-01-1259*.

Koepf, P. (1994) "Trends and Alternatives in Power Steering Systems with Particular Emphasis on Energy Consumption." *SAE Paper 945039*.

Kono, K., Itoh, H. Nakamura, S. Yoshizawa, K. Osawa, M. (1995) "Torque Converter Clutch Slip Control System." *SAE Paper 950672*.

Kang, J.M., Kolmanovsky I., Grizzle, J.W. (2001) "Approximate dynamic programming solutions for lean burn engine aftertreatment." *Journal of Dynamic Systems, Measurement, and Control*, 123, 153–160.

Kim, D. (2006) "Math Model Based Gear Shift Control Strategy for Powertrain Systems." *PhD Dissertation*, University of Michigan.

Kim, H.M., Kokkolaras, M., Louca, L.S., Delagrammatikas, G.J., Michelena, N.F., Filipi, Z.S., Papalambros, P.Y., Stein, J.L., Assanis, D.N. (2002) "Target Cascading in Vehicle Redesign: A Class VI Truck Study." *International Journal of Vehicle Design,* 29 (3), 199-225.

Kolmanovsky, I.; Van Nieuwstadt, M.; Sun, J. (1999) "Optimization of complex powertrain systems for fuel economy and emissions." *Proceedings of the 1999 IEEE International Conference on Control Applications*, 1, 833-839.

Kolmanovsky, I., Sivashankar S., Sun, J. (2005) "Optimal control-based powertrain feasibility assessment: A software implementation perspective." *Proceedings of the 2005 American Control Conference*, 7, 4452- 4457.

Kolmanovsky, I., Siverguina, I., Lygoe, B. (2002) "Optimization of powertrain operating policy for feasibility assessment and calibration: stochastic dynamic programming approach." *Proceedings of the 2002 American Control Conference*, 2, 1425-1430.

Larson, R.E. (1967) "A survey of Dynamic Programming Computational Procedures." *IEEE Transactions on Automatic Control*, 12 (6), 767-774.

Lechner, G. (1999) *Automotive transmissions: fundamentals, selection, design and application*, Springer, Berlin.

Leondes, C.T. (1980) "An Appreciation of Professor Richard Bellman." *Journal of Optimization Theory and Applications*, 32 (4), 399-406.

Leone, T.G., Pozar, M. (2001) "Fuel Economy Benefit of Cylinder Deactivation – Sensitivity to Vehicle Application and Operating Constraints." *SAE Paper 2001-01-3591*.

Lin, C-C., Filipi, Z., Wang, Y., Louca, L., Peng, H., Assanis, D., Stein, J. (2001) "Integrated, Feed-Forward Hybrid Electric Vehicle Simulation in SIMULINK and its Use for Power Management Studies." *SAE Paper 2001-01-1334*.

Lin, C-C., Peng H., Grizzle, J.W., Kang, J.M. (2003) "Power management strategy for a parallel hybrid electric truck," *IEEE Transactions on Control Systems Technology*, 11 (6), 839- 849.

Lin, C-C., Filipi, Z., Loucas, L., Peng, H., Assanis, D., Stein, J. (2004a) "Modeling and Control for a Medium-Duty Hybrid Electric Truck", *International Journal of Heavy Vehicle Systems*, 11 (3/4*), 349-370.

Lin, C-C. (2004b) "Modeling and Control Strategy Development for Hybrid Vehicles." *PhD Dissertation*, University of Michigan.

Lin, C-C., Peng H., Grizzle, J.W. (2004c) "A stochastic control strategy for hybrid electric vehicles." *Proceedings of the 2004 American Control Conference*, 5, 4710-4715.

Louca, L., Stein, J., Rideout, D. (2001) "Generating Proper Integrated Dynamic Models for Vehicle Mobility Using a Bond Graph Formulation," *Society for Computer Simulation*, Phoenix, AZ.

Maciejowski, J.M. (2002) *Predictive Control with Constraints,* Prentice Hall, New York.

Markel, T., Brooker, A., Hendricks, T., Johnson, V., Kelly, K., Kramer, B., O'K eefe, M., Sprik, S., Wipke, K.(2002) "ADVISOR: A Systems Analysis Tool for Advanced Vehicle Modeling." *Journal of Power Sources*, 110, 255–266.

Markel, T., Wipke, K. (2001) "Optimization Techniques for Hybrid Electric Vehicle Analysis Using ADVISOR." *Proceedings of the International Mechanical Engineering Congress and Exposition*, New York.

McBroom, S. (2005) "Virtual-Vehicle Product Development." *Technology Today*, Spring 2005.

McGregor, M. (12005) "Fuel Economy Measurement System Variation Pareto Chart." *Advance Quality and Blackbelt Internal Chrysler Study.*

Michelini, J., Glugla C. (2003). "Control system design for steady state operation and mode switching of an engine with cylinder deactivation." *Proceedings of the American Control Conference*, 4, 3125- 3129.

Minowa, T., Kimura, H., Ozaki, N., Ibamoto, M. (1996) "Improvement of fuel consumption for a vehicle with an automatic transmission using driven power control with a powertrain model." *JSAE Review*, 17, 375-380.

Moran, M.J., Shapiro, H.N. (1995) *Fundamentals of Engineering Thermodynamics*, John Wiley & Sons, Inc. New York.

Mortimer, J. (2002) "Squeezing Every Drop of Efficiency." *Automotive Engineer*, 27 (9), 60.

National Renewable Energy Laboratory. (2006) "Vehicle Systems Analysis: Simulation and Tools." http://www.nrel.gov/vehiclesandfuels/vsa/simulation_tools.html.

Ochi, T., Takeuchi, H., Kimura, H., Watanabe, K. (2006) "Development of a Super-Flat Torque Converter for the New Toyota FWD 6-speed Automatic Transaxle." *SAE Paper 2006-01-0149.*

Ohl, G., Prucka, M., Kanafani, F., Duty, M., DiValentin, E., Kramer, D. (2004) "Development of Powertrain Coordinator at DaimlerChrysler Corporation." *SAE Paper 2004-01-0893.*

Pasquier, M., Rousseau, A.(2001) "PSAT and PSAT-PRO an Integrated and Validated Toolkit from Modeling to Prototyping." *SAE Paper 2001-01-P178*.

Passmore, M.A., LeGood, G.M. (1994) "A Detailed Drag Study Using the Coastdown Method." *SAE Paper 940420*.

Porter, F.C. (1979) "Design for Fuel Economy – The New GM Front Drive Cars." *SAE Paper 790721*.

Powell, B.K., Sureshbabu, N., Bailey, K.E., Dunn, M.T. (1998) "Hardware-in-the-loop vehicle and powertrain analysis and control design issues." *Proceedings of the 1998 American Control Conference*, 1, 483 – 492.

Rao, H.S., Cohen, A.I., Tennant, J.A., Van Voorhies, K.L. (1979) "Engine Control Optimization via Nonlinear Programming." *SAE Paper 790177*.

Rask, E., Sellnau, M. (2004) "Simulation-Based Engine Calibration: Tools, Techniques, and Applications." *SAE Paper 2004-01-1264.*

Ren, Q., Crolla D.A., Wheatley, A. (2007) "Power Management and Control Strategies for a Hybrid Vehicle with a Dual Mode Power Split Transmission." *Proceedings of the Fifth IFAC Symposium on Advances in Automotive Control*, 1, 111-118.

Rishavy, E.A., Hamilton, S.C., Ayers, J.A., Keane, M.A. (1977) "Engine Control Optimization for Best Fuel Economy with Emissions Constraints." *SAE Paper 770075*.

Rizzoni, G., Guezennec Y., Brahma, A., Wei, X., Miller, T. (2000) "VP-SIM: A Unified Approach to Energy and Power Flow Modeling Simulation and Analysis of Hybrid Vehicles." *SAE Paper 2000-01-1565*.

Rousseau, A., Pagerit, S., Monnet, G., Feng, A. (2001) "The New PNGV System Analysis Toolkit PSAT v4.1 – Evolution and Improvement." *SAE Paper 2001-01-2536*.

Rousseau, A. (2007) "PSAT Training, Part 2: Capabilities." *Argonne National Laboratory*, www.transportation.anl.gov/pdfs/HV/298.pdf.

Society of Automotive Engineers (1996). "Road Load Measurement and Dynamometer Simulation Using Coastdown Techniques." Standard J1263.

Society of Automotive Engineers (1996). "Road Load Measurement using Onboard Anemometry and Coastdown Techniques." Standard J2263.

Society of Automotive Engineers (1999). "Stepwise Coastdown Methodology for Measuring Tire Rolling Resistance." Standard J2452.

Song, D., El-Sayed, M. (2002) "Multi-Objective Optimization for Automotive Performance." *International Journal of Vehicle Design*, 30 (4), 291-308.

Stengel, R.F. (1994) *Optimal Control and Estimation*, Dover Publications, New York.

Sumi, K., Yamamoto, K., Gielen L., Meulewaeter, L. (2002) "Powertrain noise and vibration simulation with hybrid models." *International Journal of Vehicle Design*, 29 (1-2), 149-159.

Thomann, G. (2007) "Entwicklung einer Simulationssoftware zur Vorhersage von Fahrzeugbeschleungigungsleistung." *Praxis-Bericht*, DaimlerChrysler.

Trask, N.R., Hammoud, M., Haghgooie, M., Megli, T.W., Dai, W. (2003) "Optimization Techniques and Results for the Operating Modes of a Camless Engine." *SAE Paper 2003-01-0033.*

United States Environmental Protection Agency. (2006) "Fuel Economy." http://www.epa.gov/fueleconomy.

Vahidi, A., Stefanopoulou, A., Peng, H. (2004) "Model predictive control for starvation prevention in a hybrid fuel cell system." *Proceedings of the 2004 American Control Conference*, 1, 834-839.

Vossoughi, G.R.; Rezazadeh, S. (2005) "Optimization of the calibration for an internal combustion engine management system using multi-objective genetic algorithms." *Proceedings of the 2005 IEEE Congress on Evolutionary Computation*, 2, 1254-1261.

Wagner, G., Naunheimer, H., Scherer, H., Dick, A. (2007) "Achtgang-Automatikgetriebe zur Reduzierung des Kraftstoffverbrauchs." *Automobiltechnische Zeitschrift*, June 2007, 512-519.

Wipke, K., Cuddy, M., Burch, S. (1999) "ADVISOR 2.1: a user-friendly advanced powertrain simulation using a combined backward/forward approach." *IEEE Transactions on Vehicular Technology*, 48 (6), 1751-1761.

Wong, L.T., Clemens, W.J. (1979) "Powertrain Matching for Better Fuel Economy." *SAE Paper 790045*.

Wu, B., Filipi, Z.S., Prucka, R.G., Kramer, D.M., Ohl, G.L. (2006) "Cam-phasing Optimization Using Artificial Neural Networks as Surrogate Models—Fuel Consumption and NOx Emissions." *SAE Paper 2006-01-1512*.